Development of Point-of-Care Nanoparticle Based Diagnostic Platforms

by

Jisung Kim

A thesis submitted in conformity with the requirements
for the degree of Doctor of Philosophy

Institute of Biomaterials and Biomedical Engineering
University of Toronto

Development of Point-of-Care Nanoparticle Based Diagnostic Platforms

Jisung Kim

Doctor of Philosophy

Institute of Biomaterials and Biomedical Engineering
University of Toronto

2017

Abstract

Despite the substantial improvement of diagnostic technologies over the last few decades, the most advanced diagnostic tests are centralized, require expensive facilities and expertise, and are therefore inaccessible to many patients and healthcare professionals in resource-limited areas. Point-of-Care (POC) diagnostics, which emphasize the idea that medical tests are conducted near the patients and subsequently lead to rapid clinical decisions, aim to overcome these limitations by decentralizing simple and cost-effective diagnostic approaches. Advances in nanotechnology have also shown the potential to improve POC diagnostics by offering tunable optical, electrical and magnetic properties that can transduce signals or simplify diagnostic procedures. Nonetheless, many nanoparticle-based molecular assays have been limited to the investigation of synthetic targets due to low analytical sensitivity, and clinical validation of nanodiagnostics has not been thoroughly explored yet. The work presented herein explores the development of ultrasensitive nanoparticle-based POC diagnostic platforms. Specifically, Quantum Dot (QD) barcode and multicomponent nucleic acid enzyme-gold nanoparticle (MNAzyme-GNP) assays were incorporated with Recombinase Polymerase Amplification (RPA) to demonstrate multiplexed and colorimetric detections respectively, improve the detection limits, and present clinically relevant diagnosis of infectious diseases. Overall, the combined advantages of nanotechnology and

isothermal nucleic acid amplification strategy provided highly sensitive and specific detection platforms that are promising for diagnosis of infectious diseases in resource-limited settings.

Acknowledgments

First of all, I would like to thank my supervisor, **Dr. Warren Chan**, for giving me this amazing opportunity to work in his lab. His boundless passion for new scientific discoveries has inspired me to think inventively, and will continue to motivate my desire to learn in the future. I am indebted to his incredible mentorship and continuous support throughout my study. He has consistently been resourceful to arrange numerous collaborations, and responsive with constructive feedback, which were both instrumental to keep my studies on track, and enrich the depth of my research.

I would like to also thank my committee members, **Dr. Jonathan Rocheleau** and **Dr. Ofer Levi**, who have been greatly supportive in every committee meetings, and provided insightful suggestions to improve and refine the work presented in this thesis.

This work would have not been made possible without the help from many colleagues and collaborators. I acknowledge **Dr. Kevin Ming** for his contribution and dedication towards the smartphone project. I am exceptionally appreciative to **Mohamed Mohamed** and **Dr. Kyryl Zagorovsky**, who I had pleasure of working with on MNAzyme-GNP projects. **Mohamed**'s enthusiasm has cheered me up many times when I was dampened by failed experiments, and **Kyryl**'s challenging questions aspired me to think more analytically. I was also lucky to have collaborated with **Dr. Mia Biondi** and **Dr. Jordan Feld** throughout Quantum Dot barcode projects. **Mia**'s excitement in science has invigorated our teamwork, and **Jordan**'s expertise on clinical topics were repeatedly helpful in reframing our studies.

I will not forget the days I spent with past and current members of Chan lab. **Dr. Kun Chen** was remarkably helpful, and trained me with essential skills that I needed to carry out my studies. I still remember all the fun and deep conversations I had with **Qin Dai** during our trip in Houston, the Jang Won night with everyone on St. Patrick's Day, and countless bottles of Soju I drank with **James Lazarovits** and **Dr. Carl Walkey** at Lim Ga Ne, just to list a few memorable scenes. I thank all members of Chan lab for creating such a friendly and cooperative working environment.

Finally, I would like to express the deepest gratitude to my parents, **Chul** and **Nak-Kyung Kim**, and my sister, **Dr. Danah Kim**, for their unconditional love, never-ending support and words of encouragement. I would not have been the person who I am today without their sacrifices.

Above of all, I thank **God**, for who He is.

Table of Contents

List of Tables

List of Figures

List of Abbreviations

AF647	Alexa Fluor 647
ALT	Alanine transaminases
AR	Antibiotic resistance/resistant
ATP	Adenosine triphosphate
CCFF	Concentration-controlled flow-focusing
cDNA	Complementary DNA
CFU	Colony-forming unit
CI	Confidence interval
CoreAb	Core antibody
DD	Double-distilled
DNA	Deoxyribonucleic acid
dNTP	Deoxynucleotide triphosphates
dsDNA	Double-stranded deoxyribonucleic acid
EDC	1-ethyl-3-(3-dimethylaminopropyl) carbodiimide hydrochloride
ELISA	Enzyme-linked immunosorbent assay
FITC	Fluorescein isothiocyanate
FWHM	Full with at half maximum
GNP	Gold nanoparticle
HA	Hemagglutinin
HBV	Hepatitis B virus
HBsAg	Hepatitis B virus surface antigen
HBeAg	Hepatitis B virus e-antigen
HCC	Hepatocellular carcinoma
HCV	Hepatitis C virus
HDA	Helicase dependent amplification
HIV	Human immunodeficiency virus
HPV	Human papillomavirus
HRCA	Hyperbranched RCA
InfA	Influenza A virus
LAMP	Loop mediated isothermal amplification
LFA	Lateral flow assay
LOD	Limit of detection

MDR	Multi-drug resistance/resistant
MIC	Minimum inhibitory concentration
MNAzyme	Multicomponent nucleic acid enzyme
MNP	Magnetic nanoparticle
MRSA	Methicillin-resistant *Staphylococcus aureus*
NA	Neuraminidase
NTC	No template control
PCR	Polymerase chain reaction
PG-RCA	Primer-generating RCA
PEG	Polyethylene glycol
POC	Point-of-care
QD	Quantum dot
qPCR	Quantitative PCR
qRPA	Quantitative RPA
RCA	Rolling circle amplification
RNA	Ribonucleic acid
ROC	Receiver operating characteristics
RPA	Recombinase polymerase amplification
rt-RPA	Reverse transcription RPA
SARS	Severe acute respiratory syndrome
S. aureus	*Staphylococcus aureus*
SDA	Strand displacement amplification
SNP	Single-nucleotide polymorphism
SPION	Superparamagnetic iron oxide nanoparticle
ssDNA	Single-stranded deoxyribonucleic acid
sulfo-NHS	N-hydroxysulfosuccinimid
TLC	Thin-layer chromatography
UV	Ultraviolet
YLL	Years of life lost

Chapter 1 : Introduction

1.1 Prevalence of Infectious Diseases

An infectious disease, also known as a communicable or transmissible disease, is defined as an illness caused by the transmission of infectious agents such as bacteria, virus, fungus and prion[1]. Infectious diseases remain as one of the major causes of morbidity and mortality posing a significant threat to the global health and safety[2,3]. In 2009, communicable diseases accounted for 51% of years of life lost (YLL), a measure of premature mortality[4] (Figure 1.1). Interestingly, this number is represented asymmetrically among countries of different income groups. In low-income countries, communicable diseases accounted for 68% of YLL compared to only 8% in high-income countries[4] (Figure 1.1). This discrepancy is observed primarily because there is limited access to centralized laboratory and clinical facility to run sophisticated diagnostic tests in third-world countries, and available Point-of-Care (POC) diagnostic tests lack sensitivity to detect early infections or pathogens that are presented at low concentrations[5]. Thus, undiagnosed or misdiagnosed diseases can spread to other regions of the world with international travels and worsen global morbidity and mortality. Such threat of infectious diseases on a global scale was experienced with Severe Acute Respiratory Syndrome (SARS) pandemic in 2003[6], H1N1 flu pandemic in 2009[7], Ebola epidemic in 2014[8], and Zika outbreak in 2015[9].

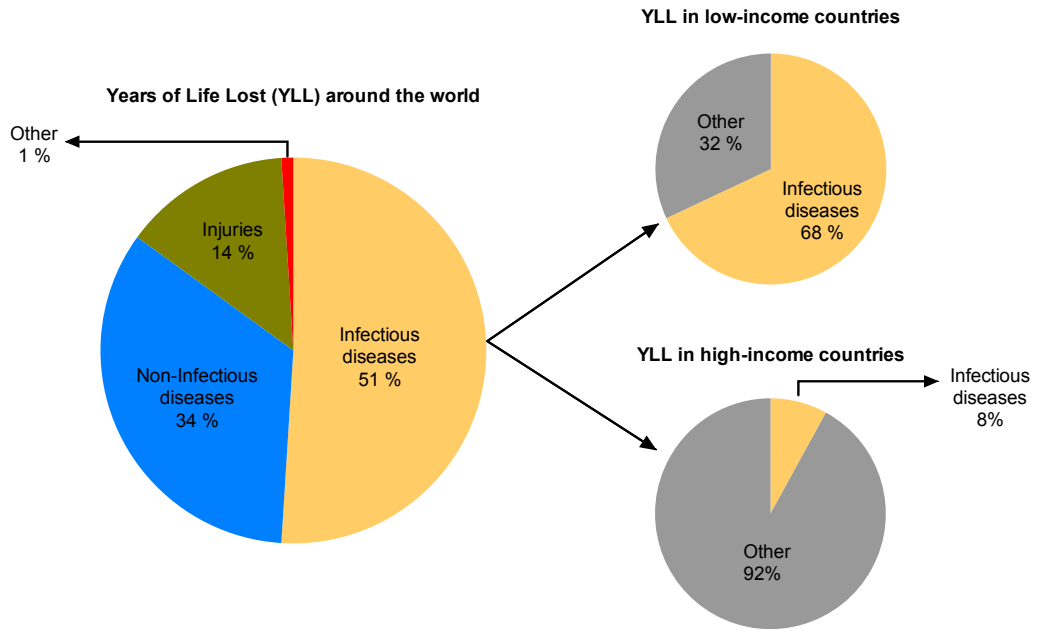

Figure 1.1: Percentage of YLL caused by Infectious Diseases[4].

1.1.1 Bloodborne Pathogens

Human immunodeficiency virus (HIV), hepatitis B virus (HBV) and hepatitis C virus (HCV) are major bloodborne pathogens, which are placed within the top 10 leading causes of infectious disease related deaths around the world[10]. Nosocomial transmission of these pathogens is a significant public health concern especially in developing countries due to inadequate sterilization of medical devices, reuse of needles and syringes, and unsafe or overuse of therapeutic injections[10,11]. Globally, about 40 million, 370 million and 130 million people are estimated to be infected with HIV, HBV and HCV respectively[10].

The majority of HIV infections, have occurred in sub-Saharan Africa (25.4 million) and Southeast Asia (7.1 million), where infections are mostly acquired through sexual contact or drug injections[12]. HIV infection can cause development of acquired immune deficiency syndrome (AIDS), which lowers cellular immunity and resistance to other infections, and can increase the risk of developing viral-induced cancers such as Kaposi's sarcoma and lymphoma[13].

HBV is the most common hepatitis virus that causes chronic infection of the liver[14]. HBV-related liver diseases like cirrhosis and hepatocellular carcinoma (HCC) account for 0.5-1 million deaths annually[15]. Chronic HBV infection is reported to be the highest in the Western Pacific (>95 million) and African (>75 million) regions, whereas the number of infections was the lowest in American region (>7 million)[16]. HBV transmission occurs mostly by perinatal and horizontal routes in sub-Saharan Africa and East Asia, whereas transmission is dominated by high-risk sexual activities and use of injection drugs in more industrialized countries[16].

HCV is the second leading cause of HCC. Unlike HIV and HBV that present high burden of infections in the sub-Saharan Africa, the highest prevalence of HCV infection has been reported in Northern Africa[17]. Industrialized nations in North America, Northern and Western Europe and Australia report lower prevalence of HCV infection[17]. In countries with high HCV prevalence, unsafe therapeutic injections are the predominant mode of HCV transmission, whereas in low prevalence countries, illegal drug injections are the predominant mode of HCV transmission[10].

HIV, HBV and HCV often present similar symptoms, and co-infection of HIV with either HBV or HCV can accelerate disease progression. Out of 40 million HIV infected individuals, 2-4 million are estimated to be co-infected with chronic HBV, and 4-5 million co-infected with chronic

HCV[10]. Hence, a combined HIV, HBV and HCV diagnostic test has been proposed as a key measure for implementing national screening programs in low-income countries[18].

1.1.2 Respiratory Viruses

The emergence and re-emergence of respiratory viruses continue to be a major global threat to the health of our community[19]. Every year, influenza has been one of the most alarming respiratory infections to humans, infecting 5 to 15% of the global population and accounting for 250,000 to 500,000 deaths[20,21]. Influenza is especially associated with a high mortality rate among people with chronic diseases, elders, and infants[22]. There are three types of influenza viruses (A, B and C), and type A is the most virulent among the three. The large-scale spreads of influenza A virus (InfA) were experienced in the past with global pandemics such as the "Spanish influenza" in 1918-1919, "Asian influenza" in 1957-1958, and "Hong Kong influenza" in 1968-1969, which were all characterized with notably increased mortality and morbidity in these years[23]. Also, InfA is associated with seasonal epidemics that can increase the rate of mortality for other diseases like congestive heart failure, pneumonia, bacterial superinfections, and chronic obstructive pulmonary disease[24].

There are many subtypes of InfA, which are classified based on the expression of hemagglutinin (HA) and neuraminidase (NA) glycoproteins on the surface of virus particles[25]. A total of 16 HA and 9 NA subtypes are known with H1N1 subtype being responsible for the recent flu pandemic in 2009[7], and H3N2 subtype dominating in the prevalence of seasonal InfA epidemics since its first appearance in 1968 (*i.e.* "Hong Kong influenza")[21]. H5N1 subtype is also considered as a potential pandemic threat since its first outbreak in human in 1997[26]

InfA viruses exist as quasi-species that are evolutionarily dynamic with high mutation rates ($1x10^{-3}$ to $8x10^{-3}$ substitutions per site per year)[22]. Antigenic variations in the HA and NA domains can result in the emergence of new InfA species or re-emergence of evolved viruses in the next epidemics or pandemics that render previous vaccinations ineffective against the new variants[27]. Hence, diagnostic platforms that can rapidly detect pre-existing InfA subtypes and newly emerging viral strains are needed for optimal selection of vaccinations and promptly administering antiviral treatments during seasonal epidemics and pandemic outbreaks[28].

1.1.3 Antibiotic Resistant Bacteria

The extensive use of antibiotics has fueled the development of many antibiotic resistant microorganisms over the last century[29]. Although various antibiotic classes have been discovered to treat bacterial infections by inhibiting the synthesis of cell walls, proteins, nucleic acids or folic acids, none of the them has completely escaped resistance mechanisms, which include the degradation or alteration of antibiotics by certain enzymes, and an active efflux of antibiotics to pump the drugs out of a cell[30]. Moreover, the antibiotic resistance is mobile, and the selected resistance genes can be transferred to other bacteria through transposons, plasmids, naked DNA or bacteriophages, which further drives the resistance problem[30,31].

Antibiotic resistance can increase the morbidity and mortality as experienced with several methicillin-resistant *Staphylococcus aureus* (MRSA), and multi-drug resistant tuberculosis outbreaks around the world. Morbidity and mortality increase because generally accepted therapy becomes ineffective, and antibiotic susceptibility tests can take hours or days, delaying the administration of an effective therapy[31]. Epidemics of antibiotic resistant pathogens occurred in the developing countries because alternative antibiotics were too expensive to administer, or due to the extensive use of non-prescription antibiotics[31,32]. The costs associated with the treatment of a disease can also increase significantly with the development of antibiotic resistance. For example, the cost of treating a tuberculosis infection is estimated to be $12,000 for an antibiotic-sensitive strain, and $180,000 for a multidrug-resistant strain[31].

Although newer drugs can be developed continuously to combat the antibiotic resistance problem, the rate of developing new antibiotics has declined as the world is approaching near the "post-antibiotic era"[31]. Also, the emergence of multi-drug resistance as seen in bacterial species like *Mycobacterium tuberculosis, Enterococcus faecium,* and *Staphylococcus aureus* (*S. aureus*) can pose a devastating threat to individuals, especially in developing countries where sanitation conditions are poor, because all available antibiotics have failed, or due to unavailability of new effective antibiotics[30].

Conservation of currently available antibiotics in conjunction with the innovation of new drugs has been proposed as an important strategy to maintain the effectiveness of antibiotics in the future[33]. This can be achieved by reducing the unnecessary use of antibiotics with inexpensive POC diagnostics that can identify the pathogen, and also its susceptibility to available antibiotics[33].

1.2 Current Infectious Disease Diagnostic Technologies

Several diagnostic techniques are currently available to determine the causative agents of infectious diseases, guide healthcare professionals to initiate proper treatments, provide control measures to quarantine the infected individuals, and monitor the disease progression. These techniques include microscopy, culture, enzyme-linked immunosorbent assay (ELISA), lateral flow assay (LFA), and polymerase chain reaction (PCR).

1.2.1 Microscopy

Numerous microscopic techniques are widely used for the diagnosis of infectious diseases like malaria[34-36], tuberculosis[37,38], and urinary tract infections[39-41]. This involves direct examination of either stained or unstained smears (blood, sputum, urine, *etc*.) at the cellular level using a variety of microscopic techniques (*e.g.* bright field, dark field, and fluorescence microscopy). Such techniques have been reported to achieve high level of diagnostic sensitivity for certain pathogens[35,37]; however, their outcomes can heavily vary depending on the training level of a microscopist, concentration of the pathogen within the clinical specimen, staining methods, and other sample preparation steps[36,40]. Hence, manual microscopy may not be a reliable screening method especially when it is performed by the non-experts due to its inherent variability[42]. Also, microscopes can be expensive with specialized optical features, which make them mostly unavailable in resource-limited and decentralized regions.

1.2.2 Culture

Culture-based tests like broth microdilution and agar diffusion (antimicrobial gradient diffusion and disc diffusion) methods are commonly used to diagnose antibiotic susceptibility of bacterial infections[43,44]. Broth microdilution method involves determining the minimum inhibitory concentration (MIC) of an antibiotic in a liquid growth medium inoculated with a bacterial suspension by observing the difference in the solution turbidity after the incubation. In the agar diffusion method, a bacterial inoculum is applied on an agar plate, and either a paper antibiotic disc, or a plastic test strip that is embedded with an antibiotic concentration gradient is placed on the agar surface. The diameter of inhibition zone qualitatively indicates the susceptibility (*i.e.* either susceptible, intermediate, or resistant) in the disc diffusion method, whereas the MIC is quantitatively measured from the strip in the antimicrobial gradient method for determination of

resistance. Despite having well standardized processes and high sensitivity for detection of antibiotic resistance, these methods are time-consuming and can take from 24 to 72 hours because sufficient incubation time is required to differentiate between resistant and susceptible bacterial isolates[43].

1.2.3 Enzyme-linked Immunosorbent Assay

Many serological diagnostic tests are performed using ELISA to detect presence of antigens or antibodies in a biological sample. There are several types of ELISA (indirect, direct, sandwich, and competitive ELISA), and all types involve the use of an enzyme-labeled antibody and a chromogenic substrate of the enzyme that changes the colorimetric or fluorescence signal in the presence of biological molecules (proteins, peptides, *etc*.)[45]. In a typical sandwich ELISA test, the target analyte is sandwiched between a capture antibody immobilized on a solid surface, and an enzyme-linked detection antibody, which converts the substrate to produce a visible color change or a fluorescence signal[46]. Despite the high sensitivity demonstrated by ELISA test, there are difficulties for practice in resource-limited settings since ELISA requires a bulky instrument for the optical detection, expensive antibody reagents, many steps of pipetting, and long hours of incubation[47,48]. Also, ELISA is susceptible to non-specific binding of the antigen or antibody to the surface of a plate, which can lead to a false-positive result, and the synthesis of antibodies that are specific to certain antigens can be challenging for diagnosis of some pathogens[45].

1.2.4 Lateral Flow Assay

LFA is by far the most widely used diagnostic technique in POC settings (*e.g.* preganancy and dipstick tests) due to its simplicity, portability, and rapid response time. In LFA, analyte travels along a polymeric strip with reporter probes by capillary force and encounters a detection zone where the analyte-reporter complex binds to immobilized capture probes producing a visible line on the pad[49]. There are several variants of LFA to detect either proteomic or genomic biomarkers. The exclusive use of antibodies as recognition molecules is known as a lateral flow immunoassay, whereas the hybridization of nucleic acids with immobilized complementary strands is called nucleic acid lateral flow assay[49]. LFAs do not require washing steps, and can be performed in one-step, which significantly reduce the amount of sample handling. However, the main disadvantage is that LFA has low sensitivity, and provides only qualitative or semi-quantitative results precluding its use for diagnosis of pathogens that are presented at low concentrations.

1.2.5 Polymerase Chain Reaction

PCR is a technique frequently used for amplification of nucleic acids (either RNA or DNA) and many infectious diseases are diagnosed using PCR to determine the presence of genetic biomarkers. Several variants of PCR have been developed to serve different purposes including quantitative and digital PCR for measuring the amount of target nucleic acids, asymmetric PCR for generating single-stranded (ss) amplicons, reverse-transcription (rt) PCR for amplifying RNA, and multiplex PCR for amplifying multiple sequences simultaneously[50-55]. In all PCR reactions, a nucleic acid sequence is amplified through repetitive cycles of dehybridization of double stranded (ds) DNA or RNA, hybridization with primers, and extension of primers with polymerase, producing a large amount of amplicons[56]. The detection of amplicons can be carried out *via* several methods such as gel electrophoresis, real-time fluorescence measurement, or sandwich hybridization assay. PCR offers the highest sensitivity, and can detect as low as 5 to 10 nucleic acid copies[57]; however, it is not well suited for use in POC settings due to the need of an expensive thermocycler and trained technicians[58].

1.2.6 Limitations of Current Diagnostic Technologies

Currently available diagnostic technologies for infectious diseases are specialized for testing in either POC or laboratory settings, and each group presents its advantages and disadvantages (Figure 1.2). POC diagnostic tests (*e.g.* LFA) can be easily performed by non-experts, are inexpensive, and can produce fast results, which render them widely accessible in the developing world; however, they provide low sensitivity. On the other hand, laboratory-based diagnostic tests (*e.g.* microscopy, culture, PCR, and ELISA) can provide higher sensitivity, but they are difficult to use, expensive and time consuming, making them largely inaccessible in the developing world.

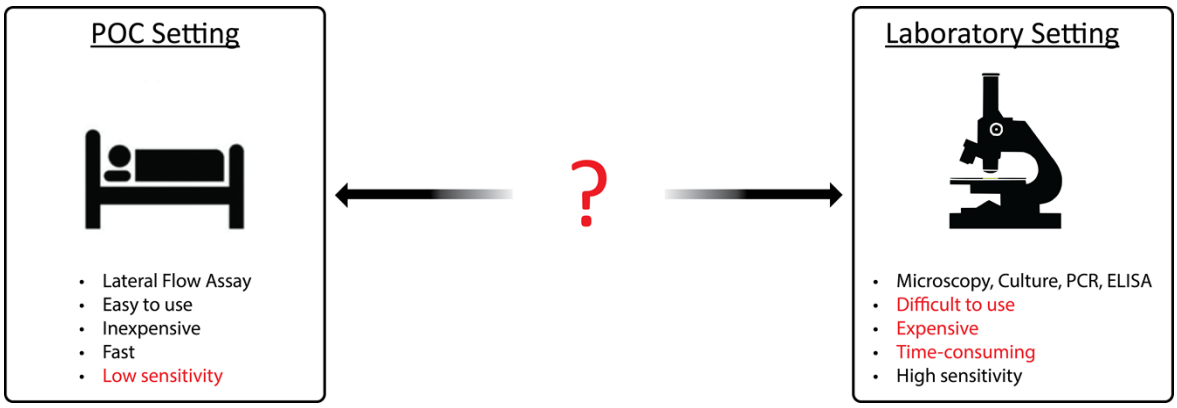

Figure 1.2: Limitations of Current Diagnostic Technologies.

1.3 Spectrum of POC Diagnostics

The World Health Organization has announced a list of criteria that defines an ideal POC diagnostic test (*i.e.* ASSURED criteria). According to this list, a POC diagnostic should be affordable, sensitive, specific, user-friendly, rapid and robust, equipment-free, and delivered[59]. Although these criteria were required when the "first-generation of POC diagnostics" (*i.e.* rapid diagnostic tests such as LFA) were introduced, they also imposed restrictions on the concept of POC diagnostics by confining them to equipment-free and cheap tests that are only used outside of laboratories and hospitals by the non-experts[60]. The emergence of the "second and third-generation POC diagnostics" such as the cartridge-based nucleic acid amplification tests, and smartphone-based diagnostic devices demand sub-classification of POC diagnostics based on how these tests can be implemented in a healthcare system[60].

Hence, POC diagnostics can be explained as a spectrum (Figure 1.3) covering different levels of technology (simple to sophisticated), user (untrained to trained), and setting (home to hospital)[60]. Despite having no universal definition, all levels of POC testing should provide a rapid turn-around that can link the test results to appropriate follow-up counseling and treatment by the healthcare providers in the same clinical encounter (*i.e.* at least on the same day of testing)[60]. For instance, many reference laboratories of developing countries use rapid diagnostic tests, but deliver their results after days, which may not be considered as a POC testing, whereas testing at a peripheral laboratory attached to a hospital may still be considered as a POC testing if the results can be disseminated on the same day of clinical encounter to initiate follow-up actions[60]. Immediate connection between the diagnostic results and follow-up care can better improve a patient's health outcome compared to a rapid diagnostic test that only identifies the cause of a disease, but leaves the patient isolated from counseling or care[61]

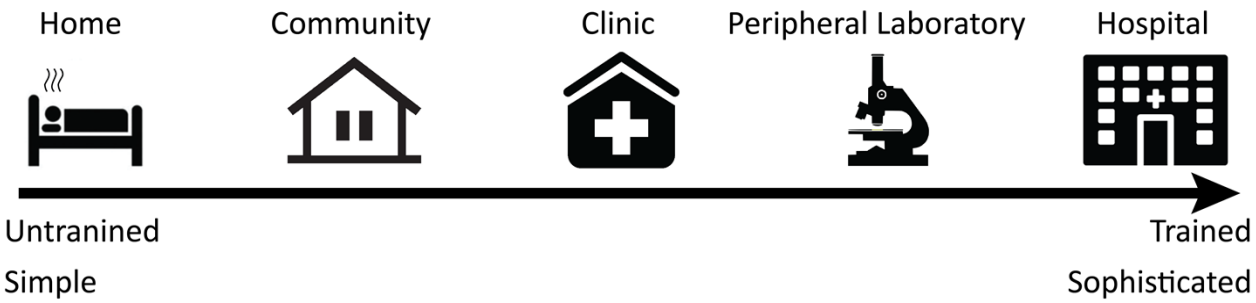

Figure 1.3: Spectrum of POC Diagnostics.
Figure recreated with permission from source[60]. Copyright (2012) Pai et al.

1.4 Nanotechnology for POC Diagnostics

The advancements in nanotechnology are offering innovative solutions to improve current diagnostic and therapeutic strategies in medicine. Nanomaterials are particularly useful for medical applications because their sizes are within the range of many biological molecules. The National Nanotechnology Initiative of the United States defined nanotechnology as the "understanding and control of matter at dimensions between approximately 1 and 100 nanometers"[62]. At this nanoscale, the ratio of surface atoms to interior atoms becomes much greater compared to a bulk material, which contributes to many unique properties of nanomaterials[63]. Contrary to macroscopic materials, nanomaterials have high surface-area-to-volume ratio, which provides a great capacity to functionalize the surface with many molecules. For example, a cube with 1-cm dimensions can be divided into 10^{21} 1-nm cubes, which will increase the surface area by 7-orders of magnitude[64]. Also, nanomaterials have tunable optical, magnetic, electrical and biological properties, and can be engineered with different shapes, sizes, chemical compositions and surface functionalities[64]. Nanomedicine aims to benefit from these properties for the diagnosis and treatment of diseases at the molecular level. Commonly used nanoparticles and their size range relative to other biological molecules is depicted in Figure 1.4. This section will discuss the properties of three nanomaterials that are commonly used in nanomedicine (quantum dots, magnetic nanoparticles, and gold nanoparticles), and their implications in the development of POC diagnostics.

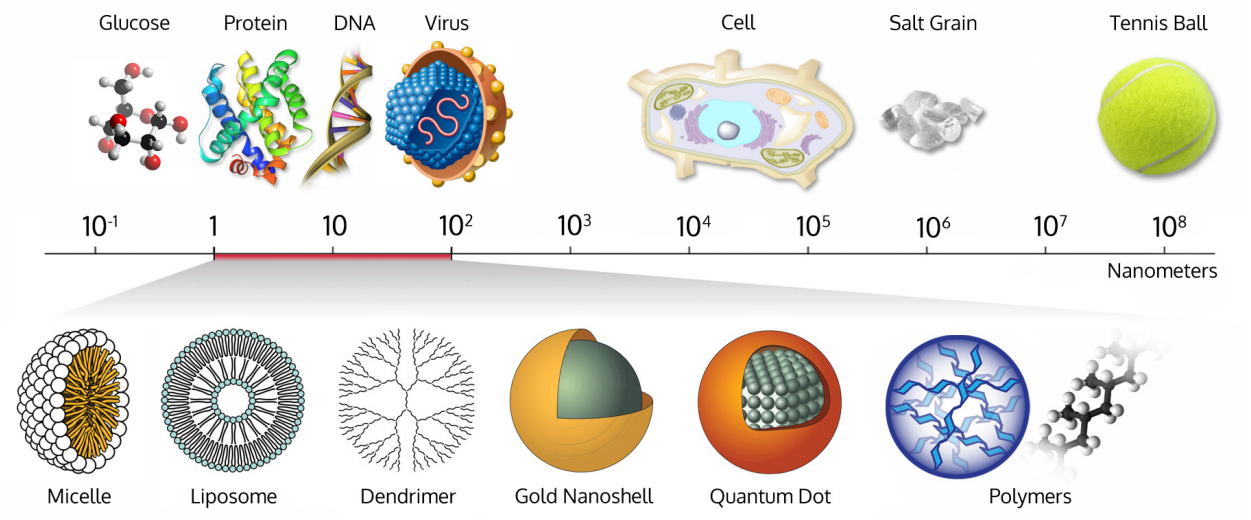

Figure 1.4: Size Range of Nanoparticles.
Figure adapted with permission from source[65]. Copyright (2015) Nachrichten aus der Chemie.

1.4.1 Quantum Dots

Quantum dots (QDs) are semiconducting nanocrystals that are usually formed as a core-shell structure, and composed of atoms from groups II-VI, IV-VI or III-V in the periodic table[66]. These nanomaterials exhibit quantum mechanical effects, which lead to size-dependent electrical and optical properties[67]. In a bulk-scale semiconductor, the energy states are grouped into energy bands, where an electron from the valence band (*i.e.* highest occupied electronic state) gets excited to the conduction band (*i.e.* lowest unoccupied electronic state) upon the absorption of a photon, leaving a vacancy in the valence band (*i.e.* hole). The excited electron and remaining hole are attracted to each other by the electrostatic force, and this electron-hole pair is referred to as an exciton. As the size of a semiconducting material becomes near or smaller than the exciton Bohr radius (~50-100 nm), which is the case for QDs, the energy bands become discrete energy levels with potential barriers that confine the electron motion (Figure 1.5A). This quantum confinement effect forms the basis of size-tunable properties of QDs. As the size of a QD increases, the discrete energy levels split and results in a narrower bandgap, which corresponds to the emission of a longer wavelength photon upon the recombination of an electron-hole pair (Figure 1.5A). Hence, the fluorescence emission of a QD can be fine-tuned to produce a variety of colors in the visible spectrum by simply adjusting its size (Figure 1.5B).

Additionally, QDs present a much broader and continuous absorption spectrum with a large separation between the excitation and emission wavelengths (*i.e.* Stokes shift) compared to organic dyes (Figure 1.5C)[68-70]. This optical property becomes useful for a diagnostic application because QDs of different emission profiles can all be excited using a single light source given that the energy of excitation is greater than the largest bandgap energy among QDs of different sizes. For instance, a light source with its wavelength in the ultraviolet (UV) range can excite all QDs that emit fluorescence in the visible range as opposed to organic dyes that typically require multiple excitation sources for different emission profiles. Also, QDs have narrower emission spectra, better photostability and are brighter than organic dyes, which are useful characteristics for many bio-labeling applications such as the cell labeling or tracking, *in vivo* imaging, *in vitro* diagnostics and encoding microbeads for a multiplexed assay[68-70]. For example, the emission spectrum of a QD is symmetric and can have a full width at half maximum (FWHM) as low as 12 nm[71], whereas an organic fluorophore is often characterized with an asymmetric emission spectrum tailing to the longer wavelength with its FWHM between 50 to 100 nm[72].

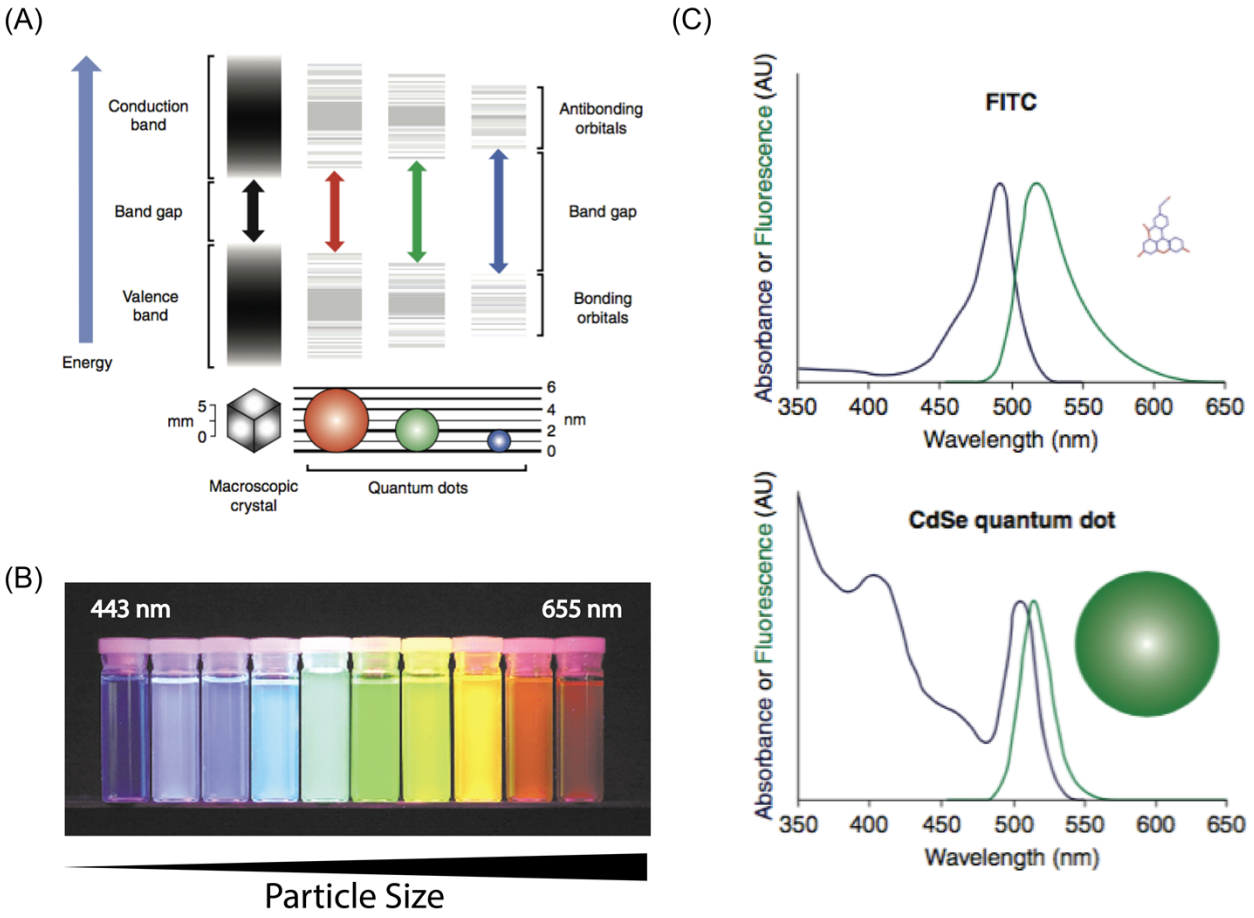

Figure 1.5: Size-tunable Optical Property of QDs. (A) Discrete energy levels of QDs compared to continuous energy states (*i.e.* energy bands) in a macroscopic semiconductor, and the size-dependent bandgap energies of QDs. Figure adapted with permission from source[73]. Copyright (2010) Dimitris Ioannou and Darren K. Griffin. (B) CdSe-ZnS (core-shell) QDs excited with a near-UV lamp showing emission peaks at 443, 473, 481, 500, 518, 543, 565, 587, 610, and 655 nm (from blue to red). Figure adapted with permission from source[74]. Copyright (2001) Nature Publishing Group. (C) Absorption and emission spectra of an organic dye (fluorescein isothiocyanate, *i.e.* FITC), and QD (CdSe). Figure adapted with permission from source[73]. Copyright (2010) Dimitris Ioannou and Darren K. Griffin.

QDs have been widely used in the development of *in vitro* biosensors, especially in the context of engineering Förester Resonance Energy Transfer (FRET) based detection systems[75-77], and multiplexed diagnostics (*i.e.* the ability to detect multiple targets simultaneously)[74,78,79]. FRET based assays utilize QDs as energy donors, which transfer the energy to acceptor fluorophores or quenchers for detection of small molecules and nucleic acids. Also, QDs have been used as reporter probes in a sandwich ELISA for multiplexed detection of chemical residues and cancer antigens[80,81]. Greater multiplexing capability of QDs was realized when different combinations of QDs were infused into polymeric microbeads to generate fluorescent barcodes. The surface of the QD tagged microbeads can be functionalized with DNA capture probes, which hybridize with the

target DNA labelled with a fluorescent dye, yielding both the barcode and detection signals (Figure 1.6)[74]. In this complex, the barcode signal can be used to determine the identity of a target DNA (*e.g.* the type of an infectious disease, antibiotic resistance, *etc.*), and the detection signal can be used to determine the presence or the absence of a target DNA (*i.e.* whether a patient is infected or not). These QD barcodes can be designed with different colors (m) and intensity levels (n) to generate (n^m-1) barcode signals[74]. For instance, combinations of 6 QD colors with 10 intensity levels can theoretically create one million barcodes[74]. Although the actual multiplexing capacity would be much lower due to the requirement of signal-to-noise ratio, spectral overlaps, and variations in the fluorescence intensity[74], QD barcodes opened up a new opportunity to further improve multiplexed diagnosis and high-throughput screening of infectious diseases. Previously, a library of 60 barcode signals was generated with 3 QD colors from a set of 5, at 3 intensity ratios *via* concentration-controlled flow-focusing (CCFF) method, which demonstrated a highly robust way of synthesizing optically encoded microbeads that are stable at a wide range of biological environments (*e.g.* temperature, pH, and buffer conditions) with good monodispersity (Figure 1.7)[82].

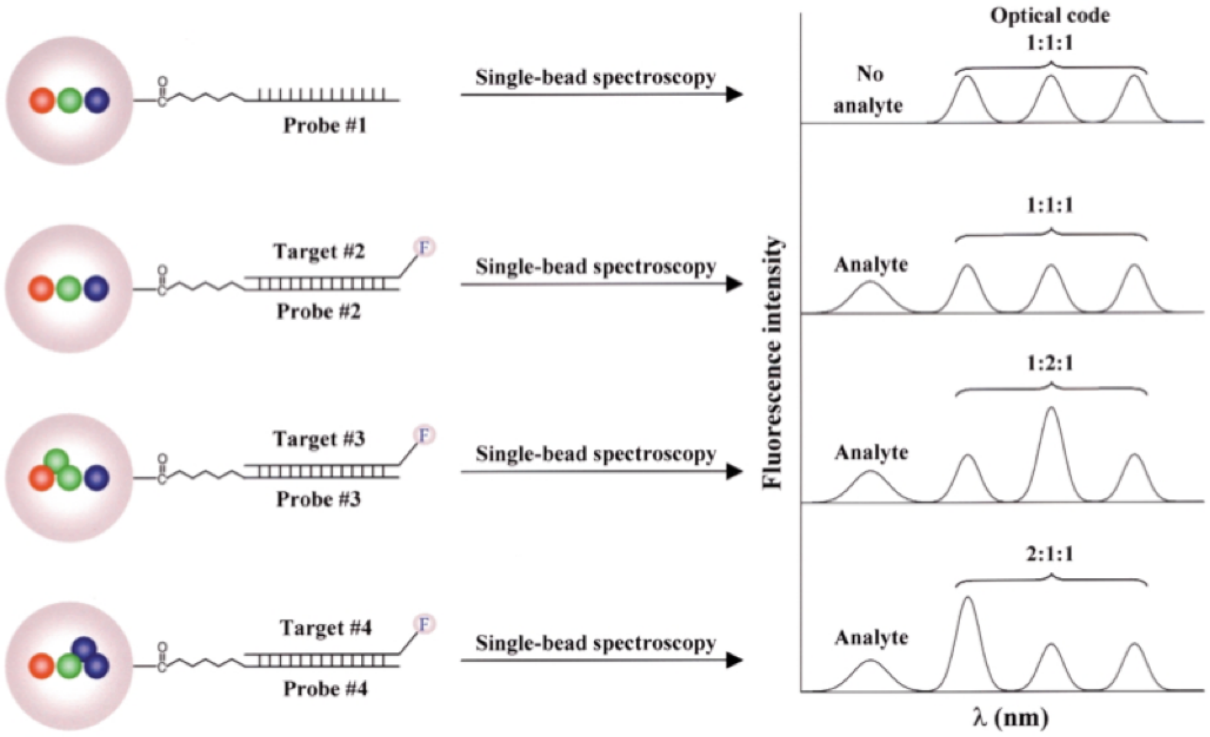

Figure 1.6: DNA Hybridization Assay using QD Barcodes. The presence of target DNA (Target #2, Target #3, and Target #4) was detected with Cascade Blue fluorescent dye, and the identify of each target DNA was determined with barcode signals in a multiplexed assay. Figure adapted with permission from source[74]. Copyright (2001) Nature Publishing Group.

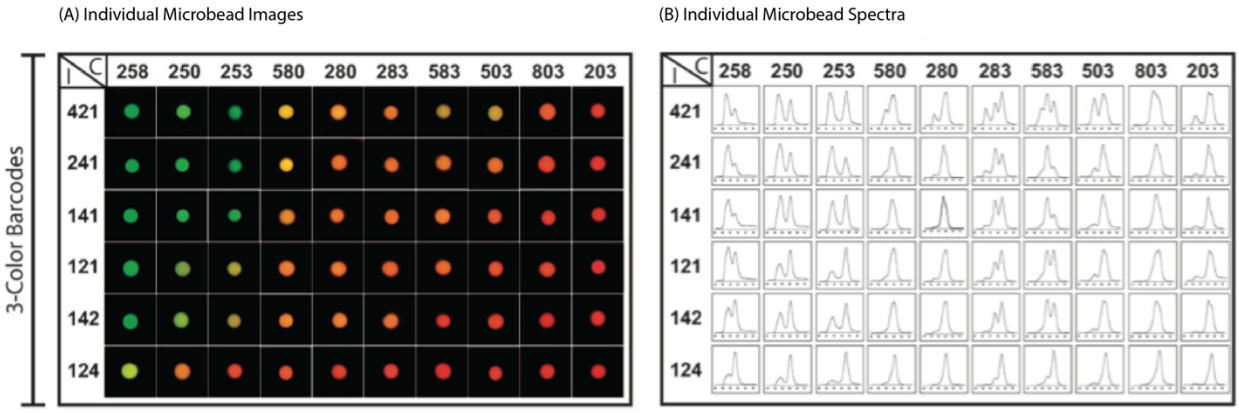

Figure 1.7: A Library of 60 QD Barcode Signals. (A) Microscope images of individual QD barcodes (5 μm) encoded with 3 colors at different relative intensity levels. (B) Fluorescence emission spectra of individual QD barcodes. Figure adapted with permission from source[82]. Copyright (2008) Wiley-VCH Verlag GmbH & Co. KGaA.

Additionally, high-throughput synthesis of QD barcodes was demonstrated using a combined membrane emulsification-solvent evaporation approach[83]. Studies have also shown multiplexed detection of several genomic and proteomic biomarkers for infectious diseases like HIV, HBV, HCV, malaria, and syphilis using QD barcodes in a sandwich assay format[78,79]. Moreover, coating the surface of QD barcodes with metal nanoshells was shown to improve the analytical sensitivity of the assay by 2-orders of magnitude due to the metal-enhanced fluorescence effect, and achieve better bead stability, fluorescence consistency and loading capacity of recognition molecules[84]. Multiplexing capability of QD barcodes is useful in the development of POC diagnostics because it can reduce labor cost and time. However, clinical validation of QD barcode technology has not been explored much yet due to the lack of a "PCR-less" signal amplification strategy that can substantially improve the limit of detection (LOD) of the assay for diagnosis of pathogens that are presented at low concentrations, but still require clinical interventions.

1.4.2 Magnetic Nanoparticles

Iron oxide nanoparticles are the most extensively explored magnetic nanoparticles (MNPs) in biomedicine due to their biocompatibility, biodegradability, and superparamagnetic properties[64,85]. In the macroscale, electrons of the magnetic particles can either spin in the opposite or same directions, in which the opposing spins cancel each other out, and weaken the localized magnetic field. On the other hand, magnetic particles at the nanoscale have more constrained electrons that only spin in the same direction, which strengthen the localized magnetic field[64]. For example, superparamagnetic iron oxide nanoparticles (SPIONs) that are smaller than 20 nm have a single

domain of electrons that spin in the same direction, whereas iron oxide macroparticles that are greater than 20 nm have multiple domains of electrons with opposite spins (Figure 1.8)[64]. Hence, SPIONs reveal much greater magnetic susceptibility to external magnetic field when compared to paramagnetic materials, and can get demagnetized with the removal of the external magnetic field unlike ferromagnetic materials that remain magnetized permanently. For this reason, there are some Food and Drug Administration (FDA) approved MNPs that are currently being used as contrast agents in Magnetic Resonance Imaging (MRI)[86], and many companies that sell MNPs for isolation of cells or extraction of biological molecules such as proteins and nucleic acids.

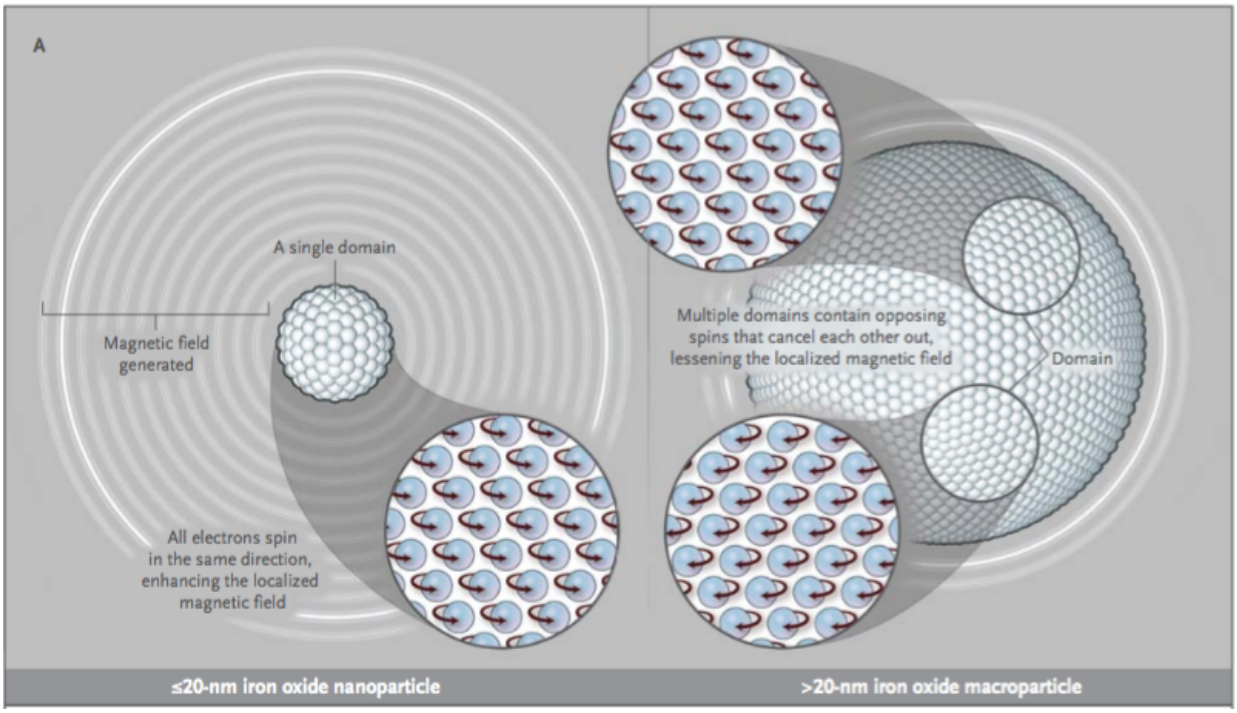

Figure 1.8: Size-dependent Properties of Iron Oxide Magnetic Particles. Figure adapted with permission from source[64]**.** Copyright (2010) Massachusetts Medical Society

MNPs have also been explored in the development of various diagnostic systems. One of the techniques measures the change in the transverse relaxation time (T_2) of a sample using a micro Nuclear Magnetic Resonance (μNMR) device by either decorating the surface of the microbeads with MNPs in the presence of the target DNA[87,88], tagging the surface of target cells with MNPs[89], or by aggregating MNPs in the presence of target analytes[90]. Magnetization of QD barcodes have also been reported by infusing MNPs in polymeric microbeads by CCFF[91] or membrane emulsification-solvent evaporation[92] methods. MNPs add another dimension to barcoding the microbeads, and can increase the number of available barcodes by several folds for multiplexing

[91]. Also, assay procedures that involve several washing and isolation steps can be simplified by using magnetic QD barcodes. For instance, washing of excess reporter probes in a typical sandwich assay can be achieved by simply applying an external magnetic field with a portable magnetic rack, which renders the assay more feasible for use in a POC setting compared to using a centrifuge device for washing. Moreover, magnetic QD barcodes can be used to automate an assay procedure in a microfluidic format. A conventional QD barcode assay has been automated with the additional encoding of the barcodes with MNPs and using permanent magnets in a microfluidic device to magnetically move the barcodes to a stream containing target DNA, move back to a stream containing reporter probes, and finally immobilize the barcodes during the washing of excess reporter probes[93].

1.4.3 Gold Nanoparticles

Gold nanoparticles (GNPs) display surface plasmon resonance effect, which contributes to their unique optical properties. When GNPs are irradiated by light, the oscillation of electric field causes synchronized oscillation of conduction band electrons as illustrated in Figure 1.9A[94]. This generates gold ions that are missing conduction band electrons and thus positively charged, creating a net charge difference or a dipole on the surface. Such induced dipole that oscillates in-phase with the electric field of the incident light causes a strong absorption of light at specific wavelengths[95]. For sub-50nm spherical GNPs, this absorption occurs near the wavelengths of blue and green colors, and reflection occurs with the wavelength of a red color (Figure 1.9B). Hence, a solution of small spherical GNPs is a red color as opposed to a bulk scale gold that presents a yellow color. The oscillation frequency or the absorption wavelength depends on the electron density, the effective mass of the electron, and the charge distribution, which can all be influenced by the size, shape and surface chemistry of the particles[94]. As the size of GNPs increases, the absorption peak becomes shifted to a longer wavelength (Figure 1.9B). As opposed to spherical GNPs that have a single absorption peak, gold nanorods have two absorption peaks: one in the visible range that corresponds to the transverse plasmon, and another in the near infrared range, which corresponds to the longitudinal plasmon[63,96] (Figure 1.9C). The inter-particle spacing also affects the absorption profile of GNPs. When the inter-particle distance becomes smaller than the diameter of GNPs, the solution color changes from red to purple or blue depending on the extent of aggregation due to the coupling of surface plasmons that shifts the absorbance peak to a longer wavelength (Figure 1.9D)[97].

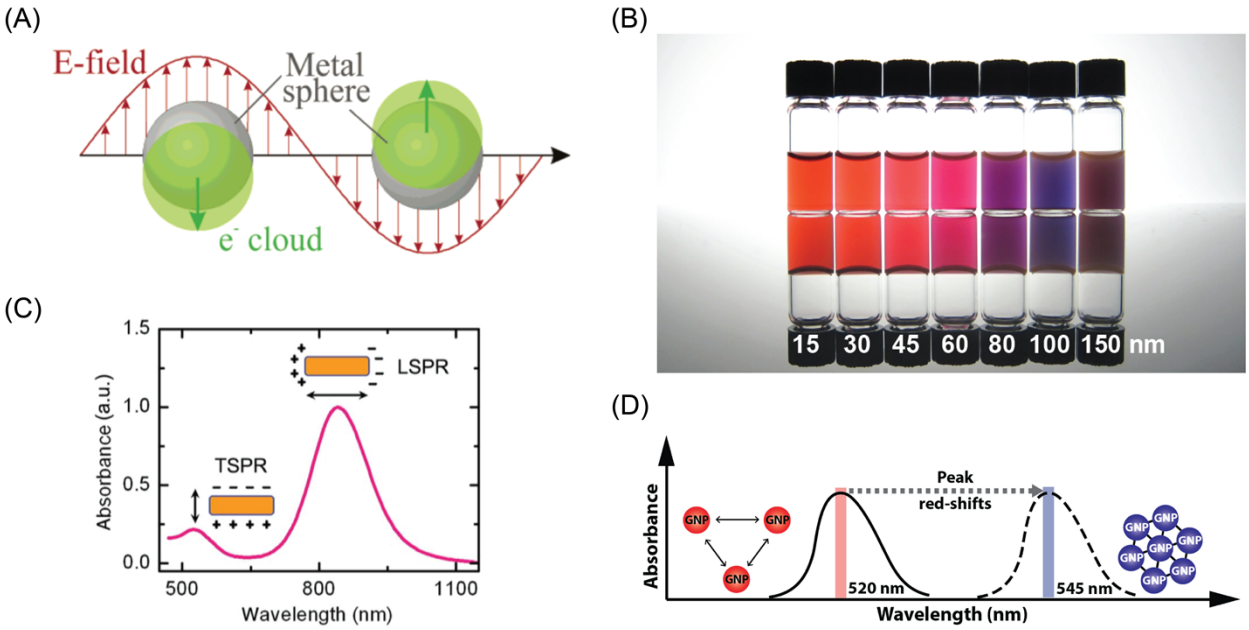

Figure 1.9: The effect of Size, Shape and Inter-particle Spacing on Optical Properties of GNPs. (A) Surface plasmon resonance of spherical GNPs showing the synchronized oscillation of conduction band electrons relative to the electric field of incident light. Figure adapted with permission from source[94]. Copyright (2003) American Chemical Society. (B) Size-dependent optical property of GNPs. As the diameter increases (15 to 150nm), the peak absorbance wavelength shifts to a longer wavelength, resulting in a darker solution color. Image courtesy of Abdullah Muhammed Syed. (C) Absorption profile of gold nanorods with two distinct peaks that correspond to transverse and longitudinal plasmons. Figure adapted with permission from source[98]. Copyright (2013) Chinese Laser Press. (D) Coupling of surface plasmons. Aggregation of GNPs shifts the absorption peak to a longer wavelength. Image courtesy of Kyryl Zagorovsky.

These optical properties of GNPs have been extensively used in the development of various *in vitro* diagnostics. Scanometric DNA array detection method has been developed using GNPs modified with oligonucleotides, which first label the target DNA with GNPs rather than fluorescent probes, followed by the reduction of silver ions at the surface of GNPs for the final readout[99]. This scanometric technique has also been incorporated in the bio-barcode assay for ultrasensitive detection of both DNA and proteins with unprecedented LODs[57,100-102]. In the bio-barcode assay, the analyte crosslinks magnetic microparticles with GNPs that are functionalized with barcode DNA, followed by the magnetic separation and dehybridization or desorption of barcode DNA. The released barcode DNA can then be detected using the scanometric method. Despite the high sensitivity of bio-barcode assay (500 zM for DNA[57] and 30 aM for proteins[101]), this assay is not well-suited for POC testing because it is time-consuming (~6 hours) and requires multiple steps.

Alternatively, a much simpler approach has been demonstrated by integrating the plasmon coupling of GNPs with multicomponent nucleic acid enzyme (MNAzyme) signal amplification strategy[103,104]. This system consists of a set of GNPs aggregated by intact linker DNA, and MNAzyme components that are activated in the presence of target DNA to cleave the linker DNA, re-distributing GNPs to a monodispersed state. The switch of GNPs from aggregated to monodispersed state shifts the absorbance peak to a shorter wavelength, and correspondingly alters the solution color from dark purple to red (Figure 1.10). Hence, MNAzyme-GNP assay can provide a simple and fast colorimetric detection of genetic targets for POC diagnosis of infectious pathogens; however, there is still a need for an additional signal amplification strategy to detect pathogens that are particularly presented at low concentrations.

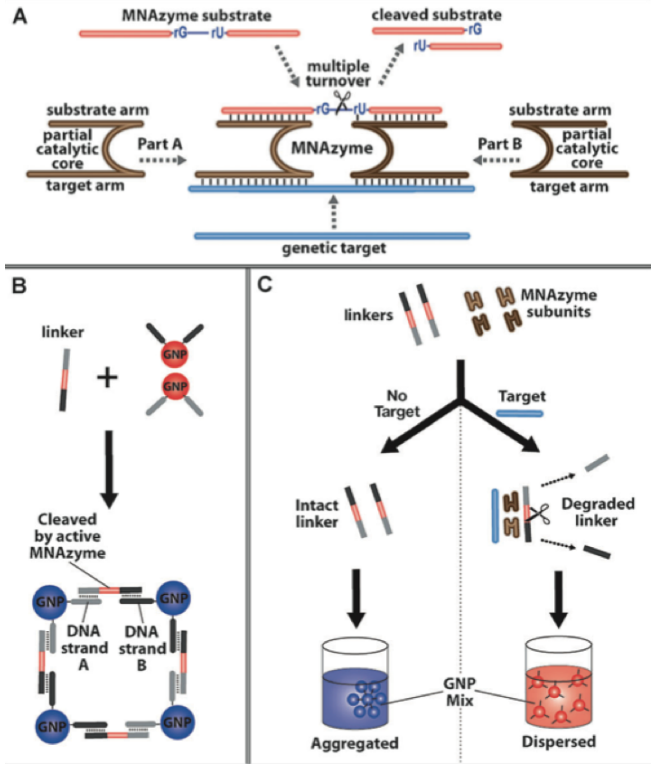

Figure 1.10: MNAzyme-GNP Assay. (A) Presence of target DNA activates catalytic activity of MNAzyme, which cleaves linker DNA. (B) Intact linker DNA crosslinks GNPs, inducing aggregation of particles. (C) In the absence of target DNA, linker DNA stay intact and induce the aggregation of GNPs resulting in a purple solution color. In the presence of target DNA, degraded linker prevents the formation of GNP aggregates, resulting in a red solution color. Figure adapted with permission from source[104]. Copyright (2013) Wiley-VCH Verlag GmbH & Co. KGaA.

1.4.4 Current Challenge of Nanodiagnostics for POC Testing

There are three main developmental stages that an emerging diagnostic technology need to experience prior to its implementation in a POC setting. The first stage is the pre-clinical testing phase, which involves characterization of analytical performance by measuring LOD and linear dynamic range using synthetic targets or spiked samples. These metrics are evaluated by first serially diluting analytes, and measuring signals at each concentration to plot a sensitivity curve. LOD is defined as three standard deviations above the mean background signal, and linear dynamic range corresponds to the concentration range at which the signal responds linearly to change in concentrations[105]. Once these pre-clinical parameters are assessed, the next step is to conduct a clinical testing using patient samples. This step involves evaluating clinical parameters such as sensitivity, specificity, predictive values, likelihood ratios, and receiver operating characteristics to assess the diagnostic performance[105]. Lastly, completion of clinical testing should lead to a field testing, where the diagnostic device is moved away from a laboratory bench, and tested in various POC settings to assess the overall diagnostic performance within the operational context.

Many of the reported nanodiagnostics have been limited to developments at the pre-clinical stage because their analytical sensitivities are low, and cannot detect pathogens that carry low number of analytes. For example, LOD of QD barcode and MNAzyme-GNP assays has been reported to be ~10^9 nucleic acid copies/reaction, which needs to be significantly improved for diagnosis of many diseases (*e.g.* HBV, HIV, and HCV) that demand much lower LOD[79,104,106]. Hence, there is a need for an amplification strategy that can substantially improve LOD of nanoparticle-based molecular assays, and allow diagnosis of patient samples for clinical testing.

1.5 Isothermal Nucleic Acid Amplification for POC Diagnostics

PCR remains as the most popular method for detecting a trace amount of nucleic acids, despite its disadvantage of requiring a bulky and expensive thermocycler, which limits its application in POC settings. To circumvent the drawbacks of PCR, alternative techniques have been developed to amplify nucleic acids at a constant temperature without the thermocycling step. This section will review isothermal nucleic acid amplification techniques that are frequently used in the development of POC diagnostics. These techniques include Rolling Circle Amplification (RCA), Strand Displacement Amplification (SDA), Loop Mediated Isothermal Amplification (LAMP), Helicase Dependent Amplification (HDA), and Recombinase Polymerase Amplification (RPA).

1.5.1 Rolling Circle Amplification

RCA involves using a circular template DNA to generate a long ssDNA of repetitive target sequences. In a linear RCA, a single DNA primer binds to the circularized target DNA, and a specialized DNA polymerase replicates the circular template DNA generating a long strand of ssDNA containing tandem repeats (Figure 1.11)[107,108]. This RCA process can be monitored in a real-time fashion using either molecular beacons, molecular zippers, or fluorescent DNA intercalating dyes[107]. Also, the resulting products can be detected by hybridization with fluorophore labeled complementary oligonucleotides[107]. Linear RCA is conducted at 37 °C, and can achieve 10^3 times amplification in 1 hour. Exponential amplification techniques have also been derived from RCA including hyperbranched RCA (HRCA) and primer-generating RCA (PG-RCA). In HRCA, the tandem repeats of long ssDNA generated from RCA contains binding sites for the reverse primers, which get extended by DNA polymerase. This reverse primer extension generates new binding sites for the forward primers in the displaced DNA strands, and also produces discrete dsDNA products containing one or more repeats[109]. HRCA has been reported to produce more than 10^9 copies in 90 minutes at 60 °C[108]. In PG-RCA, exogenous primers are not required because the target DNA can act as the primer upon binding to a circular template containing a nicking site[108]. Thus, the nicking of the target DNA by endonuclease generates many primers, which trigger further RCA and nicking processes, and exponential accumulation of target products. PG-RCA has been reported to detect as low as 60 copies of genomic DNA in 1-3 hours at 60 °C[108].

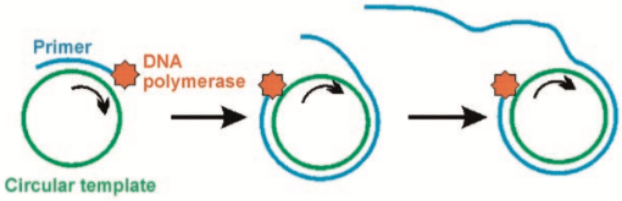

Figure 1.11: Linear RCA. Primer hybridizes to a circular template, followed by a polymerase extension generating a long strand of ssDNA containing tandem repeat sequences of template DNA. Figure adapted with permission from source[107]. Copyright (2008) Wiley-VCH Verlag GmbH & Co. KGaA.

1.5.2 Strand Displacement Amplification

SDA works based on a repeated nicking, polymerization and displacement reactions, which are catalyzed by endonuclease and exonuclease-deficient DNA polymerase[110] (Figure 1.12). The target DNA is first denatured thermally followed by the hybridization with SDA primers that form 5'-overhangs. These 5'-overhang regions from SDA primers contain DNA sequences that are recognized by the nicking endonuclease. The polymerase extension in the 3' direction generates a fully dsDNA, which gets nicked by the endonuclease at the recognition site. The nicking produces new 3'-ends, which are extended by the exonuclease-deficient DNA polymerase, displacing the downstream strand. This cycle continues, where the nicking leads to extension/displacement, and newly extended strand initiates another nicking reaction, resulting in the exponential accumulation of target nucleic acid sequences. SDA has been reported to provide 10^7-fold amplification in 2 hours at 37 °C[108]. Although the amplification step in SDA is performed at a constant temperature of 37 °C, it still requires denaturation of target dsDNA at 95 °C prior to the amplification, which adds complexity in the development of POC diagnostics.

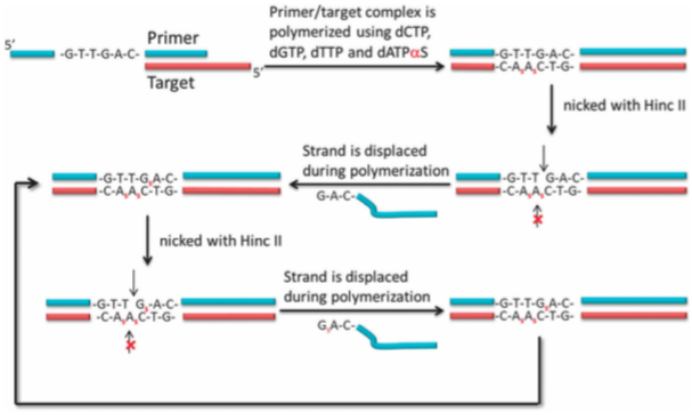

Figure 1.12: SDA. 5'-overhang from the primer contains a DNA sequence that is recognized by endonuclease. Polymerase extension generates a fully dsDNA, which gets nicked by endonuclease followed by DNA polymerase extension and displacement of downstream strand. Figure adapted with permission from source[111]. Copyright (2014) The Royal Society of Chemistry.

1.5.3 Loop Mediated Isothermal Amplification

LAMP reaction is catalyzed by DNA polymerase with strong strand displacement activity, and specially designed inner and outer primers. There are four primers involved in a LAMP reaction including the forward inner primer (FIP), backward inner primer (BIP), and two outer primers (F3 and B3) to recognize 6 distinct sites in the target DNA[108,112,113] (Figure 1.13A). The first stage of LAMP is the starting structure-producing step, which uses all four primers to produce a dumb-bell shaped DNA structure (Figure 1.13B). This DNA structure gets converted to a stem-loop DNA by self-primed DNA synthesis, and serves as the starting material for the second stage of LAMP. The second stage of LAMP is the cycling amplification step, which starts with the hybridization of an inner primer on the loop of the stem-loop DNA structure, followed by strand displacement DNA synthesis (Figure 1.13C). The final products are a mixture of stem-loop DNA of different stem lengths and number of loops consisting of alternately inverted repeats of the target sequence. LAMP can enrich a few DNA copies to 10^9 copies in less than 1 hour at 60-65 °C[108,113]. Since LAMP uses four primers in the first stage to recognize 6 distinct sequences, and two primers in the subsequent steps to recognize 4 distinct sequences, it provides high specificity and selectivity during the amplification process. However, it is difficult to design LAMP primers, and consequently, there is less degree of freedom in the selection of target sequences.

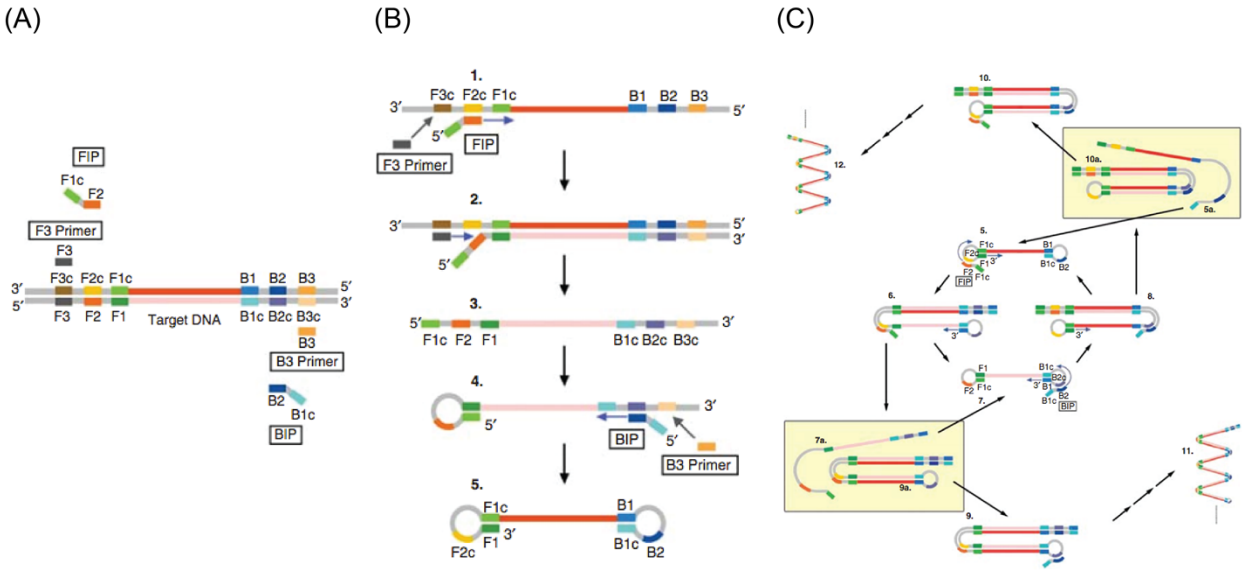

Figure 1.13: LAMP. (A) LAMP primers that recognize 6 distinct sites. (B) First stage of LAMP produces the dumb-bell shaped DNA structure, which serves as the starting material for the second stage of LAMP. (C) Second stage of LAMP produces stem-loop DNA products that contain alternately inverted repeats of the target sequence. Figure adapted with permission from source[112]. Copyright (2012) Nature America, Inc.

1.5.4 Helicase Dependent Amplification

HDA closely resembles the DNA replication process of living organisms, and follows a three-step cycle involving template separation, primer hybridization, and primer extension steps. Initially, DNA helicase is used to enzymatically unwind dsDNA and generate ssDNA templates, which become stabilized by single-stranded DNA binding proteins. Subsequently, primers bind to ssDNA templates, and get extended by DNA polymerase (Figure 1.14). This cycle repeats to achieve over a million times amplification in 0.5-2 hours at 37-65 °C[108,114,115]. Since the helicase activity allows separation of dsDNA, the initial heat denaturation and successive thermocycling steps can be removed. Also, HDA can amplify long DNA target sequences (kilobase regions), which was not possible with previously mentioned isothermal techniques.

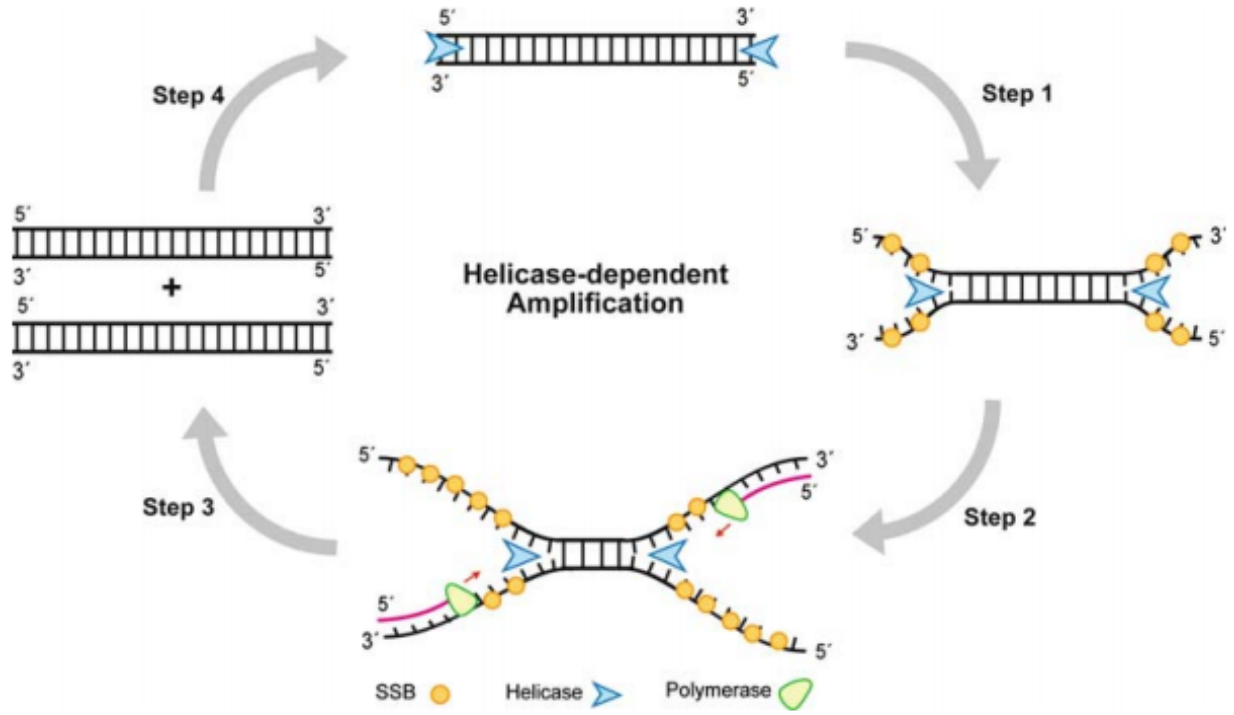

Figure 1.14: HDA. Helicase unwinds dsDNA, followed by primer binding and polymerase extension. Figure adapted with permission from source[115]. Copyright (2009) Birkihäuser Verlag.

1.5.5 Recombinase Polymerase Amplification

RPA employs recombinase to catalyze the hybridization of primers to the template DNA without thermally separating dsDNA target. In the presence of adenosine triphosphate (ATP), recombinase proteins bind to forward and reverse primers to form nucleoprotein complexes, which then scan

along dsDNA template to facilitate the strand-exchange at the homologous sequences, forming D-loop structures[116] (Figure 1.15). Single-stranded DNA binding proteins then bind to the displaced strand of template DNA and stabilize the resulting structure. As ATP gets hydrolyzed, nucleoprotein complex disassembles, and polymerase binds to 3'-end of primers. The polymerase adds deoxynucleotide triphosphates (dNTPs) to 3'-end of primers to synthesize DNA sequence that is complementary to template DNA. This process is repeated to achieve an exponential amplification, and has been demonstrated to accumulate millions of DNA copies in 40 minutes at 37-42 °C[108,116].

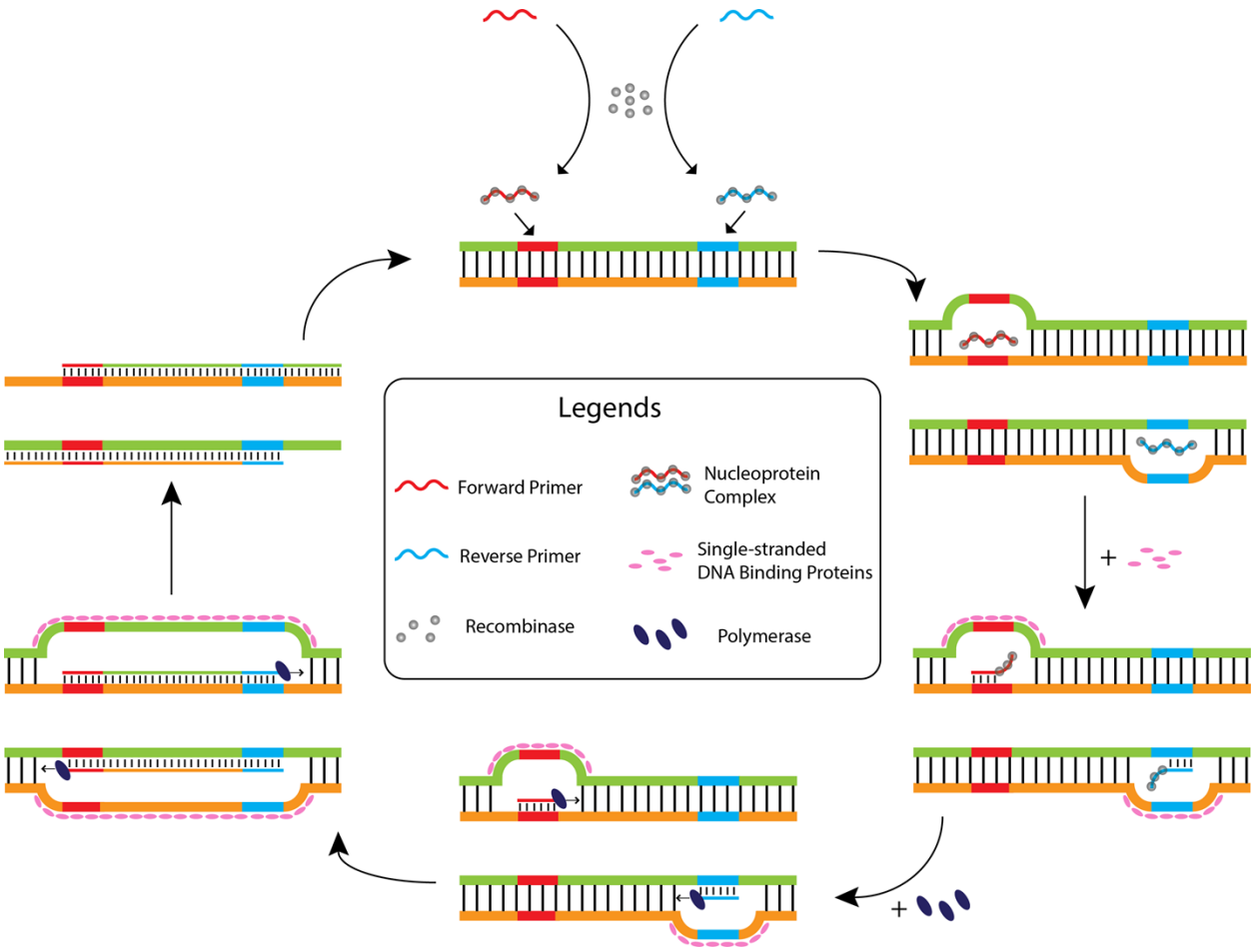

Figure 1.15: RPA. Recombinase proteins bind with a primer to form a nucleoprotein complex, which facilitates strand-exchange at the homologous sequence, where the primer hybridizes with template DNA. Primers are extended in the 3'-direction by polymerase. Figure recreated with permission from source[116]. Copyright (2006) Piepenburg et al.

1.5.6 Summary of Isothermal Nucleic Acid Amplification Techniques

A summary of isothermal nucleic acid amplification techniques is presented in Table 1.1. Although RCA is a good candidate for the amplification of circular DNA molecules such as plasmids and particular viral genomes, linear DNA molecules must be circularized *via* padlock probes prior to the amplification, which demands procedural complexity and additional enzymes[117]. Hence, RCA may not be the most suitable amplification strategy where the procedural simplicity of a diagnostic device is favored. Some of the isothermal techniques have not made significant expansion in POC markets yet mainly due to the difficulty in establishing an initial thermal or chemical denaturation step prior to the isothermal phase (*e.g.* SDA and LAMP)[118]. LAMP performance is also highly determined by the complex design of multiple primers, which has been cited as a reason for not using LAMP by many researchers[119]. Taking these limitations into account, HDA and RPA stand out to be better isothermal amplification strategies in the development of highly sensitive POC diagnostics. They require only one set of primers, the entire amplification can be performed at a low constant temperature without requiring the initial thermal denaturation step, and can achieve LOD that is comparable to conventional PCR. Out of the two techniques, RPA was used throughout this thesis due to its faster reaction time compared to HDA.

Table 1.1: Summary of Isothermal Nucleic Acid Amplification Techniques[108,117]

Method	Required Enzymes	Primers	Temperature (°C)	Time (hour)	LOD (copies)
RCA	HRCA: • ligase • DNA polymerase PG-RCA: • Nicking endonuclease • DNA polymerase	HRCA: • 2 PG-RCA: • 0	60	HRCA: • 1.5 PG-RCA: • 1-3	HRCA: • Not available PG-RCA: • 60
SDA	• Nicking endonuclease • DNA polymerase	2 or 4	37	2	10
LAMP	• DNA polymerase	4	60-65	<1	5
HDA	• Helicase • DNA polymerase	2	37-65	0.5-2	1
RPA	• Recombinase • DNA polymerase	2	37-42	0.5-1.5	1

1.6 Thesis Overview

This thesis is focused on addressing the limitations of conventional POC or laboratory-based diagnostic approaches by developing ultrasensitive nanodiagnostics and clinically validating them for POC application. The sensitivity of two nanoparticle-based molecular assays is improved with the the incorporation of an isothermal nucleic acid amplification strategy, RPA. Isothermal nucleic acid amplification eliminates the temperature cycling step involved in a PCR reaction, which makes it a better strategy to enhance the analytical sensitivity of an assay in a POC testing. Nanoparticles offer unique optical properties that are also attractive in the development of POC diagnostic systems. In **Chapters 2** and **3**, QD barcode assay integrated with RPA was investigated to demonstrate an ultrasensitive fluorescent-based diagnostic platform, which has the multiplexing capability to simultaneously detect different genetic biomarkers. MNAzyme-GNP assay combined with RPA was studied in **Chapters 4** and **5** to demonstrate an ultrasensitive colorimetric-based diagnostic platform, which does not require signal readout devices to interpret diagnostic results. The combination of the advantages that are offered by nanotechnology and isothermal nucleic acid amplification strategy is proposed to bridge the research gap that currently exists in the field of infectious disease diagnostics by offering a highly sensitive and specific diagnostic device that is feasible for testing in a resource-limited setting (Figure 1.16).

Chapter 1 introduced the prevalence of infectious diseases, current diagnostic methods and their limitations, the spectrum of POC diagnostics, and benefits and limitations of nanotechnology and isothermal nucleic acid amplification in the development of a POC diagnostic system.

Chapter 2 discusses the development of an ultrasensitive QD barcode system by integrating RPA with the assay. A pre-clinical study is conducted to evaluate the detection of HIV and HBV patient samples, and demonstrate multiplexed detection of two diseases. Additionally, the use a smartphone optical device is demonstrated for the measurement of QD barcode fluorescent signals.

Chapter 3 describes a full clinical validation of QD barcode technology for diagnosing patients infected with HBV by evaluating clinical sensitivity, specificity and Receiver Operating Characteristics (ROC). The improvement in the clinical sensitivity is also demonstrated by detecting multiple regions of the viral genome.

Chapter 4 explains the development of an ultrasensitive MNAzyme-GNP assay by incorporating RPA with the assay. The analytical sensitivity of the assay is compared with and without RPA. HBV and InfA infected patient samples were tested to assess clinical sensitivity and specificity levels.

Chapter 5 demonstrates screening genetic biomarkers of antibiotic resistance using MNAzyme-GNP assay combined with RPA. The analytical sensitivity of the assay is compared with and without the incorporation of RPA, the cross-reactivity is investigated for detection of multi-drug resistance, and three clinical isolates were screened to demonstrate the feasibility of this technique.

Chapter 6 concludes the thesis with a summary of studies presented in preceding chapters, and provides suggestions for future work.

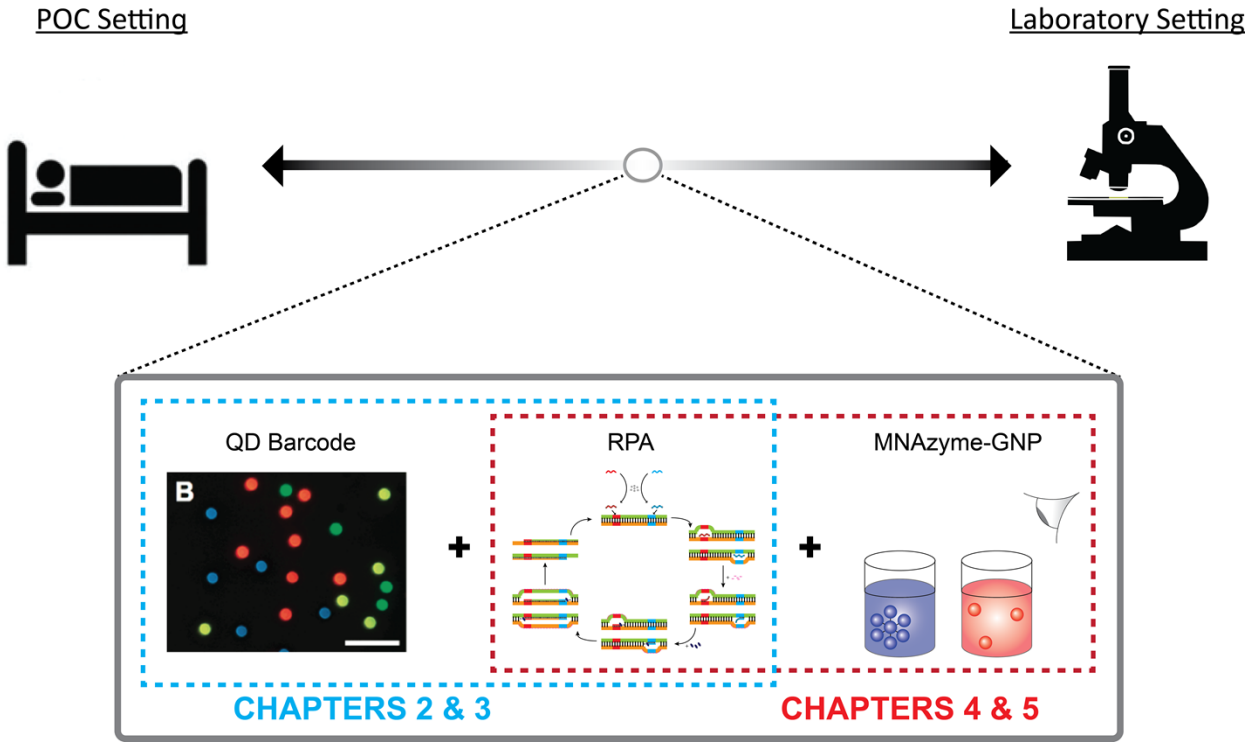

Figure 1.16: Thesis Overview. RPA integrated with QD barcode based fluorescent diagnostic platform is investigated in Chapters 2 and 3. RPA integrated with MNAzyme-GNP based colorimetric diagnostic platform is studied in Chapters 4 and 5. Two diagnostic approaches are proposed to provide high diagnostic sensitivity while being suitable for testing in POC settings, addressing the limitations of conventional diagnostic methods. QD barcode image is adapted with permission from source[78].

1.7 Author Contributions

The work presented in this thesis is conceived, designed, executed, analyzed and written by Jisung Kim and designated co-authors.

Chapter 1: Introduction. Jisung Kim performed the literature review and wrote the chapter. Warren C. W. Chan proofread and edited the chapter.

Chapter 2: Development of QD Barcode-based Isothermal Amplification Assay. Jisung Kim, Kevin Ming, and Warren C. W. Chan conceived the idea and designed the study. Jisung Kim performed RPA, QD barcode conjugation, on-chip sensitivity assays, solution-based singleplexed and multiplexed assays with clinical samples, and flow cytometry. Kevin Ming designed and constructed the smartphone device, developed MATLAB script, compared between organic dyes and QD barcodes, performed on-chip singleplexed and multiplexed assays with clinical samples. Jisung Kim and Kevin Ming analyzed the data. Mia J. Biondi, Jordan J. Feld, and Mario Ostrowski extracted and prepared HBV and HIV samples. Abdullah Syed validated QD barcode conjugation. Albert Lam synthesized QD barcodes. This chapter is adapted from the following publication.

- K. Ming[†], **J. Kim**[†], M. J. Biondi, A. Syed, K. Chen, A. Lam, M. Ostrowski, A. Rebbapragada, J. J. Feld, and W. C. W. Chan, "Integrated Quantum Dot Barcode Smartphone Optical Device for Wireless Multiplexed Diagnosis of Infected Patients," *ACS Nano*, vol. 9, no. 3, pp. 3060–3074, Mar. 2015. ([†]These authors contributed equally).

Chapter 3: Clinical Validation of QD Barcode-based Isothermal Amplification Assay. Jisung Kim and Warren C. W. Chan conceived the idea and designed the study. Jisung Kim performed QD barcodes synthesis, capture probe conjugation, RPA, singleplexed and multiplexed assays, flow cytometry, and data analysis. Mia J. Biondi completed HBV sequence analysis, designed target regions, selected diverse patient samples, collected patient data, completed viral extraction, and performed PCR. Jordan J. Feld provided clinical samples and was involved in the experimental design. This chapter is adapted from the following publication.

- **J. Kim**, M. J. Biondi, J. J. Feld, and W. C. W. Chan, "Clinical Validation of Quantum Dot Barcode Diagnostic Technology," *ACS Nano*, vol. 10, no. 4, pp. 4742–4753, Apr. 2016.

Chapter 4: Development of Colorimetric Amplification System for Clinical Diagnosis of Viral Infections. Jisung Kim, Mohamed A. A. Mohamed, Kyryl Zagorovsky and Warren C. W. Chan conceived the idea and designed the study. Jisung Kim performed RPA and rt-RPA, post-

RPA purification, gel electrophoresis, denaturation and blocking of amplicons, quantification of RPA and rt-RPA products. Mohamed A. A. Mohamed conducted denaturation and blocking of amplicons, MNAzyme-GNP assay, and peak absorbance measurement. Kyryl Zagorovsky performed synthesis and conjugation of GNPs and conducted MNAzyme-GNP assay. Jordan J. Feld and S. Mubareka provided DNA and RNA samples from clinical specimens. This chapter is adapted from the following manuscript currently under preparation.

- **J. Kim**[†], M. A. A. Mohamed[†], K. Zagorovsky, J. J. Feld, S. Mubareka, W. C. W. Chan, "Colorimetric Amplification System for Clinical Diagnosis of Viral Infections," *Manuscript in preparation.* ([†]These authors contributed equally).

Chapter 5: Screening Genetic Biomarkers of Antibiotic Resistance using Colorimetric Amplification System. Jisung Kim, Mohamed A. A. Mohamed, and Warren C. W. Chan conceived the idea and designed the study. Jisung Kim conducted RPA, post-RPA purification, gel electrophoresis, denaturation and blocking of amplicons, and optimization of multiplexed RPA. Mohamed A. A. Mohamed designed antibiotic resistance genes, extracted DNA from bacteria, performed MNAzyme-GNP assay, measured peak absorbance, optimized multiplexed RPA, and conducted antimicrobial susceptibility test. Kyryl Zagorovsky synthesized and functionalized GNPs, and performed PCR. This chapter is adapted from the following manuscript currently under preparation.

- M. A. A. Mohamed[†], **J. Kim**[†], K. Zagorovsky, W. C. W. Chan, "Colorimetric screening of antibiotic resistance using nucleic acid enzymes and gold nanoparticles," *Manuscript in preparation.* ([†]These authors contributed equally).

Chapter 6: Conclusions and Future Directions. Jisung Kim performed the literature review and wrote the chapter. Warren C. W. Chan proofread and edited the chapter.

Chapter 2: Development of QD Barcode-based Isothermal Amplification Assay

2.1 Introduction

QD barcodes are an ideal candidate for development of a POC diagnostic system due to their multiplexing capability, which can substantially reduce the amount of labor and operational time, and provide high-throughput screening of infectious pathogens[79,82,120]. QDs provide advantages over traditional organic fluorophores for barcoding because they are brighter, have narrower emission and wider absorption spectra, and are more resistant to photobleaching (Figure 2.1)[68,70,121]. Previously, 105 spectrally distinct QD barcodes were synthesized via CCFF method[82], and detection of several genomic and proteomic infectious disease biomarkers was demonstrated[78,79]. Detection occurred *via* forming a sandwich structure between surface-coated biorecognition molecule, target analyte of interest (*e.g.* antigen or DNA molecule), and fluorescently labeled detection probe. The barcode and detection probe signals then determined the identity and presence of the target molecule respectively. In addition, recent advancements in microfluidic technologies as well as the miniaturization of flow cytometry have generated greater opportunities to push the barcoding technology one step closer to POC application by automating multiple steps of the assay procedure, and detecting fluorescent signals using a portable readout device[93,122-124].

However, the LOD of current QD barcode assay needs to be significantly improved to detect clinically relevant concentrations of many pathogens. The detection limit of present QD barcode assay is only in the picomolar range (~5 pM or $3x10^9$ copies/mL)[79], which is not sufficient to diagnose pathogens that are presented at much lower concentrations, but still require clinical interventions. For instance, HBV infection is characterized with the initiation of an antiviral treatment if the viremia level exceeds 2000 IU/mL (or 10^4 copies/mL) by the international treatment guidelines[15]. Hence, the LOD of QD barcode assay needs to be improved by at least 6-orders of magnitude to diagnose HBV infections at clinically relevant concentration levels.

In this chapter, QD barcode-based isothermal amplification assay is developed by integrating QD barcode assay with an isothermal nucleic acid amplification strategy, RPA, to improve the analytical sensitivity of the assay. RPA was chosen to amplify the assay signal due to its

procedural simplicity requiring only one set of primers and no initial thermal denaturation step, high sensitivity that is comparable to PCR, and fast reaction time taking only 30 minutes. Synthetic DNA targets were first used to investigate the analytical sensitivity and specificity of the assay with the incorporation of RPA. This was followed by a pre-clinical assessment including singleplexed screening of samples collected from HBV and HIV infected patients, and multiplexed detection of the HBV/HIV co-infection model. Lastly, the use of an in-house built smartphone optical device was demonstrated to measure the fluorescent signals from QD barcodes. Such integration of a smartphone optical device with a multiplexing molecular assay and isothermal amplification is proposed to permit clinical diagnosis in the absence of a large laboratory infrastructure, and provide a wireless transmission of diagnostic results for interpretation, mapping, surveillance and prediction of infectious diseases globally.

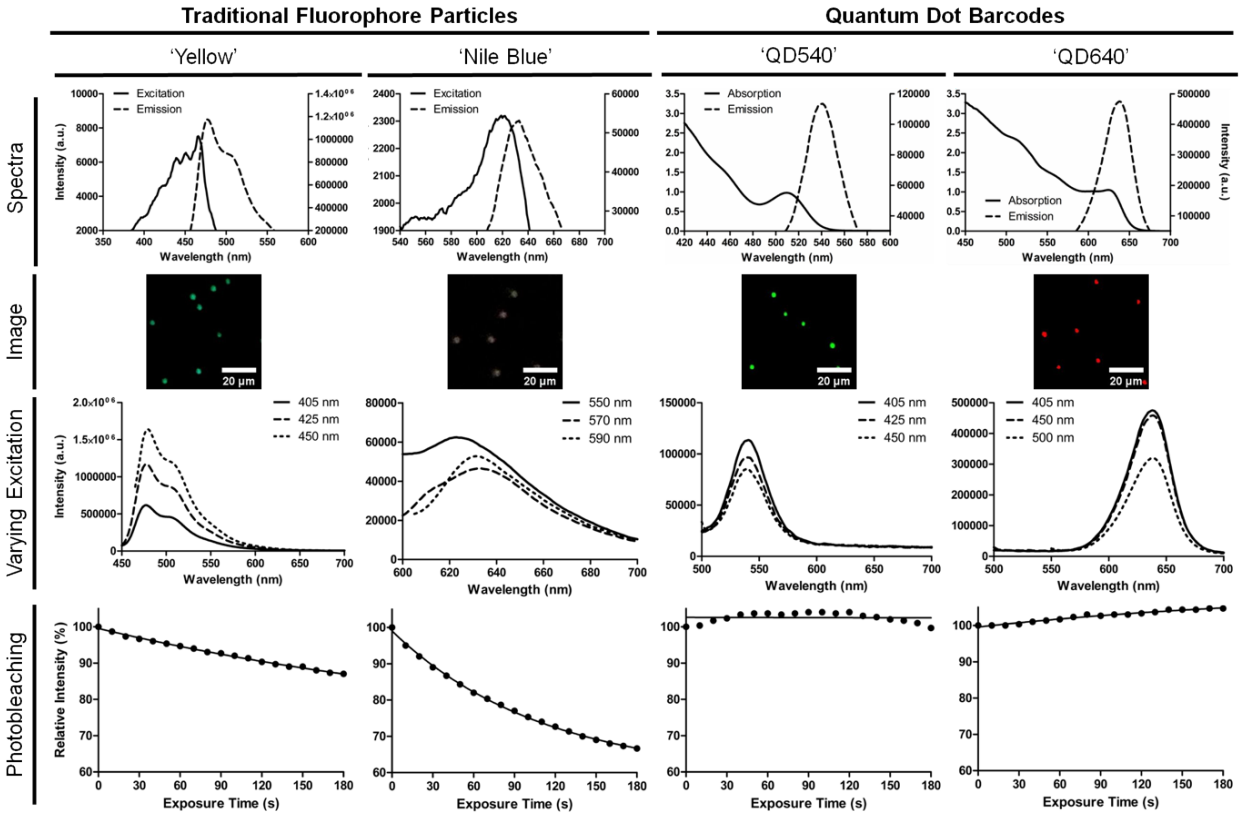

Figure 2.1: Comparison of optical properties between organic dyes and QDs inside polystyrene microbeads. Polymeric particles impregnated with organic fluorophores ("Yellow" and "Nile Blue") are compared with QD barcodes ("QD540" and "QD640"): excitation/absorption and emission spectra; visual images captured by a smartphone optical device when excited using a 405 nm laser excitation source; emission spectra under varying excitation wavelengths; and photobleaching under continuous excitation in the smartphone device, representing the average intensities of 591, 642, 1198, and 1145 barcodes analyzed, over the 180s duration, for "Yellow", "Nile Blue", "QD540", and "QD640", respectively.

2.2 Experimental Methods

2.2.1 QD Synthesis

QDs (CdSeS alloyed-ZnS capped) of peak emission wavelength 540 nm ("QD540") were purchased from CytoDiagnostics and used as instructed. QDs of peak emission wavelengths 515 nm ("QD515"), 547 nm ("QD547"), 560 nm ("QD560"), 589 nm ("QD589"), 596 nm ("QD596"), 615 nm ("QD615"), and 640 nm ("QD640") were synthesized and characterized according to published procedures[125,126] and stored in chloroform at room temperature until later use.

2.2.2 QD Barcode Synthesis

QD barcodes were prepared by mixing together the QDs (QD515, QD540, QD547, QD560, QD589, QD596, QD615 and QD640) in different ratios with a polymer-based solution (Table 2.1 and Table 2.2). The polymer solution consisted of poly(styrene-co-maleic anhydride) (32%, cumene terminated) from Sigma-Aldrich dissolved in chloroform, with the polymer concentration at 4-wt%. The resultant QD polymer solution was then introduced into a nozzle system from Ingeniatrics using a syringe pump from Harvard Apparatus at a rate of 0.9 mL/hour, as well as double-distilled (DD) water as the focusing fluid at a rate of 180 mL/hour. The nozzle system was then submerged inside a beaker partially filled with DD water. The polymeric barcode microbeads were synthesized *in situ*, and the microbeads formed a colloidal suspension in the water. After synthesis, the valve was closed and the microbeads were stabilized by overnight stirring and then collected. The microbeads were filtered using 35 μm BD Falcon nylon mesh strainer cap, and characterized using an automated Beckman Coulter Vi-Cell counter, and stored in DD water at 4 °C until later use. The QD concentrations required for preparing the barcodes are presented in Table 2.1 and Table 2.2. The barcode images and corresponding spectra along with a list of capture probe, target and secondary probe DNA sequences are summarized in Table 2.3.

Table 2.1: List of QD Barcodes Synthesized for the Synthetic Samples

Barcode	Diameter (μm)	QD540 Concentration (μL/mL)	QD589 Concentration (μL/mL)	QD640 Concentration (μL/mL)
B_H1N1	2.70 ± 1.61	60		
B_H3N2	2.70 ± 1.36		57	
B_HCV	2.70 ± 1.60	60	11.4	
B_FluB	2.70 ± 1.60	12	57	
B_HIV	2.70 ± 1.34		57	182
B_HBV	3.50 ± 1.19			910
B_H5N1	2.70 ± 1.51			182

Table 2.2: List of QD Barcodes Synthesized for the Clinical Samples

Barcode*	Diameter (µm)	QD515 Concentration (µL/mL)	QD547 Concentration (µL/mL)	QD560 Concentration (µL/mL)	QD596 Concentration (µL/mL)	QD615 Concentration (µL/mL)
CB_HIV	3.5 ± 1.66			5	5	5
CB_HBV	3.5 ± 0.96		200			
CB_Pos	3.5 ± 1.02			50		
CB_Neg	3.5 ± 0.81	100				

*All microbeads were encoded with 150 µL of 7nm FeO Magnetic Nanoparticles (36.5 ng/mL). The magnetic iron (II,III) oxide nanoparticles were synthesized *via* the thermal decomposition of iron triacetylacetonate[127].

Table 2.3: List of DNA Sequences and their Corresponding Barcodes

Disease/ Biomarker	Capture Probe Name/ Sequence*	Target / Amplicon Name and Sequence*	Secondary Probe Name/ Sequence*	Corresponding Barcode	Corresponding Barcode Spectrum
Influenza Hemagglutinin – Influenza Type A (H1N1)	**C_H1N1** CCC TCT TAG TTT GCA TAG TTT CCC GTT ATG	**T_H1N1** CGG CGA TGA ATA CCT AGC ACA CTT A CTA CA TAA CGG GAA ACT ATG CAA ACT AAG AGG G	**D** 5'-Alexa647-TAA GTG TGC TAG GTA TTC ATC GCC G-3'	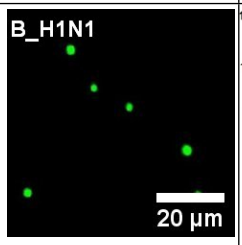	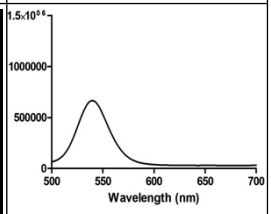
Influenza Neuraminidase – Influenza Type A (H3N2)	**C_H3N2** ACT TGG TTG TTT GGG GGG GAG TTG AAT TCA	**T_H3N2** CGG CGA TGA ATA CCT AGC ACA CTT A CTA TG AAT TCA ACT CCC CCC CAA ACA ACC AAG T		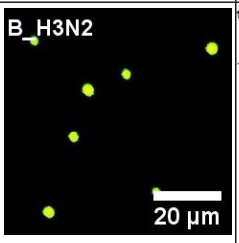	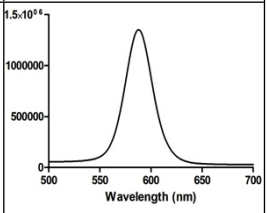
Influenza Hemagglutinin – Influenza Type A (H5N1)	**C_H5N1** CCA TTC CCT GCC ATC CTC CCT CTA TAA AAC	**T_H5N1** CGG CGA TGA ATA CCT AGC ACA CTT A CTA GT TTT ATA GAG GGA GGA TGG CAG GGA ATG G		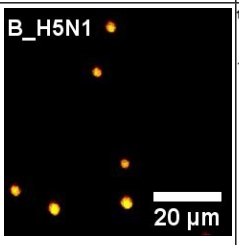	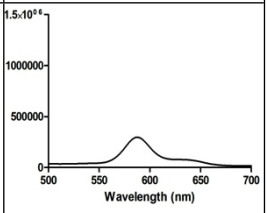
Influenza Influenza Type B	**C_FluB** CAC CGC AGT TTC AGC TGC TCG AAT TGG	**T_FluB** CGG CGA TGA ATA CCT AGC ACA CTT A CTA CC AAT TCG AGC AGC TGA AAC TGC GGT G		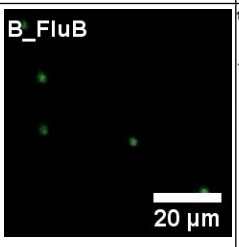	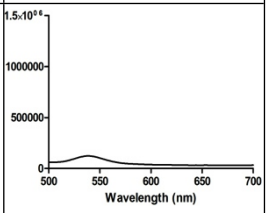

Human Immuno-deficiency Virus (HIV) SK102 HIV-1	**C_HIV** GAG ACC ATC AAT GAG GAA GCT GCA GAA TGG GAT	**T_HIV** CGG CGA TGA ATA CCT AGC ACA CTT A CTA AT CCC ATT CTG CAG CTT CCT CAT TGA TGG TCT C		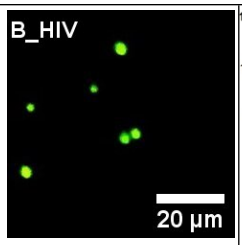	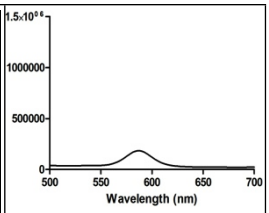
Hepatitis B (HBV) PB-2 – HBV	**C_HBV** TCA GAA GGC AAA AAA GAG AGT AAC T	**T_HBV** CGG CGA TGA ATA CCT AGC ACA CTT A CTA AG TTA CTC TCT TTT TTG CCT TCT GA		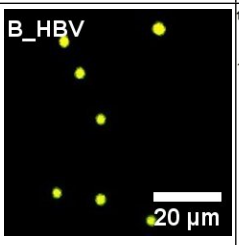	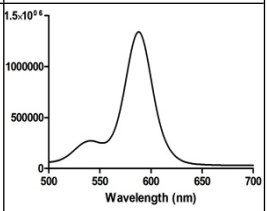
Hepatitis C (HCV) KY 150 – HCV	**C_HCV** CAT AGT GGT CTG CGG AAC CGG TGA GT	**T_HCV** CGG CGA TGA ATA CCT AGC ACA CTT A CTA AC TCA CCG GTT CCG CAG ACC ACT ATG		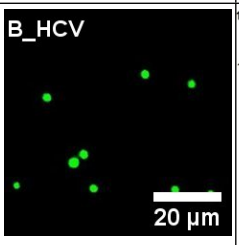	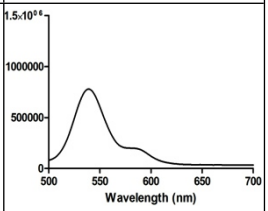
Positive Control	**C_Pos** GAC AAT GCT CAC TGA GGA TAG T	**T_Pos** CGG CGA TGA ATA CCT AGC ACA CTT A CTA AC TAT CCT CAG TGA GCA TTG TC		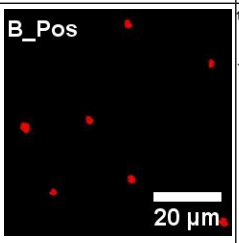	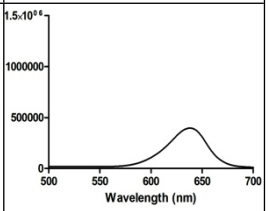
Negative Control	**C_Neg** CCA ATA TCG GCG GCC	**T_Neg** CGG CGA TGA ATA CCT AGC ACA CTT A CTA GG CCG CCG ATA TTG G		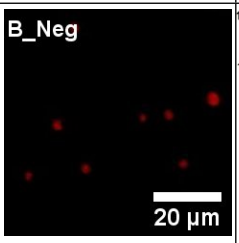	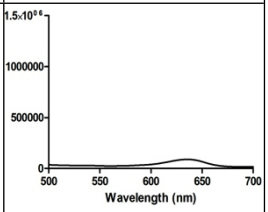
Clinical HIV Sample	**CC_HIV** GAA AGG TGA AGG GGC AGT AGT AAT ACA AGA C AAT AGT GAC ATA AAG GTA GTA CCA AGA AGA AAA GCA	**CT_HIV** TTT TTT TTT GCC ACA CAA TCA TCA CCT GCC ATC TGT TTT CCA TAA TCC CTA ATG ATC TTT GCT TTT	**CD_HIV** 5'-Alexa647-TTG GTA CTA CCT TTA TGT CAC TAT TGT CTT GTA TTA CTA CTG CCC CTT	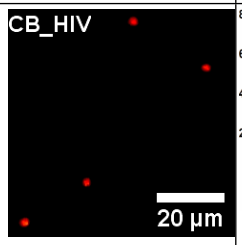	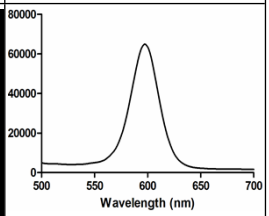

	AAG ATC ATT AGG GAT TAT GGA AAA CAG ATG GCA GGT GAT GAT TGT GTG G		CAC CTT TCC-3’		
Clinical HBV Sample	**CC_HBV** GGC ATG GAC ATT GAC CCT TAT AAA GAA TTT GGA GCT TCT GTG GAG TTA CTC TCT TTT TTG CCT TCT GAT TTC TTT CCG TCT ATT CGG GAC CTT CTC GAC A	**CT_HBV** AAA AAA AAA TGT CGA GAA GGT CCC GAA TAG ACG GAA AGA AAT CAG AAG GCA AAA AA	**CD_HBV** 5’-AAC TCC ACA GAA GCT CCA AAT TCT TTA TAA GGG TCA ATG TCC ATG CC-Alexa647-3’	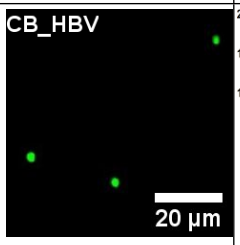	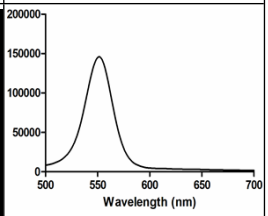
Clinical Positive Control	**CC_Pos** GAC AAT GCT CAC TGA GGA TAG T	**CT_Pos** CGG CGA TGA ATA CCT AGC ACA CTT A CTA AC TAT CCT CAG TGA GCA TTG TC		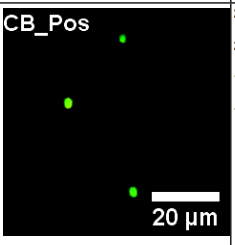	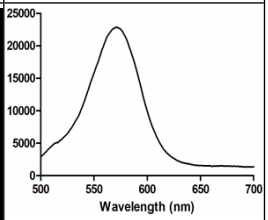
Clinical Negative Control	**CC_Neg** CCA ATA TCG GCG GCC	**CT_Neg** CGG CGA TGA ATA CCT AGC ACA CTT A CTA GG CCG CCG ATA TTG G		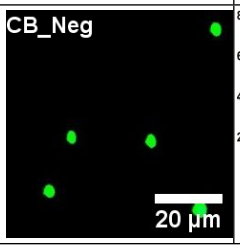	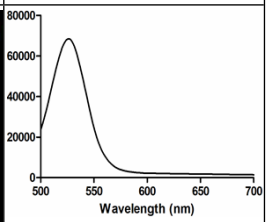

*All sequences are written from 5’ to 3’ direction.

2.2.3 QD Barcode Conjugation and Validation

For the synthetic samples, conjugation of DNA capture strands to their corresponding barcode microbeads was done through reaction with 1-ethyl-3-(3-dimethylaminopropyl) carbodiimide hydrochloride (EDC). DNA capture strands from IDT DNA Technologies, purchased HPLC-purified and used without further purification, were designed with an amine group and C12 spacer on the 5’ end. They were first prepared at a concentration of 10 pmol/µL in TE buffer and stored

at 4 °C until further use. To conjugate, EDC was first dissolved in MES buffer (pH 5, 100 mM) at a concentration of 100 mg/mL. Approximately 10^6 microbeads were mixed with 100 µL of the EDC solution, and was allowed to activate the microbead carboxyl groups for 10 minutes. Then, 2.88 µL of the DNA capture strand solution, corresponding to 28.8 pmol of DNA, was added to the microbead solution. The reaction was incubated overnight.

For the pre-clinical assessment, conjugation of DNA capture strands to their corresponding barcode microbeads was done through reaction with EDC and N-hydroxysulfosuccinimid (sulfo-NHS). DNA capture strands from Bio Basic Inc., purchased HPLC-purified and used without further purification, were designed with an amine group and C6 spacer on the 5' end. They were first prepared at a concentration of 10 pmol/µL in TE buffer and stored at 4 °C until further use. To conjugate, EDC and sulfo-NHS were dissolved in MES buffer (pH 5, 100 mM) in concentrations of 0.0192g/64µL and 0.01g/100µL, respectively. Then, approximately 10^6 microbeads were mixed with 32 µL of the EDC solution, 10 µL of the sulfo-NHS solution, 55 µL of MES buffer (pH 5, 100 mM), and 2.88 µL of the DNA capture strand solution that correspond to 28.8 pmol of DNA. The reaction was incubated overnight, at which point 0.01 g of EDC was added and the mixture was allowed to incubate for another 4 hours.

To validate the conjugation, 1 µL of DD water containing 5% Tween was added to the microbead solution, centrifuged at 3000 g for 5 minutes. Then, 50 µL of the supernatant was extracted. The same conjugation procedures described above were performed for the control cases for each barcode (*i.e.* no conjugation), except DD water was added in place of beads. In a black 96-well plate, 10 µL of the supernatants from all conjugation cases, 10 µL of the supernatants from all control cases, as well as 10 µL of four blank cases containing only DD water, were each added to individual wells. SYBR gold from Invitrogen, dissolved in DMSO, was first diluted to 0.5:10000 dilution by adding 0.5 µL of it to 10 mL of TE buffer, then 190 µL of the dilution was added to each of the sample-containing wells. All reactions were incubated at room temperature for 15 minutes before being read using a plate reader from BMG Labtech. Amount of conjugation for each barcode was then determined by comparing the fluorescence of the conjugation cases with their respective controls containing no beads. That is, lower signal indicates higher amount of conjugation. Results were converted to efficiency in percentages (Figure 2.2).

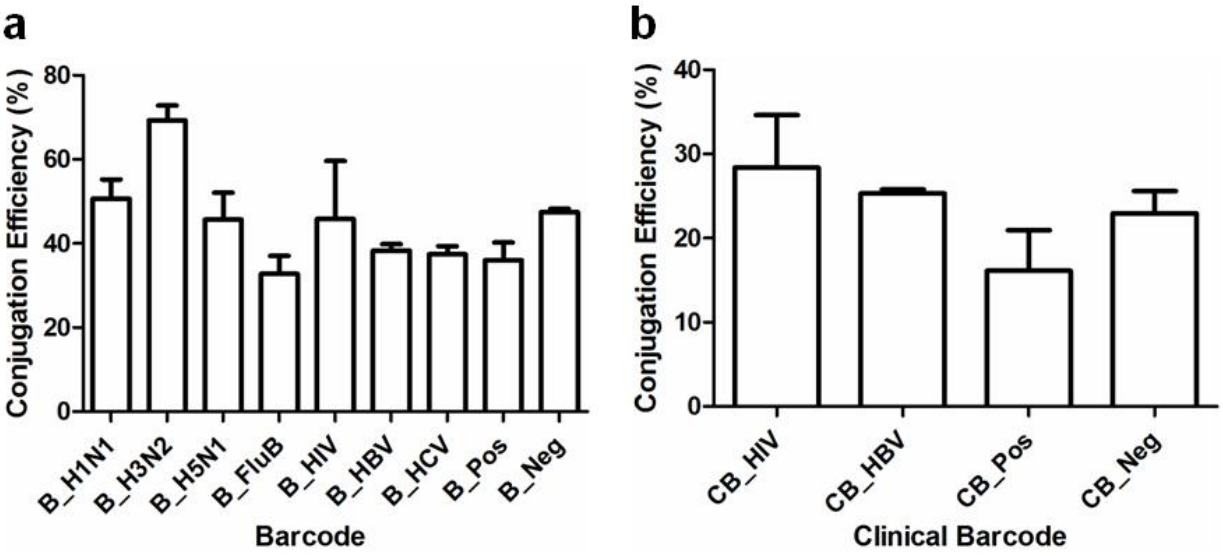

Figure 2.2: Conjugation Efficiency. Capture strand conjugation of each barcode used with (a) synthetic samples, and (b) clinical samples. Error bars were calculated as the standard deviation from two replications.

To finish the conjugation process, after the 50 µL of the supernatant was extracted for validation, the remaining supernatant was removed. Then, the conjugated microbeads were washed twice with 100 µL of DD water containing 0.05% Tween and centrifuged at 3000 g for 5 minutes to remove any non-conjugated DNA capture strands. The conjugated microbeads were then stored in 100 µL DD water containing 0.05% Tween at 4 °C until further use.

2.2.4 Excitation, Absorption, and Emission Spectra Measurement

The excitation and emission spectra of the Yellow and Nile Blue microbeads were measured using the Excitation and Emission Acquisition modes, respectively, on Horiba Jobin Yvon FluoroMax-3 fluorometer. The QD absorption spectra were measured using Shimadzu UV-1601PC UV-Visible spectrophotometer. The QD barcode emission spectra were measured using the Emission Acquisition mode on Horiba Jobin Yvon FluoroMax-3 fluorometer.

2.2.5 Viral DNA/RNA Extraction, and Reverse Transcription

De-identified clinical samples were obtained from the Toronto Western Hospital Liver Clinic and St. Michael's Hospital biobank repository. The protocol was approved by the Research Ethics Board of the University Health Network and St. Michael's Hospital, both affiliates of the University of Toronto. All patients provided written informed consent for storage and use of their specimens for research.

Whole blood was collected by venipuncture in either a Vacutainer (serum) or anticoagulant-treated tubes (plasma). Tubes were inverted several times, and stood upright for 30 – 60 minutes (for serum collection). Samples were then spun in a refrigerated centrifuge, and serum or plasma was aliquoted and stored at -80 °C. HBV or HIV nucleic acid was extracted using the Chemagic Viral DNA/RNA Kit (PerkinElmer), and HIV RNA was then reverse transcribed as per the iScript cDNA Synthesis kit (Bio-Rad).

2.2.6 RPA and post-RPA Purification

RPA was performed using either synthetic target DNA, DNA extracted from clinical specimens or reverse-transcribed cDNA using the TwistAmp Basic kit (TwistDx). For the analytical sensitivity measurement using synthetic DNA targets (Figure 2.5), a premix solution containing 2.4 µL of each forward and reverse primers (10 pmol/µL for each), 12.2 µL of nuclease-free water, 29.5 µL of rehydration buffer, and 1 µL of either water or template DNA (1 zmol/µL, 10 zmol/µL, 100 zmol/µL, 1 amol/µL, 10 amol/µL, 100 amol/µL or 1 fmol/µL) was prepared. This solution was then transferred to a tube containing the reaction pellet and mixed. The reaction was initiated by the addition of 2.5 µL of 280 mM magnesium acetate, and incubated at 37 °C for 30 minutes to produce 99 and 135 bp HPV and HIV amplicons respectively.

For the pre-clinical assessment (Figure 2.7 and Figure 2.14), 4 µL of the extracted DNA and 2 µL of the extracted and reverse-transcribed cDNA was added into the RPA reaction for HBV and HIV testing respectively. The same primer, rehydration buffer, and magnesium acetate conditions were used as before, while the water volume was adjusted in both cases to create a final reaction volume of 50 µL. The reaction was then incubated at 37 °C for 30 minutes to produce 100 and 116 bp HBV and HIV amplicons respectively. The RPA primers and target DNA sequences used in this chapter is listed in Table 2.4.

Table 2.4: List of RPA Primers and Target DNA Sequences

	Forward Primer (5' to 3')	**Reverse Primer (5' to 3')**	**Target Sequence (Only sense strand is shown, 5' to 3')**
HPV (Synthetic)	GATACTACA CGCAGTACAA ATATGTCATT ATGTGC	CCCATGTCGT AGGTACTCCT TAAAGTTAGT	TGATACTACA CGCAGTACAA ATATGTCATT ATGTGCTGCC ATATCTACTT CAGAAACTAC ATATAAAAAT ACTAACTTTA AGGAGTACCT ACGACATGGG
HIV (Synthetic)	GGACATCAAGCA GCCATGCAAATG TTAAAAGAG	TGCTATGTCACTT CCCCTTGGTTCTC TCATCTGGC	GGACATCAAGCAGCCATGCAAATGTTAAAAG AGACCATCAATGAGGAAGCTGCAGAATGGG ATAGAATGCATCCAGTGCATGCAGGGCCTAT

			TGCACCAGGCCAGATGAGAGAACCAAGGGG AAGTGACATAGCA
HIV (Pre-Clinical)	GAAAGGTGA AGGGGCAGTA GTAATACAAG ACA	CCACACA ATCATCACCT GCCATCTGTT TTCCA	GGAAAGGTGA AGGGGCAGTA GTAATACAAG ACAATAGTGA CATAAAGGTA GTACCAAGAA GAAAAGCAAA GATCATTAGG GATTATGGAA AACAGATGGC AGGTGATGAT TGTGTGGC
HBV (Pre-Clinical)	GGC ATG GAC ATT GAC CCT TAT AAA GAA TTT GG	TGT CGA GAA GGT CCC GAA TAG ACG GAA AGA	GGCATGGACA TTGACCCTTA TAAAGAATTT GGAGCTTCTG TGGAGTTACT CTCTTTTTTG CCTTCTGATT TCTTTCCGTC TATTCGGGAC CTTCTCGACA

RPA products were purified using EZ-10 Spin Column DNA Gel Extraction Kit (Bio Basic), and eluted into 50 µL for detection. Purified DNA was visualized by agarose gel electrophoresis (3% agarose, 135 V, 1 hour), and kept at 4 °C until later use.

2.2.7 PCR and post-PCR Purification

No more than 10% of the reverse-transcribed product was added to the PCR reaction, as per product guidelines. Conventional PCR was carried out using the GoTaq G2 Hot Start Colorless Master Mix (Promega) as per company amplification guidelines. The 100 base-pair amplicon for HBV was generated based on the pre-core/core open reading frame using forward primer 5'-GGCATGGACATTGACCCTTA-3' and reverse primer 5'-TGTCGAGAAGGTCCCGAATA-3' at a final concentration of 1 µM in a 50 µl reaction, and eluted into 30 µl for detection. Primers for the HIV detection product were designed to generate a 118 base-pair amplicon in the integrase gene, with forward primer 5'-GGAAAGGTGAAGGGGCAGTAGTAATAC-3' and reverse primer 5'-GCCACACAATCATCACCTGCC-3' also at a final concentration of 1 µM in a 50 µl reaction, and eluted into 30 µl. PCR programs were carried out as per Promega guidelines for small amplification products.

Amplification products were verified using gel electrophoresis and purified with the Gel/PCR DNA Fragments Extraction Kit (Geneaid) using the PCR clean-up protocol. These products were used in the barcode assay, and sent for sequencing to determine the number of single-nucleotide polymorphisms (SNPs). HBV genotyping was also conducted using conventional PCR with primers previously published[128], and genotype was determined using HBVseq from the Stanford University HIV Drug Resistance Database.

2.2.8 Singleplexed QD Barcode Assay

The following protocol was used to generate Figure 2.5C and D, Figure 2.6, and Figure 2.7A. The amplicons were denatured at 100 °C for 10 minutes and put in ice prior to running the assay. 1 µL

of denatured amplicon was then transferred to the assay solution containing 1 μL of conjugated microbeads (~10,000 beads), 1 μL of detection oligonucleotides (100 pmol/μL), 7 μL of DD water and 10 μL of hybridization buffer (10x SSC, 0.1% SDS, heated to 60 °C) making up a total volume of 20 μL. The solution was mixed and incubated at 37 °C for 30 minutes. The assay product was washed by mixing with 200 μL of washing buffer (0.5x SSC, 0.1% SDS) and let stand in a magnetic rack (MagnaRack, Life Technologies) for 10 minutes to allow magnetically encoded microbeads to settle to the wall of a microcentrifuge tube. The supernatant was removed, and the washing was repeated two more times. Washed product was resuspended in 200 μL of PBST buffer for flow cytometry (BD FACSCalibur).

2.2.9 HBV/HIV Multiplexed QD Barcode Assay

The following protocol was used to generate Figure 2.7B. Purified RPA products were denatured by heating at 100 °C for 10 minutes and stored in ice. For all multiplexing conditions, synthetic DNA strand (CT_Pos, Table 2.3) was added as a positive control, which was designed to hybridize with CC_Pos capture DNA (Table 2.3) conjugated to CB_Pos barcode. CB_Neg barcode conjugated with CC_Neg (Table 2.3) capture DNA was also added in all cases as a negative control, CB_HIV barcode was conjugated with HIV capture DNA (CC_HIV, Table 2.3), and CB_HBV barcode was conjugated with HBV capture DNA (CC_HBV, Table 2.3). A total of 2 μL of denatured amplicon (a combination of 1 μL HBV positive or healthy plus 1 μL of HIV positive or healthy corresponding to the four multiplexing cases) was added to the assay solution containing 1 μL of CB_HIV (10,000 beads), 1 μL of CB_HBV (10,000 beads), 1 μL of CB_Pos (10,000 beads), 1 μL of CB_Neg (10,000 beads), 1 μL of HIV detection oligonucleotides (100 pmol/μL, CD_HIV, Table 2.3), 1 μL of HBV detection oligonucleotides (100 pmol/μL, CD_HBV, Table 2.3), 2 μL of positive and negative control detection oligonucleotides (100 pmol/μL, CD, Table 2.3), 11 μL of hybridization buffer (10X SSC, 0.1% SDS, heated to 60 °C), and 1 μL of positive control target DNA (1 pmol/μL, CT_Pos, Table 2.3). The solution was mixed and incubated at 37 °C for 30 minutes. The assay product was washed by mixing with 200 μL of washing buffer (0.5x SSC, 0.1% SDS) and let stand in a magnetic rack (MagnaRack, Life Technologies) for 10 minutes to allow magnetically encoded microbeads to settle to the wall of a microcentrifuge tube. The supernatant was removed, and the washing was repeated two more times. Washed product was resuspended in 200 μL of PBST buffer for flow cytometry (BD FACSCalibur).

2.2.10 Assay Measurement using Smartphone Optical Device

2.2.10.1 QD Barcode Deposition on Microwell Chip

For high dispersion and microwell filling efficiency of the four barcode microbeads (B_H5N1, B_HBV, B_HCV, and B_Pos from Table 2.3) on the microwell chip, samples with concentration of $3x10^7$ bead/mL were prepared for each. Then, 2 µL of each sample was mixed with 35 µL of DD water and 5 µL of DD water containing 1% Tween to produce a final mixture concentration of $6x10^6$ beads/mL. The mixture was then sonicated for 5 minutes to reduce microbead aggregation before depositing 30 µL of it on the microwell chip, which was rinsed with DD water and allowed to dry prior to deposition. The chip was then placed in an enclosed drying chamber containing dessicant to prevent dust particle contamination, and then allowed 2 hours to dry before imaging. Note that increasing the microbead concentration in the mixture increases the microwell fill efficiency (Figure 2.10), but with greater potential for aggregation.

2.2.10.2 On-chip Analytical Sensitivity Assay

Sensitivity assays (Figure 2.12c-d) were performed directly on the microwell chips for all infectious disease DNA target strands (T_H1N1, T_H3N2, T_H5N1, T_FluB, T_HIV, T_HBV, and T_HCV) and their respective conjugated barcode microbeads (B_H1N1, B_H3N2, B_H5N1, B_FluB, B_HIV, B_HBV, and B_HCV). DNA target strands from Bio Basic Inc., purchased HPLC-purified and used without further purification, were prepared in increasing concentrations of 0, 5, 10, 50, 100, 500, 1000, and 2000 fmol/µL in TE buffer. DNA detection strand from IDT DNA Technologies with Alex Fluor 647 (AF647) fluorophore on the 5' end, purchased HPLC-purified and used without further purification, were prepared with concentration of 100 pmol/µL in TE buffer. Both DNA target and detection strand samples were stored at 4 °C until further use. To perform the assay, 1 µL of the conjugated microbead sample, corresponding to approximately 10^4 conjugated microbeads, was deposited on a microwell chip for each assay condition and let dry for 1 hour. Then, 1 µL of each DNA target strand sample was mixed with 5 µL of hybridization buffer (10x SSC, 0.1% SDS, heated to 60 °C), 3 µL of DD water, and 1 µL of DNA detection strands or DD water (for the blank condition). This resulted in a total hybridization volume of 10 µL for each assay condition, which include blank, 0, 10, 50, 100, 300, 500, 1000, and 2000 fmol target DNA. The hybridization solution for each assay condition was deposited over the conjugated microbead spots on the microwell chips and incubated at 37 °C for 20 minutes. The microwell

chips were then submerged in 10 mL of washing buffer (0.5x SSC, 0.1% SDS, heated to 37 °C), washed by agitation for 20 s, then let dry for 5 minutes before being imaged.

2.2.10.3 On-chip Multiplexing Assay

Cross-reactivity between the bloodborne virus DNA target strands (T_HIV, T_HBV, and T_HCV) and their corresponding conjugated barcodes (B_HIV, B_HBV, and B_HCV), as well as positive and negative control cases (B_Pos and T_Pos, and B_Neg and T_Neg, respectively), was studied (Figure 2.13). First, 6 μL of each conjugated barcode sample, corresponding to approximately $6x10^4$ barcodes each, were mixed together with 90 μL of DD water to produce a 4x dilution factor of the original. The dilution was to reduce microbead aggregation after deposition on chip, which may confound barcode resolution during analysis. To perform the assay, 8 μL of the diluted conjugated barcode mixture, corresponding to approximately $2x10^4$ conjugated microbeads, was deposited on a microwell chip for each multiplexing case and let dry for 4 hours. Then, 4 μL of each target case (DD water for the negative conditions, and corresponding DNA target strand sample with concentration of 2 pmol/μL for the positive conditions) was mixed with 40 μL of hybridization buffer (10x SSC, 0.1% SDS, heated to 60 °C) and 20 μL of the detection strand (concentration of 100 pmol/μL). This resulted in a total hybridization volume of 80 μL for each multiplexing case. From this, 20 μL of the hybridization solution for each multiplexing case was deposited over the conjugated barcode spots on the microwell chip and incubated at 37 °C for 20 minutes. The microwell chip was then submerged in 10 mL of washing buffer (0.5x SSC, 0.1% SDS, heated to 37 °C), washed by agitation for 20s, washed again in another 10 mL of washing buffer to further reduce non-specific binding, and then let dry for 5 minutes before being imaged.

2.2.10.4 On-chip Pre-clinical Assessment

Clinical mono-infection assays (Figure 2.14a and b) were performed directly on the microwell chips using HIV- and HBV-negative, as well as HIV- and HBV-positive samples after amplification. DNA detection strands from IDT DNA Technologies with AF647 fluorophore on either 5’ end (CD_HIV) or 3’ end (CD_HBV), purchased HPLC-purified and used without further purification, for the HIV and HBV target sequences, were prepared with concentration of 100 pmol/μL in TE buffer and stored at 4 °C until further use. To perform the assay, 1 μL of the conjugated microbead sample, corresponding to approximately 10^4 conjugated microbeads, was deposited on a microwell chip for each assay condition and let dry for 1 hour. During this time 20

µL of the amplified sample was mixed with 5 µL of the corresponding detection strand and denatured at 100 °C for 15 minutes. Then, the 25-µL denaturation solution was mixed with 25 µL of hybridization buffer (10x SSC, 0.1% SDS, heated to 60 °C). The 50-µL hybridization solution was deposited over the dried conjugated microbead spot on the microwell chip and incubated at 37 °C for 60 minutes, and let cool at room temperature for 5 minutes. The microwell chip was then submerged in 200 mL of washing buffer (0.5x SSC, 0.1% SDS, heated to 37 °C), washed by agitation for 10 s, washed again in another 200 mL of washing buffer to further reduce non-specific binding, and let dry for 5 minutes before being imaged.

Cross-reactivity between the amplified HIV and HBV clinical samples (CT_HIV and CT_HBV) and their corresponding conjugated barcodes (CB_HIV and CB_HBV), as well as positive and negative control cases (CB_Pos and CT_Pos, and CB_Neg and CT_Neg, respectively), was studied (Figure 2.14e-h). First, 5 µL of each conjugated barcode sample, corresponding to approximately $5x10^4$ barcodes each, were mixed together with 20 µL of DD water to produce a 2x dilution factor of the original. The dilution was to reduce microbead aggregation after deposition on chip, which may confound barcode resolution during analysis. To perform the assay, 1 µL of the diluted conjugated barcode mixture, corresponding to approximately $5x10^3$ conjugated microbeads, was deposited on a microwell chip for each multiplexing case and let dry for 1 hour. During this time 10 µL of each amplified sample was mixed with 5 µL of each of the corresponding detection strands (5 µL of CD_HIV, 5 µL CD_HBV, and 10 µL of CD for both CT_Pos and CT_Neg) and denatured at 100 °C for 15 minutes. Then, the 60-µL denaturation solution was mixed with 60 µL of hybridization buffer (10x SSC, 0.1% SDS, heated to 60 °C). The 120-µL hybridization solution was deposited over the dried conjugated microbead spot on the microwell chip and incubated at 37 °C for 60 minutes, and let cool at room temperature for 5 minutes. The microwell chip was then submerged in 400 mL of washing buffer (0.5x SSC, 0.1% SDS, heated to 37 °C), washed by agitation for 10 s, washed again in another 400 mL of washing buffer to further reduce non-specific binding, and let dry for 5 minutes before being imaged.

2.2.10.5 Smartphone Optical Device Design and Construction

The device was designed using SolidWorks 2012 and 3D printed commercially (Reprodux, North York, Ontario, Canada). Laser diode excitation sources of 405 nm 50 mW, and 650 nm 50 mW were purchased online and secured into the device as delivered. The device was designed such that

both lasers could excite the same spot on the chip. An excitation filter λ_{ex} = 655/15 nm (Edmund Optics) was fixed in front of the 650 nm laser diode source to reduce background signal. Both laser diodes were electrically connected to 2x AA batteries *via* a battery holder and single-pole triple-throw switch (both purchased from a local electronics shop) that switches between the two sources as well as an OFF state. A generic 160x – 200x pocket microscope was purchased online (http://www.gadgetplus.ca/science/Microscope160-200x.html). It was disassembled to extract the eyepiece and objective lenses, and installed into the device manually. The eyepiece was fixed in place but the objective was made to be movable along a track to allow focusing on the sample.

2.2.10.6 Sample Imaging

All images were acquired using the iPhone 4S from Apple (unless otherwise specified) mounted in our device. QD barcodes and AF647 fluorophore were excited using laser diodes of wavelengths 405 nm and 650 nm, respectively. Emission filters λ_{em} = 430LP (Thorlabs), λ_{em} = 530/10 (Thorlabs), λ_{em} = 580/10 (Thorlabs), λ_{em} = 640/10 (Thorlabs), and λ_{em} = 692/40 (Semrock, Brightline Cy5-4040A) were placed in the device's emission filter slot one at a time during imaging. The emission filter λ_{em} = 430LP was used in conjunction with a neutral density filter OD = 1.3 (Thorlabs) to image all barcodes to determine their size and location, while avoiding intensity saturation. The emission filters λ_{em} = 530/10, λ_{em} = 580/10, and λ_{em} = 640/10 corresponded with quantum dots QD540, QD589, and QD640, respectively, and were used to isolate for their fluorescence for resolving barcodes. The emission filter λ_{em} = 692/40 was used to isolate for the detection strand AF647 secondary label fluorescence as a means to measure the amount of analyte that hybridized with its corresponding capture strand. Image exposure times, made adjustable with the use of the NightCap app from Apple's App Store, was maintained at 1 s for all filters. In the case of fluorophore particles, they were excited using only the 405 nm laser diode source and imaged using only the emission filter λ_{em} = 430LP, the images of which were used for subsequence intensity analysis.

2.2.10.7 Image Analysis

A custom-made algorithm was written in MathWork's MATLAB for all image analysis. The algorithm accepts as inputs five emission filter images (λ_{em} = 430LP, λ_{em} = 530/10, λ_{em} = 580/10, λ_{em} = 640/10, and λ_{em} = 692/40) of a sample. The images were cropped to include microbeads of interest based on user selection. The cropped filter images were aligned with the λ_{em} = 430LP filter

image through the use of the discrete Fourier transform registration[129]. The algorithm then identified the size and location of each microbead, based on its appearances in the λ_{em} = 430LP filter image, using the Hough transform[130]. Erroneously identified microbeads (*e.g.* debris, imaging artefacts, overlapping microbeads) were excluded based on user input. Each microbead was then associated with the mean pixel intensity across its area at each of the four remaining filter images. For each microbead, the λ_{em} = 530/10, λ_{em} = 580/10, and λ_{em} = 640/10 filter image intensities comprised its intensity profile, while the λ_{em} = 692/40 filter image intensity indicated the fluorescent secondary probe intensity. In order to identify the microbeads on the chip, known barcode intensity profiles were first established (Figure 2.3).

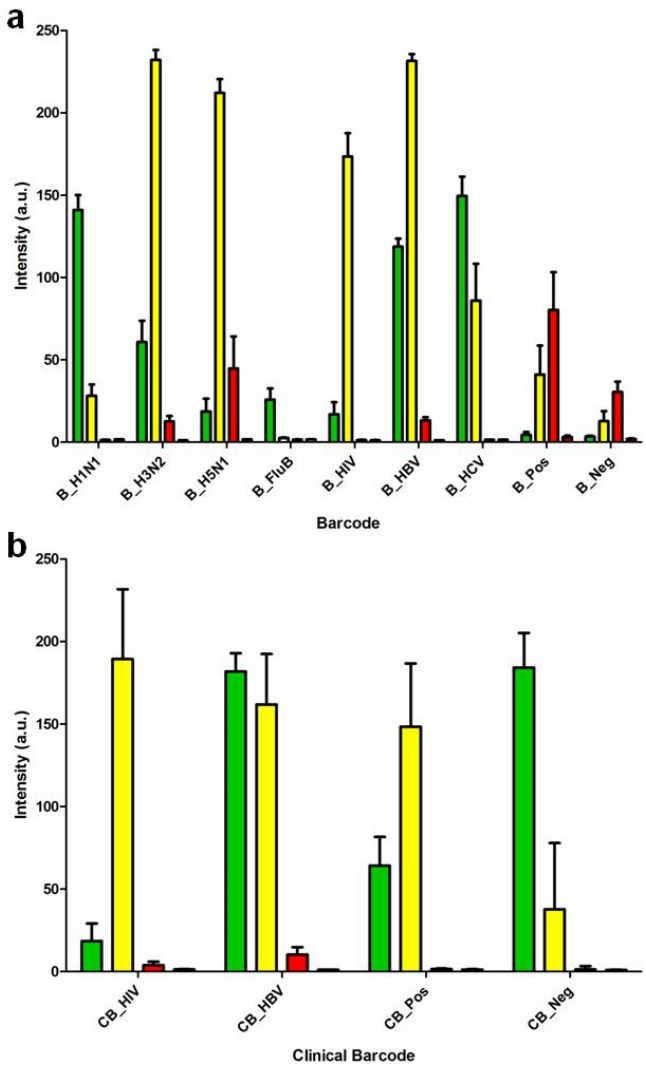

Figure 2.3: Barcode Intensity Profiles. Image intensities of QD barcodes for (a) synthetic samples, and (b) clinical samples. Known barcode intensity profiles for all barcodes used. From left to right, the colored bars represent intensity observed at the filter λ_{em} = 530/10 (■), λ_{em} = 580/10 (■), λ_{em} = 640/10 (■), and λ_{em} = 692/40 (■). Error bars were calculated as the standard deviation from three replications.

These profiles were obtained by imaging all the barcodes – B_H1N1, B_H3N2, B_H5N1, B_FluB, B_HIV, B_HBV, B_HCV, B_Pos, B_Neg, CB_HIV, CB_HBV, CB_Pos, and CB_Neg – alone (Table 2.3) and calculating the mean filter intensity across all microbeads for each filter. A microbead's intensity profile was then compared against each known barcode's intensity profile to identify the barcode of interest. Specifically, a barcode was classified according to its type (*i.e.* synthetic or clinical sample) and highest to lowest intensities among the filters λ_{em} = 530/10, λ_{em} = 580/10, and λ_{em} = 640/10. This narrowed the selection down to either one barcode, in which case the barcode of interest was identified, or two barcodes. Between the two possibilities B_{high} (with higher mean intensities) and B_{low} (with lower mean intensities) a threshold was defined for B_{low}:

$$I_{barcode} = I_{mean} + I_{STD} \qquad \textit{Equation (1)}$$

where $I_{barcode}$ is the intensity threshold for B_{low}. I_{mean} is the mean intensity of B_{low}, and I_{STD} is the intensity standard deviation of B_{low}. This threshold was calculated for the highest intensity amongst the three filters λ_{em} = 530/10, λ_{em} = 580/10, and λ_{em} = 640/10 for B_{low}. If the highest intensities were similar in value between B_{low} and B_{high}, the second highest filter intensity was used. With this, if the microbead's corresponding filter intensity was equal to or lower than $I_{barcode}$, the barcode of interest was B_{low}, otherwise B_{high} was chosen.

The presence of the analyte of interest was determined by using the intensity values from the λ_{em} = 692/40 filter, which isolates for the AF647 secondary probe signal. For the synthetic sample sensitivity assays, the intensities were used directly to establish the LOD and dynamic range for the device. However, a micobead-counting method was used to determine the optical detection of multiplex samples and clinical samples because there is greater accuracy in the measurement when the measurement is based on a comparison to negative controls. Negative and positive controls are always required in analyzing complex samples, as these control samples confirm whether a technique is working as designed. A histogram of the fluorescence intensity is developed from the secondary probe and compared to the negative sample. Equation (2) describes this analysis.

$$Q = \textit{(population of barcode whose } \lambda_{em} = 692/40 \textit{ filter intensity} \geq I_{assay}\textit{)} \,/\, \textit{(total barcode population)} \qquad \textit{Equation (2)}$$

That is, the barcodes whose secondary probe intensities were equal to or above the threshold I_{assay}, defined empirically, were counted and a percentage, relative to the barcode's total population, was calculated. In the case of multiplexed detection of synthetic bloodborne viral targets (Figure 2.13),

a detection was considered positive if $Q > 30\%$ (*i.e.* over 30% of said barcode had secondary probe signals above the threshold). In the case of amplified mono- and co-infected clinical samples (Figure 2.14), a detection was instead considered positive if $Q > 3\%$ due to their overall lower signals.

2.3 Results and Discussions

2.3.1 Integration of QD Barcode Assay with RPA

The integrated system is composed of two main steps (Figure 2.4). In the first step, template DNA is amplified *via* RPA for 30 minutes at 37 °C. Purified and denatured amplicons are then directly used in the QD barcode assay, followed by the measurement of fluorescent signals from QD barcodes and detection probes *via* flow cytometry.

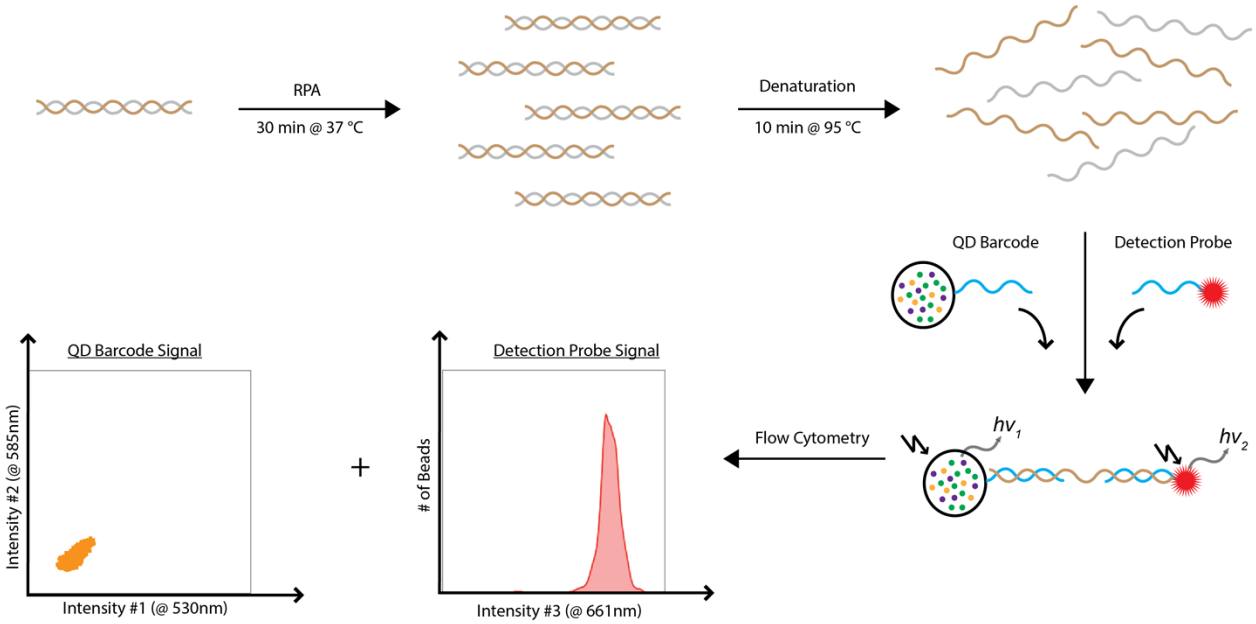

Figure 2.4: Integration of QD Barcode assay with RPA. Template DNA gets amplified *via* RPA followed by purification and denaturation of amplicons. Denatured amplicons are mixed with QD barcodes and detection probes, where both signals are measured with a flow cytometer.

The analytical sensitivity of QD barcode-based isothermal amplification assay was first examined using two synthetic DNA targets that are designed to match HIV and Human papillomavirus (HPV) sequences. Varying amounts of DNA (1 zmol to 1 fmol) were amplified *via* RPA and purified amplicons were visualized by running agarose gel electrophoresis (Figure 2.5A and B). Qualitatively, correct DNA size was observed for both DNA targets (99 bp and 135 bp for HPV and HIV respectively), and the addition of as low as 1 zmol template DNA (~600 copies) in the RPA reaction produced sufficient number of amplicons that are visible on the agarose gel compared to no template controls (NTCs). For quantitative analysis, QD barcodes and detection probes were incubated with denatured amplicons for 30 minutes at 37 °C and washed two times to remove unbound detection probes prior to flow cytometry. The intensity of AF647 from detection probes are presented in Figure 2.5C and D. For detection of both HPV and HIV amplicons,

amplification of 1 zmol template DNA (~600 copies) produced sufficient signal that was detectable by the assay, and this number was determined to be the LOD of QD barcode-based isothermal amplification assay, which is 10^6 times improvement over the LOD of conventional QD barcode assay (1 fmol = $6x10^8$ copies)[79].

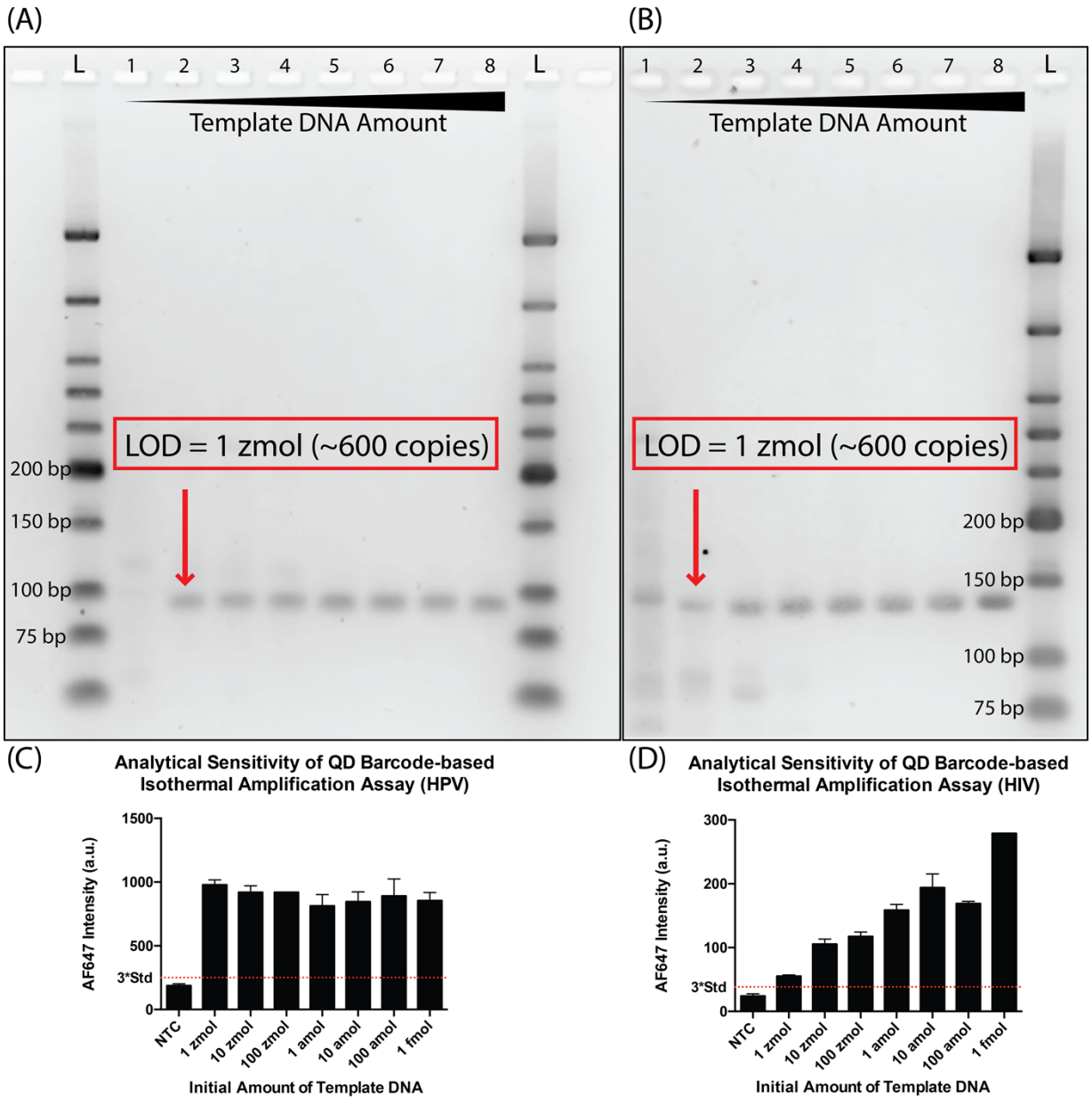

Figure 2.5: Analytical Sensitivity Measurement. Varying amounts of (A) HPV, and (B) HIV template DNA were amplified *via* RPA and visualized by running agarose gel electrophoresis (3% agarose, 135V, 1 hour). Lanes: L. DNA Ladder, 1. NTC, 2. 1 zmol, 3. 10 zmol, 4. 100 zmol, 5. 1 amol, 6. 10 amol, 7. 100 amol, 8. 1 fmol. Denatured amplicons were incubated with QD barcodes and detection probes, and detection probe signals (AF647) were measured *via* flow cytometry for (C) HPV and (D) HIV DNA targets. Dotted red lines indicate 3 times standard deviation plus the average of NTC replicates. Error bars represent standard error of the mean from experimental duplicates.

Next, the specificity of the assay was tested by comparing the assay performance between complementary (HPV), and non-complementary (HIV) amplification products to the capture probes. As depicted in Figure 2.6, only the specific RPA amplicons produced the positive assay signal, whereas non-specific and NTC RPA products produced negative assay signals. These findings suggest that the integrated QD barcode-based isothermal amplification assay has high analytical sensitivity for detection of nucleic acids extracted from clinical specimens, and high specificity for detection of multiple infectious targets. The next step was to proceed with a pre-clinical study to further evaluate this detection platform.

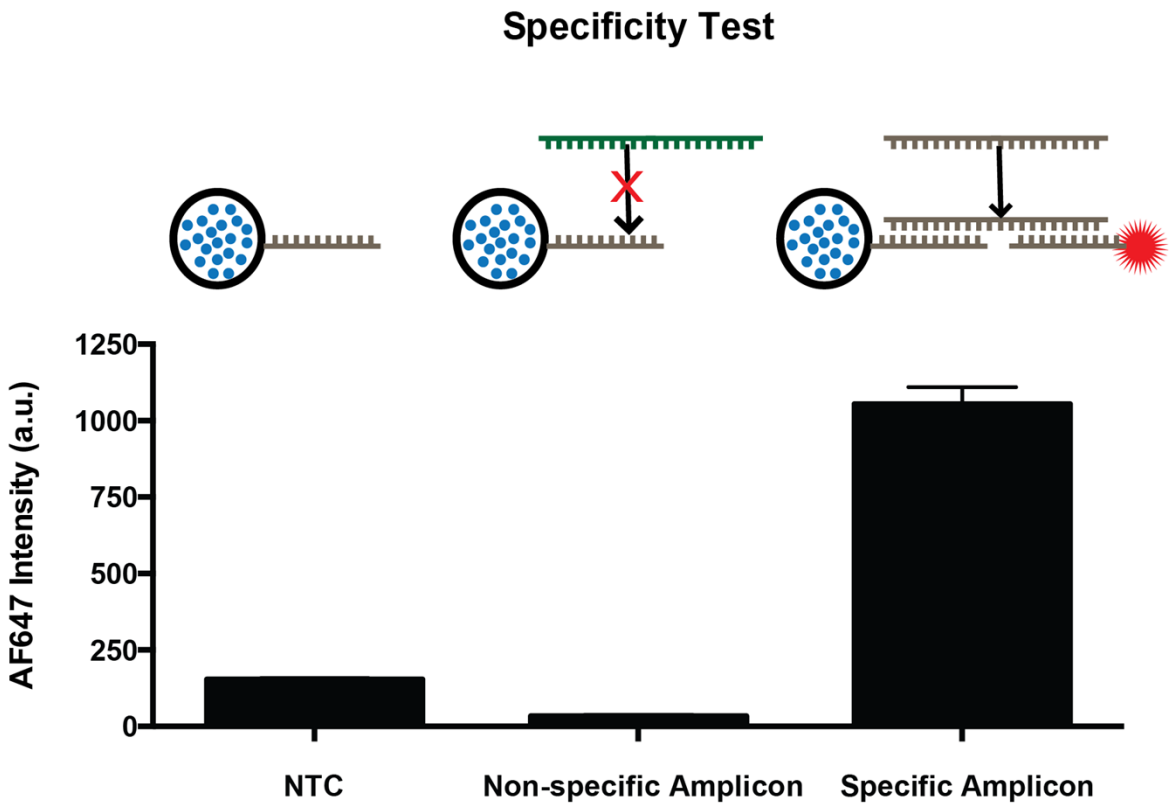

Figure 2.6: Specificity Test. Specificity was tested by incubating the assay mixture with non-specific and specific amplicons. Amplicons were produced by incubating 1 amol of template DNA in the RPA reaction. NTC contained TE buffer instead of the amplicon. All error bars represent standard error of the mean from assay duplicates.

2.3.2 Pre-clinical Assessment

For the pre-clinical assessment of QD barcode-based isothermal amplification assay, whole blood from 7 HBV-positive, 10 HIV-positive and 3 healthy subjects were collected and tested in a blinded experiment. Table 2.5 lists genotypes of HBV samples, and viral loads of HBV and HIV samples that are used in this experiment. These viral loads are reported as per a clinical setting,

and represent a viral load range from treatment-naïve patients. The HBV-infected samples were comprised of multiple genotypes to ensure wide applicability of this diagnostic system. DNA and RNA were extracted from the whole blood of HBV and HIV patients respectively, as well as from the 3 healthy subjects. The extracted viral RNA from HIV patients was reverse transcribed to generate complimentary DNA (cDNA). The extracted nucleic acids were then amplified by RPA and PCR in parallel, and both amplicons were used in QD barcode assay to compare the amplification performance. As illustrated in Figure 2.7A, all infected patient and healthy samples were correctly identified as positive and negative respectively, and RPA demonstrated to perform as effectively as PCR.

HBV/HIV co-infection model was also investigated to demonstrate the feasibility of a multiplexed detection system. Four types of QD barcodes were prepared for multiplexing: two barcodes for detecting HBV and HIV infections (CB_HBV, CB_HIV), one barcode as a positive control (CB_Pos), and one barcode as a negative control (CB_Neg). The four barcodes were synthesized to produce unique optical signatures, which appear as distinct populations on FL1 vs. FL2 measurement (Figure 2.8). Each barcode was functionalized with corresponding capture oligonucleotides, and the assay mixture was spiked with various combinations of HBV and HIV amplicons plus the positive control DNA. As presented in Figure 2.7B, only those DNA targets that are added in the assay mixture were detected without any cross-reactivity, demonstrating the feasibility of detecting multiple targets simultaneously.

Table 2.5: List of HBV Genotypes and HBV/HIV Viral Loads

HBV					HIV		
Sample ID	**HBV Genotype**	**Viral Load (IU/mL)***	**Viral Load (Copies/mL)**	**Viral Load (mol/µL)**	**Sample ID**	**Viral Load (Copies/mL)***	**Viral Load (mol/µL)**
HBV+ 1	C	4.38E7	2.55E8	4.23E-19	HIV+ 1	2.41E4	4.00E-23
HBV+ 2	C	1.7E8	9.89E8	1.64E-18	HIV+ 2	4.87E4	8.09E-23
HBV+ 3	B	1.01E6	5.88E6	9.77E-21	HIV+ 3	1.48E4	2.46E-23
HBV+ 4	D	1.68E9	9.78E9	1.62E-17	HIV+ 4	7.23E3	1.20E-23
HBV+ 5	C	4.51E5	2.63E6	4.36E-21	HIV+ 5	3.00E5	4.98E-22
HBV+ 6	B	1.31E9	7.62E9	1.27E-18	HIV+ 6	1.00E5	1.66E-22
HBV+ 7	C	1.47E5	8.56E5	1.42E-21	HIV+ 7	5.00E5	8.31E-22
					HIV+ 8	2.53E4	4.20E-23
					HIV+ 9	2.43E4	4.04E-23
					HIV+ 10	3.10E4	5.15E-23

*As reported by gold standard automated equipment.

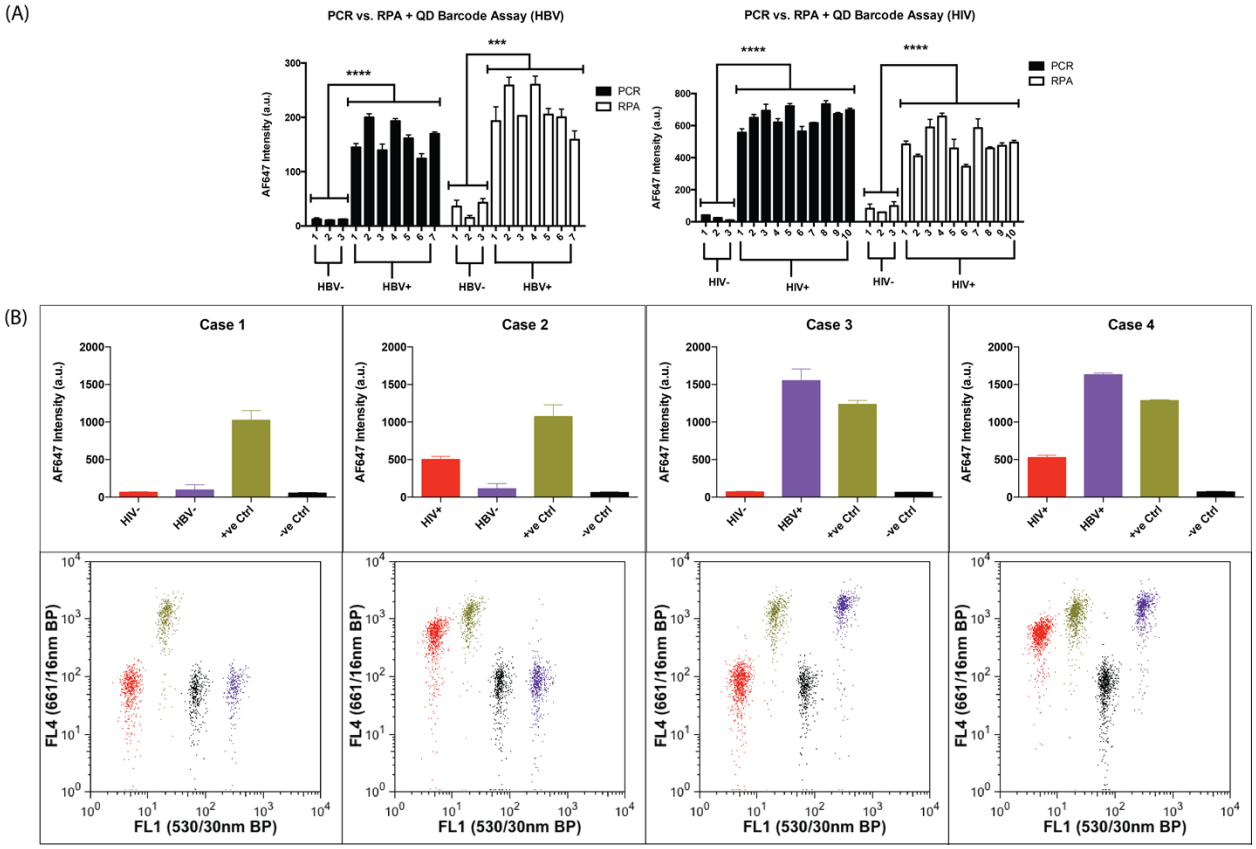

Figure 2.7: Pre-clinical Assessment of QD Barcode-based Isothermal Amplification Assay. (A) QD barcode assay using PCR and RPA products for HBV (Left) and HIV (Right) patient samples. (B) HBV/HIV multiplexed assay. Case 1) Only positive control DNA was present during hybridization. Case 2) Targets for HIV and positive control were present during hybridization. Case 3) Targets for HBV and positive control were present during hybridization. Case 4) Targets for HIV, HBV and positive control were present during hybridization. All error bars represent standard error of the mean of experimental triplicates. Note that statistical significance is indicated as *** for $p \leq 0.001$, and **** for $p \leq 0.0001$.

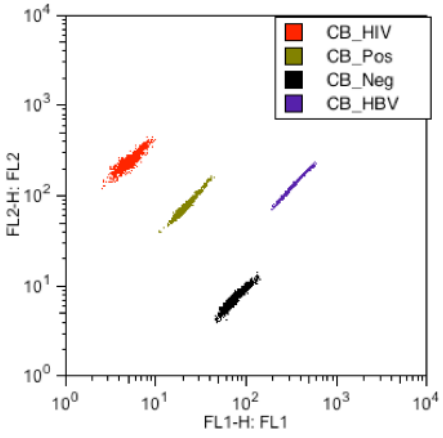

Figure 2.8: FL1 vs. FL2 Signals of Four QD Barcodes used in HBV/HIV Multiplexing. Barcode signals measured with a flow cytometer using two detection filters (FL1: 530/30 nm and FL2: 585/42 nm). Four distinct populations are shown on this plot, allowing deconvolution of the four barcode signals for multiplexed analysis.

2.3.3 Assay Measurement using Smartphone Optical Device

Despite the advances with chemical design of barcodes, nanotechnology-based barcoding has not advanced to patient care yet because the readout device (*e.g.* spectrophotometer/fluorometer, fluorescent microscope, or flow cyotometer) remains expensive, and the poor analytical sensitivity (LOD of femtomole to attomole) limits their utility for detecting many clinically relevant samples. While the sensitivity can be improved with an isothermal amplification step as demonstrated in sections **2.3.1** and **2.3.2**, current approach still relies on an expensive and bulky readout device, which renders the diagnosis impractical outside of research laboratories. To address this limitation, the use of a portable, smartphone-based readout of QD barcodes is demonstrated (Figure 2.9). While the concepts of smartphones have been proposed for diagnostic applications, they have been primarily used in direct imaging applications from identifying bacteria or viruses labeled with a fluorophore[131,132], cell counting[133-135], imaging the test lines on lateral flow immunoassays[136], and signals from custom-made lab-on-chip assays[137-139], among many other approaches[140,141]. These techniques are incapable of detecting different strains or pathogens in a high-throughput manner due to their inability to detect multiple biomarkers simultaneously.

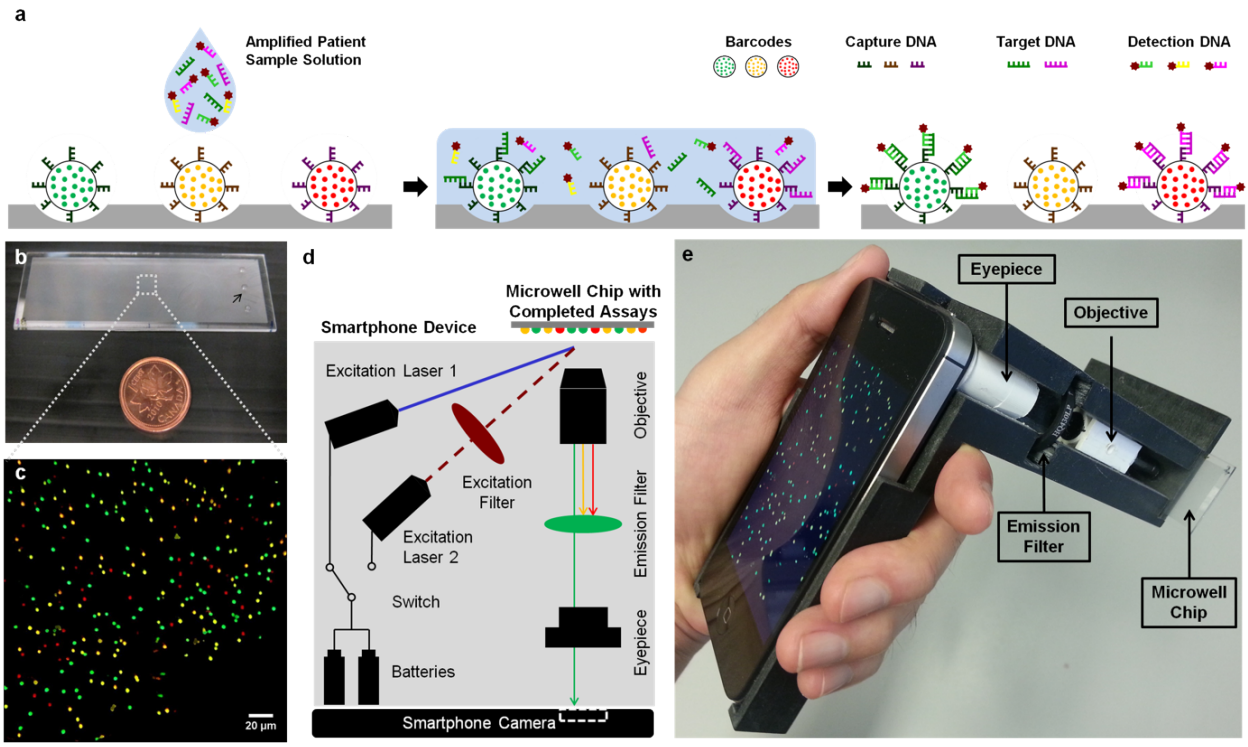

Figure 2.9: Overview of the Smartphone Device Utilizing QD Barcodes. (a) The assay involves the addition of patient samples to a chip coated with microbeads, which are optically barcoded by quantum dots and are coated with molecules that recognize a target analyte. This target analyte joins the barcode to

the detection probe. Since each barcode is conjugated with a known bio-recognition molecule for a specific pathogen target, the imaging of the optical signal from the barcode would allow for the identification of the pathogen and whether it is present in a patient sample (*i.e.* lack of detection probe signal indicates no pathogen present, in this case the yellow microbead). (b) A typical microwell chip containing different barcodes in each well. In a biological assay, a 20-µL (for multiplexing synthetic targets), or a 50-µL (for mono-infection patient samples) sample is added on the chip (see black arrow), incubated at 37 ^{o}C for 20 – 60 minutes, rinsed, and imaged. (c) A smartphone camera captures the image of four different quantum dot barcodes arrayed on the surface of the chip. These barcodes are excited with a violet laser source (λ_{ex} = 405 nm, 50 mW), optical signals collected by a set of lenses, filtered with 430 nm long-pass filter, and imaged using an Apple iPhone 4S smartphone with an exposure time of 0.05 s. (d) Two excitation sources excite the quantum dot barcoded chip independently. The optical emission is collected by a set of objective and eyepiece lenses, imaged using a smartphone camera, and interpreted as positive or negative detection using a custom-designed algorithm. The images may be sent wirelessly to a centralized facility for further evaluation or for the mapping and tracking of infectious diseases. (e) Image of the smartphone device.

The smartphone optical device is composed of a 3D-printed plastic chassis holding the smartphone, eyepiece, objective lenses, filters, and the microwell chip. The microwell chip contains 3 µm diameter wells, where the barcodes are deposited for imaging of fluorescent signals (Figure 2.9a-c). The effect of the barcode concentration and size on the filling efficiency is illustrated in Figure 2.10. The two laser diodes are switched on independently *via* a manual switch: Excitation Laser 1 (405 nm) excites the barcodes and Excitation Laser 2 (650 nm) excites the secondary label with a filter (λ_{ex} = 655/15) that controls the wavelength excitation observed by the chip (Figure 2.9d). The eyepiece and movable objective lens magnifies and focuses barcodes on the chip to allow them to be viewable clearly by the naked eye on the smartphone display. The smartphone camera, in this case Apple's iPhone 4S, then captures that view. A total of five images are acquired for each sample, corresponding to each of the five emission filters (λ_{em} = 430LP, 530/10, 580/10, 640/10, and 692/40). Specifically, the 430LP filter image is used for extracting the location and size of the barcodes in the camera field-of-view; the 530/10, 580/10, and 640/10 filter images for isolating QD signals to determine barcode signatures; and the 692/40 filter image for isolating the secondary label signal to determine the presence of target analyte bound to the barcode surface. Finally, a custom-written algorithm analyzes these images and produces the results. The algorithm develops a histogram of the optical signal from the secondary probe of all barcodes within the sample. A threshold is established in a measurement based on the highest signal from barcodes that do not contain any of the target molecules of interest (*i.e.* the negative control in the experiments). A graph of barcode numbers above this threshold is used to determine a positive or negative detection (Figure 2.11). Samples that have the target molecule of interest are expected to have more number of barcodes above this threshold.

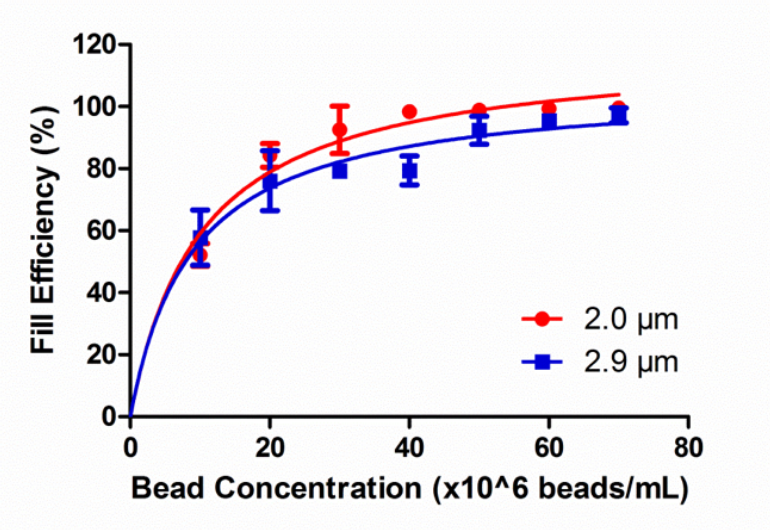

Figure 2.10: Filling Efficiency of Microbeads on a Microwell Chip. Microbead filling efficiency on the microwell chip as determined by the concentration and size of the microbeads for 2.0 µm (—) and 2.9 µm (—). Error bars were calculated as the standard deviation from three replications

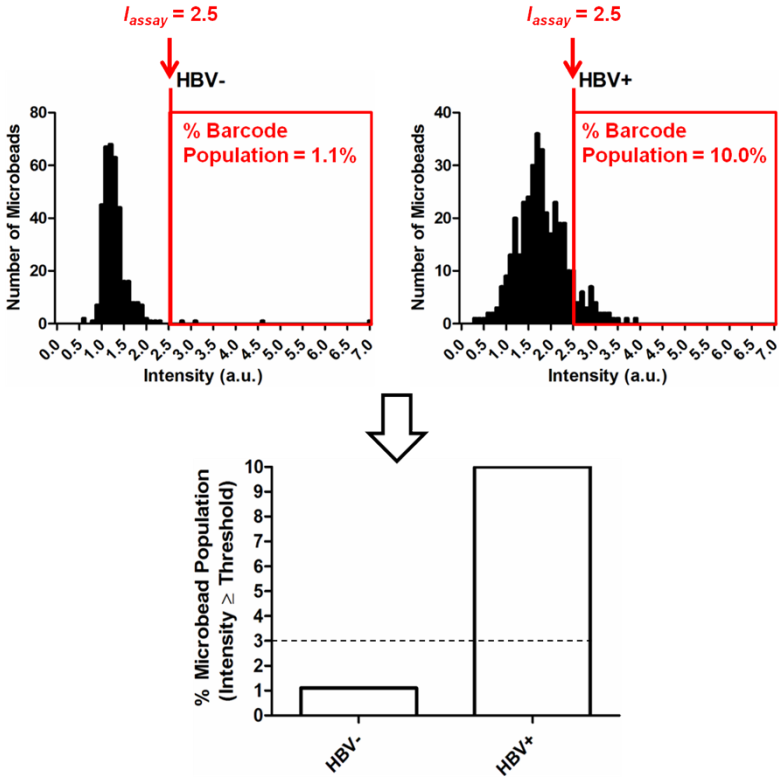

Figure 2.11: Histogram Analysis. Histogram of barcode population is plotted based on the intensity of detection probe signals. Empirically determined I_{assay} is applied to calculate the percentage of barcode population greater than or equal to I_{assay}.

2.3.3.1 Analytical Sensitivity Measurement using Smartphone Device

Figure 2.12a and b demonstrate that a smartphone camera is able to capture the distinct optical emissions of each barcode on the microwell chip, and proper filtering can differentiate the barcode optical signals from the secondary probe's signal. The analytical performance of the conventional microbead-based sandwich assay without the incorporation of RPA was first determined using the smartphone reader. Seven barcodes were designed for detecting seven infectious disease biomarker targets, plus two barcodes for the positive and negative control samples (Table 2.3). When the target is absent (*i.e.* negative detection), the optical signal from the microbead comprises only the QD signal of the barcode. When the target is present (*i.e.* positive detection), the microbead optical signal consists of emissions from both the QDs and AF647 labeled secondary probe. The LOD and linear dynamic range for all targets (HIV, HBV, HCV, H1N1, H3N2, H5N1, and Flu B) is between 10 to 50 fmol ($6x10^9$ to $3x10^{10}$ copies) and up to 40-fold, respectively, in a final hybridization sample volume of 10 µL (Figure 2.12c and d).

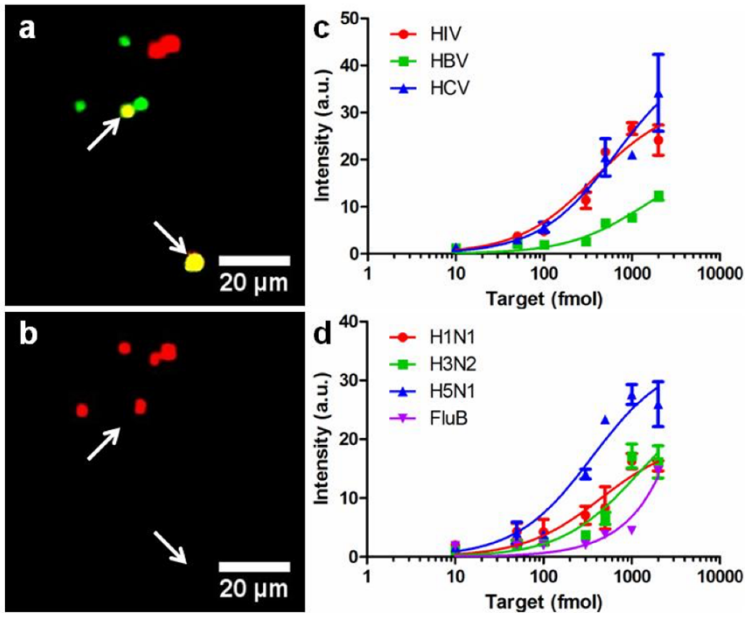

Figure 2.12: Device Assay Sensitivity. (a) Yellow, green and red barcodes (identified as B_HBV, B_HCV, and B_Pos in Table 2.3, respectively) are deposited on the chip and images using the device (λ_{ex} = 405 nm, λ_{em} = 430LP, exposure time = 1 s). (b) After the assay, the device-acquired fluorescence image of the microbeads bound with the target analyte and secondary probe (λ_{ex} = 655/15, λ_{em} = 692/40, exposure time = 1 s). Both green and red microbeads had positive signals. This demonstrates that their respective genomic targets are present in the sample but not for the yellow barcode. (c) Sensitivity curves for genetic biomarkers for the bloodborne viruses (HIV, HBV, and HCV). (d) Sensitivity curves for genetic biomarkers for the influenza A viruses H1N1, H3N5, and H5N1; and influenza B virus (FluB). All values represent the average secondary probe intensity, and error bars were calculated based on the standard deviation from three replications of each condition.

2.3.3.2 Multiplexing using Smartphone Device

Next, the ability to simultaneously detect multiple synthetic genetic targets from bloodborne virus panel was demonstrated (Figure 2.13). Six different mock genetic samples were prepared by mixing various combinations of the genetic target sequences for each of the three pathogens of interest – HIV, HBV, and HCV – plus a positive control sequence to ensure that the barcodes are working as designed, and the secondary fluorescent probe sequence. For example, a solution was spiked with the target sequences for HIV and positive control in one combination (Figure 2.13b), then with HIV, HBV, HCV and positive control sequence in another combination (Figure 2.13f). A final hybridization sample of 20 µL was added to the chip and incubated at 37 °C for 20 minutes, rinsed with a washing buffer, dried, imaged, and analyzed using the algorithm. In all cases the target sequences were correctly identified by the assay. For example, in the solution containing the sequences for HCV and positive control (Figure 2.13d), the bar graph shows difference between barcodes bound with secondary probes (*i.e.* HCV and positive control) versus those not bound (*i.e.* HIV, HBV and negative control). All of the probe recognition sequences for the bloodborne viral panels were carefully designed *in silico* to minimize cross-reactivity with closely related viruses using subtypes against the gag gene of HIV, core protein gene of HBV and nucleocapsid protein gene of HCV, as per gold standard testing guideline (Table 2.3).

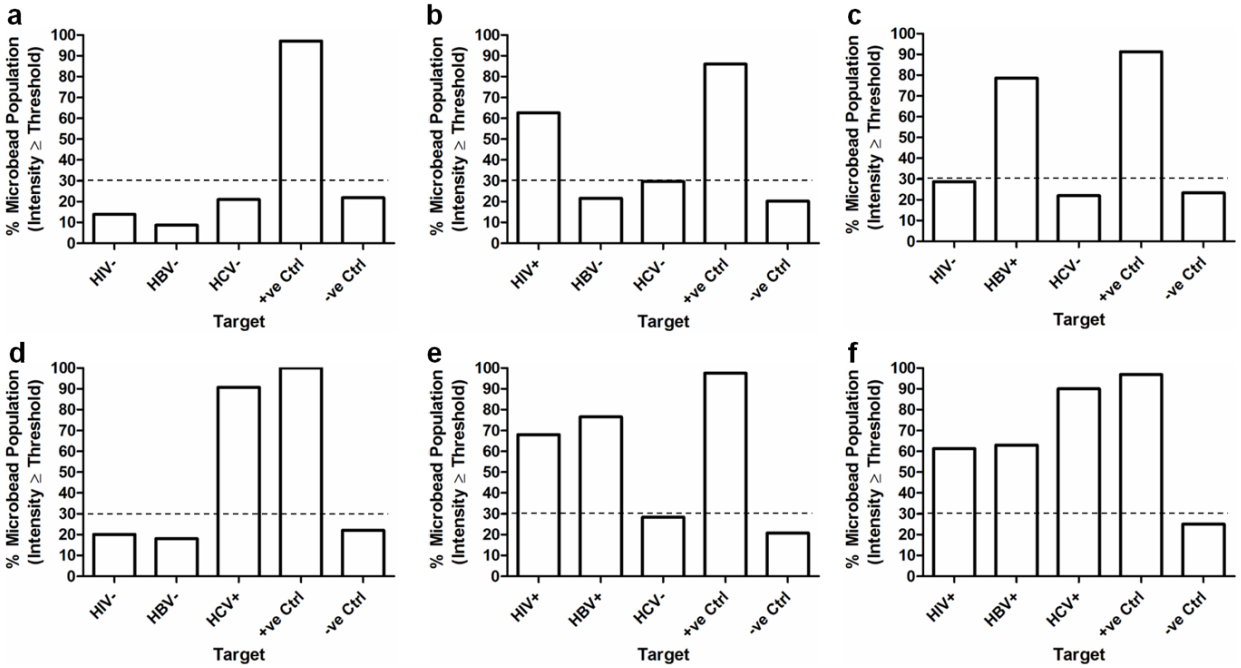

Figure 2.13: Multiplexed Detection of Synthetic Target Strands. (a) Only positive control was present during hybridization. (b) Targets for HIV and positive control were present during hybridization. (c) Targets for HBV and positive control were present during hybridization. (d) Targets for HCV and positive control were present during hybridization. (e) Targets for HIV, HBV, and positive control were present during

hybridization. (f) All targets except for negative control were present during hybridization. Results represent data from three experimental replicates of each condition combined into a single data set. Note that samples above the dashed 30% line are considered positive detection, otherwise they are considered negative detection.

2.3.3.3 Pre-clinical Assessment using Smartphone Device

After validating the device performance with synthetic targets, the pre-clinical assessment of QD barcode-based isothermal amplification assay (section **2.3.2**) was repeated using the smartphone optical device. Of the final amplified sample, 20 µL of the double-stranded DNA were denatured and added to the chip, incubated at 37 °C, rinsed with a washing buffer, dried, imaged, and analyzed using the algorithm in a manner that is similar to detection of the synthetic targets. Figure 2.14a and b demonstrate the successful diagnosis of individual patient samples infected with HIV and HBV, respectively, of varying viral loads before amplification (Table 2.5). In order to determine whether the measurement results were significant, the combined measurements from all samples of non-infected subjects were compared to the combined measurements from the infected patients with either HIV or HBV (Figure 2.14c and d, respectively). The results showed a significant difference with a p-value of 0.05 and 0.01, respectively. Hence, the smartphone optical device was capable of detecting viral loads in the range of 10^3 to 10^9 copies/mL, and of different genotypes.

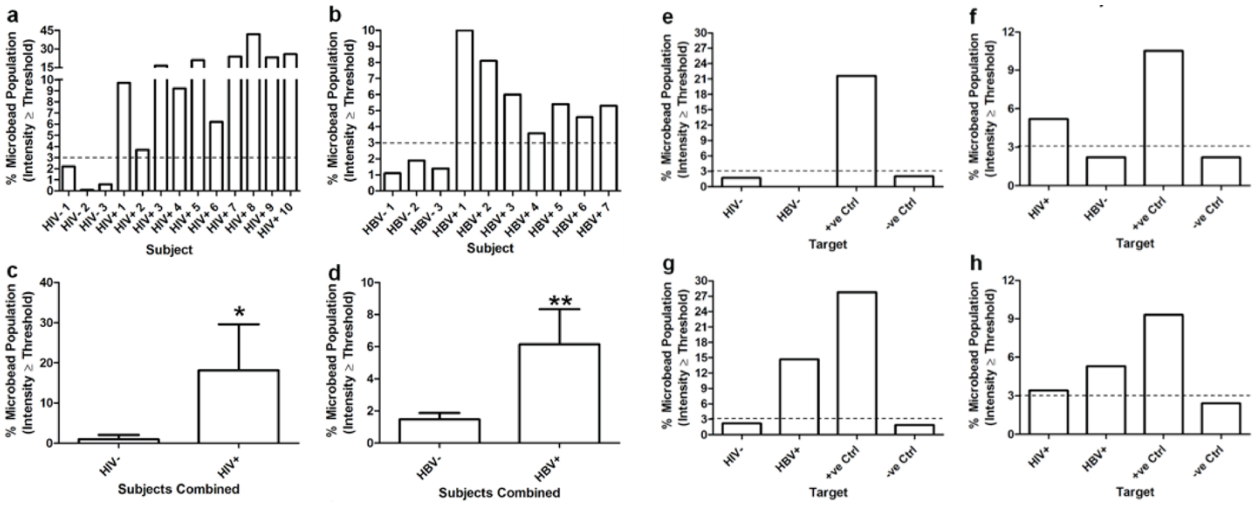

Figure 2.14: Pre-clinical Assessment using Smartphone Optical Device. (a) Detection of amplicons from 3 HIV-negative and 10 HIV-positive subjects. (b) Detection of amplicons from 3 HBV-negative and 7-HBV positive subjects. (c) Comparison between average combined statistics of all subjects of the HIV-negative group (3 subjects) and HIV-positive group (10 patients) from (a). (d) Comparison between the average combined statistics of all subjects of the HBV-negative group (3 subjects) and HBV-positive group (7 patients) from (b). (e-h) Detection of co-infection model simulated with amplified HIV- and HBV-negative, as well as HIV- and HBV-positive samples. (e) Only positive control was present during hybridization. (f) HIV-positive patient sample and positive control were present during hybridization. (g)

HBV-positive patient sample and positive control were present during hybridization. (h) HIV- and HBV-positive patient samples, and positive control were present during hybridization. Results represent data from three replications of each condition combined into a single data set (a-b, e-h). Note that samples above the dashed 3% line are considered positive detection, otherwise they are considered negative detection. All error bars (c-d) represent standard deviation with statistical significance (*$p<0.05$, **$p<0.01$) indicated and determined using a two-sided t-test.

To confirm multiplexed detection of patient samples, four-plexed assay was performed (HIV, HBV, as well as positive and negative controls) by mixing 10 μL of each amplified product with four types of barcodes, corresponding detection probes, and positive control DNA. As illustrated in Figure 2.14e-h, the smartphone optical device could differentiate between the two viruses, and also detect both viruses at the same time.

2.4 Conclusions

In this chapter, the incorporation of RPA with QD barcode assay was first demonstrated to improve the analytical sensitivity by 6-orders of magnitude. The integrated QD barcode-based isothermal amplification assay achieved a detection limit of 1 zmol template DNA (~600 copies), and was able to detect nucleic acids extracted from treatment-naïve patients infected with HBV and HIV (viral loads ranging from 10^3 to 10^9 copies/mL). Also, the cross-reactivity was investigated to demonstrate differentiation between the two diseases and simultaneous detection of both diseases using the HBV/HIV co-infection model. Lastly, a smartphone optical device was developed and integrated with QD barcodes to demonstrate a portable readout of the assay signals outside of research laboratories.

All of the pathogen targets used as test panels in this study represent major infectious threats to the global community, necessitating the development of effective and innovative diagnostics to identify infected individuals and accelerate clinical management. HIV, HBV and HCV are prevalent in resource-limited settings and pose major threats to populations, often related to unknown transmission through sexual contact, drug use and contaminated blood products[11,142]. For rapidly spreading pathogens, immediate implementation of infection control measures and enhanced surveillance to curb the spread of disease will be critical. The proposed integration of QD barcodes with isothermal amplification and smartphone technologies can provide an accurate and transportable diagnosis of infectious pathogens to prevent the rapid spread of diseases in resource-limited areas, and enable wireless transmission of diagnostic results for mapping, surveillance, and potentially prediction of diseases in real-time.

Future work needs to focus on integrating the extraction and amplification components with the existing device into a singular unit, field-testing of the device, and to conduct a clinical trial with greater sample size to evaluate clinical sensitivity and specificity in both the developed and developing worlds.

Chapter 3 : Clinical Validation of QD Barcode-based Isothermal Amplification Assay

3.1 Introduction

There has been a significant number of discussions on the need to translate academic discoveries into clinical utility for improving patient care[105,143,144]. Despite this focus, there are only a few nanotechnology-based diagnostic devices that advanced to use in clinical settings (*e.g.* GNP bio-barcode assay developed by Mirkin's group)[57,145]. In a typical translation process, the first step is to use laboratory-prepared mock samples to evaluate the technology's ability to detect biomarkers in the spiked sample *via* measurements of the analytical sensitivity, LOD, dynamic range, and cross-reactivity. This is followed by the analysis of a few clinical samples (~10 patient samples) to show feasibility of diagnostics with real-world patient samples. The final step before advancing a technology beyond the academic research objective is to conduct a full clinical evaluation (>50 patient samples) to obtain clinical sensitivity and specificity values. These numbers indicate the degree of false positive and negative detections of a diagnostic device. Interestingly, there is a large number of published studies from the initial step, less publications in the subsequent step, and only a handful of studies in the clinical validation step. As a result, the clinical feasibility of many nanotechnology-based diagnostic devices is unclear because only few published studies have explored the clinical sensitivity and specificity of these systems using patient samples.

The concept of QD barcoding was first presented by Nie and co-workers where they demonstrated the use of these barcodes to detect spiked DNA sequences in buffer[120]. They reported that QD barcodes are advantageous for multiplexed diagnostic detection over the traditional barcodes doped with organic fluorophores (*e.g.* Luminex barcodes) because one single light source can excite multiple barcode emissions[79,106], and QDs can achieve better discrimination and identification of barcodes due to narrower spectral line width and longer photostability respectively[68,69,146]. There is also a greater capacity to design more barcode signals by using QDs because the fluorescence of the QDs can be tuned by manipulating the size, shape, and chemical composition[71]. Although these QD properties would allow simplified readout and cost-effective diagnostic procedure for multiplex detection of diseases in patients, the QD barcoding technology has not advanced to the patient care yet due to the lack of its clinical validation. In this chapter, QD barcode technology is clinically validated by evaluating the feasibility of QD barcodes to

diagnose over 70 clinical samples, and assessing clinical metrics such as the clinical sensitivity, specificity and ROC. Furthermore, multiplexed QD barcodes is proposed to improve the clinical sensitivity by detecting multiple regions of the viral genome and thus increasing the rate of true positive detections.

As demonstrated in **Chapter 2**, RPA was used to improve the analytical sensitivity of conventional QD barcode assay. HBV was chosen as the model pathogen because of the global impact of the disease, the need for improved diagnostic tests and its ability to mutate, thus allowing us to confirm the stability of our platform. HBV-related liver diseases account for 0.5-1 million deaths per year, and approximately 350-400 million people are estimated to be chronic carriers for HBV surface antigen (sAg)[15]; although most are unaware of their infection. Current diagnostics for HBV involve the use of standard serological tests followed by quantification of HBV DNA by PCR. DNA detection is an essential component of HBV diagnosis as it is frequently used as an indicator of the need for treatment and is used to monitor patients during antiviral therapy[15].

However, viruses exist as quasi-species, representing a major challenge to the development of nucleic acid-based diagnostic tests. Sequence variations accumulated as a result of high mutation rates in the HBV genome pose a risk of producing false-negative results reducing diagnostic sensitivity[147]. In the absence of therapy, between 10^{11} and 10^{13} virions are produced per day, with an error rate of 10^{-4} to 10^{-5} at each base, per round of replication[148]. HBV is also categorized into genotypes A-H, which can differ by more than 8% and are concentrated in different geographical regions globally[149]. Such variability among DNA sequences can be unfavorable to the RPA process as the use of RPA has been shown to be hampered by mismatches near the 3'-end of primers, and mismatches of greater than 7-9 base pairs[150,151]. In this study, we overcome these current challenges of diagnosing HBV by (1) amplifying multiple sites within the HBV genome, and (2) using multiple QD barcodes to detect the various sequences simultaneously in a single reaction vessel (Figure 3.1). The viral DNA is first extracted from patient serum using magnetic microbeads, various regions of the extracted genome are amplified by RPA, amplified products are detected by multiplexed QD barcode assay, and finally fluorescence signals are measured *via* flow cytometry. Using this strategy, we show that the detection of multiple targets leads to a significant enhancement of the clinical sensitivity for the diagnosis of HBV. This study fosters the clinical translation of QD barcodes, and presents the clinical feasibility of QD barcodes for hospital use in the near future.

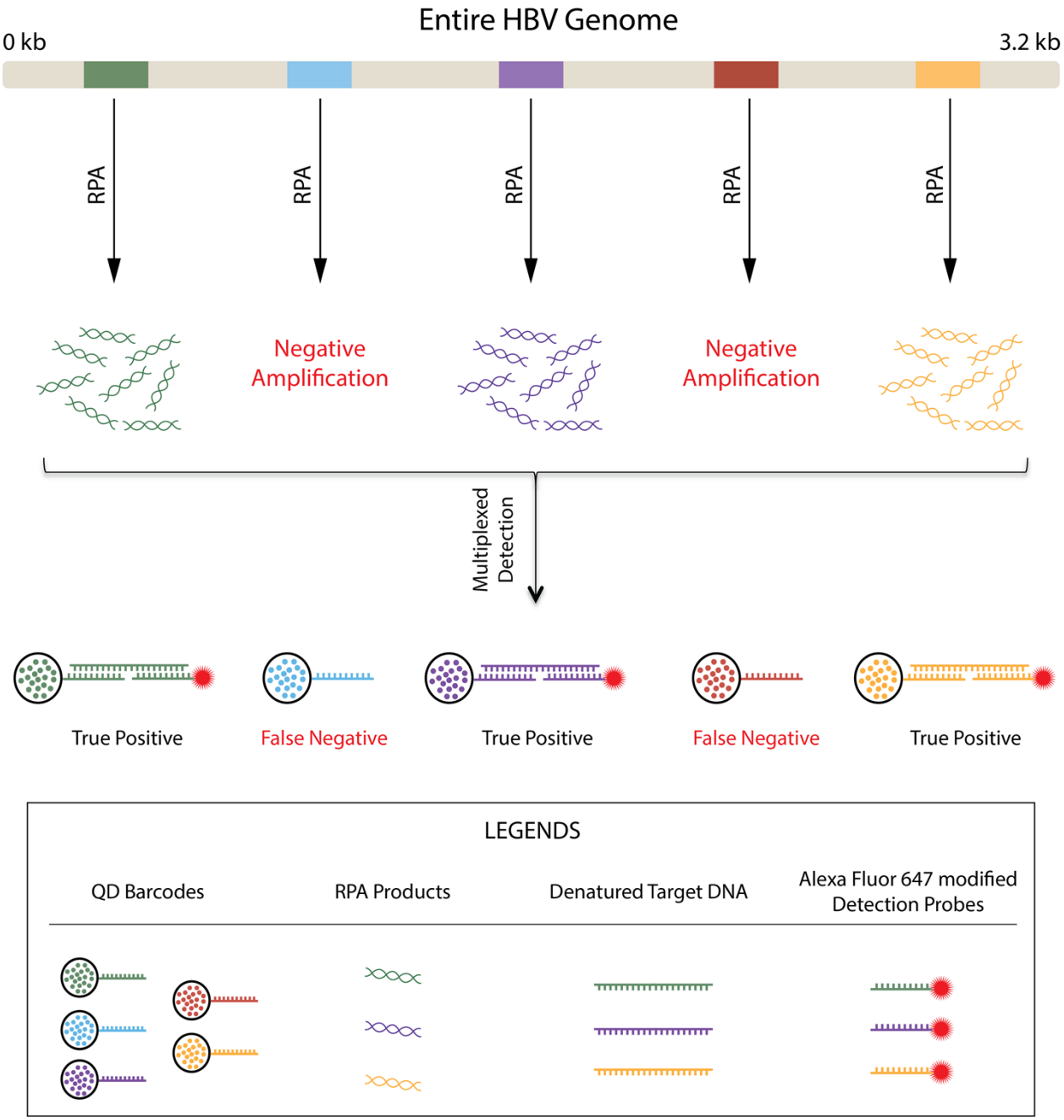

Figure 3.1: Detection of Multiple Amplification Sites *via* QD barcodes. Multiple regions within HBV genome are amplified by RPA producing positive or negative amplification products. Amplicon-specific barcodes functionalized with capture DNA molecules are then used to detect denatured amplicons in multiplexed QD barcode assay.

3.2 Experimental Methods

3.2.1 QD Synthesis

CdSe alloyed ZnS capped QDs with peak emission wavelengths of 506nm ("QD506"), 547nm ("QD547"), 560nm ("QD560"), 580nm ("QD580"), 596nm ("QD596"), and 615nm ("QD615") were synthesized and characterized according to published procedures[152,153], and stored in chloroform at room temperature in dark until later use.

3.2.2 QD Microbeads Synthesis

QD microbeads were synthesized *via* CCFF technique as outlined in the previous work[82]. Polymer solution (4 wt%) was first prepared by dissolving 400 mg of poly(styrene-*co*-maleic anhydride) (32%, cumene-terminated, Sigma-Aldrich) in 10 mL chloroform, and filtered using a 0.2 μm PTFE syringe filter (Nalgene). Various QD color and concentration ratios plus fixed concentration of FeO magnetic nanoparticles (150 μL of 36.5 ng/mL) were mixed with the polymer solution to make a final volume of 1 mL QD polymer solution as outlined in Table 3.2. The QD polymer solution and DD water were then introduced into a customized nozzle system (Ingeniatrics) submerged inside a beaker partially filled with DD water at a focused and focusing flow rates of 0.9 mL/hr and 180 mL/hr respectively using a syringe pump (Harvard Apparatus). The synthesized microbeads were stabilized by overnight stirring, filtered using a 35 μm BD falcon nylon mesh strainer cap, concentrated into a single tube, and stored at 4^{o}C in dark until later use. The size distribution (Table 3.2) and concentration of microbeads were characterized using Beckman Coulter Vi-Cell counter.

3.2.3 Conjugation of Capture Probe to Microbead Surface

Conjugation of capture DNA strands to microbead surface was done through reaction with EDC and sulfo-NHS chemistry. DNA capture strands from IDT DNA Technologies (CPP and CPN, Table 3.1) and Bio Basic Inc. (CP1-CP4, Table 3.1), purchased HPLC-purified, were designed with an amine group and C12 (CPP and CPN, Table 3.1) and C6 (CP1-CP4, Table 3.1) spacer on the 5' end, prepared at a concentration of 10 pmol/μL in TE buffer, and stored at 4^{o}C until later use. For singleplexed assay, capture probes CP1, CP2, CP3 or CP4 were conjugated with B1, and for multiplexed assay, capture probes CP1, CP2, CP3, CP4, CPP and CPN were conjugated with B1, B2, B3, B4, B5 and B6 respectively. To conjugate, EDC and sulfo-NHS were first dissolved

in MES buffer (pH 5, 100 mM) in concentrations of 0.0192g/64μL and 0.01g/100μL respectively. Then, approximately 10^6 microbeads were mixed with 55 μL of MES buffer (pH 5, 100 mM), 10 μL of the sulfo-NHS solution, 32 μL of the EDC solution, and 2.88 μL of the 10 pmol/μL capture DNA stock solution. The reaction was allowed to take place overnight, at which point additional 0.01 g of EDC was added and the mixture was allowed to incubate for another four hours.

To calculate surface density of capture probe DNA for each barcode, 1 μL of 5% Tween was added to the microbead solution, centrifuged at 3500g for 5 minutes to form bead pellet at the bottom of microcentrifuge tube, and 50 μL of the supernatant containing unbound DNA was extracted. The same conjugation procedure described above was performed for no conjugate control cases for each barcode, where DD water was added in place of the microbeads. SYBR gold (Invitrogen), dissolved in DMSO, was first diluted to 0.5:10000 ratio by adding 0.5 μL of SYBR gold to 10 mL of TE buffer, and standard curves (Figure 3.4C) were developed by activating 2.5, 5.0, 7.5 and 10.0 μL of no conjugation control samples with 197.5, 195.0, 192.5, and 190 μL of SYBR Gold (0.5X) respectively in a black 96-well plate for 5 minutes before being read by BMG Labtech plate reader. In a black 96-well plate, 10 μL of supernatants from all conjugation cases, as well as 10 μL of the four blank cases containing only DD water, were each added to individual wells, 190 μL of the diluted SYBR gold was added to each well in the plate, and incubated at room temperature for 5 minutes before being read by plate reader. The fluorescence signal from the unbound DNA was used to estimate conjugation for each barcode by comparing the fluorescence of the conjugation cases with their respective controls containing no microbeads. That is, the lower fluorescence signal indicates higher amount of conjugation. Results were first converted to efficiency percentage and normalized to surface area to determine surface density (Figure 3.4A and B). To complete conjugation, conjugated microbeads were washed twice by removing rest of the supernatant, resuspending microbead pellet in 100 μL of 0.05% Tween, and centrifuging at 3500g for 5 minutes. Washed microbeads were resuspended in 100 μL of 0.05% Tween (~10, 000 beads/μL) and stored at 4^{o}C in dark until later use.

Table 3.1: List of DNA Sequences and Corresponding Barcodes used for Multiplexed Assay

	Region #1	Region #2	Region #3
Amplicon*	**T1**: TGTT GACAAGAATC CTCACAATAC CACAGAGTCT AGACTCGTGG TGGACTTCTC TCAATTTTCT AGGGGGAACA CCCGTGTGTC CTGGCCAAAA TTCG	**T2:** CC ATCAGCGCAT GCGTGGAACC TTTGTGGCTC CTCTGCCGAT CCATACTGCG GAACTCCTAG CCGCTTGTTT TGCTCGCAGC CGGTCTG	**T3:** GCACCTCTC TTTACGCGGW CTCCCCGTCT GTGCCTTCTC ATCTGCCGGA CCGTGTGCAC TTCGCTTCAC CTCTGCACGT CGCATGGAGA CCACCGT
Capture Probe*	**CP1:** **aminoC6**-TTTTTTTTT CGAA TTTTGGCCAG GACACACGGG TGTTCCCCCT AGAAAATTGA GA	**CP2:** **aminoC6**-TTTTTTTTT CAGACCG GCTGCGAGCA AAACAAGCGG CTAGGAGTTC CG	**CP3:** **aminoC6**-TTTTTTTTT ACGGTGG TCTCCATGCG ACGTGCAGAG GTGAAGCGAA GTG
Detection Probe*	**DP1:** AGTCT AGACTCTGTG GTATTGTGAG GATTCTTGTC AACA-**Alexa647**	**DP2:** TCGGCAGAG GAGCCACAAA GGTTCCACGC ATGCGCTGAT GG-**Alexa647**	**DP3:** CGG TCCGGCAGAT GAGAAGGCAC AGACGGG-**Alexa647**
Forward Primer*	**FP1:** TGTT GACAAGAATC CTCACAATAC CACAGAGTC	**FP2:** CC ATCAGCGCAT GCGTGGAACC TTTGTGGCT	**FP3:** GCACCTCTC TTTACGCGGW CTCCCCGTCT GT
Reverse Primer*	**RP1:** CGAA TTTTGGCCAG GACACACGGG TGTTCC	**RP2:** CAGACCG GCTGCGAGCA AAACAAGCGG CTA	**RP3:** ACGGTGG TCTCCATGCG ACGTGCAGAG GTGAA
Barcode**	**B1:** 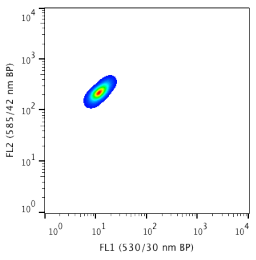	**B2:** 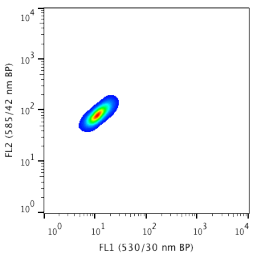	**B3:** 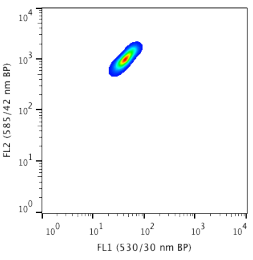

Continued...

	Region #4	Positive Control	Negative Control
Amplicon*	**T4:** CATCCCATCA TCTTGGGCTT TCGCAAAATA CCTATGGGAG TGGGCCTCAG CCCGTTTCTC CTGGCTCAGT TTACTAGTGC CATTTGTTCA GTGGTTCGTA G	**TP:** CGG CGA TGA ATA CCT AGC ACA CTT A CTA AC TAT CCT CAG TGA GCA TTG TC	**TN:** CGG CGA TGA ATA CCT AGC ACA CTT A CTA GG CCG CCG ATA TTG G
Capture Probe*	**CP4:** **aminoC6**-AAAAAAAAA C TACGAACCAC TGAACAAATG GCACTAGTAA ACTGAGCCAG GAGAAA	**CPP:** **aminoC12**-GAC AAT GCT CAC TGA GGA TAG T	**CPN:** **aminoC12**-CCA ATA TCG GCG GCC
Detection Probe*	**DP4:** AGGCCCA CTCCCATAGG TATTTTGCGA AAGCCCAAGA TGATGGGATG-**Alexa647**	**DPC:** **Alexa647**-TAA GTG TGC TAG GTA TTC ATC GCC G	
Forward Primer*	**FP4:** CATCCCATCA TCTTGGGCTT TCGCAAAATA CC	**NA**	
Reverse Primer*	**RP4:** C TACGAACCAC TGAACAAATG GCACTAGTA		
Barcode**	**B4:** 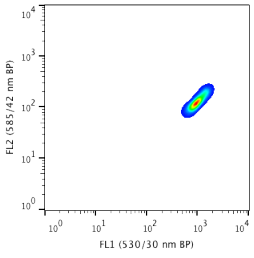	**B5:** 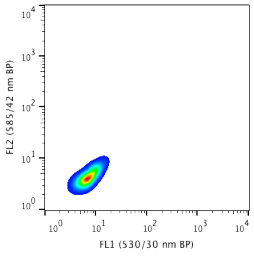	**B6:** 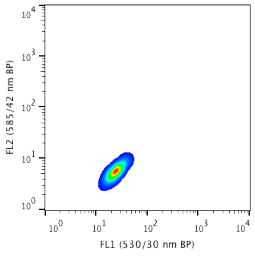

*Sequences are written in 5' to 3' direction
**FL2 *vs.* FL1 plot of barcode signal

3.2.4 Sample Selection, Collection and Viral DNA Extraction

The de-identified clinical samples were obtained from the Toronto Western Hospital Liver Clinic (protocol approved by the Research Ethics Board of the University Health Network, affiliate of the University of Toronto). All patients provided written informed consent for storage and use of their specimens for research. Patient serum was collected by venipuncture in a Vacutainer, and stood upright for 30-60 minutes. Samples were spun in a refrigerated centrifuge, and serum was aliquoted and stored at -80 °C. Viral HBV DNA was extracted using the Chemagic Viral DNA/RNA Kit (PerkinElmer).

In order to demonstrate the feasibility of using the proposed assay in a variety of settings globally, samples were chosen to represent a diverse population. Males and females were represented, with the majority of individuals being between 31-60 years of age at the time of sample collection (Figure 3.5). As HBV is a blood-borne infection, various risk factors were categorized that may have contributed to HBV infection in a clinic at a major health center in Toronto, Canada (Figure 3.5). Samples were selected to reflect diverse HBV serology, virology, and treatment. Individuals were categorized as uninfected healthy controls, anti-hepatitis B core antibodies (CoreAb) positive and hepatitis B surface antigen (HBsAg) negative (resolved infection), and various phases of chronic HBV infection including the immune tolerant phase, the immune active phase, the immune control phase, and chronic HBV on therapy. At each stage, different combinations of viral proteins may be present or absent, which also influences the level of HBV DNA. Although the assay used in this study detects viral DNA as opposed to viral proteins or ALT levels, it was essential to validate and determine whether the analytical LOD would correspond to disease stages that require immediate attention. Viral loads from 10^1 to greater than 10^9 IU/mL were included, as well as genotypes A-E, both treatment-naïve and experienced, and those with drug-resistance mutations, which were notably present in one of the regions used for our detection (Table 3.3).

3.2.5 RPA and Purification

RPA was performed using extracted DNA, primer pairs (Bio Basic Inc.), and TwistAmp® Basic kit (TwistDx). Primer pairs (FP1-FP4, and RP1-RP4, Table 3.1) were purchased HPLC-purified, and first prepared at a concentration of 100 pmol/μL in TE buffer. The stock primer solution was then diluted to 10 pmol/μL aliquots and stored at 4°C for later use. For each amplification reaction,

a premix solution containing 2.4 µL of each forward and reverse primers (10 pmol/µL), 9.2 µL of nuclease-free water, 29.5 µL of rehydration buffer, 2.5 µL of magnesium acetate (280 mM), and 4 µL of the extracted DNA was prepared in a total volume of 50 µL. For no template controls, 4 µL of nuclease-free water was added instead of extracted DNA. This solution was then transferred to a tube containing the lyophilized enzyme pellet, mixed, and incubated at 37°C for 30 minutes. For all 72 samples and no template controls, RPA was performed four times using the four primer pairs (FP1-FP4, RP1-RP4, Table 3.1) corresponding to four amplification regions (T1-T4, Table 3.1). RPA products were then purified using EZ-10 spin column DNA gel extraction kit (Bio Basic Inc.), eluted into 50 µL, visualized by agarose gel electrophoresis, and stored at 4°C until later use.

3.2.6 Singleplexed Assay

Detection probes (DP1-DP4 and DPC, Table 3.1) from IDT DNA technology were purchased HPLC-purified, modified with AF647 on 3' end (DP1-DP4, Table 3.1) or 5' end (DPC, Table 3.1), prepared at a concentration of 100 pmol/µL, and stored at 4°C in dark until later use. For each assay reaction, a premix solution containing 1 µL of conjugated microbeads (~10, 000 beads, B1-CP1, B1-CP2, B1-CP3, or B1-CP4), 1 µL of detection probes (100 pmol/µL, DP1, DP2, DP3, or DP4), 7 µL of DD water, and 10 µL of hybridization buffer (10x SSC, 0.1% SDS, heated to 60°C) making up a total volume of 19 µL was prepared. Purified RPA products were then denatured by heating at 100°C for 10 minutes and stored in ice immediately. 1 µL of denatured RPA product was mixed with 19 µL of premix solution and incubated at 37°C for 30 minutes. The assay solution was washed three times by mixing with 200 µL of washing buffer (0.5x SSC, 0.1% SDS), placing in a magnetic rack (MagnaRack, Life Technologies) for 10 minutes to allow magnetically encoded microbeads to settle to the wall of microcentrifuge tube, and removing supernatant. Washed product was resuspended in 200 µL of PBST buffer for flow cytometry (BD FACSCalibur). The assay was performed individually for all four regions across 72 samples plus no template controls using the corresponding barcode, detection probe and amplicon matches.

3.2.7 Multiplexed Assay

For all 72 samples plus 5 no template controls tested, 5 µL of RPA products from four regions were mixed into a single tube to make a final volume of 20 µL. For each assay reaction, a premix solution consisting 0.5 µL of barcode B1-CP1, 0.5 µL of barcode B2-CP2, 0.5 µL of barcode B3-

CP3, 0.5 µL of barcode B4-CP4, 0.5 µL of barcode B5-CPP, 0.5 µL of barcode B6-CPN (~5, 000 beads per barcode), 0.5 µL of detection probe DP1 (50 pmol), 0.5 µL of detection probe DP2 (50 pmol), 0.5 µL of detection probe DP3 (50 pmol), 0.5 µL of detection probe DP4 (50 pmol), 1 µL of detection probe DPC (100 pmol), 0.5 µL of positive control DNA (TP, 0.5 pmol), 1.5 µL of water, and 10 µL of hybridization buffer (10x SSC, 0.1% SDS, heated to 60^{o}C) making up a total volume of 18 µL was prepared. Mixed RPA products were then denatured by heating at 100^{o}C for 10 minutes and stored in ice immediately. 2 µL of denatured RPA product was mixed with 18 µL of premix solution and incubated at 37^{o}C for 30 minutes. The assay solution was washed three times by mixing with 200 µL of washing buffer (0.5x SSC, 0.1% SDS), placing in a magnetic rack (MagnaRack, Life Technologies) for 10 minutes to allow magnetically encoded microbeads to settle to the wall of microcentrifuge tube, and removing supernatant. Washed product was resuspended in 200 µL of PBST buffer for flow cytometry (BD FACSCalibur).

3.2.8 Data Analysis

Data was first analyzed from FlowJo software by gating the entire microbead population in FSC *vs*. SSC plot. From this subpopulation, the specific barcode population was gated, which was finally used to plot histogram of FL4 signals and calculate median intensity. For both singleplexed and multiplexed assays, FL4 signals corresponding to AF647 from detection probes were subtracted with signals from blank samples containing only conjugated barcodes in PBST buffer. FL4 median intensity values for each amplification region were then normalized to its maximum value to plot bar graphs in Figure 3.6 and Figure 3.10B. For positive and negative controls in Figure 3.10B, intensity values were normalized to the maximum intensity of positive control samples. The cutoff intensity level was calculated for each region using the following equation:

$$I_{cutoff} = Avg(I_{no\ template\ controls}) + 3*Stdev(I_{no\ template\ controls}) \qquad \textit{Equation (3)}$$

The heatmap diagram in Figure 3.10A was created using a custom-written MATLAB script that accepts normalized intensity values as an input and outputs the heatmap diagram using *imagesc* function. ROC data in Figure 3.7B, Figure 3.8, and Figure 3.14A were computed using a custom-written Matlab script that accepts normalized intensity values as an input and outputs true and false positive rates in response to varying cutoff intensity level from 0 to 1 by an increment of 0.001. Adjusted cutoff value in Figure 3.14B was determined from this output by choosing the minimum

intensity value that results in zero false positive rates. For the combinatorial analysis in Figure 3.11A, signal-to-cutoff values were first calculated for each region using the normalized intensity and I_{cutoff} values calculated above, and assigned a value of 1 or 0 according the following equations:

$$\textit{If (signal/cutoff)} \geq 1, \textit{ then } Q_{n,} = 1, \textit{ where n = barcode \#} \qquad \textit{Equation (4)}$$
$$\textit{If (signal/cutoff)} < 1, \textit{ then } Q_{n} = 0, \textit{ where n = barcode \#} \qquad \textit{Equation (5)}$$

From the above calculation, all combinations of barcodes were analyzed to determine positive or negative detection using the following equation:

$$\textit{If } [\ (Q_1 + Q_2),\ (Q_1 + Q_4),\ (Q_1 + Q_2 + Q_3),\ \textit{etc...}\ ] > 0, \textit{ then detected as positive} \qquad \textit{Equation (6)}$$
$$\textit{If } [\ (Q_1 + Q_2),\ (Q_1 + Q_4),\ (Q_1 + Q_2 + Q_3),\ \textit{etc...}\ ] = 0, \textit{ then detected as negative} \qquad \textit{Equation (7)}$$

Finally, the sensitivity and specificity are calculated using the following equation (95% confidence interval was determined using the online calculator, http://vassarstats.net/clin1.html):

$$\textit{Sensitivity} = \textit{\# of true positives / (\# of true positives + \# of false negatives)} \qquad \textit{Equation (8)}$$
$$\textit{Specificity} = \textit{\# of true negatives / (\# of true negatives + \# of false positives)} \qquad \textit{Equation (9)}$$

3.3 Results and Discussions

3.3.1 Design of QD Barcodes, RPA, and Probe Sequences.

Six QD barcodes were prepared in total by infusing various color and intensity ratios of QDs inside polymeric microbeads using CCFF[82] method (Table 3.2). To avoid overlap in the optical signals, barcode panel was prepared by using different combinations of QD concentrations and emission wavelengths. Specifically, at least 10 times difference in QD concentration between the barcodes (*e.g.* B5, B2 and B3, Table 3.2) was used which can be observed as 10 times incremental increase in the FL2 signal on flow cytometry (Figure 3.2). Also, QDs of significantly different emission wavelengths (*e.g.* B4 and B6, Table 3.2), and a combination of the various emission wavelengths (*e.g.* B1, Table 3.2) were used.

Table 3.2: List of Synthesized Microbeads

Barcode*	Diameter (µm)	Quantum Dot Concentrations (µL/mL)					
		QD506	QD547	QD560	QD580	QD596	QD615
B1	3.50 ± 1.66			5		5	5
B2	3.50 ± 1.07				10		
B3	3.50 ± 1.15				100		
B4	3.50 ± 0.96		200				
B5	2.70 ± 1.08				1		
B6	3.50 ± 0.98	168					

*All microbeads were encoded with 150µL of 7nm FeO Magnetic Nanoparticles (36.5 ng/mL). The magnetic iron (II, III) oxide nanoparticles were synthesized *via* the thermal decomposition of iron triacetylacetonate[127].

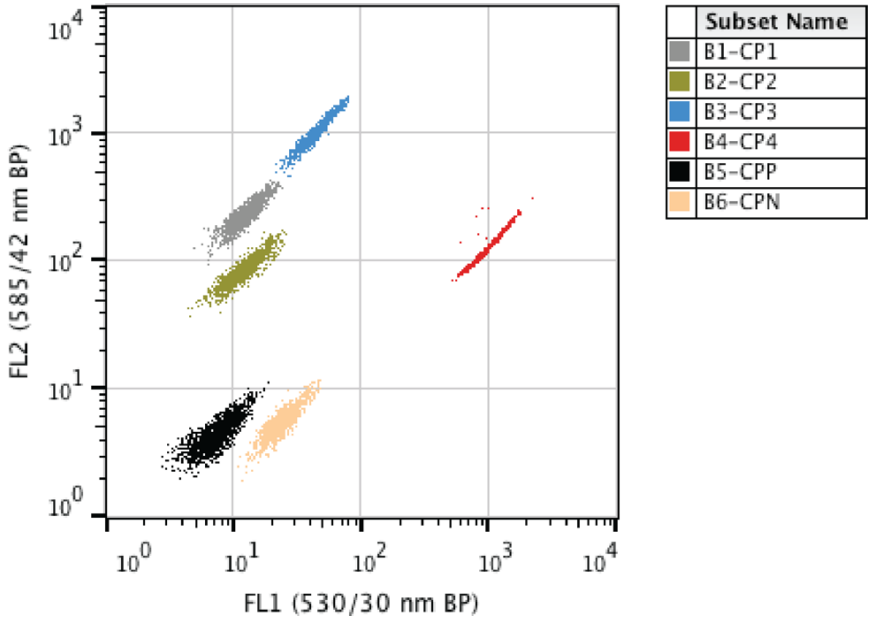

Figure 3.2: FL1 vs. FL2 Signals of Six QD Barcodes. B1-CP1, B2-CP2, B3-CP3, B4-CP4, B5-CPP, B6-CPN were used for multiplexed detection of four regions in HBV genome

For the singleplexed assay, barcode B1 was conjugated to four capture probes designed to be complementary to the first half of amplicons, and used to detect four conserved regions (R1-R4) within the HBV genome (Figure 3.3). For multiplexed assay, four barcodes were conjugated with corresponding capture probes (B1-CP1, B2-CP2, B3-CP3 and B4-CP4, Table 3.1). B5 and B6 were used as positive and negative controls during multiplexed detection and conjugated with capture probes CPP and CPN respectively. CPP and CPN sequences were designed to be complementary to genes of other sexually transmitted infectious pathogens (*Treponema pallidum* and *Neisseria gonorrhoeae* bacteria respectively), which are known to contain no similarity in their DNA sequences with respect to HBV genome, and therefore assure high specificity for the controls during our multiplexed detection.

Figure 3.3: HBV Genome. Four amplification regions in HBV genome denoted as R1, R2, R3 and R4.

The average surface density of capture probe DNA ranged from approximately $5x10^3$ to $11x10^3$ molecules/μm^2 and $3x10^3$ to $10x10^3$ molecules/μm^2 for singleplexed and multiplexed detections, respectively (Figure 3.4). The six-barcode signals were then confirmed to have unique and distinctive signatures, and to be differentiable from each other on a flow cytometer (Figure 3.2). These unique barcode signals were subsequently used for decoding multiple signals.

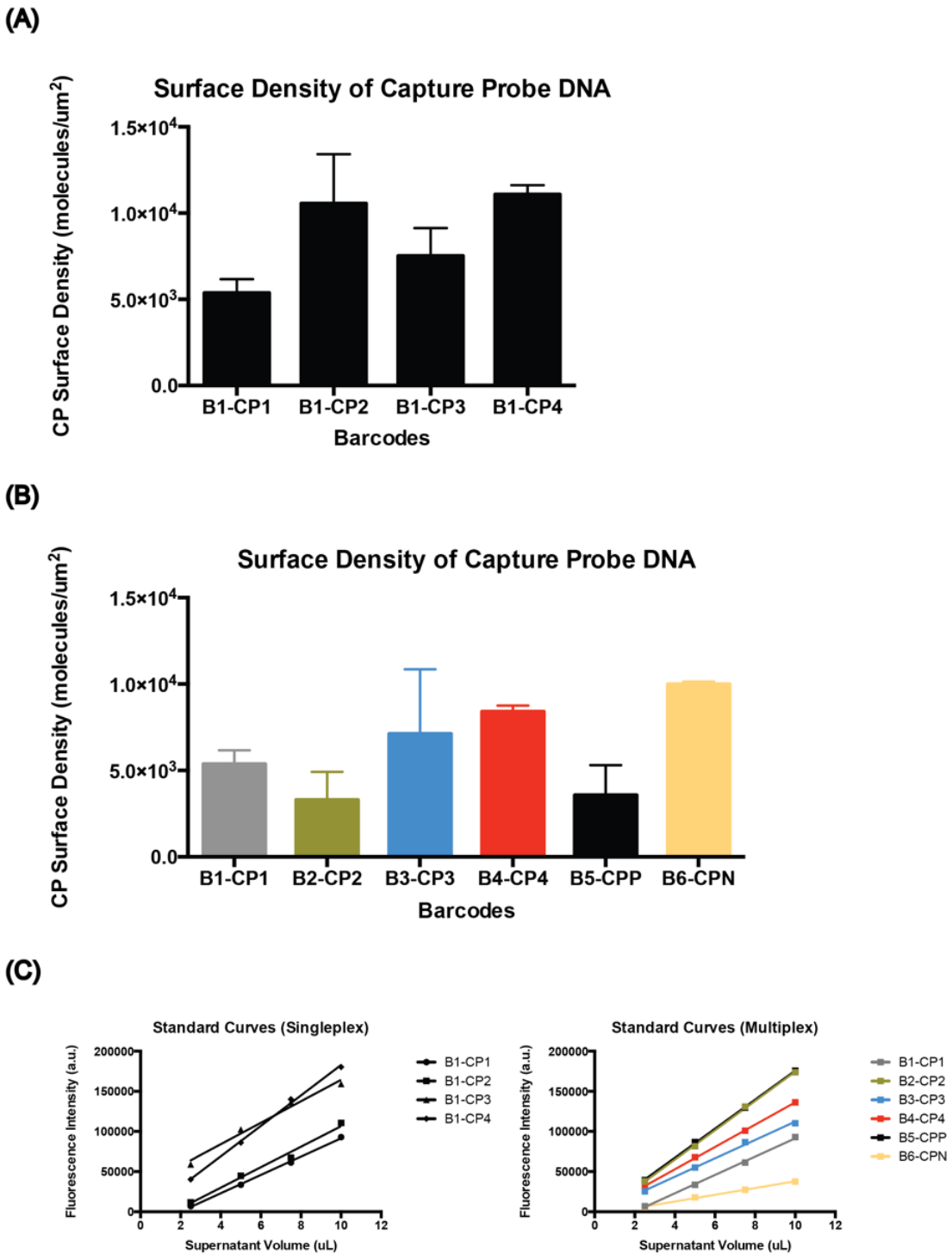

Figure 3.4: Capture Probe Surface Density. Surface density of capture probe DNA for (A) Singleplexed, and (B) Multiplexed QD barcode assays. Error bars are calculated from experimental duplicates and represent standard error of the mean. (C) Standard curves developed from no conjugation control samples for each barcode.

Sequence alignments were conducted to assess which areas of the genome would be ideal for primer binding both with respect to conservation and properties for the amplification strategy.

Ideally. amplification products would be approximately 100 nucleotides in length as longer target strands have previously been shown to lower hybridization efficiency[106], and were chosen to minimize the formation of capture and detection probe secondary structures (Table 3.1). In total, four regions within the circular HBV genome were identified as meeting all criteria for the assay (Figure 3.3). QD barcodes can then detect multiple sequences simultaneously in a single reaction, improving the probability of true-positive detection.

3.3.2 Characterization of Clinical Samples.

Seventy-two clinical samples were collected from Toronto Western Hospital Liver Clinic, and used for this study to ensure sufficient statistical power for assessing the diagnostic sensitivity (Figure 3.5). All samples were first tested by standard clinical tools to identify HBsAg, CoreAb and HBV DNA (tested by gold-standard instrument assessing HBV viral load, COBAS Amplicor HBV Monitor Test or the COBAS® AmpliPrep/COBAS® TaqMan® HBV Test, v2.0) with a lower LOD of 20-60 IU/mL. Healthy controls were negative for all markers (n=5), those with resolved past infection were negative for HBsAg and HBV DNA with detectable CoreAb (n=5) and those with chronic infection were positive for HBsAg and CoreAb with varying levels of HBV DNA (n=62). HBV DNA titres were undetectable in 11 patients on suppressive antiviral therapy and ranged from 10^1 to greater than 10^9 IU/mL in those with untreated infection (n=51). These 51 samples were identified as patients positive for HBV covering genotypes A-E, accounting for the five most common genotypes globally. Serological and clinical data are shown in Table 3.3.

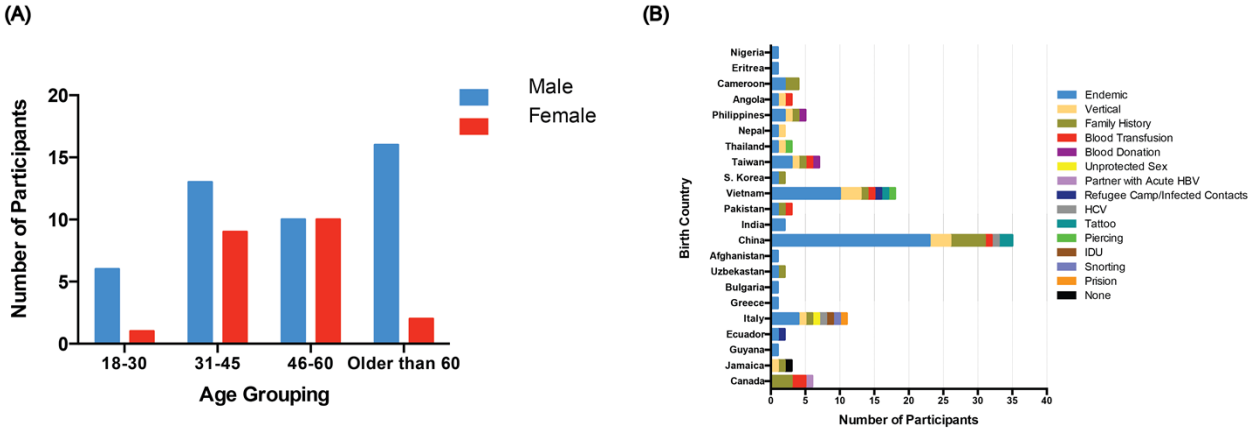

Figure 3.5: Participant Demographics. Participant demographics categorized by (A) Age and sex, and (B) Birth countries and risk factors of HBV infection.

Table 3.3: Samples Categorized by HBV Disease Markers and Viral Characteristics

Sample ID	Serology			Genotype	HBV DNA (IU/mL)[1]	ALT (U/L)[2]	Treatment History	Polymerase Drug Resistance Mutations	Detection by Barcode Region			
	Core Ab	HBsAg	HBeAg						R1	R2	R3	R4
Healthy Volunteers												
21	-	-	-	N/A	N/A	N/A	N/A	N/A	-	-	-	-
22	-	-	-	N/A	N/A	N/A	N/A	N/A	-	-	-	-
23	-	-	-	N/A	N/A	N/A	N/A	N/A	-	-	-	-
24	-	-	-	N/A	N/A	N/A	N/A	N/A	-	-	-	-
25	-	-	-	N/A	N/A	N/A	N/A	N/A	-	-	-	-
CoreAb Positive, sAg Negative (Resolved HBV Infection)												
26	+	-	-	N/A	N/A	19	N/A	N/A	-	-	-	-
27[3]	+	-	U/A	N/A	N/A	16	N/A	N/A	-	-	-	-
28	+	-	-	N/A	N/A	31	N/A	N/A	-	-	-	-
29	+	-	U/A	N/A	N/A	190	N/A	N/A	-	-	-	-
30	+	-	-	N/A	N/A	19	N/A	N/A	-	-	-	-
Immune Tolerant Phase (Detectable HBV DNA and HBeAg without Active Liver Disease)												
43	+	+	+	U/A	6.89E+04	19	Naive	N/A	-	+	+	-
39	+	+	+	U/A	3.30E+05	40	Naive	N/A	+	-	-	+
40	+	+	+	U/A	4.49E+05	18	Naive	N/A	-	+	+	-
16	+	+	+	E	9.26E+07	37	Naive	N/A	+	+	+	+
36	+	+	+	U/A	1.28E+08	37	Naive	N/A	+	+	+	+
42	+	+	+	U/A	1.70E+08	18	Naive	N/A	+	+	+	+
44	+	+	+	B	1.70E+08	39	Naive	N/A	+	+	+	+
41	+	+	+	B	1.69E+08	20	Previous Treatment[4]	U/A	+	+	+	+
45	+	+	+	U/A	1.70E+08	24	Previous Treatment[4]	U/A	+	+	+	+
Immune Active Phase (Chronic Hepatitis B with Active Liver Disease)												
15	+	+	+	B	3.66E+04	44	Naive	N/A	-	+	-	+
72	+	+	+	U/A	3.17E+05	43	Naive	N/A	+	+	+	+
70	+	+	+	E	3.80E+06	53	Naive	N/A	+	+	+	+
68	+	+	+	C	4.51E+06	48	Naive	N/A	+	+	+	+
62	+	+	+	U/A	6.15E+06	82	Naive	N/A	+	+	+	+
57	+	+	+	U/A	9.23E+06	49	Naive	N/A	+	+	+	+
63	+	+	+	U/A	1.32E+07	74	Naive	N/A	+	+	+	+
19	+	+	+	E	3.29E+07	69	Naive	N/A	-	+	+	+
18	+	+	+	B	4.31E+07	191	Naive	N/A	+	+	+	+
1	+	+	+	B	5.14E+07	353	Naive	N/A	+	+	+	+
14	+	+	+	D	6.89E+07	453	Naive	N/A	+	+	+	+
71	+	+	+	B	7.25E+07	200	Naive	N/A	+	+	+	+
5	+	+	+	B	7.33E+07	154	Naive	N/A	+	+	+	+
17	+	+	+	B	3.65E+08	284	Naive	N/A	+	+	+	+
10	+	+	+	B	5.61E+08	115	Naive	N/A	+	+	+	+
11	+	+	+	A	4.90E+04	281	*On Treatment*[4,5]	U/A	-	+	-	+
60	+	+	+	U/A	2.85E+06	90	*On Treatment*[4]	U/A	+	+	+	+
64	+	+	+	U/A	3.72E+06	686	*On Treatment*	U/A	+	+	+	+
58	+	+	+	A	6.40E+05	60	*Previous Treatment*[4]	U/A	-	-	+	+
20	+	+	-	D	6.82E+05	71	Naive	N/A	+	+	+	+
4	+	+	-	B	1.51E+06	106	Naive	N/A	+	+	+	+
47	+	+	-	U/A	8.16E+06	64	*On Treatment*	Lamivudine Resistance	-	-	+	+

46	+	+	-	U/A	1.66E+07	1034	*On Treatment*	Lamivudine Resistance	+	+	+	+
54	+	+	-	C	6.07E+08	160	*On Treatment*[4]	L180M/M204I	+	+	+	+
48	+	+	-	B	>10E+09	544	*On Treatment*[4]	Mutations at L528 and M552	+	+	+	+
Immune Control Phase (Low Level HBV DNA without HBeAg or Active Liver Disease)												
3	+	+	-	C/D	4.45E+03	28	Naive	N/A	-	+	-	-
9	+	+	-	C	2.24E+04	40	Naive	N/A	-	+	+	-
12	+	+	-	C	3.80E+04	30	Naive	N/A	-	-	-	+
Chronic Hepatitis B, on Suppressive Antiviral Therapy												
66	+	+	+	U/A	Not Detectable	13	*On Treatment*	U/A	+[6]	-	-	-
37	+	+	+	C	<20	22	On Treatment[4, 5]	U/A	-	-	-	-
2	+	+	+	C	8.33E+01	59	*On Treatment*[4]	M204I	-	+	-	-
38	+	+	+	U/A	3.88E+02	22	On Treatment[5]	U/A	-	-	-	-
8	+	+	+	A	9.76E+02	42	On Treatment	U/A	-	-	-	+
56	+	+	+	U/A	1.22E+03	49	On Treatment[5]	L80V/I, L180M, Mutation at V173, M204I	-	-	-	-
59	+	+	-	U/A	Not Detectable	29	*On Treatment*[4,5]	L80I, L180M, M204I	-	-	-	-
31	+	+	-	U/A	Not Detectable	16	*On Treatment*	U/A	-	-	-	-
32	+	+	-	U/A	Not Detectable	20	*On Treatment*	U/A	-	-	-	-
33	+	+	-	C	Not Detectable	13	*On Treatment*[4,5]	U/A	-	-	-	-
34	+	+	-	U/A	Not Detectable	25	*On Treatment*[4,5]	L80I/V, M204I	-	-	-	-
35	+	+	-	U/A	Not Detectable	36	*On Treatment*[4,5]	None	-	-	-	-
61	+	+	-	U/A	Not Detectable	14	*On Treatment*[5]	U/A	-	-	-	-
65	+	+	-	U/A	Not Detectable	30	*On Treatment*[5]	U/A	-	-	-	-
67	+	+	-	U/A	Not Detectable	17	*On Treatment*[4,5]	U/A	+[6]	-	+[6]	+[6]
69	+	+	-	U/A	Not Detectable	34	*On Treatment*[4]	U/A	-	-	-	-
53	+	+	-	U/A	1.20E+01	17	*On Treatment*[5]	Lamivudine Resistance	-	-	-	-
55	+	+	-	U/A	1.23E+02	31	*On Treatment*	Lamivudine Resistance	-	-	-	-
7	+	+	-	D	4.88E+02	41	*On Treatment*	U/A	-	-	-	-
50	+	+	-	U/A	1.23E+03	20	*On Treatment*	L180I/M204I	-	-	-	+
51	+	+	-	D	4.70E+03	35	*On Treatment*	Lamivudine Resistance	-	-	-	-
52	+	+	-	U/A	5.09E+03	13	*On Treatment*[4,5]	M204I	-	-	-	-
49	+	+	-	U/A	1.15E+04	19	*On Treatment*[4,5]	M204I	-	-	-	-
13	+	+	U/A	D	3.70E+03	49	*On Treatment*	U/A	-	-	-	-
Chronic Hepatitis B, Indeterminate Phase												
6	+	+	-	B	2.28E+08	27	Naive	N/A	+	+	+	+

[1]As reported by gold standard automated equipment.
[2]ALT >40 U/L considered elevated[154].
[3]Confirmed hepatitis C antibody positive. All other participants were either not tested or were negative for hepatitis C and/or HIV-1 and HIV-2 antibodies.
[4]Break in therapy occurred at some point during treatment history, possibility to contribute to the presence of polymerase drug resistance mutations.
[5]Treatment experience consisted of two or more polymerase inhibitors.
[6]False positive detection by multiplexing.
U/A – Unavailable
N/A – Not Applicable

3.3.3 Clinical Sensitivity and Specificity of Singleplex Assay.

A singleplex assay refers to the detection of a single genetic target. The clinical sensitivity and specificity of the four selected genetic HBV targets were determined by comparing results from the gold-standard instrument with a singleplexed QD barcode assay. Extracted viral DNA was directly used for amplification in RPA, where for each sample, the amplification was performed four times using the four primer pairs (FP1-FP4 and RP1-RP4 for forward and reverse primers respectively, Table 3.1) to produce four amplicons (T1-T4, Table 3.1). Purified and denatured amplicons were directly incubated with corresponding detection probes that are labeled with AF647 and designed to be complementary to the second half of amplicons (DP1-DP4, Table 3.1), hybridization buffer, and QD barcodes at 37^{o}C for 30 minutes, washed three times with a washing buffer, and stored in PBST buffer for flow cytometry.

Singleplexed detection of four regions is first presented as normalized detection probe intensity plots (Figure 3.6). The cutoff intensity levels (*i.e.* 3 standard deviations above the background signal) were then determined by analyzing water control samples. The results are shown in Figure 3.7A. Signal-to-cutoff value greater than or equal to 1 was considered as positive detection, whereas signal-to-cutoff value lower than 1 was considered as negative detection. The results show that detection of each individual genomic region achieved an overall clinical sensitivity ranging from 58.8% (95% CI: 44.2-72.1%) to 64.7% (95% CI: 50.0-77.2%), and a specificity of 100% (95% CI: 80.8%-100%) (Figure 3.7A). The difference in sensitivity among the four amplification regions highlights sequence-dependent amplification performance behavior, which directly affected the assay. ROC curves were also developed from the normalized intensity plots (Figure 3.7B). These ROC curves describe the tradeoff or relationship between sensitivity and specificity as the cutoff intensity level is varied from 0 to 1 on the normalized detection probe intensity plots[155], and can also be used to preset cutoff intensity values if one desires to achieve a certain target sensitivity or specificity. Lines that are closer to the top left corner on this plot indicate that

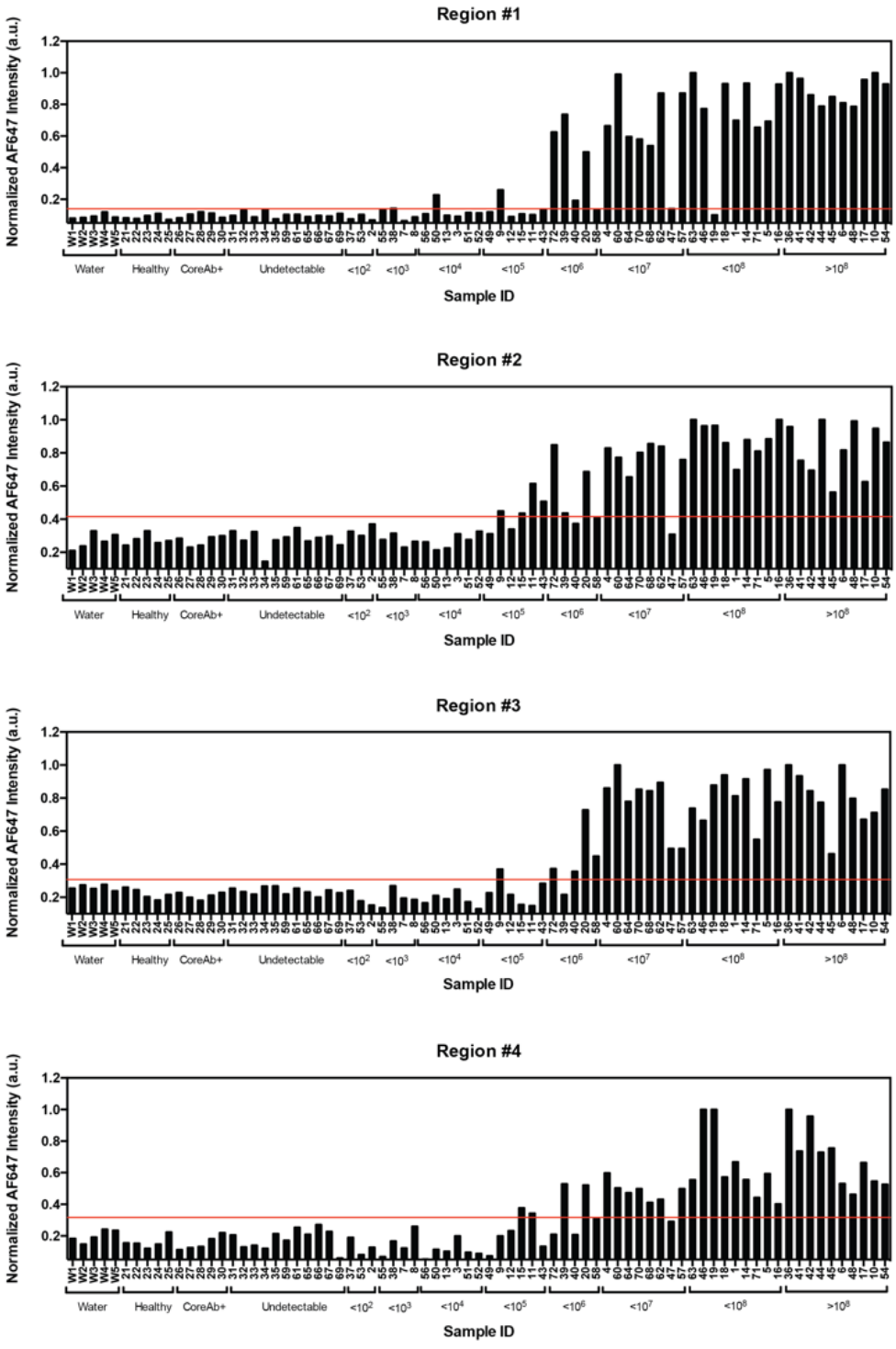

Figure 3.6: Normalized AF647 Intensity from Singleplexed Detection of Four Amplicons. Bar graphs representing normalized AF647 intensity across 72 samples screened with four amplification regions. Red lines represent cutoff intensity levels calculated from five water controls (W1-W5, 3 standard deviations above average water intensity). Samples are ordered from left to right as the following: water controls, healthy subjects, CoreAb positive, undetectable by gold standard and DNA positive samples. HBV positive samples (sample ID 1-20, 36-58, 60, 62-64, 68, 70-72) are ordered from the lowest to highest viral load in IU/ml.

they are approaching higher sensitivity and specificity levels, and any point along the diagonal line (*i.e.* Line of No Discrimination) means that the diagnostic result is no better than random guess estimations. In general, sensitivity and specificity levels were higher with Region #1 and #2 compared to Region #3 and #4. For instance, at a specificity level of 0.8, the sensitivities of Region #1 and # 2 were ~0.77 and 0.84 respectively, whereas for Region #3 and #4 sensitivities were ~0.69 and 0.67 respectively. Similarly, at a sensitivity level of 0.8, the specificities of Region #1 and #2 were ~0.67 and 0.81 respectively, whereas for Region #3 and #4 specificities were ~0.1 and 0.24 respectively. Such discrepancies suggest that RPA is favored in some regions due to more efficient primer-template binding, and the level of non-specific binding by the detection probes varies from one sequence to another. Additionally, the assay performance was analyzed to examine whether it varies among two different patient groups: 1) patients who are currently on-treatment or have previous treatment record, and 2) treatment-naïve patients (Figure 3.8). Interestingly, ROC curves are much closer to the top left corner of the plot for treatment-naïve group, suggesting that our diagnostic technique provides a better prediction of infectivity when the patients have not received treatment before.

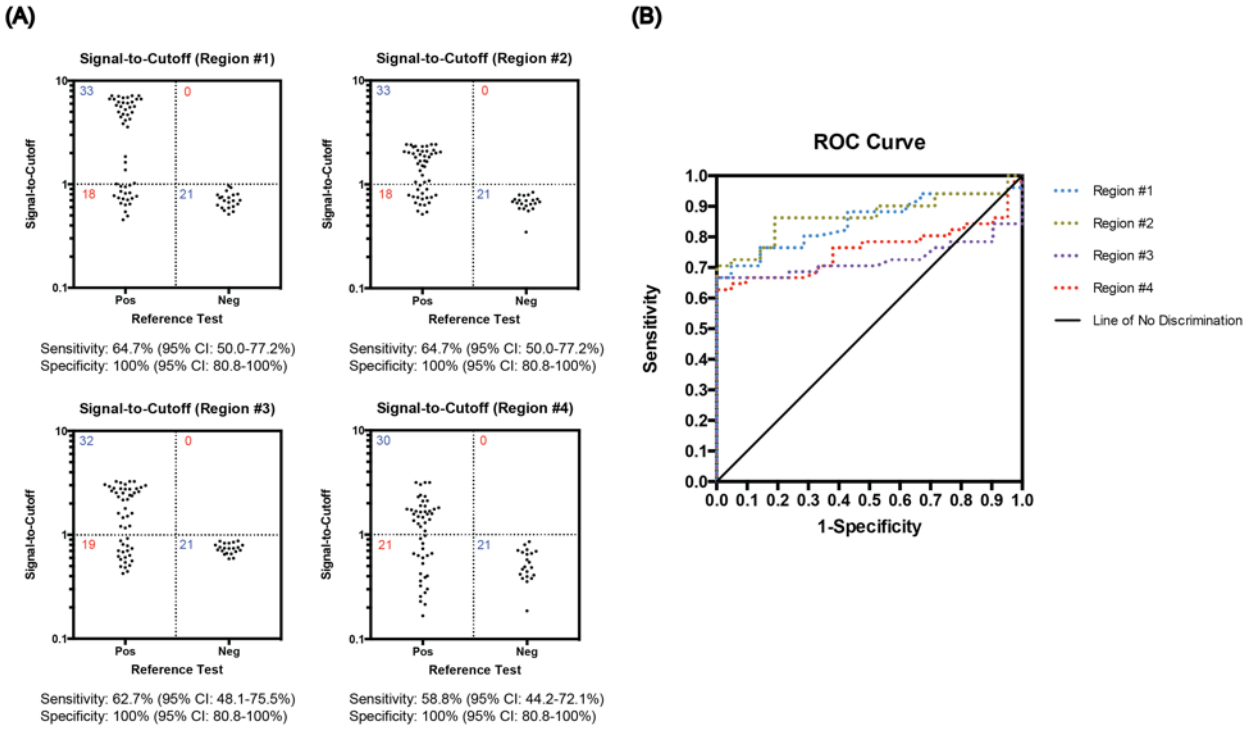

Figure 3.7: Signal-to-Cutoff ratios and ROC Curves from Singleplexed Detection. (A) Signal-to-cutoff ratios of four amplification regions relative to its reference test. (B) ROC curves developed for each region by varying cutoff intensity value from 0 to 1 by an increment of 0.001. Line of no discrimination predicts sensitivity and specificity by random guess estimations.

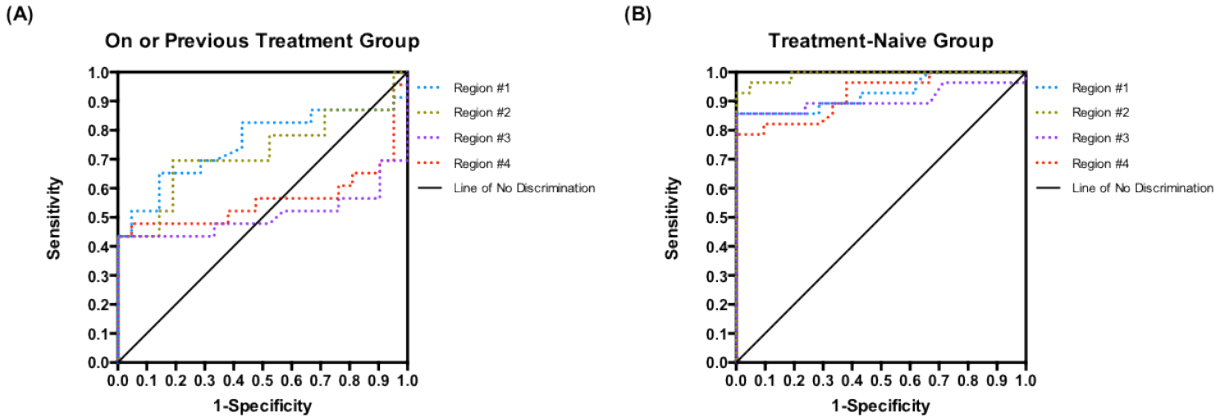

Figure 3.8: ROC Curve Analysis. Singleplexed assay performance was analyzed by separating patients into two groups: (A) Patients who are currently on-treatment or have previous treatment record, and (B) Treatment-naïve patients.

3.3.4 Multiplexed Detection of Four Amplification Regions

Next, multiplexed detection of four amplification regions was performed. Table 3.1 summarizes the six barcodes and corresponding DNA sequences used for this assay. For each sample, amplicons produced from the four regions (T1-T4) were pre-mixed, denatured and incubated with the six barcodes (B1-CP1, B2-CP2, B3-CP3, B4-CP4, B5-CPP and B6-CPN), positive control DNA (TP), detection probes (DP1-DP4 and DPC), and hybridization buffer at 37°C for 30 minutes, washed three times with a washing buffer, and stored in PBST buffer for flow cytometry. The barcode signals were then deconvoluted as shown in Figure 3.9. First, the entire barcode population was gated from debris, aggregates or artifacts using forward vs. side scatter (FSC vs. SSC) plots followed by the gating of specific barcode populations in FL1 *vs.* FL2 plot. The histogram of FL4 signal corresponding to AF647 signal from the detection probe is plotted to calculate the median

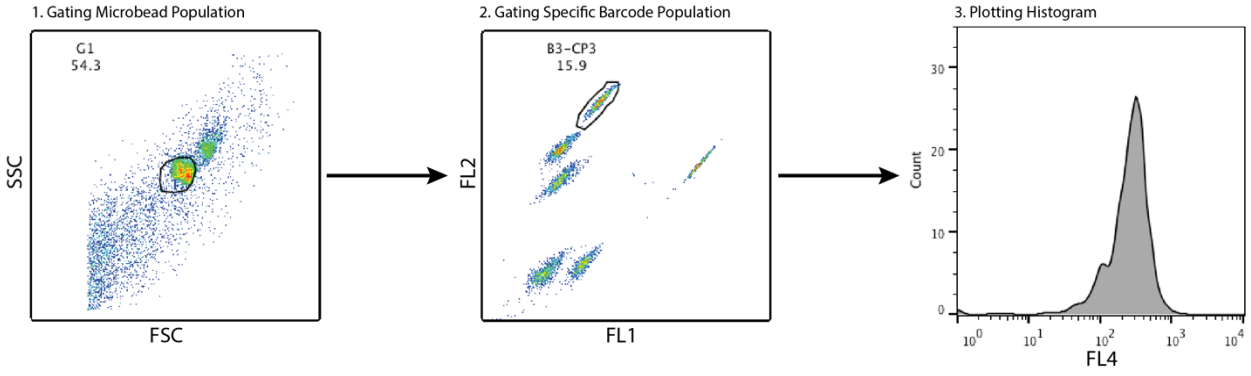

Figure 3.9: Deconvolution of Barcode Signals. Microbead population is gated in FSC *vs.* SSC plot, followed by gating of specific barcode population in FL1 (530/30 nm BP) *vs.* FL2 (585/42 nm BP) plot. Fiinally, histogram of FL4 (661//16 nm BP) signal is plotted from the gated population

intensity level. The presence of corresponding amplicons enables the formation of a sandwich structure between capture probe functionalized microbeads and detection probes, thereby producing strong FL4 signal, whereas in the absence of amplicons, there should be minimal FL4 signal detected.

For all samples tested, positive control barcodes produced signals that are at least 3-fold higher than the corresponding signals produced from negative control barcodes confirming that the assay worked correctly in a 6-plexed format (Figure 3.10). As expected from the singleplexed assay, each amplification region produced intensity profiles unique to itself across 72 samples that are screened (Figure 3.10). Similar to the singleplexed detection, five water controls were used for each region to calculate cutoff intensity levels (*i.e.* 3 standard deviations above the average water signals).

As illustrated in the heat map diagram (Figure 3.10A), it was confirmed that multiple barcodes that detect different HBV genomic regions could be performed in a single reaction vial with minimal cross-reactivity between barcodes. The genomic regions were identified by the emission of the original barcodes, and the presence of the genetic targets was identified by the emission from the secondary probes. As hypothesized, unique signals were detected across the 72 samples. There were regions that produced higher intensity signals compared to the other regions of the same HBV genome even at high viral loads, and the presence of several barcodes enhanced the rate of detection (*e.g.* samples 19, 47 and 58, Table 3.4). This finding signifies the importance of using multiple barcodes to reduce false-negative detections, and to increase the likelihood of producing true-positive diagnostic results. There are in total 4 false-positive across the four regions and out of the 21 negative samples tested. Interestingly, all false-positives were on suppressive antiviral therapy with undetectable viral loads on PCR. Also, 3 of the false-positive are from the same patient (#67), suggesting further confirmatory testing may be useful for this patient. On the other hand, all of the healthy volunteers (n=5), and resolved infection group (n=5) were correctly identified as true-negatives on the assay. Regarding the false-negatives, much of the false-negative signals arose from the on-treatment patient group or patients with previous treatment experiences (55/92 = 60%, 23 samples in this group x 4 regions = 92 in total), whereas treatment-naïve group produced significantly lower false-negative rate (17/112 = 15%, 28 samples in this group x 4 regions = 112 in total). It is speculated that this is primarily due to suppressed viral loads for on-treatment patients, and development of drug-resistant mutations after the treatment.

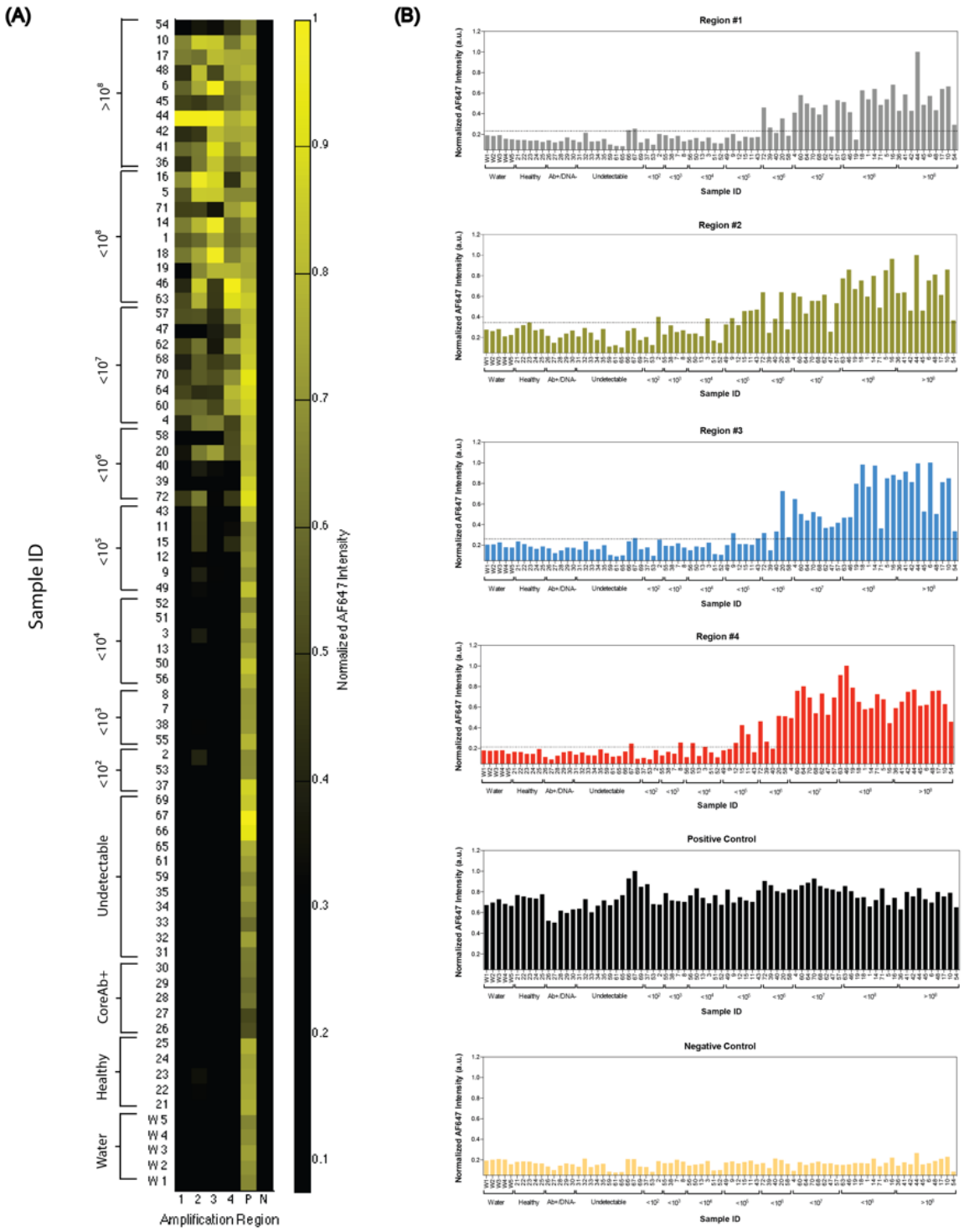

Figure 3.10: Multiplexed Detection of Four Amplification Regions. Normalized AF647 intensity across 72 samples screened with four barcodes corresponding to four amplification regions plus positive and negative control barcodes. (A) Heat map diagram (P: Positive control, N: Negative control). (B) Bar graphs. Dotted lines represent cutoff intensity levels calculated from five water controls (W1-W5, 3 standard deviations above average water intensity). Samples are ordered from left to right as the following: water controls, healthy subjects, CoreAb positive, undetectable by gold standard, and DNA positive samples.

HBV positive samples (sample ID 1-20, 36-58, 60, 62-64, 68, 70-72) are ordered from the lowest to highest viral load in IU/mL.

Table 3.4: Summary of Discordant Sample Detection

Sample ID	Viral Load IU/mL[1]	Detection by Barcode Region			
		Region 1	Region 2	Region 3	Region 4
2	8.33E+01	-	+	-	-
8	9.76E+02	-	-	-	+
50	1.23E+03	-	-	-	+
3	4.45E+03	-	+	-	+
9	2.24E+04	-	+	+	-
15	3.66E+04	-	+	-	+
12	3.80E+04	-	-	-	+
11	4.90E+04	-	+	-	+
43	6.89E+04	-	+	+	-
39	3.30E+05	+	-	-	+
40	4.49E+05	-	+	+	-
58	6.40E+05	-	-	+	+
47	8.16E+06	-	-	+	+
19	3.29E+07	-	+	+	+

[1]As reported by gold standard automated equipment.

3.3.5 Combinatorial Analysis

As a next step, we evaluated whether the combinatorial signal arising from the detection of the different genomic regions can lead to an increase in clinical sensitivity. Combinatorial analysis of clinical sensitivity was performed by calculating sensitivity for various combinations of barcodes. Positive detection was determined if one or more barcodes produced a signal above the cutoff intensity as defined in Figure 3.10. As shown in Figure 3.11, there was a systematic increase in clinical sensitivity up to combinations of two barcodes and saturation in sensitivity was observed with three and four barcodes. Also, there was an increase in the sensitivity as various sample inclusion criteria was applied (*i.e.* samples that have viral loads greater than 200, 2,000, and 20,000 IU/mL). An analytical threshold of 2,000 IU/mL was chosen because this corresponds to the level of viremia for which antiviral treatment is recommended by international treatment guidelines[15]. Individuals with viral loads greater than or equal to 2,000 IU/mL, and with elevated alanine transaminases (ALTs) require further assessment and potentially initiation of antiviral treatment (Table 3.3)[15]. For all criteria tested, a combination of B4 and B2 (Region #4 and 2 in Figure 3.10) was enough to saturate the sensitivity curves and therefore was used to calculate clinical sensitivity and specificity for samples containing viral loads greater than the clinically relevant threshold levels of 2,000 and 20,000 IU/mL. The signal-to-cutoff values shown in Figure 3.11B demonstrate

that the clinical sensitivities of 90.5% (95% CI: 76.5-96.9%) and 100% (95% CI: 88.3-100%) are achieved when 2,000 and 20,000 IU/mL thresholds are applied respectively, and clinical specificity of 95.2% (95% CI: 74.1-99.8%) is achieved. More detailed analysis of samples can be

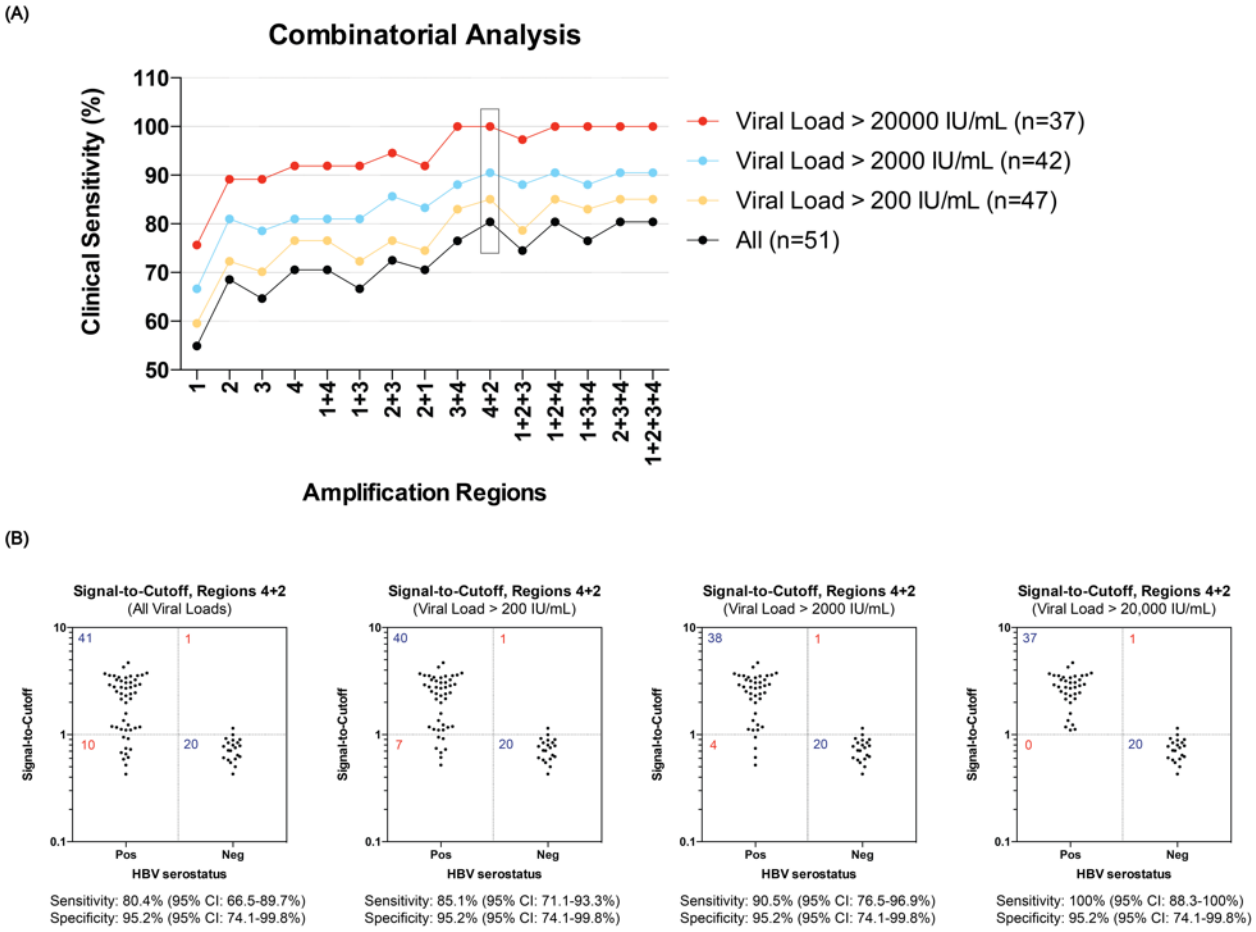

Figure 3.11: Combinatorial Analysis. (A) Effect of various barcode/amplification region combinations on clinical sensitivity. Different sample inclusion criteria were applied (samples containing viral loads greater than 200, 2000, and 20,000 IU/mL). (B) Signal-to-cutoff values with combination of Region #4 and 2 (B4 and B2) relative to its reference test for samples containing different viral loads (All, >200 IU/mL, >2000 IU/mL, and >20,000 IU/mL).

seen on Figure 3.12. The reduction in specificity compared to singleplexed detection is speculated to be caused by a higher level of non-specific binding of detection probes to the barcode surface as there are 3 times more detection probes added for multiplexed assay compared to a singleplexed assay (15 pmol/uL *vs.* 5 pmol/uL). The presence of more than one positive barcode provided a better prediction of true-positive signals. For example, only one false-positive showed positive signals arising from multiple barcodes (sample 67) and all samples with only a single positive barcode were either false positives (n=1, sample 66) or had low levels of HBV DNA (n=5, samples 2, 3, 8, 12, and 50), suggesting that further confirmatory testing may be useful for samples yielding

a single positive barcode. Furthermore, the level of non-specific binding can be reduced with various blocking strategies (*e.g.* BSA or digested BSA surface modification, Figure 3.13). An alternative method to mitigate this reduction in specificity is to preset cutoff threshold intensity

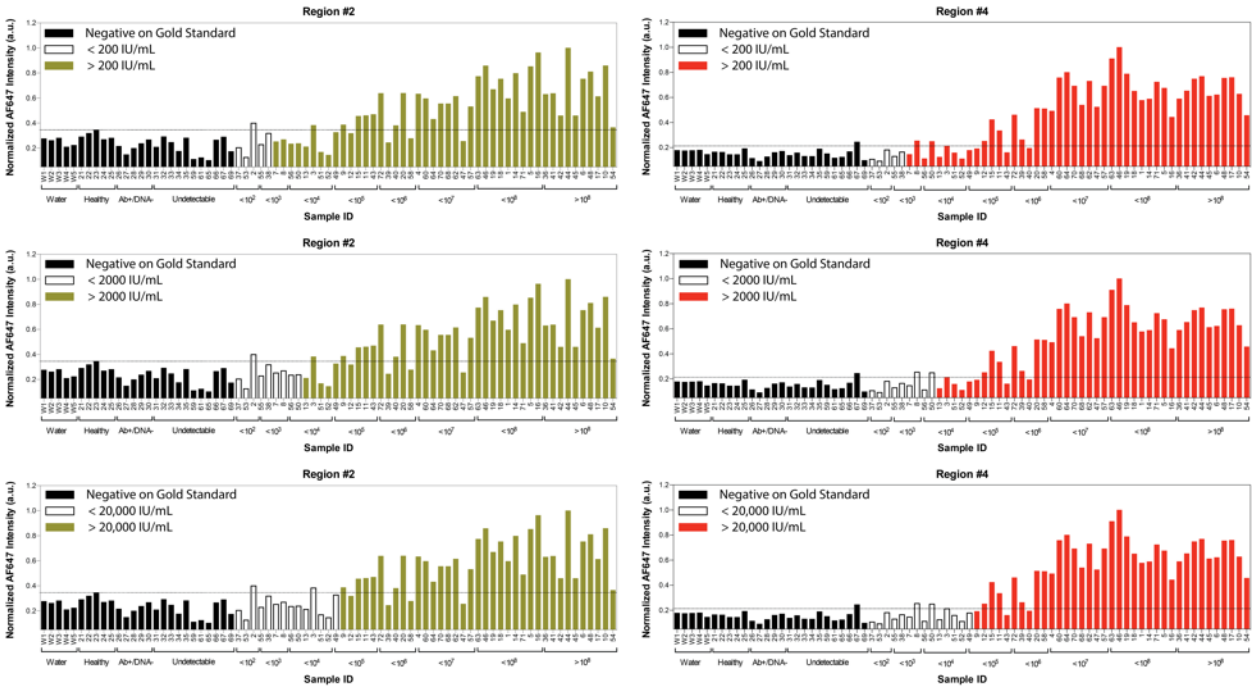

Figure 3.12: Combination Analysis of Different Viral Load Groups. Intensity bar graphs of Region #2 and #4 indicating which samples are included and excluded for clinical sensitivity calculation with various threshold levels applied (200, 2000 and 20,000 IU/mL).

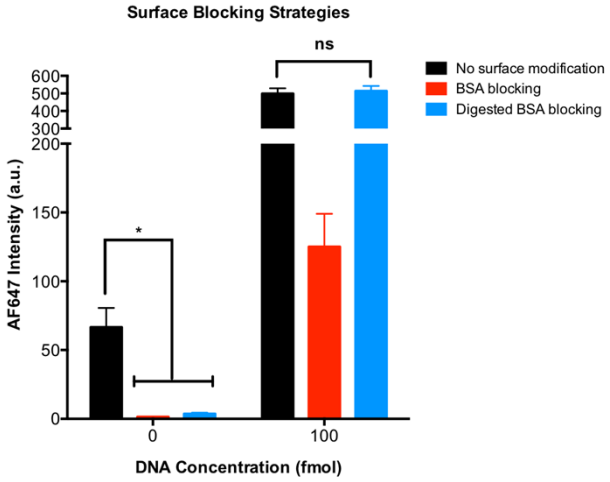

Figure 3.13: Reducing non-specific binding of detection probes. Microbead surface was passivated by BSA and Trypsin digested BSA. Both modifications sufficiently reduced the level of non-specific binding, but only digested BSA modification maintained the assay performance (*i.e.* positive signal is maintained compared to no surface modification at 100 fmol DNA concentration). Error bars are calculated from experimental duplicates and represent standard error of the mean. Statistics were calculated using unpaired, two-tailed t-test (*$p<0.05$, ns = no statistical significance).

levels by developing ROC curves as shown in Figure 3.14. Here, ROC curves were developed again for each region based on Figure 3.10, and adjusted cutoff intensity levels to achieve 100% specificity for all four regions. Applying this new threshold gave 100% specificity (95% CI: 80.8-100%) while maintaining the sensitivity level (90.5%, CI: 76.5-96.9%). Thus, these results suggest we can achieve near perfect clinical diagnosis of patients infected with HBV by using multiple QD barcodes in the detection process.

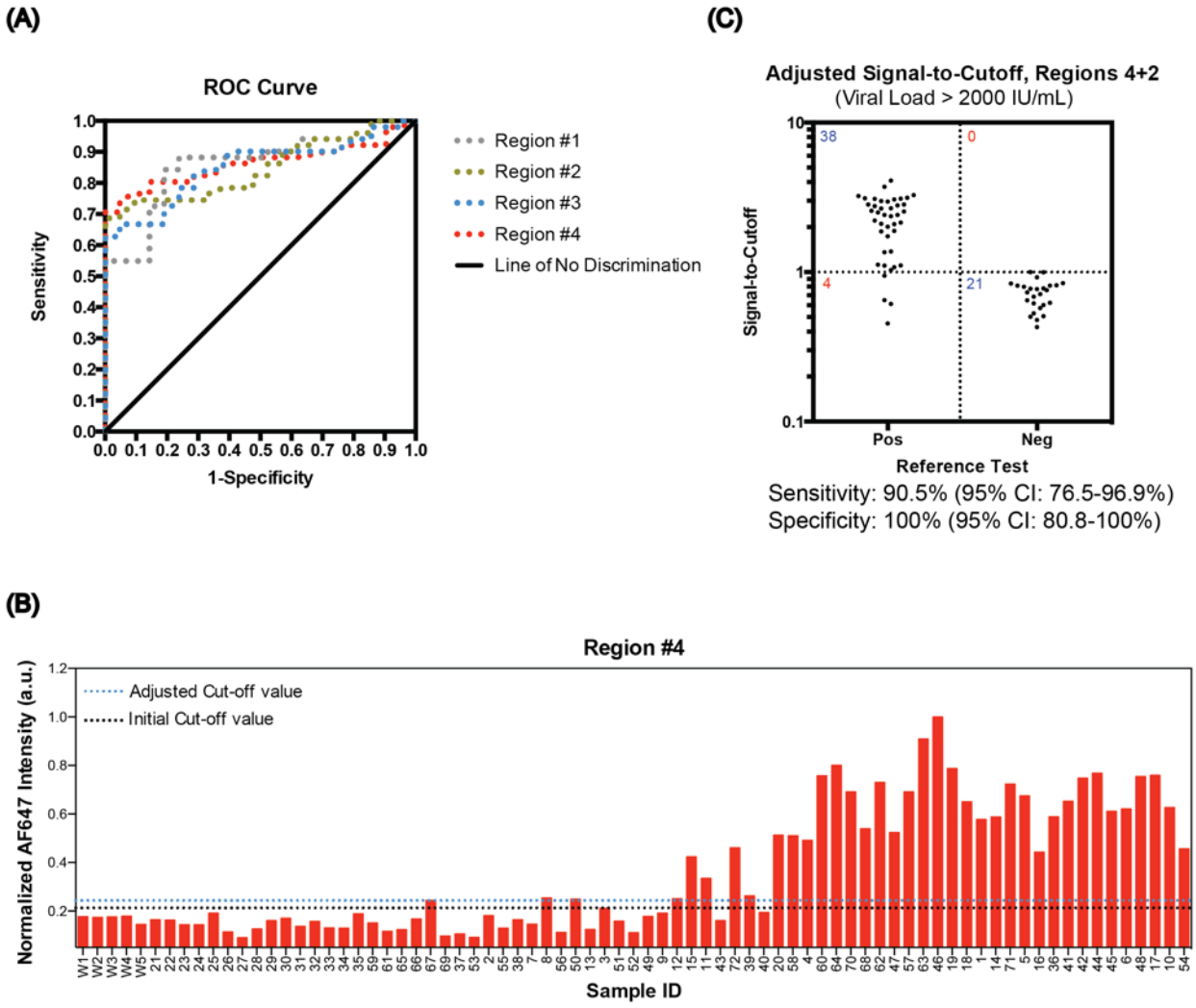

Figure 3.14: Adjusted Cutoff Intensity Level from ROC Curve. (A) ROC curves developed for each barcode/amplification region based on Figure 3.10. (B) Cutoff intensity level was adjusted according to the ROC curve to achieve 100% specificity. (C) Adjusted signal-to-cutoff values showing 100% specificity and 90.5% sensitivity with new cutoff value.

3.4 Conclusions

The work presented herein describes a full clinical validation of QD barcode technology for the diagnosis of a large number of clinical samples that represent the spectrum of disease of HBV with differing viral loads, relevant viral genotypes and both treatment-experienced and treatment-naïve populations. This combinatorial analysis demonstrated that the QD barcode diagnostic sensitivity is 54.9% (95% CI: 40.5-68.6%) with a single barcode but can be improved to 80.4% (95% CI: 66.5-89.7%) with two barcodes combination when all samples are included, and from 66.7% (95% CI: 50.4-80.0%) with a single barcode to 90.5% (95% CI: 76.5-96.9%) with two barcodes combination if the clinically relevant threshold level (2000 IU/mL) is applied (Figure 3.11). We also demonstrated that ROC curves can be developed to preset cutoff intensity levels to achieve desired specificity (Figure 3.14). With respect to those samples that are not detected by all four barcodes, there is a relationship between viral load and number of barcodes, where higher viral loads are more likely to be detected by two or more barcodes (Table 3.4). For instance, 75% (3/4) of the discordant samples with viral loads less than 10^4 IU/mL were detected by only one barcode, whereas 90% (9/10) of the discordant samples with viral loads greater than 10^4 IU/mL were detected by two or more barcodes. Thus, while the data suggest that sensitivity of a single barcode increases as the viral load increases, it is also identified that for a subset of samples, multiple barcodes are required even in the presence of high viral load.

In theory, any false-negative samples identified in this assay that were above the clinically relevant threshold of 2,000 IU/mL could fall within the error of the diagnostic assay, and therefore if repeated, the clinical sensitivity of our assay may be closer to 100%. This is evidenced by the discrepancy in clinical sensitivities reported by independent groups for the gold-standard automated HBV detection system, which are affected by HBV e antigen (eAg) status, HBV genotype, and by intra-assay variability of serum samples (reported coefficients of variation ranged from 1.22 to 8.22% for TaqMan assay)[156]. Based on the clinical data that were available, there was no difference in detection of various HBV genotypes, or samples with differing eAg status, even when these samples had viral loads near the defined analytical cut-off. Furthermore, samples with polymerase drug resistance mutations selected by available treatment (Table 3.3) were also detected by the assay, which is an important finding, as one of the detection regions included these mutations (R4, Figure 3.3). This confirms that even single nucleotide substitutions in the primer

regions will not affect the diagnostic accuracy of the test, an important consideration for constantly evolving viral pathogens.

Additionally, depending on the desired clinical need, if the diagnostic test was only to be utilized to determine patients with obviously active chronic hepatitis (*i.e.* high ALT levels and serum DNA levels greater than 20,000 IU/mL), the sensitivity would increase to 100%. These patients require therapy immediately[15]. This would be particularly applicable in settings that lack the equipment and training to perform liver biopsies and/or other investigations used to make treatment decisions.

Although HBV, a DNA virus, was used as the model for this study, this technique can also be applied to improve the diagnosis of RNA viruses like HCV or HIV by using a reverse-transcription RPA (rt-RPA) to amplify the signal. In fact, for viruses that either have similar presentations, or often no clinical presentation at all (HBV, HCV, HIV), several barcodes for each virus could be combined allowing for multiplexing of a single virus with improved sensitivity, as well as multiplexing for several viruses simultaneously. Because of the size and shape-dependent optical properties of QDs, using different combinations of QDs and varying the intensity level can theoretically design over 1 million barcodes. Thus, the use of the proposed combinatorial strategy could enable the diagnosis of a multitude of infectious pathogens with high clinical sensitivity.

Finally, the presented procedure utilizes techniques that are ideal for application in POC settings. RPA was used to replace conventional PCR for nucleic acid amplification because RPA can be performed in 30 minutes, is simple to use, and operates at a low constant temperature (37^{o}C); hence, eliminating the complexity of using an expensive thermocycler for application in low resource or remote settings[116]. RPA is also advantageous over other well-known isothermal amplification techniques like RCA, LAMP, or HDA because it is cheaper, extremely quick, power saving, and does not require complex primer design[157]. Furthermore, it has been recently demonstrated that human body heat may be employed for incubation of RPA reactions suggesting an extremely low-cost solution for operation in resource-limited settings[158]. Also, various microfluidic approaches have been shown to automate the RPA procedure and simplify sample-handling steps. Likewise, the QD barcode assay can be easily automated, and the signals can be detected using a smartphone camera as demonstrated in the previous work[93,159]. In the near future, a final black box device is envisioned with various chambers to encompass all necessary components and automate our diagnostic procedure. Each compartment will contain lyophilized

reagents to be dissolved by corresponding buffers and samples will be transferred from one compartment to another using capillaries or electrically driven flow. The barcodes will then be deposited on a substrate, imaged using the smartphone camera accompanied with various optics and excitation source, and signals will be deconvoluted *via* custom software algorithm. Such smartphone-based diagnostic system can facilitate wireless transmission of diagnostic data enabling surveillance, mapping and prediction of diseases.

One of the limitations of the current design is that RPA for multiple amplification regions was performed in a parallel setup requiring more operational time than the detection of a single amplification region. This challenge can be addressed in the near future by implementing multiplexed RPA, where multiple regions are simultaneously amplified, as demonstrated by Nickisch-Rosenegk and colleagues[160]. Also, quantification of initial viral loads will improve monitoring of disease progression and treatment response, which should be further examined by following quantitative RPA (qRPA) approach suggested by Richards-Kortum and colleagues[161]. The influence of sequence mismatches on RPA specificity and barcode detection can be further analyzed by high-throughput sequencing, and can be used for not only detecting pathogens, but also for identification of various genotypes and subspecies. Although there was a small reduction in clinical specificity with the multiplexed detection scheme, it is speculated that this is primarily due to increase in the level of non-specific binding, which can be mitigated by various surface passivation strategies, or by simply presetting cutoff intensity values that would result in desired specificity from previously developed ROC curves. In a complete POC system, extraction of genetic targets of interest need to be employed in a more streamlined format either by integrating microcapillary with FTA membrane or microfluidic approach[162-164]. Finally, the integration of extraction, amplification and detection steps into a single device unit will accelerate the transition to the POC application.

Chapter 4: Development of Colorimetric Amplification System for Clinical Diagnosis of Viral Infections

4.1 Introduction

As discussed in **Chapter 1**, infectious diseases remain as one of the major causes of morbidity and mortality posing a significant threat to global health and safety[2]. Current diagnostic approaches to combat the spread of infectious diseases include microscopy, culture, LFA, and ELISA, but these methods are slow, expensive, or have poor detection limit, precluding their use in the developing world[5]. PCR is an alternative diagnostic technique that offers high sensitivity for detection of genetic materials, but requires expensive equipment and skilled technicians[165]. As a result, there has been an increasing demand for rapid, cost-effective and sensitive POC diagnostic tests in resource-limited areas[5,166,167].

A colorimetric based diagnostic assay offers a unique advantage over other types of biosensors (*e.g.* electrochemical, magnetic, or fluorescence based assays) because it does not require an instrument for readout of the assay signals, and thus is well-suited for POC testing. As described in section **1.4.3**, a solution of GNPs changes its color from red to purple as the inter-particle distance decreases due to the coupling of surface plasmons. Owing to this optical property, GNPs have been widely explored to develop colorimetric assays based on the aggregation of nanoparticles[97,168-173]. Although these colorimetric assays are simple, fast and do not require expensive instrumentation, they are significantly limited by the low sensitivity as there are no amplification steps.

To improve the sensitivity of GNP-based colorimetric assay, the catalytic activity of MNAzyme was previously integrated with plasmon coupling of GNPs (*i.e.* MNAzyme-GNP assay)[104]. This system consists of a set of GNPs aggregated by intact linker DNA, and MNAzyme components that are activated in the presence of target DNA to cleave the linker DNA, re-distributing GNPs to a monodispersed state. The switch of GNPs from an aggregated to monodispersed state shifts the absorbance to a shorter wavelength, and correspondingly alters the solution color from dark purple to red. The inclusion of MNAzyme was demonstrated to provide multiple turnovers of catalytic activity and improve the analytical sensitivity of the assay by 600 times (10^7 – 10^9 copies/μL)[104]. Furthermore, this assay was recently used to successfully detect bacterial pathogens in clinical

urinary tract infection samples based on their 16S rRNA signatures, which are expressed in bacteria at high copy number. Nonetheless, an additional signal amplification strategy is needed to detect pathogens that require much lower detection limit for clinical diagnosis (*e.g.* 10^2-10^4 copies/μL), which is the case for many viral infections.

In this chapter, colorimetric amplification system is developed by combining RPA with MNAzyme-GNP assay to further improve the analytical sensitivity. RPA was used for nucleic acid amplification as it has been demonstrated to be a successful alternative to PCR in **Chapters 2** and **3**, which removes the difficulty of using an expensive thermocycler[108,116]. Two viral disease, HBV and InfA, were used in this study to represent diagnosis of both DNA and RNA viruses, and a major sexually transmitted and viral respiratory infections respectively.

4.2 Experimental Methods

4.2.1 Synthesis and Conjugation of 13nm GNPs

13 nm GNPs were synthesized using citrate reduction method. 1 mL of 1% HAuCl4 was added to a 250 mL flask containing 100 ml of de-ionized water under heating. When boiling add 1 ml of 3% of sodium citrate tribasic solution under vigorous stirring and at boiling temperatures. After 10 min, transfer the flask into ice box until cool down. GNPs were centrifuged down at 16000g for 35 min and the concentration of GNPs was adjusted to 100 nM. 100 μL of 100 nM gold nanoparticles was transferred into 2 clean tubes containing 40 μL 0.1% (v/v) Tween-20 and 60 μL water. 100 μL of 2.5 μM DNA-SH probe 1 was added to the first tube and 100 uL of 10 μM DNA-SH probe 2 was added to the second tube. All tubes were then incubated for 30 min at 60 °C. The GNPs were then incubated with 50 uL of 2 mM 1kDa mPEG-SH1000 to backfill the surface of the gold nanoparticles. Finally, the sample is centrifuged at 16000g for 35 min and concentration of each GNPs probe was adjusted to 11 nM and mixed together in a single tube.

4.2.2 Extraction of DNA and RNA from Clinical Specimens

DNA samples for HBV test were extracted from serum of patients and healthy subjects. Serum samples were collected by venipuncture in a Vacutainer, which were stood upright for 0.5 to 1 hour, spun in a refrigerated centrifuge, aliquoted and stored at -80 °C until later use. DNA was extracted from the aliquots using Chemagic Viral DNA/RNA Kit (PerkinElmer).

RNA samples for InfA test were extracted from mid-turbinate nasal from patients presenting with febrile respiratory illness at a tertiary acute care centre. Samples (200 μL) were extracted with EZ1 XL or EZ1 virus mini kit version (Qiagen), eluted in 60 μL and stored at -80 °C until later use.

4.2.3 RPA and rt-RPA, and Purification

RPA was performed using the TwistAmp Basic kit (TwistDx), forward and reverse primer pairs (Bio Basic Inc.), and extracted DNA samples. HPLC-purified primers (Table 4.1) were purchased, and prepared at a concentration of 100 pmol/μL in TE buffer, diluted to 10 pmol/μL aliquots, and stored at 4 °C until later use. For measurement of analytical sensitivity, a premix solution containing 2.4 μL of each forward and reverse primers (10 pmol/μL), 29.5 μL of rehydration buffer, 12.2 μL of nuclease-free water, and 2.5 μL of magnesium acetate (280 mM), and 1 μL of

the serially diluted DNA samples (10^{-1} to 10^{10} or 10^{11} copies/μL) was prepared to make a total volume of 50 μL. For the negative controls, 1 μL of nuclease-free water was added instead of template DNA. For measurement of clinical sensitivity and specificity, the premix solution contained 9.2 μL of nuclease-free water and 4 μL of the extracted DNA, and NTCs included 4 μL of nuclease-free water instead of extracted DNA. This solution was then transferred to a tube containing the lyophilized enzyme pellet, mixed and incubated at 37 °C for 30 minutes.

rt-RPA was performed using the TwistAmp Basic RT kit (TwistDx), forward and reverse primer pairs (Bio Basic Inc.), RNAse Inhibitor (BioShop Canada Inc.), and extracted RNA samples. A premix solution containing 2.6 μL of forward primer (10 pmol/μL), 3.0 μL of reverse primer (10 pmol/μL), 29.5 μL of rehydration buffer, 1.4 μL of nuclease-free water, 1 μL of RNAse Inhibitor (40 units/μL), and 2.5 μL of magnesium acetate (280 mM), and 10 μL of extracted RNA was prepared to make a total volume of 50 μL. For NTCs, 10 μL of nuclease-free water was added instead of extracted RNA. This solution was then transferred to a tube containing the lyophilized enzyme pellet, mixed and incubated at 40 °C for 30 minutes.

RPA and rt-RPA products were then purified using EZ-10 spin column DNA gel extraction kit (Bio Basic Inc.), eluted into 50 μL, visualized by agarose gel electrophoresis, and stored at 4 °C until later use.

4.2.4 Denaturation and Blocking of Amplicons

For the measurement of analytical sensitivity, 1 μL of purified RPA product, 2 μL of blocking strands mix (final concentration of 50 pmol/μL for each strand) and 2 μL of TE buffer were mixed, incubated at 95 °C for 10 minutes, and incubated for 10 minutes at 40 °C. For the measurement of HBV clinical sensitivity and specificity, 2 μL of purified RPA product, 4 μL of blocking strands mix (final concentration of 50 pmol/μL for each strand) and 4 μL of TE buffer were mixed, incubated at 95 °C for 10 minutes, and incubated for 10 minutes at 40 °C. For the measurement of InfA clinical sensitivity and specificity, 5 μL of purified rt-RPA product and 2 μL blocking strands mix (final concentration of 50 pmol/μL for each strand) were mixed, incubated at 95 °C for 10 minutes, and incubated for 10 minutes at 40 °C

For the chemical denaturation, 1 μL of RPA product, 2 μL of blocking strands mix (final concentration of 50 pmol/μL for each strand), and 1 μL of NaOH (0.1 M) were mixed, incubated at room temperature for 5 minutes, and neutralized by adding 1 μL HCL (0.1 M).

4.2.5 MNAzyme-GNP Assay

For the measurement of analytical sensitivity of HBV and InfA, 4 μL of blocked RPA amplicons of HBV or InfA samples was mixed with 1 μL of 10X MNAzyme buffer (0.1 M Tris-HCl, 0.5 M KCl, pH 8.3), 1 μL of 300 mM $MgCl_2$, 1 μL of HBV or InfA MNAzyme (4 μM), 1 μL of 1 μM Linker for HBV or 1 μL of 0.7 μM Linker for InfA, and 2 μL of water. For negative control, 5 μL of elution buffer and blocking strands mix was used. The mixture was incubated at 50 °C for 1 hr. After incubation, 10 μL of GNPs probe mixture was then added to the samples and negative control and incubated at 50 °C for 20 min to allow aggregation of GNPs. 3 μL of sample was then deposited on the surface of TLC plate. The remaining of the sample was then measured using UV-Vis spectrophotometer to record the peak absorbance wavelength. For the measurement of HBV and InfA clinical sensitivity and specificity, the same method mentioned above was used except that 6 μL of the blocked RPA amplicons were used for both HBV and InfA.

4.2.6 Quantification of RPA and rt-RPA products

The plasmid of known concentration (725 ng/μL) was serially diluted to make the following concentrations: 10, 5, 2.5, 1.25, 0.625, 0.312, 0.156 and 0 ng/μL. 6 μL of the DNA samples were mixed with 114 μL of SYBR Green (1X) to develop the standard curves, and measure the fluorescence signal of RPA or rt-RPA products. The fluorescence signals were measured using BMG Labtech plate reader. To calculate the concentration of RPA or rt-RPA products, the fluorescence signal of the sample was fitted into the equation of the line obtained from the standard curves. For instance, for HBV RPA product that was used to measure the analytical sensitivity, fluorescence signal of 123151 a.u. was fitted into the equation (y=19383x-991.5) to obtain the x-value of 6.4 ng/μL. This number was divided by the molecular weight of the amplicon (60586.25 g/mol for HBV and 149568.76 g/mol for InfA) to obtain the molar concentration and number of copies per μL.

4.3 Results and Discussions

4.3.1 Colorimetric Amplification System

Figure 4.1 demonstrates the schematic of colorimetric amplification system. Extracted viral DNA or RNA from a patient's serum (HBV) or nasal swab (InfA) is first amplified *via* RPA or rt-RPA respectively. Purified amplification products are then thermally denatured, and hybridized with blocking oligonucleotides to prevent re-hybridization with anti-sense strands. Such blocking strategy has been previously demonstrated to be an effective strategy for making binding sites available to other probes[174], and was confirmed to be an essential step in obtaining positive signals in our assay (Figure 4.2). Blocked amplicons are then mixed with MNAzyme and linker DNA, where the binding of the MNAzyme to amplicons activate the cleavage of linker DNA. Lastly, the reaction mixture is incubated with GNPs functionalized with DNA probes that are designed to hybridize with linker DNA. In the presence of target DNA, degraded linker fails to crosslink GNPs, leaving the particles monodispersed in the solution. This in turn results in a red color solution. When there is no target presence, intact linker crosslinks GNPs resulting in a dark purple color. DNA sequences of primers, blocking oligonucleotides, MNAzyme, linker DNA and GNP probes for HBV and InfA are summarized in Table 4.1.

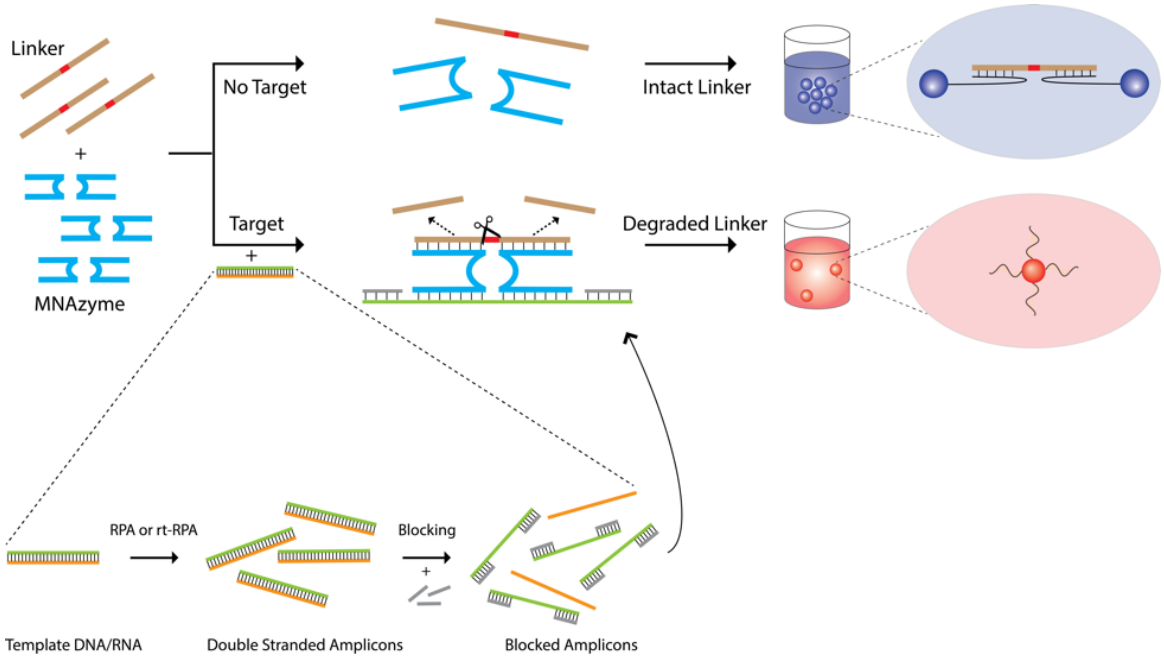

Figure 4.1: Schematic of Colorimetric Amplification System. Viral DNA or RNA is amplified *via* RPA or rt-RPA respectively followed by thermal denaturation and blocking of amplicons from re-hybridization. MNAzymes are activated by blocked amplicons, which cleave the linker DNA, distributing GNPs into a mono-dispersed state. GNPs aggregate with intact linkers in the absence of target DNA.

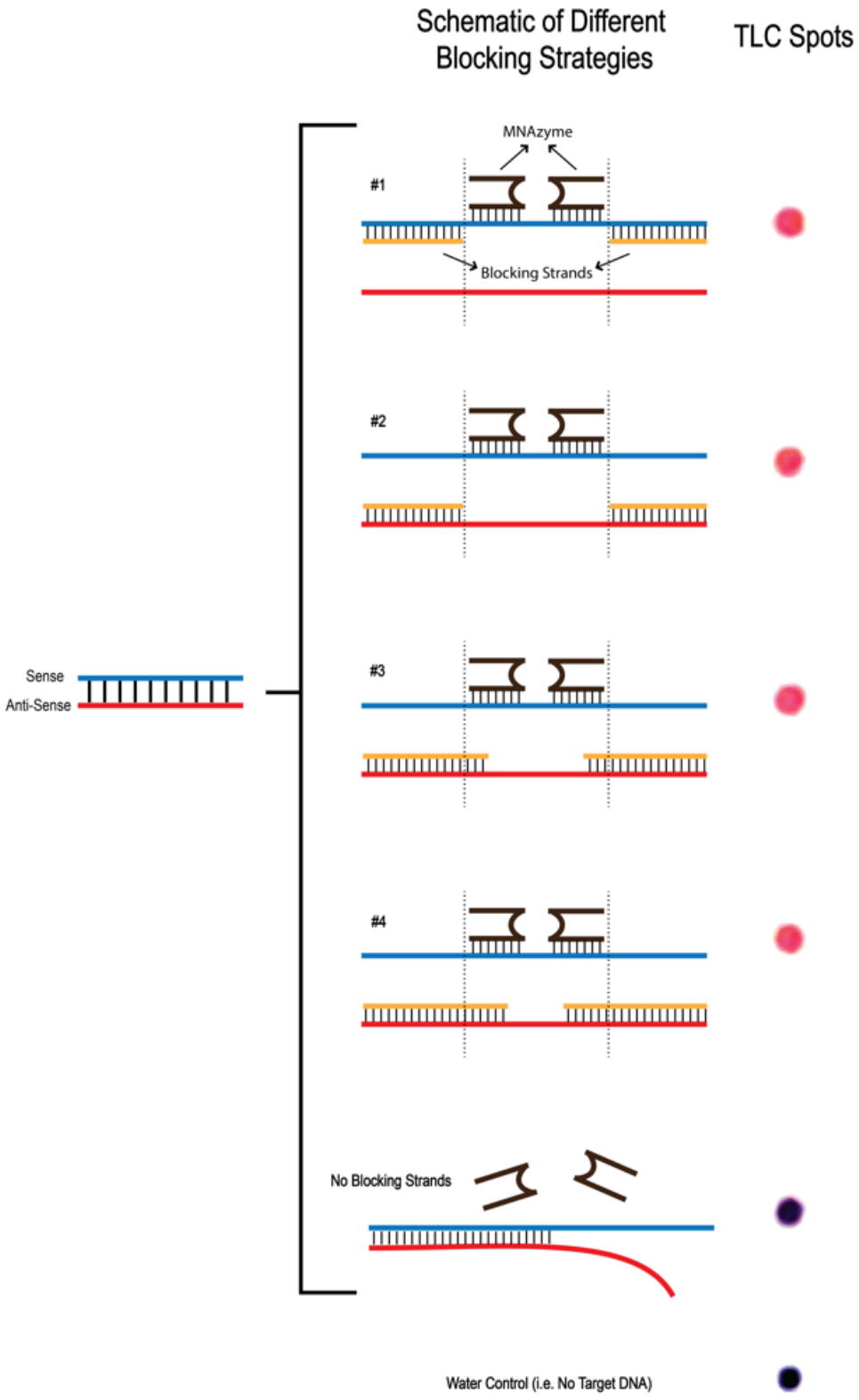

Figure 4.2: Schematic of Blocking Strategies and TLC Spot Images. Four blocking strategies were investigated and compared to the absence of blocking strands or target DNA: #1. 30 bp blocking strands hybridize to sense strand of the amplicon, #2. 30 bp blocking strands hybridize to anti-sense of the amplicon, #3. 35 bp blocking strands hybridize to anti-sense strand of the amplicon, #4. 40 bp blocking strands hybridize to anti-sense strand of the amplicon.

Table 4.1: List of DNA Sequences

	HBV (5' to 3')	InfA (5' to 3')
Forward Primer	TGTT GACAAGAATC CTCACAATAC CACAGAGTC	ATGAGYCTTY TAACCGAGGT CGAAACG
Reverse Primer	CGAA TTTTGGCCAG GACACACGGG TGTTCC	TGGACAAANC GTCTACGCTG CAG
Target	TGTT GACAAGAATC CTCACAATAC CACAGAGTCT AGACTCGTGG TGGACTTCTC TCAATTTTCT AGGGGGAACA CCCGTGTGTC CTGGCCAAAA TTCG	ATGAG TCTTCTAACC GAGGTCGAAA CGTACGTTCT CTCTATCATC CCGTCAGGCC CCCTCAAAGC CGAGATCGCG CAGAAACTTG AAGATGTCTT TGCAGGAAAG AACAC**C**GATC T**C**GAGGCTCT CATGGA**G**TGG CTAAAGACAA GACCAATCCT GTCACCTCTG ACTAAAGGGA TTTTGGGATT TGTATTCACG CTCACCGTGC CCAGTGAGCG AGGACTGCAG CGTAGACGCT TTGTCCA
Blocking Strand #1	TGTG GTATTGTGAG GATTCTTGTC AACA	CTTTCCTGCA AAGACATCTT CAAGTTTCTG CGCGATCTCG GCTTTGAGGG
Blocking Strand #2	CGAA TTTTGGCCAG GACACACGGG TGTTC	GGCCTGACGG GATGATAGAG AGAACGTACG TTTCGACCTC GGTTAGAAGA CTCAT
Blocking Strand #3	NA	TGGACAA AGCGTCTACG CTGCAGTCCT CGCTCACTGG GCACGGTGAG
Blocking Strand #4		CGTGAATACA AATCCCAAAA TCCCTTTAGT CAGAGGTGAC AGGATTGGT
MNAzyme Left arm	GACACAAAGAAGGCTAGCTGTCCACCA CGAGTCTAGACTC	CAAGATCGCTAGGCTAGCTGAGAGCCTCAA GATCTGTGTT
MNAzyme Right arm	CCCCTAGAAAATTGAGAGAAACAACGA TCTCTACGACT	CTTGTCTTTAGCCATTCCAT ACAACGAATAGTGTCACA
Linker DNA	GCGTCCCTCCTCGTATAGTCGTAGAGAR GRUTCTTTGTGTCTTCATACAATTGCACT	CGTCGCACTCACTCGTTGTGACACTATRGR UAGCGATCTTGTTGACTGTAAGCCACC
GNPs probe 1	SS—AAAAAAAAAATACGAGGAGGGACGC	HS--AAAAAAAAAACGAGTGAGTGCGACG
GNPs probe 2	AGTGCAATTGTATGAAAAAAAAAAA--SS	GGTGGCTTACAGTCAAAAAAAAAAA--SH

4.3.2 Analytical Sensitivity

The analytical sensitivity of the assay was first compared with and without the incorporation of RPA for HBV and InfA genetic targets (Figure 4.3). To make 10^{10} and 10^{11} copies/μL target DNA samples for HBV and InfA, DNA and RNA extracted from clinical specimens (Sample# 41 in Table 4.2, and Sample# 40 in Table 4.3) were first amplified using RPA and rt-RPA respectively, and the concentrations were measured by mixing with SYBR Green and developing standard curves with a plasmid of known concentration (Figure 4.4). For instance, the post-RPA HBV DNA concentration was measured to be 6.4 ng/μL (Figure 4.4A), which is equal to 6.4×10^{10} copies/μL. Compared to the initial HBV DNA concentration in the RPA mixture (=1.8×10^4 copies/μL), this corresponds to an increase in the DNA concentration by 6-orders of magnitude. The amplification products were then serially diluted from 10^{10} to 10^{-1} copies/μL for HBV and 10^{11} to 10^{-1} copies/μL for InfA. The serially diluted samples were either directly denatured and blocked, or re-amplified *via* RPA, denatured and blocked prior to mixing with the assay components. After running

MNAzyme-GNP assay, 3μL of the samples were deposited on a thin-layer chromatography (TLC) plate, and the peak absorbance wavelength of the solution was measured with a spectrometer to confirm the TLC plate result.

The inclusion of the additional amplification step demonstrated a significant improvement in the analytical sensitivity of the assay for both genetic targets. In the case of HBV detection, the TLC image reveals a shift in the spot color from dark purple to red at 10^4 DNA copies/reaction with RPA, and 10^{10} DNA copies/reaction without RPA (Figure 4.3A). This corresponds to an enhancement in the detection limit by 6-orders of magnitude, and matches the amount of increase in the DNA concentration after RPA. Quantitatively, statistically significant difference ($p<0.001$) was measured in the peak absorbance wavelength at greater than or equal to 10^4 DNA copies with RPA, and 10^{10} DNA copies without RPA when compared to the negative controls. In the case of InfA detection, there was an even greater enhancement in the analytical sensitivity. TLC image reveals a shift in the spot color at 10^3 DNA copies/reaction with RPA, and 10^{11} DNA copies/reaction without RPA (Figure 4.3B), which corresponds to an improvement in the detection limit by 8-orders of magnitude. Partially dispersed particles at 10^3 DNA copies with RPA are qualitatively seen on the plate with a red ring surrounding the black spot image, and confirmed to have a statistically significant difference ($p<0.05$) in the peak absorbance wavelength when compared to the negative control. The difference in the improvement of analytical sensitivities between HBV and InfA tests may be due to several factors. First, RPA efficiency can be hampered by the number and distribution of sequence mismatches as a result of genetic mutations at the primer binding sites[150], or due to primer-dependent artifacts[175]. Also, the catalytic activity of MNAzyme and aggregation of GNPs are dependent on the genetic sequences of amplicon and linker DNA respectively. These factors may account for the variance in the detection limits between HBV and InfA targets.

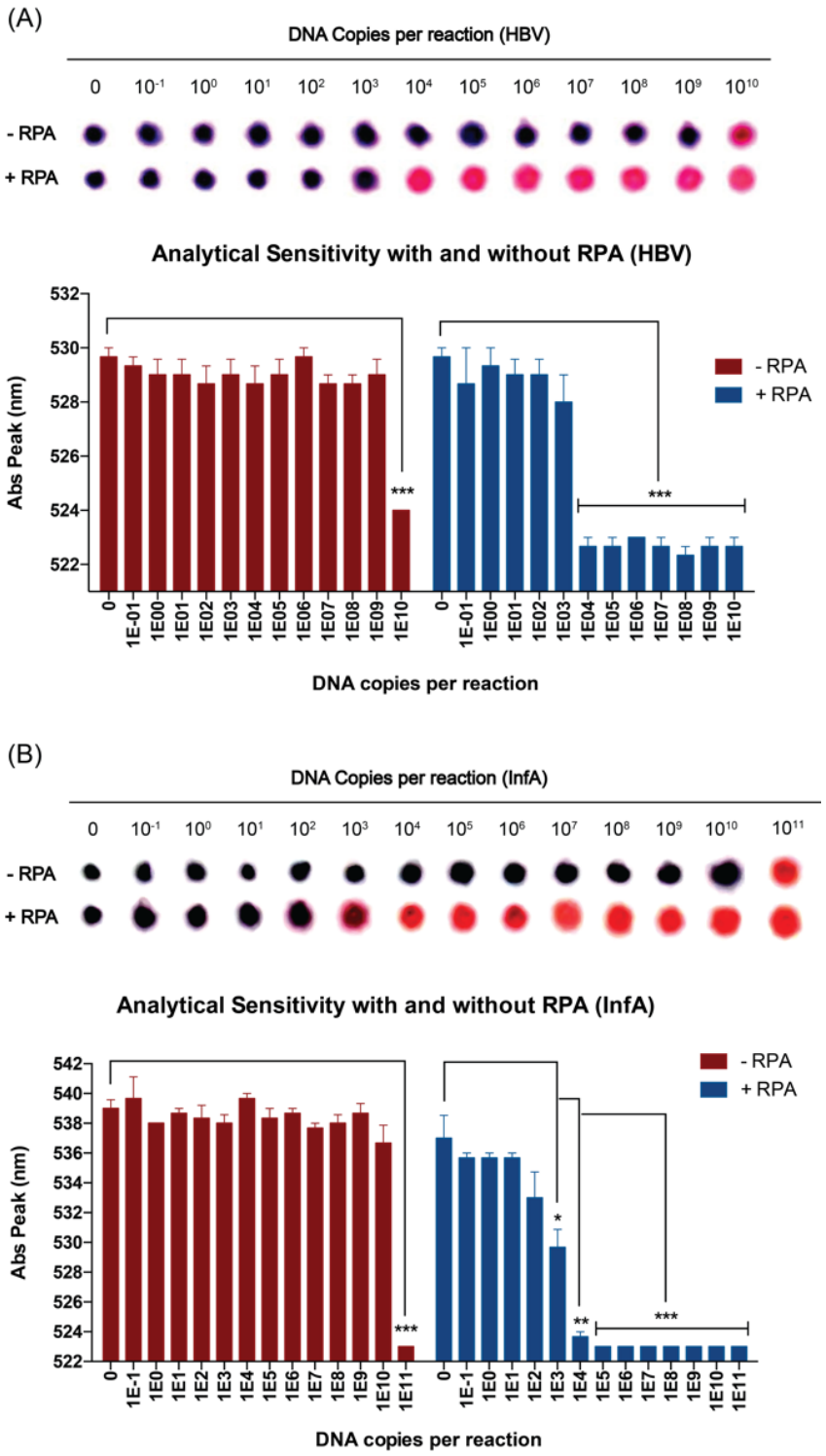

Figure 4.3: Analytical Sensitivity with and without RPA. Varying amount of (A) HBV and (B) InfA DNA was amplified *via* RPA and detected with MNAzyme-GNP assay. Spot images represent colorimetric readout on a TLC plate after adjusting for brightness and contrast on ImageJ. DNA copies refer to the amount of DNA per reaction. Bar graphs represent the wavelength of the absorbance peak. Error bars represent standard error of the mean from experimental triplicates. All statistics were calculated on excel using a two-tailed unpaired T-test assuming two-sample equal variance (*$p<0.05$, **$p<0.01$, and ***$p<0.001$).

Table 4.2: List of HBV Samples

Sample #	Serology			Genotype	HBV DNA (copies/µL)	Treatment History
	Core Ab	sAg	eAg			
Negative Samples						
1	-	-	-	N/A	N/A	N/A
2	-	-	-	N/A	N/A	N/A
3	-	-	-	N/A	N/A	N/A
4	-	-	-	N/A	N/A	N/A
5	-	-	-	N/A	N/A	N/A
6	+	-	-	N/A	N/A	N/A
7	+	-	U/A	N/A	N/A	N/A
8	+	-	-	N/A	N/A	N/A
9	+	-	U/A	N/A	N/A	N/A
10	+	-	-	N/A	N/A	N/A
11	+	+	-	U/A	Not Detectable	*On Treatment*
12	+	+	-	U/A	Not Detectable	*On Treatment*
13	+	+	-	U/A	Not Detectable	*On Treatment*
14	+	+	-	U/A	Not Detectable	*On Treatment*
15	+	+	-	U/A	Not Detectable	*On Treatment*
16	+	+	-	U/A	Not Detectable	*On Treatment*
17	+	+	-	U/A	Not Detectable	*On Treatment*
18	+	+	-	U/A	Not Detectable	*On Treatment*
19	+	+	+	U/A	Not Detectable	*On Treatment*
20	+	+	-	U/A	Not Detectable	*On Treatment*
21	+	+	-	U/A	Not Detectable	*On Treatment*
Positive Samples						
22	+	+	-	C	1.30E+02	Naive
23	+	+	-	C	2.00E+02	Naive
24	+	+	+	B	2.13E+02	Naive
25	+	+	+	A	2.58E+02	*On Treatment*
26	+	+	+	U/A	4.01E+02	Naive
27	+	+	+	U/A	1.84E+03	Naive
28	+	+	+	U/A	1.92E+03	Naive
29	+	+	+	U/A	2.61E+03	Naive
30	+	+	-	D	3.59E+03	Naive
31	+	+	+	A	3.72E+03	*Previous Treatment*
32	+	+	-	B	7.94E+03	Naive
33	+	+	+	U/A	1.66E+04	*On Treatment*
34	+	+	+	U/A	2.17E+04	*On Treatment*
35	+	+	+	U/A	3.58E+04	Naive
36	+	+	-	U/A	4.75E+04	*On Treatment*
37	+	+	+	U/A	5.37E+04	Naive
38	+	+	+	U/A	7.68E+04	Naive
39	+	+	-	U/A	9.66E+04	*On Treatment*
40	+	+	+	E	1.73E+05	Naive
41	+	+	+	B	2.27E+05	Naive
42	+	+	+	B	2.70E+05	Naive
43	+	+	+	D	3.62E+05	Naive
44	+	+	+	B	4.22E+05	Naive
45	+	+	+	E	4.87E+05	Naive
46	+	+	+	U/A	7.45E+05	Naive
47	+	+	+	B	9.84E+05	Previous Treatment
48	+	+	+	U/A	9.89E+05	Naive
49	+	+	+	B	9.89E+05	Naive
50	+	+	+	U/A	9.89E+05	Previous Treatment
51	+	+	-	B	1.20E+06	Naive
52	+	+	-	B	1.38E+06	*On Treatment*

53	+	+	+	B	1.92E+06	Naive
54	+	+	+	B	2.95E+06	Naive
55	+	+	-	C	3.19E+06	*On Treatment*
56	+	+	+	B	3.86E+05	Naive

U/A – Unavailable
N/A – Not Applicable

Table 4.3: List of InfA Samples

Sample #	Virus[1]	Year	InfA RNA (copies/μL)	RVP Fast MFI	
				Matrix	H3
Negative Samples					
1	ENR	U/A	N/A	N/A	N/A
2	ENR	U/A	N/A	N/A	N/A
3	ENR	U/A	N/A	N/A	N/A
4	HMPV	U/A	N/A	N/A	N/A
5	ENR	U/A	N/A	N/A	N/A
6	ENR	U/A	N/A	N/A	N/A
7	ENR	U/A	N/A	N/A	N/A
8	HMPV	U/A	N/A	N/A	N/A
9	ENR	U/A	N/A	N/A	N/A
10	PIV4	U/A	N/A	N/A	N/A
11	RSV	2014	N/A	N/A	N/A
12	ENR	2016	N/A	N/A	N/A
13	ENR	2016	N/A	N/A	N/A
14	RSV	2015	N/A	N/A	N/A
15	NEG	2016	N/A	N/A	N/A
16	NEG	2016	N/A	N/A	N/A
17	NEG	2016	N/A	N/A	N/A
18	RSV	2015	N/A	N/A	N/A
19	RSV	2015	N/A	N/A	N/A
20	ENR	2016	N/A	N/A	N/A
Positive Samples					
22	H3N2	2014	3.35E+04	2.87E+03	3.54E+03
23	H3N2	U/A	3.28E+05	2.49E+03	6.60E+02
24	H3N2	2015	7.83E+04	2.45E+03	1.80E+03
25	H3N2	2015	1.32E+05	2.87E+03	2.90E+03
26	H3N2	2015	5.04E+05	3.07E+03	3.92E+03
27	H3N2	2015	3.99E+03	2.61E+03	3.47E+02
28	H3N2	2015	2.11E+05	2.67E+03	2.70E+03
29	H3N2	2016	9.24E+05	1.75E+03	2.22E+03
30	H3N2	2016	4.80E+06	2.06E+03	1.99E+03
31	H3N2	2016	3.51E+06	2.40E+03	2.58E+03
32	H3N2	2016	1.21E+05	2.31E+03	8.58E+02
33	H3N2	2016	6.99E+04	2.44E+03	3.83E+02
34	H3N2	2016	3.31E+05	2.32E+03	1.57E+03
35	H3N2	2016	3.14E+06	2.45E+03	2.79E+03
36	H3N2	2016	4.69E+05	2.52E+03	1.70E+03
37	H3N2	2016	7.37E+05	2.20E+03	2.31E+03
38	H3N2	2016	1.75E+06	2.17E+03	1.19E+03
39	H3N2	2016	9.04E+05	6.03E+03	3.39E+03
40	H3N2	2016	U/A	2.06E+03	1.99E+03
41	H3N2	2016	U/A	2.52E+03	1.70E+03
42	H3N2	2016	U/A	2.20E+03	2.31E+03

43	H3N2	2016	U/A	2.45E+03	2.79E+03
44	H3N2	2016	U/A	2.17E+03	1.19E+03
45	H3N2	2016	2.49E+05	2.98E+03	1.36E+03
46	H3N2	2015	1.91E+05	2.93E+03	3.56E+03
47	H3N2	2015	2.60E+04	2.68E+03	1.24E+03
48	H3N2	2016	1.73E+06	2.04E+03	2.15E+03
49	H3N2	2016	7.66E+05	2.27E+03	1.79E+03

[1]ENR – Enterovirus, HMPV – Human metapneumovirus, PIV4 – Parainfluenza virus type 4, RSV – Respiratory syncytial virus, H3N2 – Influenza A virus subtype H3N2, NEG – Negative
U/A – Unavailable
N/A – Not Applicable

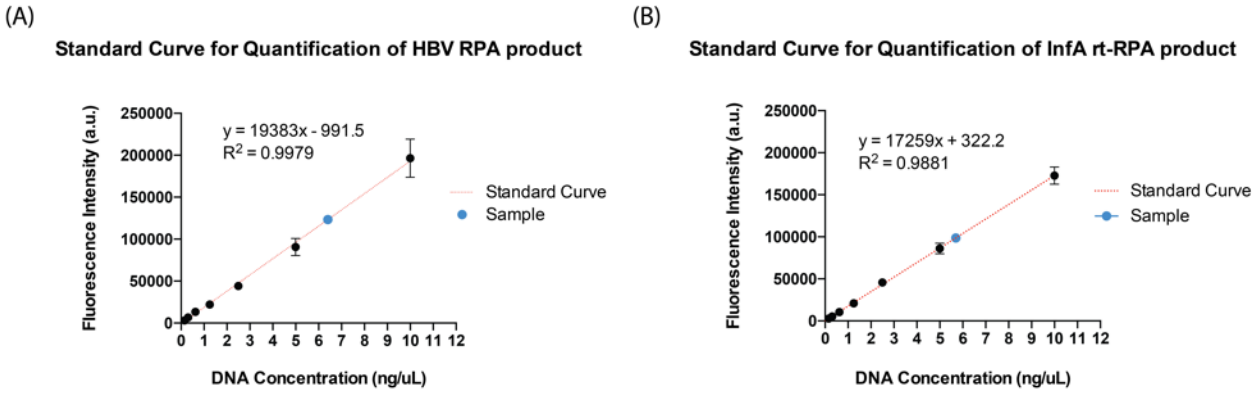

Figure 4.4: Quantification of RPA and rt-RPA products. Standard curves developed for the quantification (A) HBV RPA and (B) InfA rt-RPA products. Serially diluted plasmid of known concentration was mixed with SYBR Green (1X), and the fluorescence signal was measured using a plate reader. The fluorescence intensity of InfA rt-RPA sample was obtained from 18 times diluted concentration because the full concentration generated intensity level that is beyond the standard curve range. Error bars represent standard error of the mean from experimental triplicates.

4.3.3 Clinical Sensitivity and Specificity

Next, the clinical sensitivity and specificity of colorimetric amplification system was measured by screening clinical specimens in a blinded-experiment (Figure 4.5). The evaluation of emerging diagnostic technologies using clinical metrics is an important step in the translation of bench-side research work to clinical applications[105]. Clinical sensitivity and specificity indicate the degree of true-positive and true-negative rates compared to a reference diagnostic test respectively, and can directly influence the diagnostic decisions of healthcare providers[176,177]. HBV samples of various genotypes (A-E) and viral loads ($1x10^2$ to $3x10^6$ copies/μL) were selected to represent different spectrum of the disease (Table 4.2). For InfA test, H3N2 subtype was chosen with the viral loads ranging from $4x10^3$ to $5x10^6$ copies/μL (Table 4.3). For testing HBV, a total of 56 clinical samples (21 negative and 35 positive) were collected from Toronto Western Hospital Liver Clinic, and the presence of the infection was confirmed according to current clinical procedures by testing for HBsAg, anti-hepatitis B CoreAb, and HBV DNA (COBAS Amplicor HBV Monitor Test or

COBAS AmpliPrep/COBAS TaqMan HBV Test v2.0). For InfA test, a total of 48 clinical samples (20 negative and 28 positive) were collected from Sunnybrook Health Sciences Centre, and tested for InfA RNA using the Luminex xTAG Respiratory Viral Panel Fast test. Extracted viral DNA and RNA from clinical specimens were amplified *via* RPA and rt-RPA respectively. Purified, denatured and blocked amplicons were then incubated with the MNAzyme assay components, transferred to GNP solutions, and spotted on a TLC plate.

Detection of HBV viral DNA achieved a clinical sensitivity of 91.4% (95% CI, 75.8-97.8%), and a specificity of 95.2% (95% CI, 74.1-99.8%). InfA test achieved a clinical sensitivity of 92.9% (95% CI, 75.0-98.8%), and a specificity of 100.0% (95% CI, 80.0-100.0%). Two types of negative controls were used in these experiments to ensure correct interpretation of diagnostic results. The first control was EBS control composed of elution buffer of DNA purification kit and blocking strands. This control was mixed with MNAzyme assay components and transferred to GNP solutions to confirm proper aggregation of GNPs with inactive MNAzyme and intact linker DNA. The second control was NTC, which replaced viral DNA or RNA with water in RPA or rt-RPA reactions to ensure that there is no target nucleic acid contamination in the reagents. These two controls confirmed that the positive signals are obtained by the selective activation of MNAzyme in the presence of corresponding amplicons, and not due to improper aggregation of GNPs or contamination in RPA or rt-RPA reactions.

The false-negative results (sample# 23-25 for HBV, and 27 and 47 for InfA, Figure 4.5) may be caused by genetic mutations that are prevalent in viral genomes hampering RPA and rt-RPA reactions[150], or the hybridization of amplicons to MNAzyme binding sites. Bioinformatics analysis on sequence variability can alleviate these problems by allowing the design of better degenerate primers and MNAzyme components that can tolerate few genetic mutations.

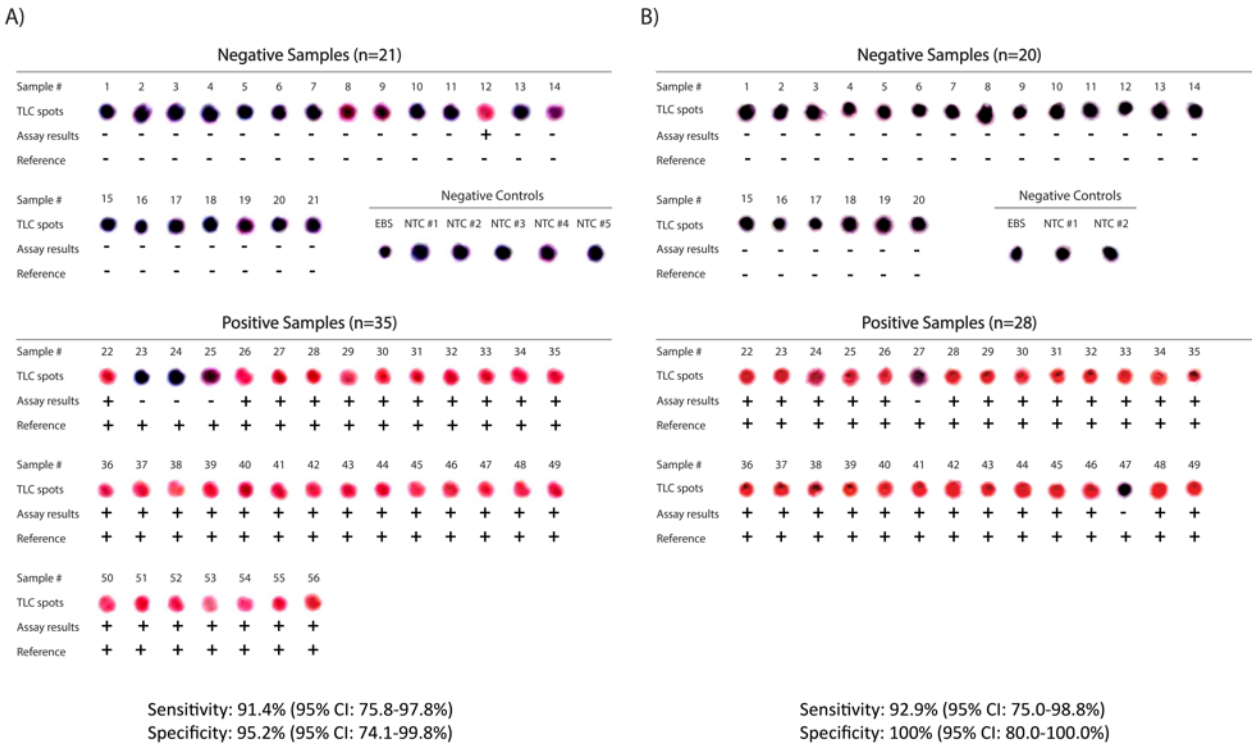

Figure 4.5: Clinical Sensitivity and Specificity Measurements. Colorimetric readout of clinical samples on a TLC plate after adjusting for brightness and contrast on ImageJ for detection of (A) HBV viral DNA, and (B) InfA viral RNA. "EBS" refers to elution buffer blocking strands control, which was used to test the aggregation of GNPs. "NTC" refers to no template control, which was used to test contamination in RPA. "Reference" row indicates the diagnostic results from standard clinical tests. 95% confidence intervals were determined using the online calculator (http://vassarstats.net/clin1.html).

4.4 Conclusions

In summary, the work presented herein describes the integration of RPA with MNAzyme-GNP assay for POC diagnosis of viral infections. The incorporation of RPA improved the analytical sensitivity of the assay by 6-orders of magnitude for the detection of HBV, and by 8-orders of magnitude for the detection of InfA. Over 90% clinical sensitivity and 95% clinical specificity were measured when clinical specimens were screened using the colorimetric amplification system in a blinded manner. This system is well-suited for rapid, cost-effective and sensitive diagnosis of viral diseases in POC settings since the entire assay can be performed within 2 hours, does not require expensive equipment, and can detect as low as 10^3 copies of genetic materials. Although MNAzyme was incubated with amplicons and linker DNA for 1 hour in the experiments, the assay performance was also investigated at shorter incubation periods, and demonstrated that the assay can produce the same level of positive signals with 10 minutes of MNAzyme incubation (Figure 4.6). Hence, the entire assay can potentially be performed within 1 hour (30 minutes of RPA, 10 minutes of MNAzyme, and 20 minutes of GNP aggregation steps).

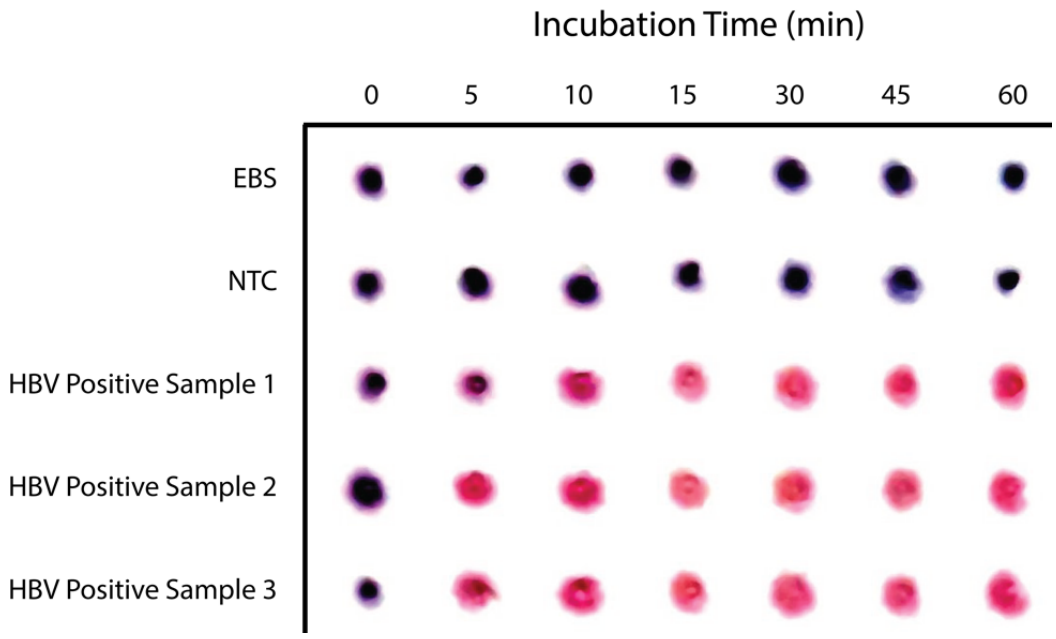

Figure 4.6: Shortening MNAzyme Incubation Time. Different MNAzyme incubation time periods (0, 5, 10, 15, 30, 45 and 60 minutes) were investigated with 3 HBV-positive samples. MNAzyme activation was effective down to 10 minutes of incubation.

Chemical denaturation method will be incorporated in the near future to replace the thermal denaturation of amplification products[178]. The denaturation of double-stranded RPA products was examined using NaOH, which was proven to be as effective as thermal denaturation method for

generating single-stranded DNA that can hybridize with blocking oligonucleotides to prevent re-hybridization with anti-sense strands (Figure 4.7). This strategy will be useful in resource-limited settings where heating devices are unavailable for thermal denaturation of amplicons.

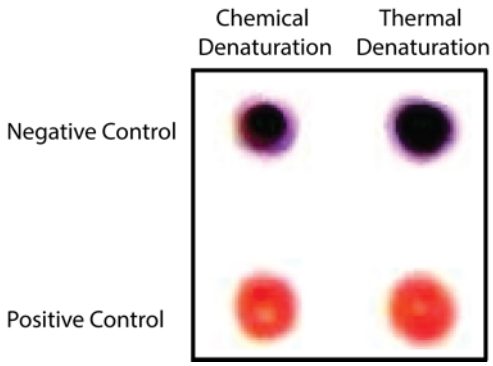

Figure 4.7: Chemical *vs.* Thermal Denaturation of RPA products. RPA products mixed with blocking oligonucleotides were denatured either chemically by incubating with NaOH or thermally by incubating at 95 °C.

The current post-RPA purification step involves the use of spin-columns to collect amplified DNA while removing proteins used in the RPA reaction. This step is unfeasible in resource-poor areas with limited availability of centrifuge instruments, and can be simplified using proteinase K (Figure 4.8). Proteinase K can rapidly digest proteins involved in the RPA reaction[179], which can prevent undesirable interaction of RPA proteins with DNA in MNAzyme-GNP assay after the amplification.

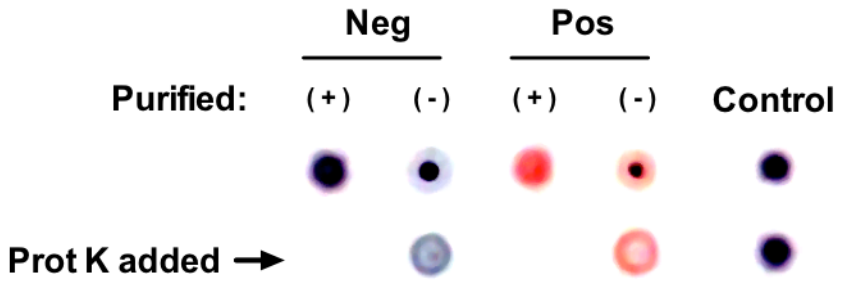

Figure 4.8: Post-RPA Purification by Proteinase K. RPA products were compared with and without spin-column purification. Unpurified samples that produced aggregated spots at the core were mixed with Proteinase K to prevent undesirable interaction between RPA proteins and DNA in MNAzyme-GNP assay.

In addition, panels of colorimetric amplification system components can be developed in the future to demonstrate a parallel detection of related sexually transmitted diseases (*e.g.* HBV, HCV and HIV), or respiratory viruses (*e.g.* InfA, influenza B virus, rhinovirus, and respiratory syncytial

virus), and also their respective subtypes. Non-specific MNAzymes do not get activated allowing analysis of multiple targets in parallel (Figure 4.9).

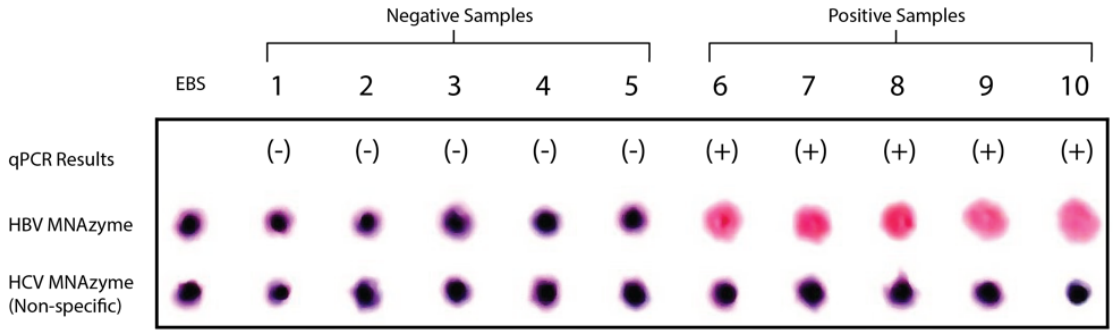

Figure 4.9: Cross-reactivity of MNAzyme-GNP assay. Five HBV-positive RPA products were incubated with specific HBV MNAzyme, and non-specific HCV MNAzyme.

Lastly, a field testing with larger sample size is required to fully assess the capability of diagnosing patients in POC settings.

Chapter 5: Screening Genetic Biomarkers of Antibiotic Resistance using Colorimetric Amplification System

5.1 Introduction

Extensive and improper use of antibiotics have led to rapid evolution of antibiotic resistance (AR) over the past decades[29,180]. Particularly, there is an emerging trend of multi-drug resistant (MDR) pathogens, which have acquired resistances to multiple antibiotics. Rapid, accurate and sensitive diagnostic approaches that can detect multiple AR determinants are needed to enable healthcare professionals to provide appropriate therapy and reduce the development of new resistance mechanisms[44,181-183]. These techniques should be simple, instrument-free and adaptable for use in remote locations and in countries with limited resources where screening for AR is inadequate[33]. Currently, there are two major laboratory techniques for detection of AR, which are culture-based phenotypic test and molecular-level genotypic test. Although phenotypic culture methods such as agar diffusion, microdilution, or selective chromogenic media are cost-effective, they take 24-72 hours to achieve an accurate diagnosis[44,183-186]. In addition, pathogens that carry AR genes can appear as phenotypically antibiotic sensitive due to the lack of gene expression or the decreased potency of the antibiotic, producing false-negative results[187-190]. This lack of resistance gene expression or the decreased potency of the antibiotic can be influenced by several environmental factors such as temperature, pH and NaCl content of the culture medium, and therefore the results might not represent actual bacterial resistance in human host[191,192]. In contrast, genotypic tests can directly detect the presence of AR genes, are not affected by testing conditions, and are often used to confirm inconclusive phenotypic test results[193-196] (Figure 5.1). Another advantage of these genotypic tests includes the improved safety, since they can be carried out using inactivated or sterilized samples[182]. The gold standard technique for genetic detection is quantitative polymerase chain reaction (qPCR), which offers high sensitivity. However, qPCR is expensive, uses complex equipment, and requires highly skilled technicians, precluding its use in resource-limited areas. To circumvent the problems with current AR screening technologies, there has been an effort to develop new methods for screening AR such as microfluidic culture based techniques and nanomaterial-based nucleic acid assays[116,197-203]. However, these techniques are either phenotypic, have insufficient sensitivity, focus on detection of only a single AR determinant, or still rely on PCR for amplification of target DNA.

This chapter describes the development of an instrument-free, rapid, simple and highly sensitive technique that can detect multiple AR determinants. As a continuation of **Chapter 4**, this system utilizes RPA to achieve high sensitivity[116], followed by the colorimetric readout that is based on MNAzyme-GNP system[104]. Multiplexed RPA was incorporated into the system to demonstrate simultaneous amplification of multiple AR genes, followed by parallel detection of amplified products using a panel of MNAzyme-GNP designs. The assay was developed to detect 10 different genes responsible for resistance to 5 major antibiotics in MRSA, which is the most common AR pathogen[204,205]. The analytical sensitivity and cross-reactivity of the assay were examined, followed by the genotypic AR profiling of 3 clinical isolates, which was compared with phenotypic test results. The described system presents a method for simple and cost effective clinical detection and profiling of antibiotic resistance in bacterial pathogens, which can be easily adapted to both centralized and remote testing locations.

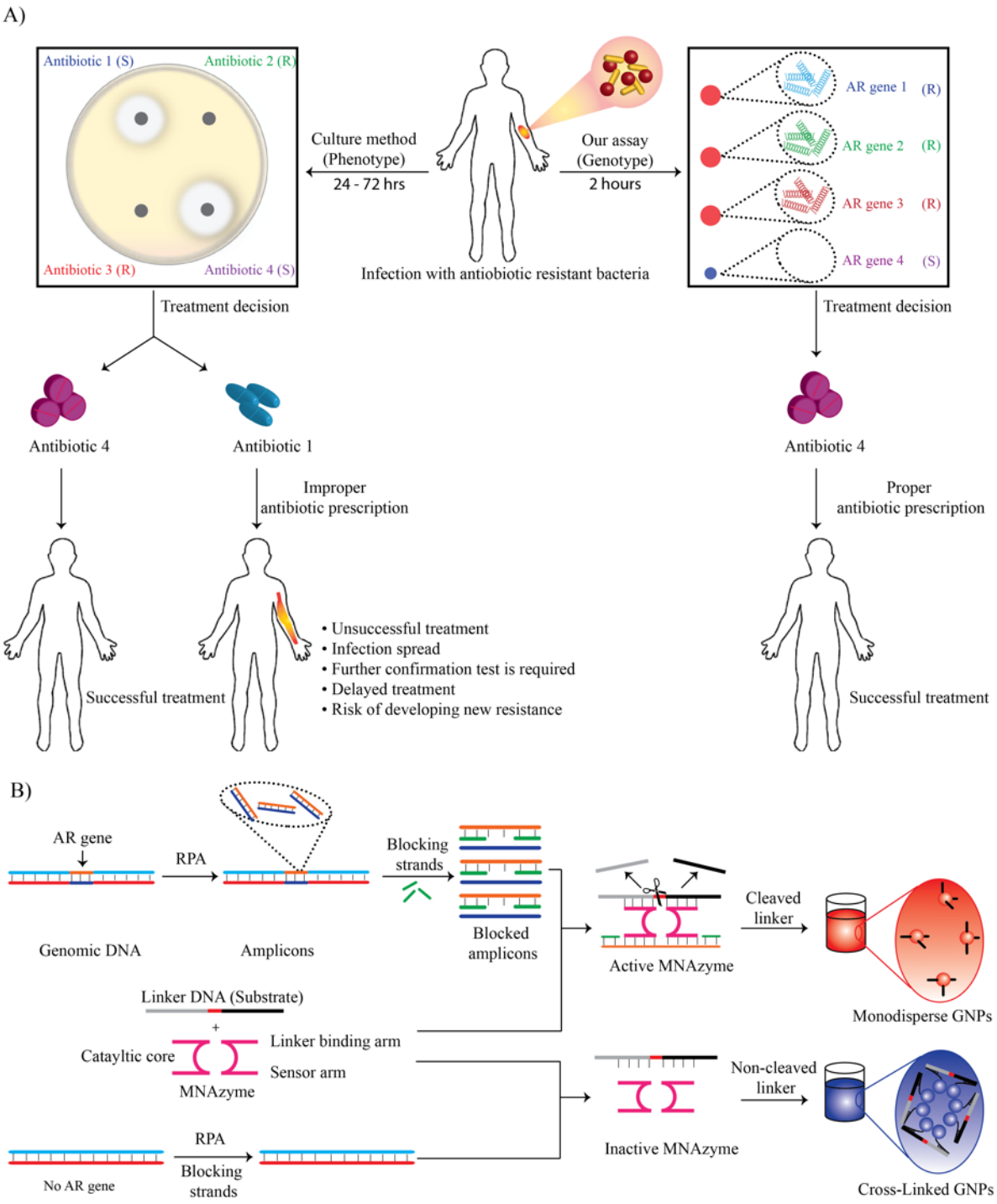

Figure 5.1: Utility of MNAzyme-GNP assay for Detection of AR. A) Culture method can lead to a lack of gene expression and increased risk of prescribing an improper antibiotic. On the other hand, MNAzyme-GNP assay can detect AR genes directly and lead to proper antibiotic prescription. B) AR gene is amplified *via* RPA followed by chemical denaturation and blocking of amplicons from re-hybridization. MNAzyme is activated by blocked amplicons, which cleaves the linker DNA rendering GNPs monodispersed. In absence of AR gene, the linker DNA remains intact due to inactive MNAzyme, causing GNPs to aggregate.

5.2 Experimental Methods

5.2.1 Design of AR target regions, primers and MNAzyme constructs.

Ten different AR genes that represent five families of antibiotics were selected for this study. The genes were selected based on their common presence in *Staphylococcus aureus* (*S. aureus*) strains. The gene sequences were obtained from AR genes database (https://ardb.cbcb.umd.edu) and the national center for biotechnology information (https://www.ncbi.nlm.nih.gov). Then the gene sequences were aligned using Basic Local Alignment Search Tool (BLAST) (https://www.ncbi.nlm.nih.gov) to select the most conserved region. Primers were then designed for each conserved region using primerQuest Tool from Integrated DNA Technologies, Inc. (https://www.idtdna.com/Primerquest/Home/Index) to produce amplicon sizes of 100 (*mecA* and *balZ*), 125 (*vanA* and *vanB*), 150 (*tetK* and *tetM*), 201 (*ermC*) and 219 (*ermA*) bp. The cross reactivity of all primers were examined using OligoAnalyzer 3.1 from Integrated DNA Technologies, Inc. (https://www.idtdna.com/calc/analyzer). All DNA oligonucleotides were purchased from Bio Basic Canada Inc.

5.2.2 Synthesis and Surface Modification of GNPs

Solution containing 98 mL of water and 1 mL of 25 nM $HAuCl_4$ were brought to a rapid boil in aqua regia (30 mL HCl, 10 mL nitric acid) prewashed 250 mL flask on a benchtop stir plate (set to 300°C). 1 mL of 33 mg/mL of sodium citrate tribasic solution was then quickly added, and solution was kept heated and stirring for another 10 min, then cooled on ice. Nanoparticle size and monodispersity (PDI < 0.1 accepted) were measured by dynamic light scattering. Tween-20 was then added to a final concentration of 0.01% (v/v) and nanoparticles concentrated by centrifugation at 12,000g for 35 minutes. Nanoparticle concentration was measured by UV-Vis spectroscopy at λ=520 nm (extinction coefficient 2.33×10^8 M^{-1} cm^{-1}), then adjusting to 100 nM using 0.01% (v/v) Tween-20 solution. To functionalize nanoparticle surface with thiolated DNA, 100 µL of 100 nM GNPs were mixed with 100 µL of DNA strand (2.5 µM for GNPs probe 1 and 10 µM for GNPs probe 2), 40 µL 0.1% (v/v) Tween-20 and 60 µL water. Solution was incubated for 5 min at room temperature, 100 µL of 100 mM trisodium citrate (pH 3) buffer was then added, and mixture further incubated for 30 min at room temperature to allow DNA to adsorb onto GNPs. Nanoparticle surface was then backfilled with polyethylene glycol (PEG) by adding 50 µL of 2 mM 1000 kDa methoxy and thiol terminated PEG and incubating for 30 min at 60°C. Particles were washed by

3X centrifugation at 16,000g for 45 min, re-suspended in 0.01% (v/v) Tween-20 solution, and concentration adjusted to 11 nM.

5.2.3 DNA extraction from bacterial cells

DNA was extracted from bacterial cells using commercial DNA extraction kit (GeneJET Genomic DNA Purification kit, ThermoFisher Scientific Inc.). For sensitivity curve, the number of freshly grown cells was adjusted to 10^7 CFU/ml and serially diluted to 10^0 CFU/ml in LB media. Cells were centrifuged at 5000g for 10 min. The supernant was removed and the cells were re-suspended in 160 µL of lysis buffer (2x TE, 1.2% triton x-100) followed by 10 µL of lysostaphine (Sigma Aldrich) and 10 µL of 20mg/ml lysozyme (Bioshop Canada). The cells were incubated at 37 ^oC for 30 min. After incubation, 200 µL of lysis solution (kit component) were added and the mixture was incubated at 56 ^oC for 30 min. The mixture was treated with 20 µL of proteinase K and 20 µL of RNAse. 400 µL of 50% ethanol was added and the mixture was added to the column. The DNA was then purified following the kit guideline. The purified DNA was then eluted in 50 µL and stored at 4^oC for further use. For multiplex reaction, the DNA was extracted from bacterial cells at concertation of 10^5 CFU/ml and purified following the same procedure.

5.2.4 Recombinase Polymerase Amplification

RPA was performed using the TwistAmp Basic kit (TwistDx), forward and reverse primers (Bio Basic Inc.), and target DNA samples. HPLC-purified primers were prepared at a concentration of 100 pmol/µL in TE buffer, diluted to 10 pmol/µL aliquots, and stored at 4 °C until later use. For the measurement of analytical sensitivity using synthetic DNA targets, a premix solution containing 2.4 µL of each forward and reverse primers (10 pmol/µL), 29.5 µL of rehydration buffer, 12.2 µL of nuclease-free water, 2.5 µL of magnesium acetate (280 mM), and 1 µL of serially diluted DNA samples (10^0 to 10^{11} copies/µL) was prepared to make a total volume of 50 µL. For the NTCs, 1 µL of TE buffer was added instead of target DNA. For the measurement of analytical sensitivity using AR genes extracted from MRSA isolate (MRSA-44), a similar premix solution was prepared using 3.2 µL of nuclease-free water and 10 µL of extracted DNA from serially diluted bacteria (10^7-10^0 CFU/mL). For the NTCs, 10 µL of solution extracted from the media without bacteria was added instead of extracted DNA. This solution was then transferred to a tube containing the lyophilized enzyme pellet, mixed and incubated at 37 °C for 30 minutes.

For cross-reactivity test of the first multiplexed RPA group, a premix solution containing 7 μL of *blaZ* forward and reverse primer mix (5 pmol/μL per primer), 8 μL of *vanA* primer mix (5 pmol/μL per primer), 2.5 μL of *tetK* primer mix (5 pmol/μL per primer), 13 μL of *aph3iiia* primer mix (5 pmol/μL per primer), 3.5 μL of *ermA* primer mix (5 pmol/μL per primer), 145 μL of rehydration buffer, 53.5 μL of nuclease-free water, and 12.5 μL of magnesium acetate (280 mM) was prepared to make a total volume of 245 μL. The premix solution was then mixed with a target mix containing 1 μL of *blaZ* (10^5 copes/μL), 1 μL of *vanA* (10^5 copes/μL), 1 μL of *tetK* (10^5 copes/μL), 1 μL of *aph3iiia* (10^5 copes/μL), and 1 μL of ermA (10^5 copes/μL) synthetic target DNA for "All" condition, or 1 μL of one of the five genes plus 4 μL of nuclease-free water to make a final volume of 250 μL. "None" condition contained 5 μL of nuclease-free water instead of target DNA. For screening clinical isolates, a similar premix solution was prepared using 8.5 μL of nuclease-free water and 50 μL of DNA extracted from bacteria (10^5 CFU/mL). NTC contained 50 μL of water instead of extracted DNA. This solution was then transferred to a tube containing 5 lyophilized enzyme pellets, mixed, and incubated at 37 °C for 30 minutes.

For cross-reactivity test of the second multiplexed RPA group, a premix solution containing 4.8 μL of *mecA* forward and reverse primer mix (5 pmol/μL per primer), 4.8 μL of *vanB* primer mix (5 pmol/μL per primer), 3.5 μL of *tetM* primer mix (5 pmol/μL per primer), 4 μL of *acc6* primer mix (5 pmol/μL per primer), 3.6 μL of *ermC* primer mix (5 pmol/μL per primer), 118 μL of rehydration buffer, 45.5 μL of nuclease-free water, and 10 μL of magnesium acetate (280 mM) was prepared to make a total volume of 194.2 μL The premix solution was then mixed with a target mix containing 1 μL of *mecA* (10^5 copes/μL), 1 μL of *vanB* (10^5 copes/μL), 1 μL of *tetM* (10^5 copes/μL), 1 μL of *acc6* (10^5 copes/μL), and 1 μL of *ermC* (10^5 copes/μL) synthetic target DNA for "All" condition, or 1 μL of one of the five genes plus 4 μL of nuclease-free water to make a final volume of 199.2 μL. "None" condition contained 5 μL of nuclease-free water instead of target DNA. For screening clinical isolates, a similar premix solution was prepared using 50 μL of DNA extracted from bacteria (10^5 CFU/mL) without nuclease-free water. NTC contained 50 μL of water instead of extracted DNA. This solution was then transferred to a tube containing 4 lyophilized enzyme pellets, mixed, and incubated at 37 °C for 30 minutes. RPA products were then purified using EZ-10 spin column DNA gel extraction kit (Bio Basic Inc.), eluted to 50 μL, visualized by

agarose gel electrophoresis (135 V, 3% agarose gel, 30-45 minutes), and stored at 4 °C until later use.

For singleplex screening of AR genes from bacteria, RPA was performed using DNA extracted from 10^7 CFU/mL MRSA-44, MRSA-41 and MSSA isolates. A premix solution containing 2.4 µL of each forward and reverse primers (10 pmol/µL), 29.5 µL of rehydration buffer, 12.2 µL of nuclease-free water, 2.5 µL of magnesium acetate (280 mM), and 1 µL of extracted DNA was prepared to make a total volume of 50 µL. For the NTC, 1 µL of water was added instead of extracted DNA. This solution was transferred to a tube containing the lyophilized enzyme pellet, mixed and incubated at 37 ^oC for 30 minutes. RPA products were then purified using EZ-10 spin column DNA gel extraction kit (Bio Basic Inc.), eluted to 50 µL, visualized by agarose gel electrophoresis (135 V, 3% agarose gel, 30-45 minutes), and stored at 4 ^oC until later use. Low molecular weight DNA ladder (New England Biolabs) was used to estimate the size of amplicons.

5.2.5 Polymerase Chain Reaction

PCR reactions were set up separately for each AR gene by mixing 12.5 µL of 2X PCR master Mix (Thermo Fisher), 0.5 µL of 10 µM primer mix, 11 µL nuclease free water, and 1 µL of template DNA product extracted from bacterial clinical isolates. 1 µL of 10^5 copies/µL of synthetic DNA was used as a positive control, and 1 µL of nuclease free water was used as a negative control. PCR included 40 seconds 95ºC initial denaturation step, and was carried out for 40 cycles with each cycle including 30 seconds 95ºC denaturation, 30 seconds primer melting step (51ºC for *ermC*; 54ºC for *mecA*, *blaZ*, *tetK*, *tetM*, *acc6*; 58ºC for *vanA*, *vanB*, *aph3iiia*, *ermA*), and 30 seconds 72ºC polymerase extension. The reaction was terminated by 4 minutes 72ºC extension, and cooling of the product to 4ºC. 3 µL of the product were visualized on 3% agarose gel.

5.2.6 Denaturation and Blocking of RPA products

For the measurement of analytical sensitivity using synthetic DNA targets and DNA extracted from clinical isolates, 1 µL of purified RPA product or elution buffer (negative control), 2 µL of blocking strand mix (final concentration of 50 pmol/µL for each strand), and 1 µL of NaOH (0.1 M) were mixed, incubated at room temperature for 5 minutes, and neutralized by adding 1 µL of HCl (0.1 M) to the solution mix.

For cross-reactivity test and screening clinical isolates of the first multiplexed RPA group, 12 μL of purified RPA product, 1 μL of 5 blocking strands mix (20 pmol/μL of each strand mix), and 2.5 μL of NaOH (0.1M) were mixed, incubated at room temperature for 5 minutes, and neutralized by adding 2.5 μL of HCL (0.1M) to the solution mix.

For cross-reactivity test and screening clinical isolates of the second multiplexed RPA group, 6 μL of purified RPA product, 6 μL of 5 blocking strands mix (24 pmol/μL of each strand mix), and 3 μL of NaOH (0.1M) were mixed, incubated at room temperature for 5 minutes, and neutralized by adding 3 μL of HCL (0.1M) to the solution mix.

5.2.7 MNAzyme-GNP assay

For the measurement of analytical sensitivity of synthetic DNA targets and DNA extracted from clinical isolates, 5 μL of blocked RPA amplicons of each gene or elution buffer was mixed with 1 μL of 10X MNAzyme buffer (0.1 M Tris-HCl, 0.5 M KCl, pH 8.3), 1 μL of 300 mM $MgCl_2$, 1 μL of MNAzyme (4 μM), 1 μL of 1 μM of Linker DNA, and 1 uL of water. The mixture was incubated at 50 ^oC for 1 hr. After incubation, 10 uL of GNPs probe mixture was then added to the samples and negative control and incubated at 50 ^oC for 20 min to allow aggregation of GNPs. 3 μL of sample was then deposited on the surface of TLC plate. The remaining of the sample was then measured using UV-vis spectrophotometer to record the peak absorbance wavelength.

For cross-reactivity test and screening clinical isolates of the first multiplexed group, 18 μL of multiplexed blocked amplicons of the 5 genes of each group or elution buffer was mixed with 3 μL of 10X MNAzyme buffer (0.1 M Tris-HCl, 0.5 M KCl, pH 8.3), 3 μL of 300 mM $MgCl_2$, 3 μL of 5 MNAzyme mixtures of the 5 genes (4 μM) and 3 μL of 1 μM of 5 different DNA linkers. The mixture was incubated at 50 ^oC for 1 hr. After incubation, both the positive and negative control mixtures were pipetted out into 5 different tubes (5 μL in each tube), 5 μL of 5 different GNPs probes was then added to the samples and negative control and incubated at 50 ^oC for 20 min to allow aggregation of GNPs. 3 μL of sample was then deposited on the surface of TLC plate.

For singleplex screening of clinical isolates, 5 μL of blocked RPA amplicons of each gene or elution buffer was mixed with 1 μL of 10X MNAzyme buffer (0.1 M Tris-HCl, 0.5 M KCl, pH 8.3), 1 μL of 300 mM MgCl2, 1 μL of MNAzyme (4 μM) 1 μL of 1 μM of Linker DNA and 1 μL

of water. The mixture was incubated at 50 ^{o}C for 1 hr. After incubation, 10 uL of GNPs probe mixture was then added to the samples and negative control and incubated at 50 ^{o}C for 20 min to allow aggregation of GNPs. 3 μL of sample was then deposited on the surface of TLC plate.

5.2.8 Antimicrobial susceptibility test using agar diffusion method

Eight different antibiotic discs were purchased from Bacterius LTD (US) and used in this experiment: penicillin (10 units), oxacillin (1 μg), vancomycin (30 μg), tetracycline (30 μg), minocycline (30 μg), gentamicin (10 μg), kanamycin (30 μg) and erythromycin (15 μg). The procedure was done following the Clinical and Laboratory Standards Institute (CLSI) antimicrobial susceptibility testing guideline[184]. Briefly, fresh cultures of *S. aureus* strains were prepared from single colony on fresh Luria agar (LA) plates. Plates were incubated at 37 ^{o}C for 24 hr. Three to five colonies of each culture were then transferred to 1 ml of 0.85% NaCl solution and the turbidity of the solution was adjusted to 0.5 McFerland standard. A sterile cotton swab was immersed into the cell suspension and rotated firmly several times against the upper inside wall of the tube to remove excess fluid. The swab was then used to inoculate the surface of Muller Hinton agar (MHA) plates by spreading the swab over the agar surface. The desired antibiotic discs were applied to the surface of the MHA plates using sterile forceps. The plates were incubated at 35 ^{o}C for 16 hr. After incubation, the diameter of inhibition zone was measured and compared to the Clinical and Laboratory Standards Institute (CLSI) antimicrobial susceptibility testing guideline tables to determine the antibiotic susceptibility of the bacterial strains.

5.3 Results and Discussions

5.3.1 Design of the Assay

Ten different AR genes were selected to represent 5 classes of antibiotics: *blaZ* gene for penicillin resistance, *mecA* gene for oxacillin resistance, *vanA* and *vanB* genes for vancomycin resistance, *tetK* and *tetM* genes for tetracycline resistance, *tetM* gene for minocycline, *acc6* and *aph3iiia* genes for gentamicin and kanamycin resistance, and *ermA* and *ermC* for erythromycin resistance. These genes were selected based on their common presence in *S. aureus* strains[193,206-210]. All the gene sequences were first screened using BLAST to select the most conserved region. Then, the primers were designed for each conserved region to achieve high specificity and minimal cross reactivity. Figure 5.1b depicts the schematic and description of the assay. Genomic DNA is first extracted from bacterial cells, followed by isothermal amplification of AR genes *via* RPA at 37^{o}C. The purified amplicons are then chemically denatured using NaOH[178]. This chemical denaturation step was adapted instead of thermal denaturation since heating devices are usually unavailable in resource-limited areas, thus making the proposed diagnostic procedure more feasible for remote testing locations. The denatured amplicons are then mixed with blocking strands and the solution is neutralized with HCL to allow hybridization of blocking stands with the sense strand of a target gene. Such blocking strategy has been proven to be effective in preventing re-hybridization of denatured DNA, thus allowing hybridization with any other available DNA probes[174]. The blocked amplicons are then mixed with MNAzyme solution to allow hybridization of blocked amplicons with the MNAzyme sensor arms, which triggers the catalytic activity of MNAzyme. Target-activated MNAzyme binds to "linker DNA" and cleaves it. The cleaved linker DNA fails to crosslink the GNPs rendering them monodispersed, which results in a distinct red color. In the absence of the target, the linker DNA remains intact and hybridizes with DNA probes on the surface of GNPs to produce a dark purple color due to crosslinking of GNPs. DNA sequences of RPA primers, target DNA, MNAzyme components, linker DNA, GNP probes, and blocking strands are presented in Table 5.1 and Table 5.2.

Table 5.1: List of DNA Sequences for the First Group

	***blaZ* (5' to 3')**	***vanA* (5' to 3')**	***tetK* (5' to 3')**	***aph3* (5' to 3')**	***ermA* (5' to 3')**
FP	AAGATGATAT AGTTGCTTATT CTCC	CAGTGCCGCG TTAGTTGTTG	CTGGAACCAT GAGTGTTATTG	CGCGCGAGCT GTATGATTT	AAGCGGTAAA CCCCTCTGA

RP	TTATCACTATA TGTCATTGAAG CC	GGTCTGCGGG AACGGTTAT	TCAACCACAT ACTAAACTCA AC	CGGATGCAGA AGGCAATGT	CCAAAGCTCG TTGCAGATT
Target	AAGATGATAT AGTTGCTTATT CTCCT ATTTTAGAAA AATATGTAGG AAAAGATATC ACTTTAAAAG CACTTATTG AGGCTTCAAT GACATATAGT GATAA	CAGTGCCGCG TTAGTTGTTGG CGAGGTGGAC CAAATCAGGC TGCAGTACGG AATCTTTCGTA TTCATCAGGA AGTCGAGCCG GAAAAAGGCT CTGAAAACGC AGTT ATAACCGTTCC CGCAGACC	CTGGAACCAT GAGTGTTATTG TTTTTGGTTAT TTTGGTGGTTT TTTAGTGGATA GAAAAGGATC ATTATTTGTTT TTATTTTAGGA TCATTGTCTAT CTCTATAAGTT TTTTAACTATT GCATTTTTT GTTGAGTTTAG TATGTGGTTGA	CGCGCGAGCT GTATGATTTTT TAAAGACGGA AAAGCCCGAA GAGGAACTTG TCTTTTCCCAC GGCGACCTGG GAGACAGCAA CATCTTTGTGA AAGATGGCAA AGTAAGTGGC TTTATTGATCT TGGGAGAAGC GGCAGGGCGG ACAAGTGGTA TG ACATTGCCTTC TGCATCCG	AAGCGG TAAACCCCTC TGAGAATATA AAAGTGATTC AAACGGATAT TCTAAAATTT TCCTTCCCAA AACATATAAA CTATAAGATAT ATGGTAATA TTCCTTATAA CATCAGTACG GATATTGTCA AAAGAATTAC CTTTGAAAGT CAGGCTAAAT ATAGCTATCT TATCGTTGAG AAGGGATTTG CGAAAAGATT GCAAAATCTG CAACGAGCTTT GG
MNAzyme Left arm	GACACAAAGA AGGCTAGCTCT TTTCCTACATA TTTTTCTA	GAATAGGTGC AGGCTAGCTA CGAAAGATTC CGTACTGCAG	CACGTGTTCTC AGGCTAGCTA AATAAAAACA AATAATGATC	AATCCTATACA GGCTAGCTTCT TTCACAAAGA TGTTGCTG	CAAGATCGCT AGGCTAGCTTC CGTACTGATGT TATAAGGA
MNAzyme Right arm	AAGTGCTTTTA AAGTGATATA CAACGATCTCT ACGACT	GGCTCGACTTC CTGATGAATA CAACGATCGG AATTAAC	AGAGATAGAC AATGATCCTA ACAACGATAT GGTTTGCG	TAAAGCCACTT ACTTTGCCAAC AACGATCTGTC CAGCA	AGGTAATTCTT TTGACAATAA CAACGAATAG TGTCACA
Linker DNA	GCGTCCCTCCT CGTATAGTCGT AGAGARGRUT CTTTGTGTCTT CATACAATTGC ACT	GCCTTACTGCA ACCCTGTTAAT TCCGARGRUG CACCTATTCTC TCCCTGGTAGC TCG	ACATACATCG GCCATTCGCA AACCATARGR UGAGAACACG TGTAGCCTACT TTCCTCT	GAGTAACACC AATAATTGCTG GACAGARGRU GTATAGGATTT ACTACATGCCC TACA	CGTCGCACTCA CTCGTTGTGAC ACTATRGRUA GCGATCTTGTT GACTGTAAGC CACC
GNPs probe 1	SS-- AAAAAAAAAA TACGAGGAGG GACGC	SS-- AAAAAAAAAA GGGTTGCAGT AAGGC	SS-- AAAAAAAAAA ATGGCCGATG TATGT	SS-- AAAAAAAAAA TTATTGGTGTT ACTC	HS-- AAAAAAAAAA CGAGTGAGTG CGACG
GNPs probe 2	AGTGCAATTGT ATGAAAAAAA AAAA--SS	CGAGCTACCA GGGAGAAAAA AAAAA--SS	AGAGGAAAGT AGGCTAAAAA AAAAA--SS	TGTAGGGCAT GTAGTAAAAA AAAAA--SS	GGTGGCTTAC AGTCAAAAAA AAAAA--SH
BS #1	AAAT AGGAGAATAA GCAACTATATC ATCTT	CCTGATTTGGT CCACCTCGCCA ACAACTAACG CGGCACTG	CTTTTCTATC CACTAAAAAA CCACCAAAAT AACCAAAAAC AATAACACTC ATGGTTCCAG	TCTCCC AGGTCGCCGT GGGAAAAGAC AAGTTCCTCT	ATATTACCAT ATATCTTATA GTTTATATGT TTTGGGAAGG AAAATTTTAG
BS #2	TTATCACTATA TGTCATTGAAG CCT CAAT	GGTCTGCGGG AACG GTTATAACTGC GTTTTCAGAGC CTTTTTCC	TCAACCACAT ACTAAACTCA ACAAAAAATG CAATAGTTAA AAAACTTAT	TCGGGCTTTT CCGTCTTTAA AAAATCATAC AGCTCGCGCG	AATATCCGTT TGAATCACTT TTATATTCTC AGAGGGGTTT ACCGCTT
BS #3	NA	NA	NA	CGGAT GCAGAAGGCA ATGTCATACC ACTTG	CCAAAGCTCG TTGCAGATTT TGCAATCTTT TCGCAAATCC

BS #4	NA	NA	NA	TCCGC CCTGCCGCTT CTCCCAAGAT CAA	CTTCTCAACG ATAAGATAGC TATATTTAGC CTGACTTTCAA

Table 5.2: List of DNA Sequences for the Second Group

	***mecA* (5' to 3')**	***vanB* (5' to 3')**	***tetM* (5' to 3')**	***acc6* (5' to 3')**	***ermC* (5' to 3')**
FP	AAGATATGAA GTGGTAAATG GT	CATGATGTGTC GGTAAAATCC G	GTGGAGCGAT TACAGAATTA G	AGATTTGCCA GAACATGAA	AGTACAGAGG TGTAATTTCG
RP	CTTACTGCCTA ATTCGAGTG	TCCGTACATGG CTTCTTGCA	CTGGCGTGTCT ATGATGTT	CACACTATCAT AACCACTACC	ACAATTTTGCG TATTATATCC
Target	AAGATATGAA GTGGTAAATG GT AATATCGACTT AAAACAAGCA ATAGAATCAT CAGATAACAT TTTCTTTGCTA GAGTAG CACTCGAATTA GGCAGTAAG	CATGATGTGTC GGTAAAATCC GCAATAGAAA TTGCTGCGAA CATTAATACTG AAAAATTCG ATCCGCACTA CATCGGAATT ACAAAAAACG GCGTATGGAA GCTATGCAAG AAGCCATGTA CGGA	GTGGAGCGAT TACAGAATTA GGAAGCGTGG ACAAAGGTAC AACGAGGACG GATAATACGC TTTTAGAACGT CAGAGAGGAA TTACAATTCAG ACAGGAATAA CCTCTTTTCAG TGGGAAAATA CGAAGGTG AACATCATAG ACACGCCAG	AGATTTGCCA GAACATGAAT TACACGAGGG CAAAAAAGAA GATTGTTATTT AATGGAATAT AGATATGATG ATAATGCCAC AAATGTTAAG GCAATGAAAT ATTTAATTGAG CATTACTTTGA TAATTTCAAAG TAGATAGTATT GAAATAATC GGTAGTGGTT ATGATAGTGT G	AGT ACAGAGGTGT AATTTCGTAA CTGCCATTGA AATAGACCAT AAATTATGCA AAACTACAGA AAATAAACTT GTTGATCACG ATAATTTCCA AGTTTTAAAC AAGGATATAT TGCAGTTTAA ATTTCCTAAA AACCAATCCT ATAAAATATA TGGTAATATA CCTTATAACA TAAGTACGGA TATAATACGC AAAATTGT
MNAzyme Left arm	GACACAAAGA AGGCTAGCTG ATTCTATTGCT TGTTTTAAG	GAATAGGTGC AGGCTAGCT GAATTTTTCAG TATTAATGTT	CACGTGTTCTC AGGCTAGCTTC TGACGTTCTAA AAGCGTAT	AATCCTATACA GGCTAGCTAA CATTTGTGGCA TTATCATC	CAAGATCGCT AGGCTAGCTC AACAAGTTTAT TTTCTGTAG
MNAzyme Right arm	CAAAGAAAAT GTTATCTGATA CAACGATCTCT ACGACT	ATTCCGATGTA GTGCGGATCA CAACGATCGG AATTAAC	TGTCTGAATTG TAATTCCTCAC AACGATATGG TTTGCG	ATTAAATATTT CATTGCCTTAC AACGATCTGTC CAGCA	AACTTGGAAA TTATCGTGATA CAACGAATAG TGTCACA
Linker DNA	GCGTCCCTCCT CGTATAGTCGT AGAGARGRUT CTTTGTGTCTT CATACAATTGC ACT	GCCTTACTGCA ACCCTGTTAAT TCCGARGRUG CACCTATTCTC TCCCTGGTAGC TCG	ACATACATCG GCCATTCGCA AACCATARGR UGAGAACACG TGTAGCCTACT TTCCTCT	GAGTAACACC AATAATTGCTG GACAGARGRU GTATAGGATTT ACTACATGCCC TACA	CGTCGCACTCA CTCGTTGTGAC ACTATRGRUA GCGATCTTGTT GACTGTAAGC CACC
GNPs probe 1	SS-- AAAAAAAAAA TACGAGGAGG GACGC	SS-- AAAAAAAAAA GGGTTGCAGT AAGGC	SS-- AAAAAAAAAA ATGGCCGATG TATGT	SS-- AAAAAAAAAA TTATTGGTGTT ACTC	HS-- AAAAAAAAAA CGAGTGAGTG CGACG
GNPs probe 2	AGTGCAATTGT ATGAAAAAAA AAAA--SS	CGAGCTACCA GGGAGAAAAA AAAAA--SS	AGAGGAAAGT AGGCTAAAAA AAAAA--SS	TGTAGGGCAT GTAGTAAAAA AAAAA--SS	GGTGGCTTAC AGTCAAAAAA AAAAA--SH
BS #1	TCGATATT ACCATTTACCA CTTCATATCTT	CGCAGCAAT TTCTATTGCG GATTTTACCG ACACATCATG	TATC CGTCCTCGTT GTACCTTTGT CCACGCTTCC	ATATCTATAT TCCATTAAAT AACAATCTTC	TTTTGC ATAATTTATG GTCTATTTCA

			TAATTCTGTA ATCGCTCCAC		
BS #2	CTTACTGCCTA ATTCGAGTG CTACTCTAG	TCCGT ACATGGCTTC TTGCATAGCT TCCATACGCC GTTTTTTGTA	CTGGCGTGTC TATGATGTTC ACCTTCGTAT TTTCCCACTG AAAAGAGGTT ATTCC	TTTTTTGCCC TCGTGTAATT CATGTTCTGG CAAATCT	ATGGCAGTTA CGAAATTACA CCTCTGTACT
BS #3	NA	NA	NA	CACACTATCA TAACCACTAC CGATTATTTC	ACAATTTTGCG TATTATATCC GTACTTATGT TATAAGGTAT ATTACCATAT
BS #4	NA	NA	NA	AATACTATCT ACTTTGAAAT TATCAAAGTA ATGCTCA	ATTTTATAGG ATTGGTTTTT AGGAAATTTA AACTGCAATA TATCCTTGTT TAA

5.3.2 Analytical Sensitivity of Detecting Synthetic AR Genes

In a previous study, a standalone MNAzyme-GNP assay was demonstrated to detect 10^7 to 10^9 synthetic DNA copies/µL[104]. However, this LOD is insufficient for clinical detection of antimicrobial resistance in *S. aureus,* which requires the analytical sensitivity level of 10^5 CFU/ml (or 10^2 copies/µL)[184,211]. Therefore, RPA was incorporated into MNAzyme-GNP assay to significantly improve the detection limit of the system. This was investigated by comparing the analytical sensitivity of the assay with and without RPA. For the RPA condition, the 10 synthetic AR genes were serially diluted (10^{11} – 10^0 copies/µL), and amplified using RPA. The amplified products were then qualitatively assessed using agarose gel electrophoresis (Figure 5.2). Both the amplified and non-amplified (*i.e.* serially diluted genes without RPA) targets were chemically denatured, blocked and added to the MNAzyme assay mixture to allow the cleavage process to occur, followed by the addition of GNPs for the signal readout. The samples (3 µL) were then deposited on a TLC plate and observed for a color shift from purple to red as an indication for a positive signal. Figure 5.3 illustrates increase in the analytical sensitivity for all genes by 8-9 orders of magnitude with the incorporation of RPA, yielding a detection limit of 10^2-10^3 DNA copies/reaction (2-20 DNA copies/µL). This was indicated by the color shift of GNPs from purple to red on the TLC plate and was confirmed quantitatively by measuring the peak absorbance wavelength using UV-Vis spectrophotometer (Figure 5.4). Statistically significant difference was observed in the peak absorbance wavelength at or greater than 10^2 DNA copies/reaction for *tetM*, *acc6*, *aph3iiia* and *ermA* genes (*P* value <0.0001 or <0.00001) and at or greater than 10^3 DNA copies/uL for all other genes (*P* value <0.0001 or <0.00001) when RPA is used compared to NTCs.

This confirms the need for RPA as a pre-amplification step in the assay to achieve clinically relevant LOD.

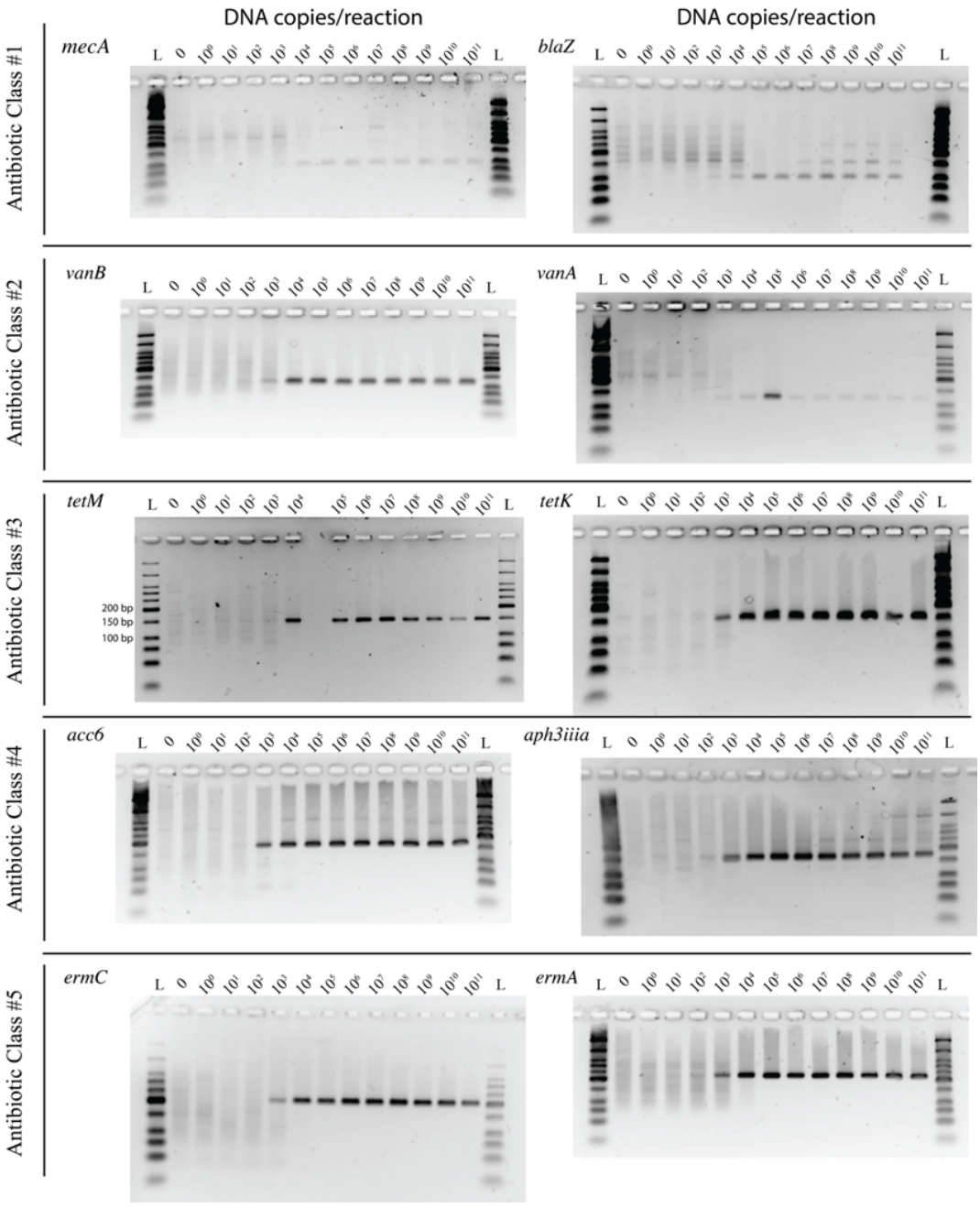

Figure 5.2: Qualitative Assessment of Amplified AR Genes using Gel Electrophoresis. Serially diluted AR genes were amplified *via* RPA and visualized on agarose gel. Clear bands that correspond to each gene can be observed when 10^2-10^3 DNA copies were used in the RPA reaction. This is in correlation with the MNAzyme-GNP assay results (Figure 5.3). (**L**: low molecular weight DNA ladder).

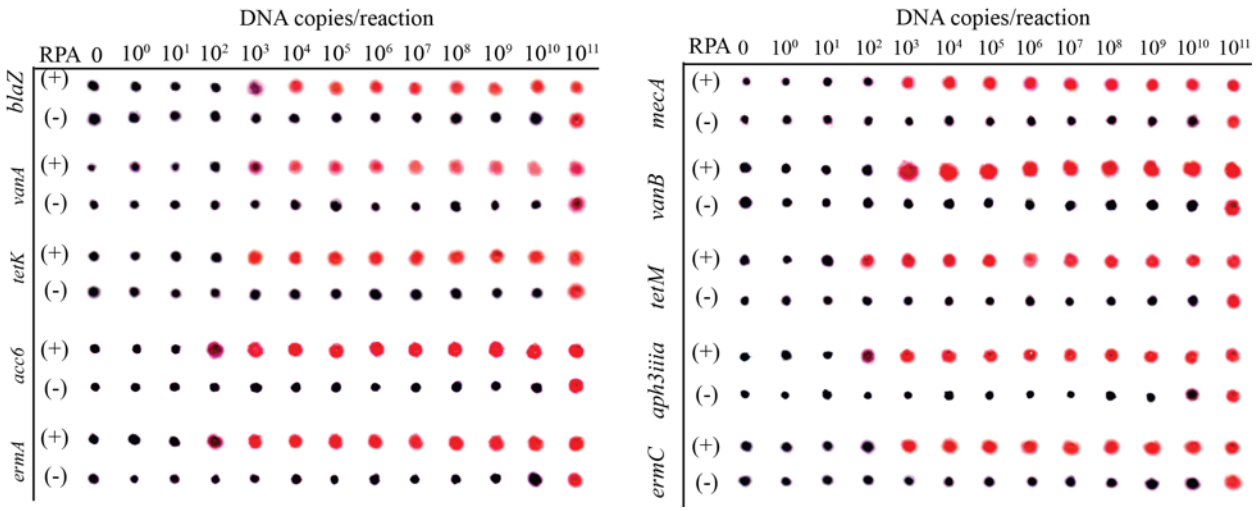

Figure 5.3: Analytical Sensitivity of Detecting AR Genes with and without RPA. 10 synthetic AR genes were serially diluted, amplified *via* RPA and detected with MNAzyme-GNP assay. The assay results were compared to no RPA conditions. Spot images represent colorimetric readout on a TLC plate after adjusting for brightness and contrast on Image J.

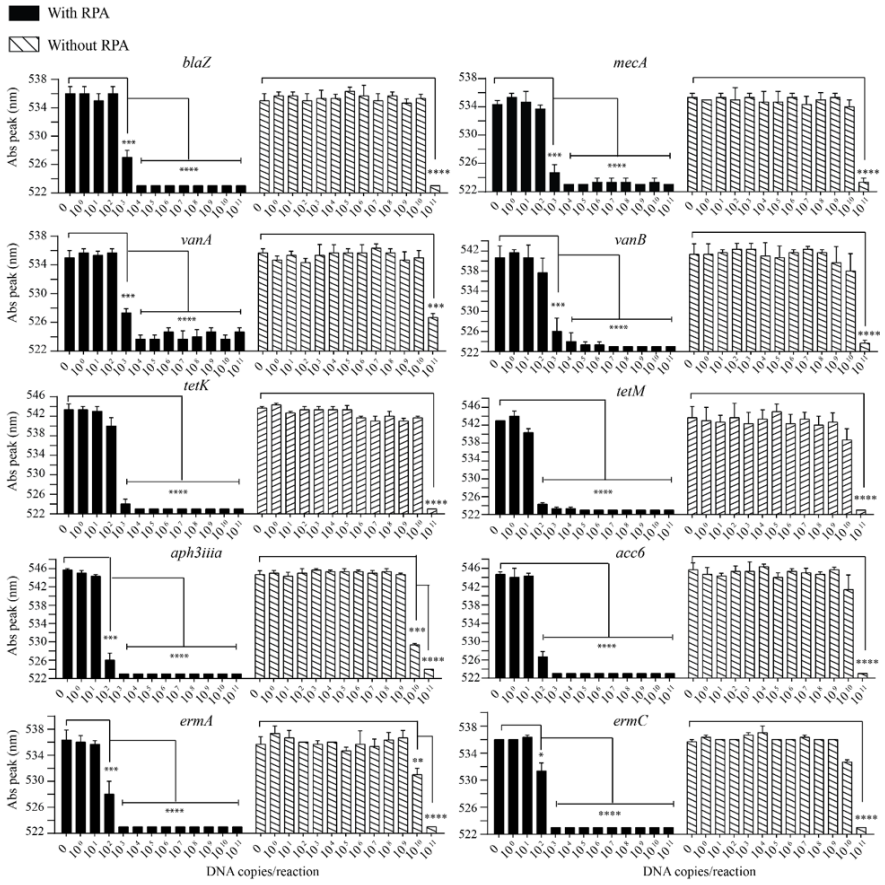

Figure 5.4: Quantitative Measurement of Analytical Sensitivity of AR Genes with and without RPA. Wavelength peak absorbance measurement reveals the analytical sensitivity of MNAzyme-GNP assay at 10^2-10^3 DNA copies/reaction when RPA is used compared to 10^{11} DNA copies/reaction without RPA. Error bars denote the standard deviation where n=3. (*p≤0.05, **p<0.001, ***p<0.0001 and ****p<0.00001)

5.3.3 Detection of Multiple Synthetic AR Genes

The ability to identify multiple AR determinants is critical for detecting MDR bacteria, which will facilitate more accurate treatment decisions in a time effective manner. Hence, the ability to detect multiple AR genes in parallel is demonstrated. AR genes were first divided into 2 groups based on the gene size and to minimize cross-reactivity between the primers. Group 1 included *blaZ*, *vanA*, *tetK*, *aph3iiia* and *ermA* genes, and group 2 included *mecA*, *vanB*, *tetM*, *acc6* and *ermC* genes. For each group, 5 synthetic AR genes were added simultaneously to the multiplexed RPA solution containing primers for *blaZ*, *vanA*, *tetK*, *aph3iiia* and *ermA* for group 1, and *mecA*, *vanB*, *tetM*, *acc6* and *ermC* for group 2. The amplicons were then blocked and added to MNAzyme solution containing mixture of the 5 MNAzymes for each group. This was followed by parallel signal readout by 5 different GNP detection probes. Figure 5.5 illustrates amplicons of 5 AR genes produced from multiplex RPA reaction and visualized on agarose gel electrophoresis. Subsequently, all AR genes were detected in parallel with MNAzyme-GNP assay (Figure 5.6). This is indicated by the red color spots of "All" condition in which all genes were added simultaneously to the RPA reaction mixture. These red spots represent positive signals when compared to the purple color spots of the NTC condition. For NTCs, water was added instead of AR genes in the multiplex RPA reaction to check for any false-positive signals arising from the contamination of RPA reagents with AR genes or non-specific RPA products. Also, to examine

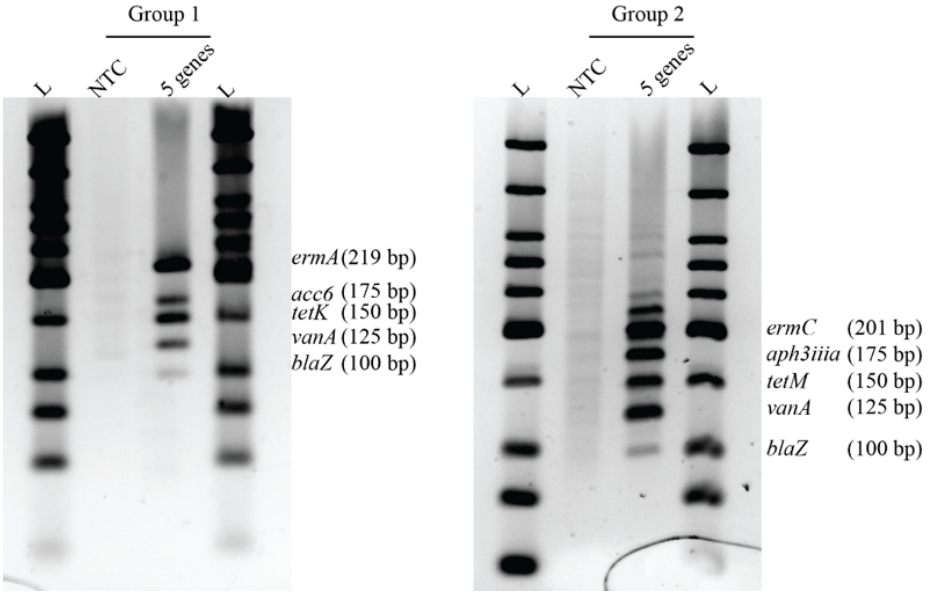

Figure 5.5: Multiplex RPA of 5 AR Genes. Gel electrophoresis images show the presence of the amplified products of the 5 AR genes with different band sizes. (**L**: low molecular weight DNA ladder)

any false-positive signals that could arise from improper aggregation of GNPs, "EBS" control composed of elution buffer of DNA purification kit and blocking strands was used. This control was mixed directly with MNAzyme assay components and transferred to GNP solutions to confirm proper aggregation of GNPs with inactive MNAzyme and intact linker DNA. Furthermore, the cross-reactivity in both RPA and MNAzyme reactions was investigated by incubating one of the five AR genes of each group in the multiplexed RPA reaction, and using the amplified products in the MNAzyme-GNP assay. No cross-reactivity was observed for all conditions tested (Figure 5.6), and only the gene that was added to the multiplexed RPA reaction gave a positive signal. This confirms that the assay can selectively detect multiple AR genes without any cross-reactivity.

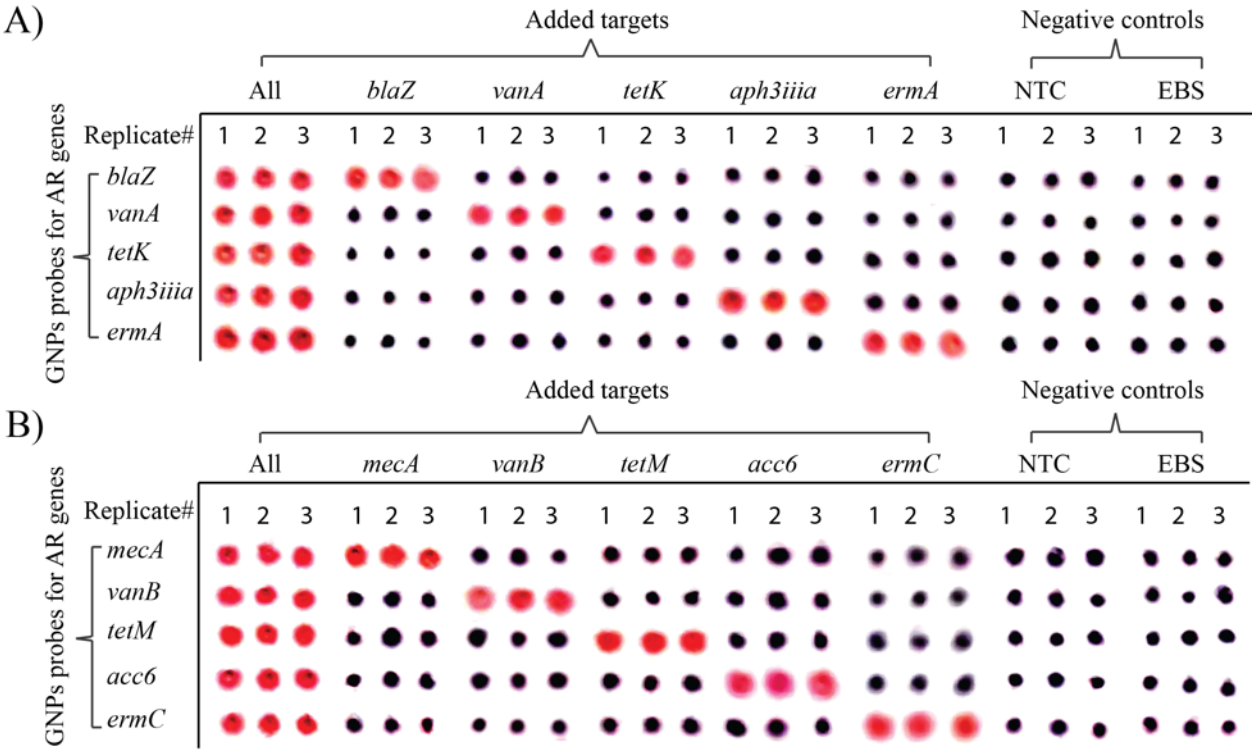

Figure 5.6: Cross-reactivity Test. Synthetic AR gene(s) were added to the multiplexed RPA solution containing primers for (A) *balZ*, *vanA*, *tetK*, *aph3iiia*, and *ermA*, or (B) *mecA*, *vanB*, *tetM*, *acc6*, and *ermC*. Amplicons were detected with MNAzyme-GNP assay. "None" indicates no template control of multiplexed RPA reaction. "All" indicates that all AR genes of the group are added to multiplexed RPA reaction. "EBS" control is composed of elution buffer of DNA purification kit and blocking strands to test aggregation of GNPs. Spot images represent colorimetric readout on a TLC plate after adjusting for brightness and contrast on Image J.

5.3.4 Validation of Analytical Sensitivity using Clinical Isolates

Next, DNA extracted from clinical isolates was used to validate the analytical sensitivity measured using synthetic DNA targets, and to confirm that clinically relevant detection limit ($\leq 10^5$ CFU/ml) can be achieved. Three isolates of *S. aureus* were first screened: *S. aureus* ATCC BAA-44 (MRSA-44), *S. aureus* ATCC BAA-41 (MRSA-41) and *S. aureus* ATCC 29213 (MSSA) for the presence of AR genes. Bacteria were grown at a high concentration of 10^7 CFU/ml, to ensure that negative detection of genes is not due to insufficient amount of target DNA. DNA was extracted from the three isolates and then screened for the presence of AR genes in a singleplex reaction. Both NTC and EBS controls were used to ensure correct interpretation of test results. MRSA-44 had the highest abundance of genes denoted by 5 AR genes: *blaZ*, *mecA*, *tetM*, *acc6* and *ermA* genes, followed by MRSA-41 which contained 3 AR genes: *balZ*, *mecA* and *ermA*, while MSSA contained only *blaZ* gene (Figure 5.7). The presence of these AR genes was also confirmed by PCR (Figure 5.8), which detected the same genes in the three MRSA isolates.

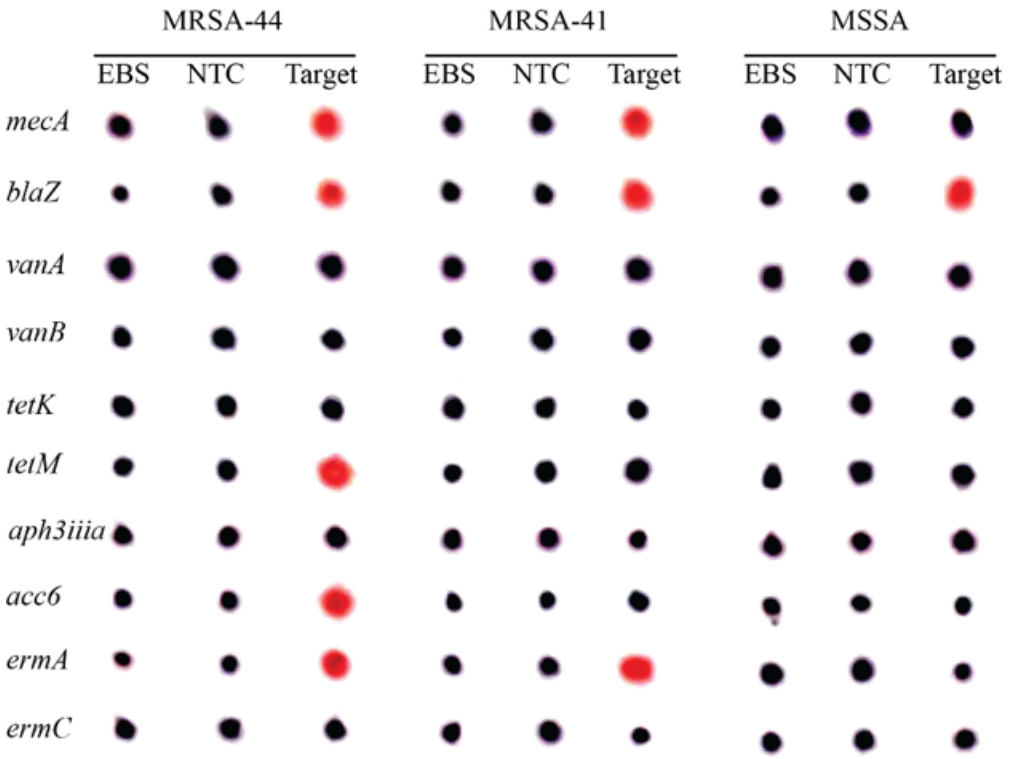

Figure 5.7: Screening Clinical Isolates using Singleplex RPA and MNAzyme-GNP Assay. Three *Staphylococcus aureus* strains (MRSA-44, MRSA-41, and MSSA) were screened to test for presence of the 10 AR genes. Spot images represent colorimetric readout on a TLC plate after adjusting for brightness and contrast on Image J. Red spots indicate the presence of genes while dark purple/blue spots indicate the absence of gene.

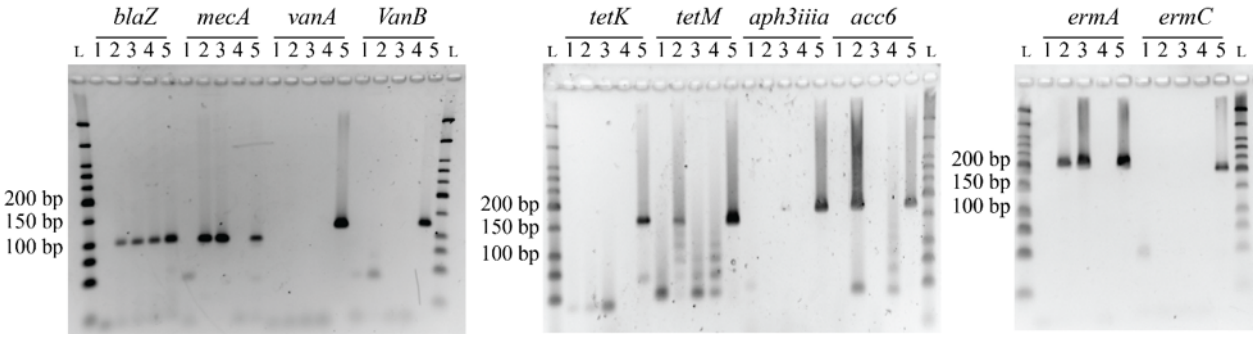

Figure 5.8: Detection of AR Genes in Bacterial Strains using PCR. The gel electrophoresis images show the presence of AR genes in MRSA-44 (lane 2), MRSA-41 (lane 3) and MSSA (lane 4) strains. Synthetic AR genes (lane 5) was used as positive control while NTC (lane 1) was used as a negative control. (**L**: low molecular weight DNA ladder).

Subsequently, the analytical sensitivity was measured for the five AR genes that were present in MRSA-44 using serial dilutions of this bacteria (10^7-10^0 CFU/ml). Media without bacteria served as a negative control (*i.e.* 0 CFU/mL). Detection limit of 10^2-10^3 CFU/ml, which corresponds to 20-200 DNA copies/µL, was measured. This LOD is much lower than clinically relevant threshold (10^5 CFU/mL), and was similar to the analytical sensitivity measured using synthetic AR genes. This was also confirmed quantitatively by measuring the peak absorbance wavelength using UV-Vis spectrophotometer. Statistically significant difference was measured in the peak absorbance wavelength at or greater than 10^2 CFU/ml for *mecA* and *tetM* genes, and 10^3 CFU/ml for *balZ*, *acc6* and *ermA* genes (*P* value <0.0001 or <0.00001) when compared to the negative control. Thus, AR genes in MRSA isolates can be detected using this assay at concentrations that are relevant for clinical applications.

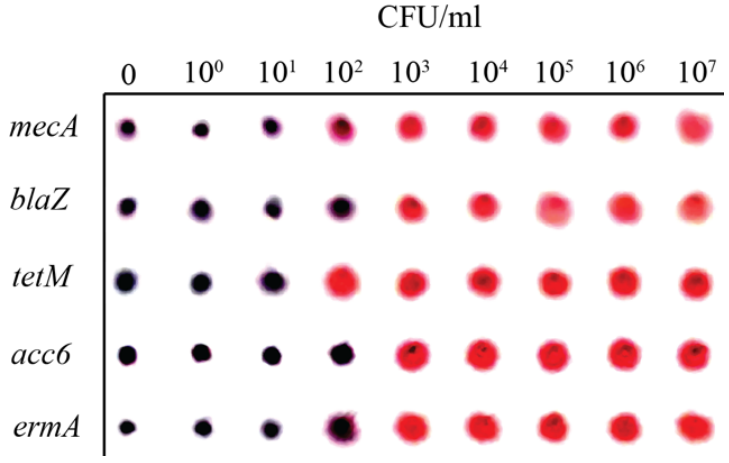

Figure 5.9: Analytical Sensitivity of Detecting AR Genes from MRSA-44. DNA extracted from serially diluted MRSA-44 was amplified *via* RPA and detected with MNAzyme-GNP assay. Spot images represent colorimetric readout on a TLC plate after adjusting for brightness and contrast on Image J.

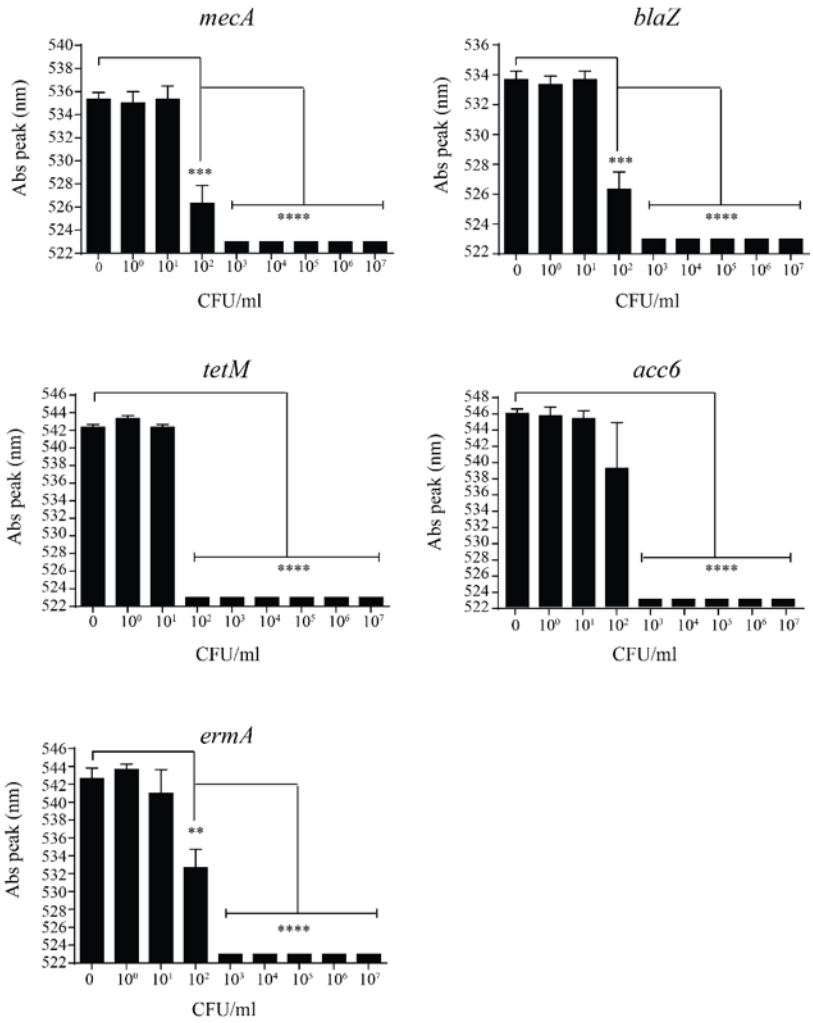

Figure 5.10: Quantitative Measurement of Analytical Sensitivity of AR Genes from MRSA-44. Wavelength peak absorbance measurement reveals the analytical sensitivity of the assay at 10^2-10^3 CFU/ml. Error bars denotes the standard deviation where n=3. (*p≤0.05, **p<0.001, ***p<0.0001 and ****p<0.00001).

5.3.5 Screening AR Genes in Clinical Isolates

As a final step, the ability to detect multiple AR genes in parallel is demonstrated with three *S. aureus* strains, and compared with one of the most commonly used phenotypic assays. DNA was first extracted from three isolates at 10^5 CFU/ml. Extracted DNA was then added to the multiplexed RPA reaction, and blocked amplicons were added to MNAzyme reaction as mentioned in the previous sections, followed by parallel colorimetric readout. As shown in Figure 5.11A and B, following AR genes were detected from three isolates: *blaZ*, *mecA*, *tetM*, *acc6* and *ermA* genes in MRSA-44 strain, *blaZ*, *mecA* and *ermA* genes in MRSA-41 strain, and *blaZ* gene in MSSA strain. These results perfectly match with the singleplex results that were obtained in

Figure 5.7. Using the agar diffusion method, it was confirmed that MRSA-44 strain is resistant to penicillin, oxacillin, gentamicin, kanamycin, tetracycline and erythromycin, and intermediate resistant to minocycline (Figure 5.11C and Figure 5.12). This is in agreement with the results of MNAzyme-GNP assay, which detected the presence of *blaZ*, *mecA*, *tetM*, *acc6* and *ermA* genes. It was also confirmed that MRSA-41 strain is resistant to penicillin, oxacillin and erythromycin which corresponds to the presence of *blaZ*, *mecA* and *ermA* genes respectively, and MSSA strain is resistant to penicillin which corresponds to the presence of *blaZ* gene. Overall, MNAzyme-GNP assay can detect multiple AR genes from MRSA isolates at 10^5 CFU/ml with the same predictive capability of phenotypic method and PCR (Table 5.3).

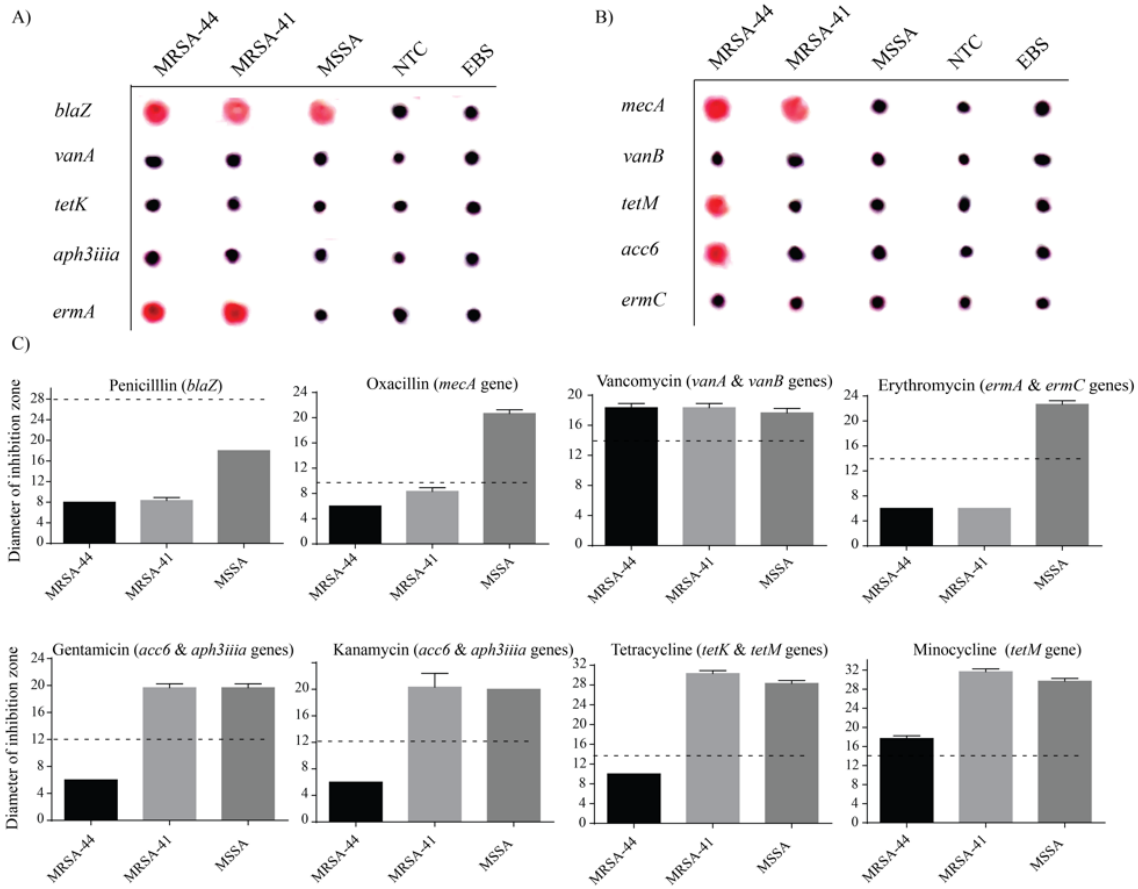

Figure 5.11: Screening Clinical Isolates for Detection of Multiple AR Genes. Three *Staphylococcus aureus* strains (MRSA-44, MRSA-41, and MSSA) were screened to test for presence of 10 AR genes. DNA extracted from 3 isolates were tested for the presence of (A) *balZ*, *vanA*, *tetK*, *aph3iiia*, and *ermA* genes, and (B) *mecA*, *vanB*, *tetM*, *acc6*, and *ermC* genes. "EBS" control is composed of elution buffer of DNA purification kit and blocking strands to test aggregation of GNPs. "NTC" indicates no template control of multiplexed RPA reaction. Spot images represent colorimetric readout on a TLC plate after adjusting for brightness and contrast on Image J. (C) Culture-based agar diffusion test. Bar graphs represent the diameter of inhibition zone, where the diameter below the horizontal dotted line indicates AR. Error bars represent standard deviation of the mean from experimental triplicates.

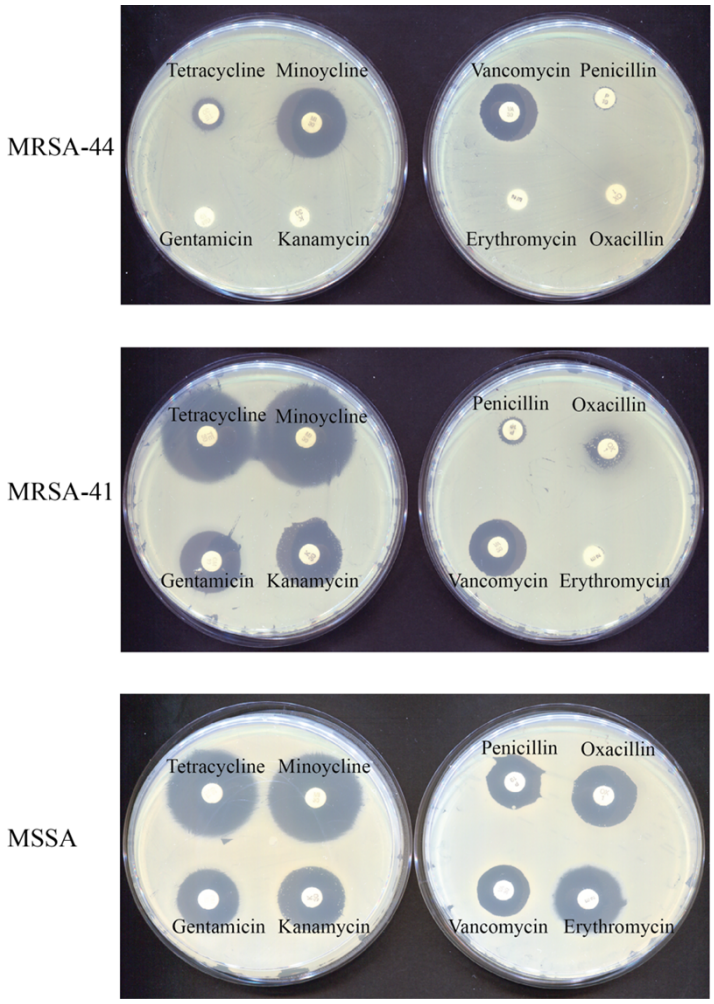

Figure 5.12: Antibiotic Susceptibility Assay using Agar Diffusion Method. Photos show the susceptibility of MRSA-44, MRSA-41 and MSSA strains to antibiotics based on the diameter of inhibition zone.

Table 5.3: Comparison Between MNAzyme-GNP Assay, PCR and Agar Diffusion Method

Antibiotic family	Antibiotic name	Genes	MNAzyme-GNP Assay			PCR			Agar Diffusion Method		
			MSSA	MRSA-41	MRSA-44	MSSA	MRSA-41	MRSA-44	MSSA	MRSA-41	MRSA-44
B-lactam	Penicillin	*balZ*	+	+	+	+	+	+	+	+	+
	Oxacillin	*mecA*	-	+	+	-	+	+	-	+	+
Glycopeptides	Vancomycin	*vanA*	-	-	-	-	-	-	-	-	-
		vanB	-	-	-	-	-	-			
Tetracyclines	Tetracycline/ Minocycline	*tetK*	-	-	-	-	-	-	-	-	+
		tetM	-	-	+	-	-	+			
Aminoglycosides	Gentamicin/ Kanamycin	*acc6*	-	-	+	-	-	+	-	-	+
		aph3iii a	-	-	-	-	-	-			
Macrolides	Erythromycin	*ermA*	-	+	+	-	+	+	-	+	+
		ermC	-	-	-	-	-	-			

5.4 Conclusions

The work presented herein describes the development of a rapid diagnostic technique that can detect AR profiles of MRSA isolates within 2 hours. In clinical practices, physicians usually prescribe broad-spectrum antibiotics as initial therapy. Once, the antibiotic susceptibility test results are available, a more specific narrow-spectrum antibiotic is prescribed[186]. This time window between initial and definitive therapy is very critical. Previous studies have shown that a delay in the administration of appropriate antibiotics due to long diagnostic times of current clinical methods (24-72 hours) can lead to increased risk of patients mortality, higher costs due to prolonged hospitalization times and increased risk of AR development[186,212,213]. Therefore, the ability of MNAzyme-GNP assay to provide the antibiotic susceptibility results much sooner than the current laboratory techniques will significantly improve the treatment outcomes, reduce healthcare costs, and prevent emergence of AR. The assay demonstrated high analytical sensitivity of 10^2-10^3 CFU/ml, detection of 10 AR genes in parallel for profiling resistance to 5 antibiotic classes, and produced results that matched standard laboratory techniques (*e.g.* PCR and agar diffusion methods, Table 5.3).

In **Chapter 3**, it has been shown that the detection of multiple genes for diagnosis of a pathogen can increase the diagnostic sensitivity of an assay[214]. Similarly, 2 genes were used to test for resistance to the same antibiotic class, which demonstrated better predictive capability compared to using a single gene. For instance, testing for erythromycin resistance in MRSA-41 and 44 resulted negative for *ermC* and positive for *ermA* genes (Figure 5.11). If only *ermC* gene was tested, one could have falsely predicted MRSA-41 and 44 to be susceptible to erythromycin. On the other hand, screening for both *ermA* and *ermC* genes correctly identified the resistance of MRSA-41 and 44 to erythromycin. Current panel includes two AR genes for each antibiotic class; however, this can be easily expanded to include multiple AR genes for each class, which can further increase the diagnostic sensitivity of the assay. Moreover, high detection selectivity was achieved through both RPA and MNAzyme-GNP assay steps. This was confirmed with a cross-reactivity test that demonstrated selective amplification of the AR genes *via* multiplexed RPA followed by specific activation of MNAzyme in response to the presence of corresponding amplification products.

AR can be acquired *via* acquisition of genetic mobile elements or single point mutation in chromosomal genes[215-217]. However, current design can only detect conserved genetic mobile elements responsible for AR. Thus, MNAzyme-GNP assay need to be improved in the future to detect point mutations that are responsible for AR[103].

In conclusion, the proposed assay is simple, instrument-free and provides colorimetric readout. It can be easily adapted to both centralized and remote testing locations in resource-limited countries. This technique is also versatile and can be easily applied to detect different AR genes from different pathogens by simply modifying primer and MNAzyme sequences. Moreover, the ability to detect multiple AR determinants in MDR pathogens will help to minimize the improper use of antibiotics and select for antibiotics that can effectively treat patients who are infected with bacterial pathogens.

Chapter 6: Conclusions

6.1 Summary

In summary, this thesis described pre-clinical development and clinical assessment of two nanoparticle-based assays for POC diagnosis of infectious pathogens. Specifically, fundamental limitations of conventional diagnostic tests were addressed by improving the analytical sensitivity of QD barcode (**Chapters 2** and **3**) and MNAzyme-GNP (**Chapters 4** and **5**) assays *via* the incorporation of an isothermal nucleic acid amplification strategy, RPA.

In **Chapter 2**, the incorporation of RPA with QD barcode assay demonstrated to improve the analytical sensitivity by 6-orders of magnitude, yielding a detection limit of 1 zmol template DNA (~600 copies) per reaction. The integrated QD barcode-based isothermal amplification assay was then used to diagnose treatment-naïve patients infected with HBV and HIV, and to demonstrate simultaneous detection of both diseases using the HBV/HIV co-infection model. Lastly, the assay signals were measured using a smartphone optical device to demonstrate replacement of an expensive and bulky signal readout instrument (*e.g.* flow cytometer, fluorescent microscope, and spectrophotometer) with a portable device for POC testing.

In **Chapter 3**, a thorough clinical validation of QD barcode technology was conducted, where a total of 72 clinical samples of diverse backgrounds that represent a wide spectrum of HBV disease was tested to determine clinical sensitivity, specificity and ROC. Detecting multiple regions of the viral genome using multiplexed QD barcodes demonstrated to improve the diagnostic sensitivity without significantly reducing the specificity level. Also, it has been shown that the proposed diagnostic platform provided better prediction of infectivity when the patients have not received treatment before (*i.e.* treatment-naïve patients) compared to patients who are currently on-treatment or have previous treatment record.

In **Chapter 4,** an improvement in the analytical sensitivity of MNAzyme-GNP assay was demonstrated by 6- and 8-orders of magnitude for HBV and InfA genetic targets respectively with the incorporation of RPA pre-amplification step. Over 90% clinical sensitivity and 95% clinical specificity were measured after screening a total of 56 and 48 clinical samples for HBV and InfA testing respectively.

In **Chapter 5**, detection of multiple AR genetic biomarkers was demonstrated using multiplexed RPA and parallel MNAzyme-GNP assay. Detection limits of 10^2-10^3 DNA copies/reaction, and 10^2-10^3 CFU/mL were achieved with synthetic DNA targets and DNA extracted from MRSA isolate respectively. Three clinical isolates were screened to demonstrate detection of multiple AR genes and determine their corresponding AR profiles. The results from MNAzyme-GNP assay were in a perfect agreement with the results from the gold standard methods for testing AR (*i.e.* PCR and agar diffusion).

6.2 Future Directions

This section gives suggestions to further exploit QD barcode and MNAzyme-GNP assays for POC diagnosis of infectious diseases, and accelerate their translations from academic bench to real-world applications in the future. A total of seven different future studies will be highlighted.

6.2.1 Future Studies for QD Barcode System

[Study #1] HBV Genotyping using Multiplexed RPA and QD Barcodes

The lack of proofreading activity of DNA polymerase in HBV has led to mutations during viral replications and development of eight known HBV genotypes (A-H) that differ by at least 8% of the genome[149]. Various studies have been reported that indicate strong correlation of HBV genotypes with disease progression. For instance, many studies concluded that genotype C is highly associated with rapid liver cirrhosis, and HCC development, recurrence and metastasis when compared to genotype B[218]. Also, some studies suggest that patients who are HBV e-antigen (HBeAg) positive, and carry genotype B or A respond better to interferon (IFN) antiviral therapy than genotype C or D respectively[218]. Sequencing and phylogenetic analyses are considered to be the gold standard HBV genotyping technique; nevertheless, these techniques are expensive, time-consuming and can only detect the most prevalent genotype in the genotype mixture[218]. Other alternative techniques like INNO-LiPA® and multiplex or real-time PCR require DNA amplification using a thermocycler, which is not feasible in POC settings.

A future study can further explore the multiplexing capabilities of RPA and QD barcodes to develop a simple, rapid and "PCR-less" HBV genotyping technique, which can be used in the resource-limited settings to not only diagnose the infection, but also to guide subsequent treatment decisions. There are three specific aims for this study. The first aim is to design HBV genotype-

specific RPA primers based on the unique sequence mutations that are conserved within the five most prevalent genotypes (A-E), and to test for cross-reactivity between different genotypes. The second aim is to develop multiplexed RPA by using a mixture of genotype-specific primers, where the amplification products will be detected *via* QD barcode assay. The third aim is to evaluate diagnostic sensitivity and specificity of screening various HBV genotypes using multiplexed RPA-QD barcode assay.

The overall schematic of multiplexed RPA-QD barcode genotyping assay is illustrated in Figure 6.1. HBV sample of unknown genotype is first amplified *via* multiplexed RPA containing a mixture of genotype-specific primers (GTA-GTE), followed by multiplexed QD barcode assay to identify the unknown genotype. The detection probe signal determines the presence or absence of HBV DNA, and the barcode signal identifies its genotype.

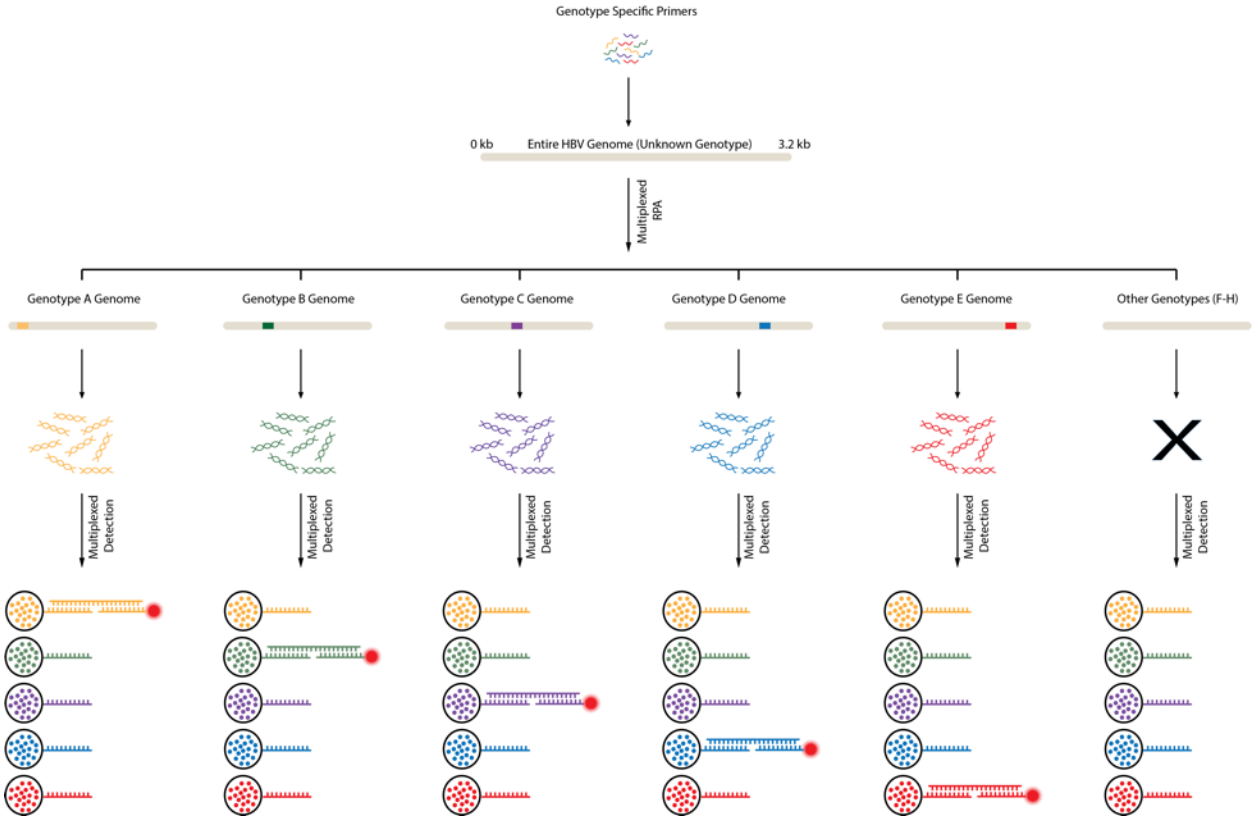

Figure 6.1: Schematic of Multiplexed RPA-QD Barcode Genotyping Assay. A mixture of genotype-specific primers (GTA-GTE) is used to amplify unknown HBV target. After multiplexed RPA, multiplexed QD barcode assay is performed to identify the unknown genotype. The detection probe signal determines the presence or absence of HBV DNA, and the barcode signal identifies the HBV genotype. Other genotypes (F-H) shall not produce RPA products, and result in a negative signal after the assay.

In a preliminary experiment, genotype B (GTB), D (GTD) and E (GTE) specific primers were designed and tested for cross-reactivity in a singleplexed manner (Figure 6.2). For example, GTB-specific primer set was used to amplify GTB, GTC, GTD and GTE samples, and the amplicons were individually incubated with QD barcode conjugated with GTB-specific capture probes. As shown in Figure 6.2A, no cross-reactivity was observed using GTB-specific primer set (*i.e.* none of GTC, GTD and GTE samples produced false-positive signal), and 11/12 (91.7%) GTB samples were correctly identified. Likewise, GTD-specific primer showed 1/3 coverage among GTD samples, and no cross-reactivity with GTB and GTC samples (Figure 6.2B). GTE-specific primer achieved 2/2 coverage among GTE samples, and no cross-reactivity with GTB, GTC and GTD samples (Figure 6.2C).

This preliminary data suggests that RPA and QD barcode assay offer high specificity that allow differentiation between various HBV genotypes. Hence, the next step would be to complete designing HBV genotype-specific primers for the remaining of five most prevalent genotypes (GTA and GTC), demonstrate minimal cross-reactivity in a singleplexed reaction for each genotype as demonstrated in Figure 6.2, optimize multiplex RPA as demonstrated in **Chapter 5**, and finally evaluate the diagnostic sensitivity and specificity of screening various HBV genotypes (GTA-GTE) using multiplexed RPA-QD barcode assay.

Future study can also explore the incorporation of a smartphone optical device used in **Chapter 2** with multiplexed RPA-QD barcode genotyping assay to measure the optical signals of QD barcodes, and remove flow cytometry in the detection process for POC testing. The proposal for this ancillary study has been recently approved by Hepatitis B Research Network (HBRN), where a total of 240 samples will be received through collaboration with Dr. Jordan Feld (University Health Network). Completion of this study can lead to further exploration of the full multiplexing potential of QD barcodes, which will be further discussed in section **6.3**.

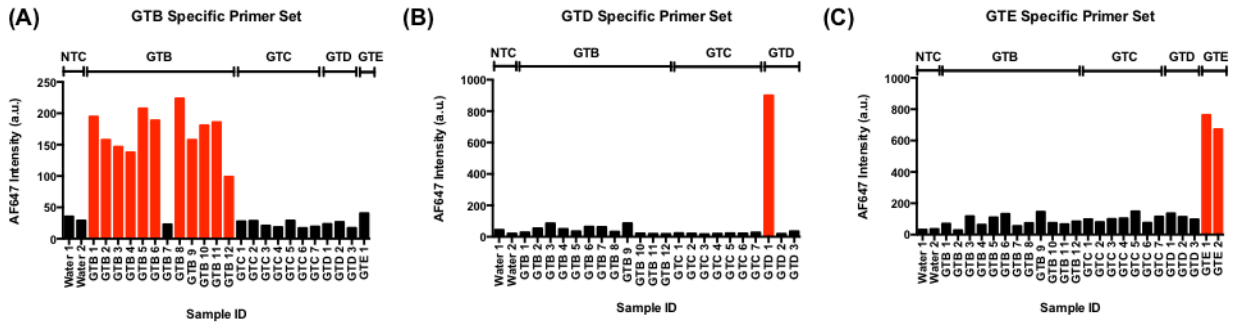

Figure 6.2: Testing Genotype-Specific Primer Sets. Genotype-specific primer sets were tested for cross-reactivity with other genotypes and detection of (A) GTB, (B) GTD, and (C) GTE samples. Red bars indicate positive detection from singleplexed QD barcode assay.

[Study #2] One-step QD Barcode-based Isothermal Amplification Assay

Current QD barcode-based isothermal amplification assay consists of two major steps: 1) amplification using RPA, and 2) post-RPA QD barcode assay. The separation of these two reactions imposes extra minor steps in between including the purification of amplicons after RPA, and thermal or chemical denaturation of RPA products prior to running the QD barcode assay. Combining the amplification and microbead-based assay into a single reaction step can greatly reduce the operational labor and eliminate post-RPA purification and denaturation steps.

A future study can simplify QD barcode-based isothermal amplification assay by using AF647 labelled forward primer and reverse primer conjugated QD barcodes. The schematic of one-step QD barcode-based isothermal amplification assay is illustrated in Figure 6.3. Forward primer is labelled with AF647 and the surface of QD barcode is conjugated with reverse primers, which are then directly used in the RPA reaction as described in previous chapters. First cycle of amplification generates two amplicons that are each labeled with either AF647 or QD barcode. Subsequently, repeated cycles further label the amplicons with AF647 or QD barcode to produce RPA products that are fully labelled with both AF647 and QD barcode. Similar approach has been demonstrated, where magnetic bead and GNP labelled primers were used in RPA for electrochemical detection of *Leishmania* DNA[219]. Such development of a one-step isothermal nucleic acid amplification and microbead hybridization assay can simplify the diagnostic procedure by reducing the number of operational interventions, and thus render QD barcode assay more attainable in areas with limited availability of skilled technicians.

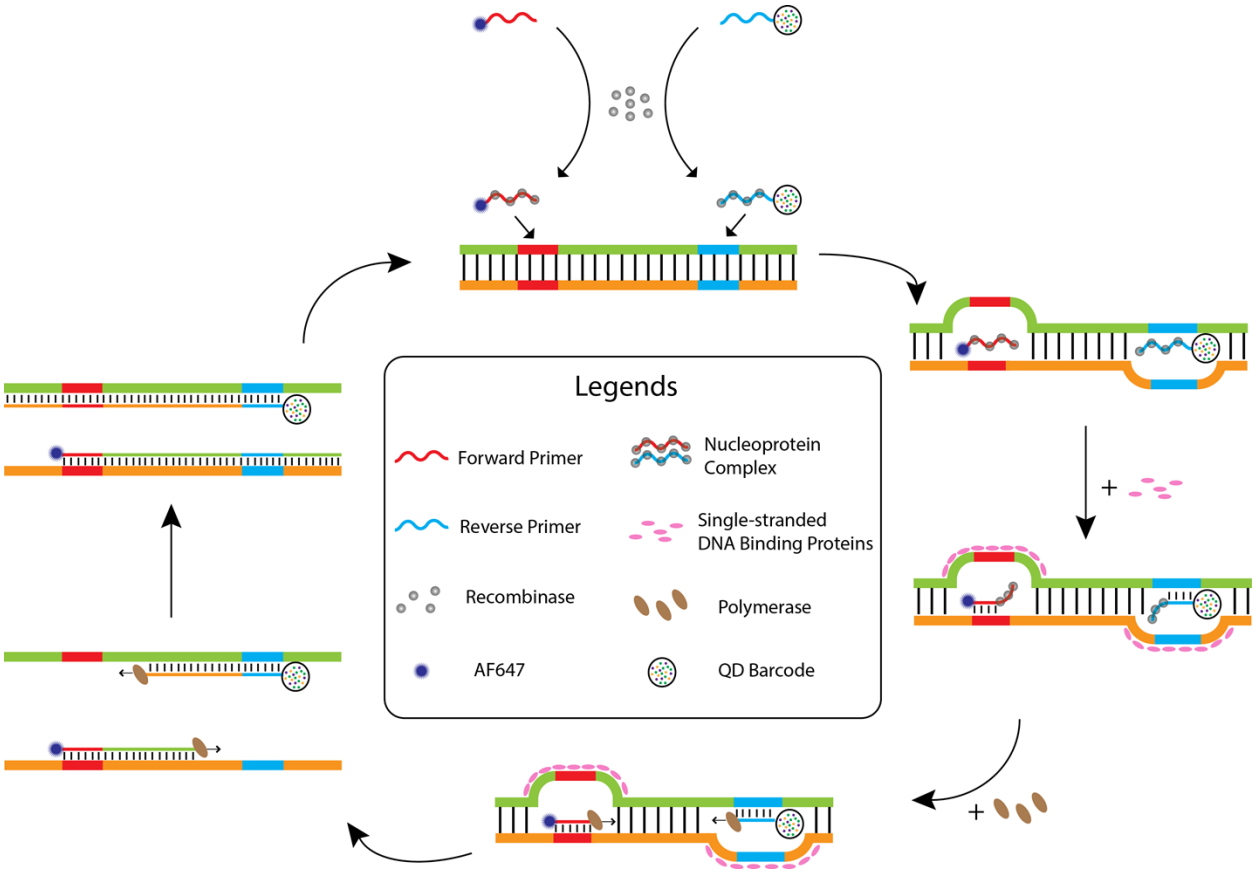

Figure 6.3: One-step QD Barcode-based Isothermal Amplification Assay. The surface of QD barcode is conjugated with reverse primer and the forward primer is labeled with AF647 dye. Repeated amplification cycles generate RPA products that are labeled with both QD barcode and AF647.

6.2.2 Future Studies for MNAzyme-GNP System

[Study #3] Detection of Point Mutations that Confer Antibiotic Resistance

Current MNAzyme-GNP assay cannot differentiate between wildtype and mutated sequences upto ~3 mutations. Nonetheless, many studies have demonstrated that a single point mutation at the gene encoding the target of an antibiotic can confer resistance to that antibiotic[215-217,220,221]. For example, in *S. aureus*, point mutations in *mprF* gene can result in daptomycin resistance, and in *Salmonella enterica,* point mutations in penicillin-binding proteins (PBP3, PBP4, and PBP6) can result in resistance to beta-lactam antibiotics. Hence, there is a need to selectively identify these point mutations by improving the specificity of the assay.

A future study can investigate modifying the current MNAzyme-GNP system to select for point-mutations among wild-type sequences. This can be achieved by re-designing current MNAzyme with truncated sensor and stabilizer arms as demonstrated by Mokany *et al.* (Figure 6.4)[103].

Truncated sensor arm is designed to perfectly match target sequence containing the point-mutation, which will activate the cleavage of linker DNA. On the other hand, wildtype sequence does not activate modified MNAzyme, and linker DNA stays intact. As a result, degraded linker DNA will disaggregate GNPs in a solution in the presence of the point mutation sequence, and intact linker DNA will aggregate GNPs in the presence of the wild-type sequence.

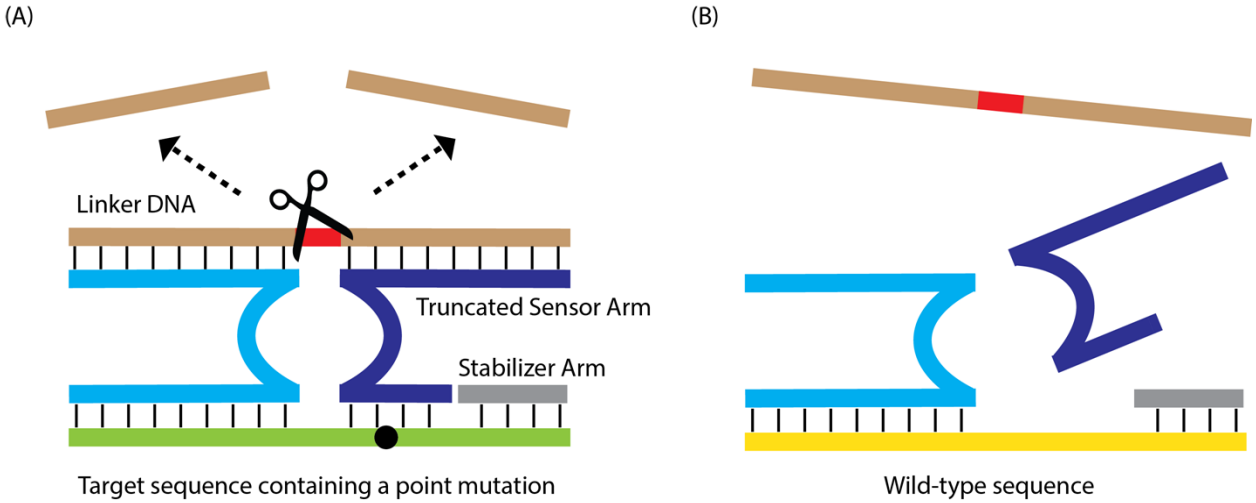

Figure 6.4: Modified MNAzyme Design for Detection of Point Mutations. (A) Modified MNAzyme gets activated by a target sequence containing a point mutation, and cleaves the linker DNA. (B) Modified MNAzyme does not get activated by a wild-type sequence, and linker DNA stays intact.

[Study #4] Clinical Validation of Screening Antibiotic Resistance

Screening of AR using MNAzyme-GNP assay was demonstrated with synthetic DNA targets and DNA extracted from three *S. aureus* isolates in **Chapter 5**. As a follow-up study, a full clinical validation can be conducted to evaluate clinical sensitivity and specificity, and demonstrate the wider utility of this approach

The clinical validation can be accomplished with three major aims. The first aim can explore screening a much larger set of clinical isolates (~100-200) to evaluate the clinical sensitivity and specificity levels. The second aim can explore detection of MDR from different pathogens (*e.g. Streptococcus pneumoniae*, *Enterococcus faecalis*, *Neisseria gonorrhoeae*, *Helicobacter pylori, etc*.) that are extracted from diverse biological fluids (*e.g.* blood, urine, nasal swabs, *etc*.) to demonstrate the versatility of this technique. The third aim can demonstrate improvement on clinical sesntivitiy level with the addition of more AR genes that confer resistance to the same antibiotic class.

The protocol for this study has been recently submitted for Research Ethics Board (REB) approval, and a total of 100 clinical isolates are currently being collected in collaboration with **Dr. Tony Mazzulli** from Mount Sanai Hospital.

6.2.3 Future Studies for Both Systems

[Study #5] Detection of Circulating Tumour DNA for Colorectal Cancer

Although this thesis was focused on the diagnosis of various infectious diseases, the work developed in this study can be easily adopted for diagnosis of other diseases such as cancers. Cancers are the leading cause of global morbidity and mortality, accounting for 8.2 million cancer-related deaths in 2012[222]. Among different types of cancers, colorectal cancer (CRC) represents roughly 26% of all cancer cases. There are approximately 25% of metastatic patients and 50% of later metastasis development upon initial diagnosis[223]. More importantly, the five-year mortality rate of metastatic CRC is about 40%, which can be reduced by at least 16% with annual screening of the disease[224]. Nevertheless, current diagnostic strategies used to screen CRC such as fecal occult blood testing, colonoscopy, or Computed Tomography (CT) colonography provides either poor diagnostic sensitivity, is invasive and expensive requiring highly trained operators, or presents low sensitivity for imaging small lesions respectively. On the other hand, detection of cell-free circulating tumour DNA (ctDNA) offers a promising alternative that is less-invasive, cost-effective and highly sensitive to track disease progression and response to treatment.

Thus, a future study can investigate detection of tumor-specific alterations in ctDNA using either QD barcode or MNAzyme-GNP assays. ctDNA carries genetic and epigenetic alterations such as point mutations, rearranged genomic sequences, degree of integrity, copy number variation, microsatellite instability, DNA methylation, and loss of heterozygosity, which differentiate ctDNA from normal cell-free DNA, and thus can be used in a diagnostic and prognostic liquid biopsy for cancer patients[225]. Specifically, several regions of the *ID4* genes can be amplified *via* RPA, where the cytosines of the gene is aberrantly methylated in tumours compared to healthy subjects. Non-methylated cytosines from healthy subjects will convert to uracil by sodium bisulfate, and therefore will not undergo cytosine-specific nucleic acid amplification. Amplified DNA products can then can be detected using either QD barcode or MNAzyme-GNP assays. The management of CRC necessitates continuous monitoring to track the disease progression and therapeutic success. Current screening techniques are inefficient in repeated monitoring due to low sensitivity and

invasive nature of the diagnosis. The proposed study will demonstrate clinical relevance of detecting ctDNA using nanoparticle-based assays for repeated monitoring of CRC patients and their prognosis.

[Study #6] Streamlining Diagnostic Procedures

The extraction of nucleic acids from biological fluids is a pre-requisite for many DNA or RNA-based *in vitro* diagnostics, which has not been discussed in much detail in this work. Extraction was mostly carried out by using commercially available magnetic beads or silica columns that capture and release nucleic acids on the bead surface or the column membrane depending on the buffer conditions. Such extraction procedure demands multiple additions of the buffers and removal of the supernatants. Also, RPA and both QD barcode and MNAzyme-GNP assays currently require several pipetting steps, which need to be automated to facilitate the usage by non-experts.

Therefore, a single device unit can be engineered in the near future to automate the steps that are involved in running the extraction, amplification, and QD barcode and MNAzyme-GNP assays. Such device is currently being developed by **Pranav Kadhiresan**, a Ph.D. candidate in Chan Lab, who has proposed high-level schematics of the device as shown in Figure 6.5. The proposed device consists of a miniature peristaltic pump, which is used to drive the flow of reagents between tubes. The device accepts patient samples (*e.g.* blood, urine, sputum, nasal swap, *etc*.) from the input, processes the raw samples, and outputs the assay products, which are to be deposited on either a microwell chip for QD barcode assay or TLC plate for MNAzyme-GNP assay, and imaged with a smartphone optical device.

The imaged data can be analyzed using a custom-written software. For QD barcode assay, the software algorithm for de-convoluting QD barcode signals and determining positive and negative signals have already been developed by a colleague, **Dr. Kevin Ming**. The next step is to develop a graphical user interface and re-package this algorithm into a smartphone app. Although the results of MNAzyme-GNP assay can be interpreted using a naked eye, some diagnostic results may become harder to interpret due to weak signals or reader's bias. In such case, a software algorithm can be applied to quantify the amount of red intensity in comparison to green and blue channels (developed by **Abdullah Syed**, Ph.D. Candidate in Chan Lab). The algorithm can also start analyzing the spot sizes in the assessment of signals since spots of aggregated GNPs are

smaller than the spots of dispersed GNPs. It is expected that using both parameters (*i.e.* the color intensity ratios and spot sizes) in the analysis can improve the overall diagnostic accuracy, especially for those results that are harder to determine using a naked eye.

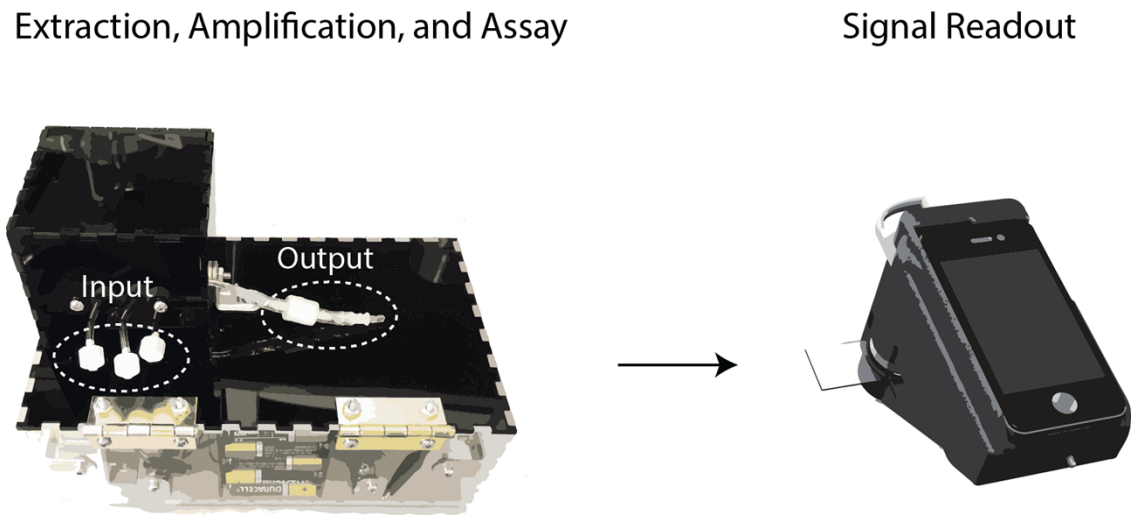

Figure 6.5: Automation of the Extraction, Amplification and Assay. The raw sample is inserted into the device, and the device processes the sample (extraction, amplification and assay). The output from the device gets deposited on a microwell chip (QD barcode assay) or a TLC plate (MNAzyme-GNP assay), imaged using the smartphone optical device, and analyzed using a custom-written software. Figure adapted with permission from Pranav Kadhiresan.

[Study #7] Field Testing and Evaluating Diagnostic Efficacy

Field testing can be conducted in various POC settings (Figure 1.3) to evaluate the diagnostic efficacy of proposed diagnostic platforms. Diagnostic efficacy evaluates the combination of the diagnostic accuracy and clinical effectiveness of POC testing[166]. For instance, it can be defined as the product of positive likelihood ratio and patient notification rate, in which the positive likelihood ratio is calculated as the sensitivity divided by 1 minus specificity, and the patient notification rate is the percentage of patients receiving diagnostic results over a fixed time. Alternatively, these terms can be replaced with other clinical metrics that are used to characterize diagnostic accuracy and clinical effectiveness such as diagnostic odds ratio, Area Under the Curve (AUC) of ROC plot, rate of antibiotic misuse, and time to treatment initiation.

This metric can therefore be used to describe the overall diagnostic performance by capturing the aspect of patient outcome from the implementation of a new POC testing in the field, and accounting for test inaccuracies, delays, and clinical consequences as a result of missing or delaying diagnosis[166].

6.3 Significance

The presented integration of nanoparticle-based molecular assays and isothermal nucleic acid amplification can address the limitations of currently available diagnostic systems by delivering highly sensitive and specific diagnostic platforms that are feasible for testing in resource-poor areas. QD barcode-based diagnostic provides a great capacity for multiplexing, which becomes advantageous for simultaneously diagnosing multiple infectious pathogens that are difficult to differentiate clinically due to common symptoms, or for the investigation of co-infections. For instance, HBV and HCV infections are highly prevalent among HIV-infected patients due to the shared transmission routes, and HIV can modify the natural history of either HBV or HCV infections by accelerating the liver disease progression[226-228]. Hence, QD barcodes can be used to effectively diagnose three diseases in a single test.

Moreover, further multiplexing can be performed by designing additional number of optically distinct QD barcodes to determine genotypes and subtypes of each disease as described in section **6.2.1**. Similar to HBV, HCV is classified into 6 major genotypes that differ in the sequences by 30 to 35%, and respond much differently to interferon-based therapy[148]. For example, HCV genotypes dictate the optimal duration of peginterferon-α2a and ribavirin combined treatment, antiviral dosing, and the likelihood of treatment response[17,229]. HIV is also divided into two major types (HIV-1 and HIV-2), and HIV-1 is further divided into groups and subtypes. Determining the subtypes is important for HIV diagnosis because some of the subtypes are known to be more virulent or resistant to antiviral medications[230]. Therefore, multiple QD barcodes can be designed to not only diagnose various pathogens, but also to identify genotypes and subtypes of each disease to guide subsequent treatment decisions, and improve diagnostic sensitivity using the approach described in **Chapter 3**. Such design would enable diagnosis of multitude of infectious pathogens with high clinical sensitivity, and identification of genotypes and subtypes for better clinical management and outcomes, which can potentially demonstrate high diagnostic efficacy.

Colorimetric diagnosis using MNAzyme-GNP assay becomes significant especially near the left-side of the POC diagnostics spectrum (Figure 1.3). In these settings (*i.e.* home and community) of low-income countries, there are notably limited access to devices and availability of trained technicians; therefore, there is a high demand for simpler and cost-effective diagnostics that can be performed by the non-experts. MNAzyme-GNP assay offers the simplicity and cost-

effectiveness since the diagnostic results are displayed into two different colors, and can be easily acquired and interpreted by a non-expert with an unaided eye. Particularly, the presented colorimetric MNAzyme-GNP diagnostic system will become useful for profiling MDR in the developing countries, where development of MDR in bacterial species pose a greater devastating threat than developed regions due to poor sanitation conditions, failure of available antibiotics, and unavailability of new effective antibiotics.

The smartphone optical device used in **Chapter 2**, and discussed in section **6.2.5**, can concievably accelerate knowledge transfer of emerging or urgent disease threats among healthcare and military organizations in real time. With over 6.8 billion subscriptions globally, handheld mobile-cellular devices can also be programmed to spatially map, temporally track and transmit information of infections over wide geographical space and boundaries. This would enable collaborative clinical management, global surveillance of infectious transmission events, and prediction of temporal infection trends through crowd-sourced data collection.

Bibliography

1. Barreto, M. L., Teixeira, M. G. & Carmo, E. H. Infectious diseases epidemiology. *Journal of Epidemiology & Community Health* **60,** 192–195 (2006).

2. Jones, K. E. *et al.* Global trends in emerging infectious diseases. *Nature* **451,** 990–993 (2008).

3. Fauci, A. S., Touchette, N. A. & Folkers, G. K. Emerging Infectious Diseases: a 10-Year Perspective from the National Institute of Allergy and Infectious Diseases. *Emerging Infectious Diseases* **11,** 519–525 (2005).

4. World Health Organization. World Health Statistics 2009. 47 (2009).

5. Hauck, T. S., Giri, S., Gao, Y. & Chan, W. C. W. Nanotechnology diagnostics for infectious diseases prevalent in developing countries. *Advanced Drug Delivery Reviews* **62,** 438–448 (2010).

6. Zhong, N. S. *et al.* Epidemiology and cause of severe acute respiratory syndrome (SARS) in Guangdong, People's Republic of China, in February, 2003. *The Lancet* **362,** 1353–1358 (2003).

7. Neumann, G., Noda, T. & Kawaoka, Y. Emergence and pandemic potential of swine-origin H1N1 influenza virus. *Nature* **459,** 931–939 (2009).

8. Gostin, L. O., Lucey, D. & Phelan, A. The Ebola Epidemic. *JAMA* **312,** 1095–1096 (2014).

9. Samarasekera, U. & Triunfol, M. Concern over Zika virus grips the world. *The Lancet* **387,** 521–524 (2016).

10. Alter, M. J. Epidemiology of viral hepatitis and HIV co-infection. *J. Hepatol.* **44,** S6–S9 (2006).

11. Yerly, S. *et al.* Nosocomial Outbreak of Multiple Bloodborne Viral Infections. *The Journal of Infectious Diseases* **184,** 369–372 (2001).

12. McCutchan, F. E. Global epidemiology of HIV. *Journal of Medical Virology* **78,** S7–S12 (2006).

13. Vogel, M. *et al.* The Treatment of Patients With HIV. *Deutsches Arzteblatt International* **107,** 507–515 (2010).

14. Lavanchy, D. Worldwide epidemiology of HBV infection, disease burden, and vaccine prevention. *J. Clin. Virol.* **34,** S1–S3 (2005).

15. EASL. EASL Clinical Practice Guidlines: Management of chronic heptitis B virus infection. *J. Hepatol.* **57,** 167–185 (2012).

16. Schweitzer, A., Horn, J., Mikolajczyk, R. T., Krause, G. & Ott, J. J. Estimations of worldwide prevalence of chronic hepatitis B virus infection: a systematic review of data published between 1965 and 2013. *The Lancet* **386,** 1546–1555 (2015).

17. Shepard, C. W., Finelli, L. & Alter, M. J. Global epidemiology of hepatitis C virus infection. *The Lancet Infectious Diseases* **5,** 558–567 (2005).

18. Kania, D. *et al.* Combining rapid diagnostic tests and dried blood spot assays for point-of-care testing of human immunodeficiency virus, hepatitis B and hepatitis C infections in Burkina Faso, West Africa. *Clinical Microbiology and Infection* **19,** E533–E541 (2014).

19. Al-Tawfiq, J. A. *et al.* Surveillance for emerging respiratory viruses. *The Lancet Infectious Diseases* **14,** 992–1000 (2014).

20. Russell, C. A. *et al.* The Global Circulation of Seasonal Influenza A (H3N2) Viruses. *Science* **320,** 340–346 (2008).

21. Rambaut, A. *et al.* The genomic and epidemiological dynamics of human influenza A virus. *Nature* **453,** 615–619 (2008).

22. Taubenberger, J. K. & Kash, J. C. Influenza Virus Evolution, Host Adaptation, and Pandemic Formation. *Cell Host and Microbe* **7,** 440–451 (2010).

23. Simonsen, L. *et al.* Pandemic versus Epidemic Influenza Mortality: A Pattern of Changing Age Distribution. *The Journal of Infectious Diseases* 53–60 (1998).

24. Thompson, W. W. *et al.* Mortality Associated With Influenza and Respiratory Syncytial Virus in the United States. *JAMA* **289,** 179–186 (2003).

25. Olsen, B. *et al.* Global Patterns of Influenza A Virus in Wild Birds. *Science* **312,** 384–388 (2006).

26. Guan, Y. *et al.* H5N1 influenza: A protean pandemic threat. *Proc. Natl. Acad. Sci.* **101,** 8156–8161 (2004).

27. Cox, N. J. & Subbarao, K. Global Epidemiology of Infleunza: Past and Present. *Annual Review of Medicine* **51,** 407–421 (2000).

28. Vemula, S. *et al.* Current Approaches for Diagnosis of Influenza Virus Infections in Humans. *Viruses* **8,** 96–111 (2016).

29. Neu, H. C. The Crisis in Antibiotic Resistance. *Science* **257,** 1064–1073 (1992).

30. Levy, S. B. & Marshall, B. Antibacterial resistance worldwide: causes, challenges and responses. *Nature Medicine* **10,** S122–S129 (2004).

31. Cohen, M. L. Epidemiology of Drug Resistance: Implications for a Post-Antimicrobial Era. *Science* **257,** 1050–1055 (1992).

32. Morgan, D. J., Okeke, I. N., Laxminarayan, R., Perencevich, E. N. & Weisenberg, S. Non-prescription antimicrobial use worldwide: a systematic review. *The Lancet Infectious Diseases* **11,** 692–701 (2011).

33. Laxminarayan, R. Antibiotic effectiveness: Balancing conservation against innovation. *Science* **345,** 1299–1301 (2014).

34. Murray, C. K., Gasser, R. A., Magill, A. J. & Miller, R. S. Update on Rapid Diagnostic Testing for Malaria. *Clinical Microbiology Reviews* **21,** 97–110 (2008).

35. Wongsrichanalai, C., Barcus, M. J., Muth, S., Sutamihardja, A. & Wernsdorfer, W. H. A Review of Malaria Diagnostic Tools: Microscopy and Rapid Diagnostic Test (RDT). *Am. J. Trop. Med. Hyg.* **77,** 119–127 (2007).

36. Payne, D. Use and limitations of light microscopy for diagnosing malariaattheprimaryhealthcarelevel. *Bulletin of the World Health Organization* **66,** 621–626 (1988).

37. Steingart, K. R. *et al.* Fluorescence versus conventional sputum smear microscopy for tuberculosis: a systematic review. *The Lancet Infectious Diseases* **6,** 570–581 (2006).

38. Singhal, R. & Myneedu, V. P. Microscopy as a diagnostic tool in pulmonary tuberculosis. *International Journal of Mycobacteriology* **4,** 1–6 (2015).

39. Vickers, D., Ahmad, T. & Coulthard, M. G. Diagnosis of urinary tract infection in children: fresh urine microscopy or culture? *The Lancet* **338,** 767–770 (1991).

40. Wilson, M. L. & Gaido, L. Laboratory Diagnosis of Urinary Tract Infections in Adult Patients. *Medical Microbiology* **38,** 1150–1158 (2004).

41. Jenkins, R. D., Fenn, J. P. & Matsen, J. M. Review of Urine Microscopy for Bacteriuria. *JAMA* **255,** 3397–3403 (1986).

42. Tek, F. B., Dempster, A. G. & Kale, I. Computer vision for microscopy diagnosis of malaria. *Malar J* **8,** 153–167 (2009).

43. Pulido, M. R., Garcia-Quintanilla, M., Martin-Pena, R., Cisneros, J. M. & McConnell, M. J. Progress on the development of rapid methods for antimicrobial susceptibility testing. *Journal of Antimicrobial Chemotherapy* **68,** 2710–2717 (2013).

44. Jorgensen, J. H. & Ferraro, M. J. Antimicrobial Susceptibility Testing: A Review of General Principles and Contemporary Practices. *CLIN INFECT DIS* **49,** 1749–1755 (2009).

45. Gan, S. D. & Patel, K. R. Enzyme Immunoassay and Enzyme-Linked Immunosorbent Assay. *Journal of Investigative Dermatology* **133,** e12–e14 (2013).

46. Wright, P. F., Nilsson, E., Vanrooij, E. M. A., Lelenta, M. & Jeggo, M. H. Standardisation and validation of enzyme-linked immunosorbent assay techniques for

the detection of antibody in infectious disease diagnosis. *Rev. sci. tech. Off. int. Epiz.* **12,** 435–450 (1993).

47. Sia, S. K., Linder, V., Parviz, B. A., Siegel, A. & Whitesides, G. M. An Integrated Approach to a Portable and Low-Cost Immunoassay for Resource-Poor Settings. **43,** 498–502 (2004).

48. Li, X. J., Nie, Z. H., Cheng, C. M., Goodale, A. B. & Whitesides, G. M. PAPER-BASED ELECTROCHEMICAL ELISA. *14th International Conference on Miniaturized Systems for Chemistry and Life Sciences* 1487–1489 (2010).

49. Posthuma-Trumpie, G. A., Korf, J. & van Amerongen, A. Lateral flow (immuno)assay: its strengths, weaknesses, opportunities and threats. A literature survey. *Anal Bioanal Chem* **393,** 569–582 (2008).

50. Heid, C. A., Stevens, J., Livak, K. J. & Williams, P. M. Real Time Quantitative PCR. *Genome Research* **6,** 986–994 (1996).

51. Vogelstein, B. & Kinzler, K. W. Digital PCR. *Proc Natl Acad Sci USA* **96,** 9236–9241 (1999).

52. Sanchez, J. A., Pierce, K. E., Rice, J. E. & Wangh, L. J. Linear-After-The-Exponential (LATE)–PCR: An advanced method of asymmetric PCR and its uses in quantitative real-time analysis. *Proc Natl Acad Sci USA* **101,** 1933–1938 (2004).

53. Bustin, S. A. Quantification of mRNA using real-time reverse transcription PCR (RT-PCR): trends and problems. *Journal of Molecular Endocrinology* **29,** 23–39 (2002).

54. Henegariu, O., Heerema, N. A., Dlouhy, S. R., Vance, G. H. & Vogt, P. H. Multiplex PCR: Critical Parameters and Step-by-Step Protocol. *BioTechniques* **23,** 504–511 (1997).

55. Edwards, M. C. & Gibbs, R. A. Multiplex PCR: Advantages, Development and Applications. *Genome Research* **3,** S65–S75 (1994).

56. Mullis, K. *et al.* Specific Enzymatic Amplification of DNA In Vitro: The Polymerase Chain Reaction. *Cold Spring Harbor Symposia on Quantitative Biology* 263–273 (1986).

57. Nam, J.-M., Stoeva, S. I. & Mirkin, C. A. Bio-Bar-Code-Based DNA Detection with PCR-like Sensitivity. *J. Am. Chem. Soc.* **126,** 5932–5933 (2004).

58. Espy, M. J. *et al.* Real-Time PCR in Clinical Microbiology: Applications for Routine Laboratory Testing. *Clinical Microbiology Reviews* **19,** 165–256 (2006).

59. Peeling, R. W. & Mabey, D. Point-of-care tests for diagnosing infections in the developing world. *Clinical Microbiology and Infection* **16,** 1062–1069 (2010).

60. Pai, N. P., Vadnais, C., Denkinger, C., Engel, N. & Pai, M. Point-of-Care Testing for

Infectious Diseases: Diversity, Complexity, and Barriers in Low- And Middle-Income Countries. *PLoS Med* **9,** e1001306–7 (2012).

61. The PLoS Medicine Editors. Speed and Convenience Aren't Everything with Diagnostics. *PLoS Med* **8,** e1001113–2 (2011).

62. Balogh, L. P. Why do we have so many definitions for nanoscience and nanotechnology? *Nanomedicine: Nanotechnology, Biology, and Medicine* **6,** 397–398 (2010).

63. Link, S. & El-Sayed, M. A. Shape and size dependence of radiative, non-radiative and photothermal properties of gold nanocrystals. *International Reviews in Physical Chemistry* **19,** 409–453 (2000).

64. Kim, B. Y. S., Rutka, J. T. & Chan, W. C. W. Nanomedicine. *The New England Journal of Medicine* **363,** 2434–2443 (2010).

65. Wich, P. R. Baukasten der Natur. *Nachrichten aus der Chemie* **63,** 128–132 (2015).

66. Reiss, P., Protière, M. & Li, L. Core/Shell Semiconductor Nanocrystals. *Small* **5,** 154–168 (2009).

67. Alivisatos, A. P. Semiconductor Clusters, Nanocrystals, and Quantum Dots. *Science* **271,** 933–937 (1996).

68. Kairdolf, B. A. *et al.* Semiconductor Quantum Dots for Bioimaging and Biodiagnostic Applications. *Annu. Rev. Anal. Chem.* **6,** 143–162 (2013).

69. Alivisatos, P. The use of nanocrystals in biological detection. *Nat. Biotechnol.* **22,** 47–52 (2003).

70. Jin, Z. & Hildebrandt, N. Semiconductor quantum dots for in vitro diagnostics and cellular imaging. *Trends Biotechnol.* **30,** 394–403 (2012).

71. Chan, W. C. W. & Nie, S. Quantum Dot Bioconjugates for Ultrasensitive Nonisotopic Detection. *Science* **281,** 2016–2018 (1998).

72. Isola, N. R., Stokes, D. L. & Vo-Dinh, T. Surface-Enhanced Raman Gene Probe for HIV Detection. *Anal. Chem.* **70,** 1352–1356 (1998).

73. Ioannou, D. & Griffin, D. K. Nanotechnology and molecular cytogenetics: the future has not yet arrived. *Nano Reviews* **1,** 5117 (2010).

74. Han, M., Gao, X., Su, J. Z. & Nie, S. Quantum-dot-tagged microbeads for multiplexed optical coding of biomolecules. *Nat. Biotechnol.* **19,** 631–635 (2001).

75. Zhang, C.-Y. & Hu, J. Single Quantum Dot-Based Nanosensor for Multiple DNA Detection. *Anal. Chem.* **82,** 1921–1927 (2010).

76. Medintz, I. L. *et al.* Self-assembled nanoscale biosensors based on quantum dot FRET

donors. *Nature Materials* **2,** 630–638 (2003).

77. Zhang, C.-Y. & Johnson, L. W. Quantum-Dot-Based Nanosensor for RRE IIB RNA−Rev Peptide Interaction Assay. *J. Am. Chem. Soc.* **128,** 5324–5325 (2006).

78. Klostranec, J. M. *et al.* Convergence of Quantum Dot Barcodes with Microfluidics and Signal Processing for Multiplexed High-Throughput Infectious Disease Diagnostics. *Nano Lett.* **7,** 2812–2818 (2007).

79. Giri, S., Sykes, E. A., Jennings, T. L. & Chan, W. C. W. Rapid Screening of Genetic Biomarkers of Infectious Agents Using Quantum Dot Barcodes. *ACS Nano* **5,** 1580–1587 (2011).

80. Park, J., Park, Y. & Kim, S. Signal Amplification via Biological Self-Assembly of Surface-Engineered Quantum Dots for Multiplexed Subattomolar Immunoassays and Apoptosis Imaging. *ACS Nano* **7,** 9416–9427 (2013).

81. Peng, C. *et al.* Simultaneous and sensitive determination of multiplex chemical residues based on multicolor quantum dot probes. *Biosensors and Bioelectronics* **24,** 3657–3662 (2009).

82. Fournier Bidoz, S. *et al.* Facile and Rapid One-Step Mass Preparation of Quantum-Dot Barcodes. *Angew. Chem.* **47,** 5577–5581 (2008).

83. Wang, G. *et al.* Highly Efficient Preparation of Multiscaled Quantum Dot Barcodes for Multiplexed Hepatitis B Detection. *ACS Nano* **7,** 471–481 (2013).

84. Chen, K., Chou, L. Y. T., Song, F. & Chan, W. C. W. Fabrication of metal nanoshell quantum-dot barcodes for biomolecular detection. *Nano Today* **8,** 228–234 (2013).

85. Reddy, L. H., Arias, J. L., Nicolas, J. & Couvreur, P. Magnetic Nanoparticles: Design and Characterization, Toxicity and Biocompatibility, Pharmaceutical and Biomedical Applications. *Chem. Rev.* **112,** 5818–5878 (2012).

86. Prijic, S. & Sersa, G. Magnetic nanoparticles as targeted delivery systems in oncology. *Radiology and Oncology* **45,** 1–16 (2011).

87. Chung, H. J., Castro, C. M., Im, H., Lee, H. & Weissleder, R. A magneto-DNA nanoparticle system for rapid detection and phenotyping of bacteria. *Nature Nanotechnology* **8,** 369–375 (2013).

88. Liong, M. *et al.* Magnetic barcode assay for genetic detection of pathogens. *Nature Communications* **4,** 1752–9 (1AD).

89. Haun, J. B. *et al.* Micro-NMR for Rapid Molecular Analysis of Human Tumor Samples.pdf. *Science* **3,** 1–14 (2011).

90. Lee, H., Sun, E., Ham, D. & Weissleder, R. Chip–NMR biosensor for detection and molecular analysis of cells. *Nature Medicine* **14,** 869–874 (2008).

91. Giri, S., Li, D. & Chan, W. C. W. Engineering multifunctional magnetic-quantum dot barcodes by flow focusing. *Chem. Commun.* **47,** 4195 (2011).

92. Wang, G. *et al.* Efficient preparation of magnetic quantum dot barcodes. *Journal of Materials Chemistry B: Materials for biology and medicine* **2,** 8310–8313 (2014).

93. Gao, Y., Lam, A. W. Y. & Chan, W. C. W. Automating Quantum Dot Barcode Assays Using Microfluidics and Magnetism for the Development of a Point-of-Care Device. *ACS Appl. Mater. Interfaces* **5,** 2853–2860 (2013).

94. Kelly, K. L., Coronado, E., Zhao, L. L. & Schatz, G. C. The Optical Properties of Metal Nanoparticles: The Influence of Size, Shape, and Dielectric Environment. *J. Phys. Chem. B* **107,** 668–677 (2003).

95. Ghosh, S. K. & Pal, T. Interparticle Coupling Effect on the Surface Plasmon Resonance of Gold Nanoparticles: From Theory to Applications. *Chem. Rev.* **107,** 4797–4862 (2007).

96. Gao, J., Bender, C. M. & Murphy, C. J. Dependence of the Gold Nanorod Aspect Ratio on the Nature of the Directing Surfactant in Aqueous Solution. *Langmuir* **19,** 9065–9070 (2003).

97. Elghanian, R., Storhoff, J. J., Mucic, R. C., Letsinger, R. L. & Mirkin, C. A. Selective Colorimetric Detection of Polynucleotides Based on the Distance-Dependent Optical Properties of Gold Nanoparticles. *Science* **277,** 1078–1081 (1997).

98. Li, J., Guo, H. & Li, Z.-Y. Microscopic and macroscopic manipulation of gold nanorod and its hybrid nanostructures [Invited]. *Photon. Res.* **1,** 28–41 (2013).

99. Taton, T. A., Mirkin, C. A. & Letsinger, R. L. Scanometric DNA Array Detection with Nanoparticle Probes. *Science* **289,** 1757–1760 (2000).

100. Stoeva, S. I., Lee, J.-S., Thaxton, C. S. & Mirkin, C. A. Multiplexed DNA Detection with Biobarcoded Nanoparticle Probes. *Angew. Chem.* **118,** 3381–3384 (2006).

101. Nam, J.-M., Thaxton, C. S. & Mirkin, C. A. Nanoparticle-Based Bio–Bar Codes for the Ultrasensitive Detection of Proteins. *Science* **301,** 1884–1886 (2003).

102. Stoeva, S. I., Lee, J.-S., Smith, J. E., Rosen, S. T. & Mirkin, C. A. Multiplexed Detection of Protein Cancer Markers with Biobarcoded Nanoparticle Probes. *J. Am. Chem. Soc.* **128,** 8378–8379 (2006).

103. Mokany, E., Bone, S. M., Young, P. E., Doan, T. B. & Todd, A. V. MNAzymes, a Versatile New Class of Nucleic Acid Enzymes That Can Function as Biosensors and Molecular Switches. *J. Am. Chem. Soc.* **132,** 1051–1059 (2010).

104. Zagorovsky, K. & Chan, W. C. W. A Plasmonic DNAzyme Strategy for Point-of-Care Genetic Detection of Infectious Pathogens. *Angewandte Chemie International Edition* **52,** 3168–3171 (2013).

105. Chan, W. C. W. *et al.* Patients, Here Comes More Nanotechnology. *ACS Nano* **10,** 8139–8142 (2016).

106. Gao, Y., Stanford, W. L. & Chan, W. C. W. Quantum-Dot-Encoded Microbeads for Multiplexed Genetic Detection of Non-amplified DNA Samples. *Small* **7,** 137–146 (2010).

107. Zhao, W., Ali, M. M., Brook, M. A. & Li, Y. Rolling Circle Amplification: Applications in Nanotechnology and Biodetection with Functional Nucleic Acids. *Angewandte Chemie International Edition* **47,** 6330–6337 (2008).

108. Zhao, Y., Chen, F., Li, Q., Wang, L. & Fan, C. Isothermal Amplification of Nucleic Acids. *Chem. Rev.* **115,** 12491–12545 (2015).

109. Lizardi, P. M. *et al.* Mutation detection and single-molecule counting using isothermal rolling-circle amplification. *Nature Genetics* **19,** 225–232 (1998).

110. Walker, G. T., Little, M. C., Nadeau, J. G. & Shank, D. D. Isothermal in vitro amplification of DNA by a restriction enzyme/DNA polymerase system. *Proc Natl Acad Sci USA* **89,** 392–396 (1992).

111. Yan, L. *et al.* Isothermal amplified detection of DNA and RNA. *Mol. BioSyst.* **10,** 970–1003 (2014).

112. Tomita, N., Mori, Y., Kanda, H. & Notomi, T. Loop-mediated isothermal amplification (LAMP) of gene sequences and simple visual detection of products. *Nat Protoc* **3,** 877–882 (2008).

113. Notomi, T. *et al.* Loop-mediated isothermal amplification of DNA. **28,** e63 (2000).

114. Vincent, M., Xu, Y. & Kong, H. Helicase-dependent isothermal DNA amplification. *EMBO Rep* **5,** 795–800 (2004).

115. Jeong, Y.-J., Park, K. & Kim, D.-E. Isothermal DNA amplification in vitro: the helicase-dependent amplification system. *Cell. Mol. Life Sci.* **66,** 3325–3336 (2009).

116. Piepenburg, O., Williams, C. H., Stemple, D. L. & Armes, N. A. DNA Detection Using Recombination Proteins. *PLoS Biol.* **4,** 1115–1121 (2006).

117. Craw, P. & Balachandran, W. Isothermal nucleic acid amplification technologies for point-of-care diagnostics: a critical review. *Lab on a Chip* **12,** 2469–2486 (2012).

118. Piepenburg, O. & Armes, N. Biochemical solutions for portable nucleic acid testing. *BioWorld EUROPE* 38–41 (2007).

119. Mori, Y. & Notomi, T. Loop-mediated isothermal amplification (LAMP): a rapid, accurate, and cost-effective diagnostic method for infectious diseases. *Journal of Infection and Chemotherapy* **15,** 62–69 (2009).

120. Han, M., Gao, X., Su, J. Z. & Nie, S. Quantum-dot-tagged microbeads for multiplexed optical coding of biomolecules. *Nat. Biotechnol.* **19,** 631–635 (2001).

121. Alivisatos, P. The use of nanocrystals in biological detection. *Nat. Biotechnol.* **22,** 47–52 (2003).

122. Huh, D., Gu, W., Kamotani, Y., Grotberg, J. B. & Takayama, S. Microfluidics for flow cytometric analysis of cells and particles. *Physiol. Meas.* **26,** R73–R98 (2005).

123. Chung, T. D. & Kim, H. C. Recent advances in miniaturized microfluidic flow cytometry for clinical use. *Electrophoresis* **28,** 4511–4520 (2007).

124. Jani, I. V., Janossy, G. & Brown, D. W. G. Multiplexed immunoassays by flow cytometry for diagnosis and surveillance of infectious diseases in resource-poor settings. *The Lancet* **2,** 243–250 (2002).

125. Hines, M. A. & Guyot-Sionnest, P. Synthesis and Characterization of Strongly Luminescing ZnS-Capped CdSe Nanocrystals. *J. Phys. Chem.* **100,** 468–471 (1996).

126. Peng, X., Schlamp, M. C., Kadavanich, A. V. & Alivisatos, A. P. Epitaxial Growth of Highly Luminescent CdSe/CdS Core/Shell Nanocrystals with Photostability and Electronic Accessibility. *J. Am. Chem. Soc.* 7019–7029 (1997).

127. Xu, Z., Shen, C., Hou, Y., Gao, H. & Sun, S. Oleylamine as Both Reducing Agent and Stabilizer in a Facile Synthesis of Magnetite Nanoparticles. *Chem. Mater.* **21,** 1778–1780 (2009).

128. Huy, T. T.-T. *et al.* Genotype C of hepatitis B virus can be classified into at least two subgroups. *Journal of General Virology* **85,** 283–292 (2004).

129. Guizar-Sicairos, M., Thurman, S. T. & Fienup, J. R. Efficient subpixel image registration algorithms. *OPTICS LETTERS* **33,** 156–158 (2008).

130. Ballard, D. H. Generalizing the Hough Transform to Detect Arbitrary Shapes. *Pattern Recognition* **13,** 111–122 (1981).

131. Breslauer, D. N., Maamari, R. N., Switz, N. A., Lam, W. A. & Fletcher, D. A. Mobile Phone Based Clinical Microscopy for Global Health Applications. *PLoS One* **4,** e6320 (2009).

132. Wei, Q. *et al.* Fluorescent Imaging of Single Nanoparticles and Viruses on a Smart Phone. *ACS Nano* **7,** 9147–9155 (2013).

133. Zhu, H., Mavandadi, S., Coskun, A. F., Yaglidere, O. & Ozcan, A. Optofluidic Fluorescent Imaging Cytometry on a Cell Phone. *Anal. Chem.* **83,** 6641–6647 (2011).

134. Zhu, H., Yaglidere, O., Su, T.-W., Tseng, D. & Ozcan, A. Cost-effective and compact wide-field fluorescent imaging on a cell-phone. *Lab on a Chip* **11,** 315–322 (2011).

135. Zhu, H. *et al.* Cost-effective and rapid blood analysis on a cell-phone. *Lab on a Chip* **13,** 1282–1288 (2013).

136. Mudanyali, O. *et al.* Integrated rapid-diagnostic-test reader platform on a cellphone. *Lab on a Chip* **12,** 2678–2686 (2012).

137. Wang, S. *et al.* Integration of cell phone imaging with microchip ELISA to detect ovarian cancer HE4 biomarker in urine at the point-of-care. *Lab on a Chip* **11,** 3411–3418 (2011).

138. Stedtfeld, R. D. *et al.* Gene-Z: a device for point of care genetic testing using a smartphone. *Lab on a Chip* **12,** 1454–1462 (2012).

139. Preechaburana, P., Gonzalez, M. C., Suska, A. & Filippini, D. Surface Plasmon Resonance Chemical Sensing on Cell Phones. *Angewandte Chemie International Edition* **51,** 11585–11588 (2012).

140. Zhu, H., Isikman, S. O., Mudanyali, O., Greenbaum, A. & Ozcan, A. Optical imaging techniques for point-of-care diagnostics. *Lab on a Chip* **13,** 51–67 (2013).

141. Preechaburana, P., Suska, A. & Filippini, D. Biosensing with cell phones. *Trends Biotechnol.* **32,** 351–355 (2014).

142. Chu, C.-W. *et al.* Comparison of clinical, virologic and pathologic features in patients with acute hepatitis B and C. *Journal of Gastroenterology and Hepatology* **16,** 209–214 (2001).

143. Chan, W. C. W. A Call for Clinical Studies. *ACS Nano* **8,** 4055–4057 (2014).

144. Mitragotri, S. *et al.* Accelerating the Translation of Nanomaterials in Biomedicine. *ACS Nano* **9,** 6644–6654 (2015).

145. Thaxton, S. *et al.* Nanoparticle-based bio-barcode assay redefines '"undetectable"' PSA and biochemical recurrence after radical prostatectomy. *Proc. Natl. Acad. Sci.* **106,** 18437–18442 (2009).

146. Jin, Z. & Hildebrandt, N. Semiconductor quantum dots for in vitro diagnostics and cellular imaging. *Trends Biotechnol.* **30,** 394–403 (2012).

147. Bartholomeusz, A. & Schaefer, S. Hepatitis B virus genotypes: comparison of genotyping methods. *Rev. Med. Virol.* **14,** 3–16 (2004).

148. Margeridon-Thermet, S. & Shafer, R. W. Comparison of the Mechanisms of Drug Resistance among HIV, Hepatitis B, and Hepatitis C. *Viruses* **2,** 2696–2739 (2010).

149. Sunbul, M. Hepatitis B virus genotypes: Global distribution and clinical importance. *World J. Gastroenterol.* **20,** 5427–5434 (2014).

150. Daher, R. K., Stewart, G., Boissinot, M., Boudreau, D. K. & Bergeron, M. G.

Influence of sequence mismatches on the specificity of recombinase polymerase amplification technology. *Mol. Cell. Probes* **29,** 116–121 (2015).

151. Boyle, D. S. *et al.* Rapid Detection of HIV-1 Proviral DNA for Early Infant Diagnosis Using Recombinase Polymerase Amplification. *mBio* **4,** e00135–13 (2013).

152. Peng, X., Schlamp, M. C., Kadavanich, A. V. & Alivisatos, A. P. Epitaxial Growth of Highly Luminescent CdSe/CdS Core/Shell Nanocrystals with Photostability and Electronic Accessibility. *J. Am. Chem. Soc.* **119,** 7019–7029 (1997).

153. Hines, M. A. & Guyot-Sionnest, P. Synthesis and Characterization of Strongly Luminescing ZnS-Capped CdSe Nanocrystals. *J. Phys. Chem.* **100,** 468–471 (1996).

154. Papatheodoridis, G. V., Manolakopoulos, S. & Lok, A. Follow-up and indications for liver biopsy in HBeAg-negative chronic hepatitis B virus infection with persistently normal ALT: A systematic review. *J. Hepatol.* **57,** 196–202 (2012).

155. McClish, D. K. Analyzing a Portion of the ROC Curve. *Medical Decision Making* **9,** 190–195 (1989).

156. Yeh, M.-L. *et al.* Comparison of the Abbott RealTime HBV assay with the Roche Cobas AmpliPrep/Cobas TaqMan HBV assay for HBV DNA detection and quantification. *J. Clin. Virol.* **60,** 206–214 (2014).

157. Zaghloul, H. & Mahmoud, E.-S. Recombinase polymerase amplification as a promising tool in hepatitis C virus diagnosis. *World Journal of Hepatology* **6,** 916–922 (2014).

158. Crannell, Z. A., Rohrman, B. & Richards-Kortum, R. Equipment-Free Incubation of Recombinase Polymerase Amplification Reactions Using Body Heat. *PLoS One* **9,** e112146 (2014).

159. Ming, K. *et al.* Integrated Quantum Dot Barcode Smartphone Optical Device for Wireless Multiplexed Diagnosis of Infected Patients. *ACS Nano* **9,** 3060–3074 (2015).

160. Kersting, S., Rausch, V., Bier, F. F. & Nickisch-Rosenegk, Von, M. Multiplex isothermal solid-phase recombinase polymerase amplification for the specific and fast DNA-based detection of three bacterial pathogens. *Microchim. Acta* **181,** 1715–1723 (2014).

161. Crannell, Z. A., Rohrman, B. & Richards-Kortum, R. Development of a Quantitative Recombinase Polymerase Amplification Assay with an Internal Positive Control. *J. Visualized Exp.* e52620 (2015). doi:10.3791/52620

162. Zhang, L. *et al.* Integrated Microcapillary for Sample-to-Answer Nucleic Acid Pretreatment, Amplification, and Detection. *Anal. Chem.* **86,** 10461–10466 (2014).

163. Breadmore, M. C. *et al.* Microchip-Based Purification of DNA from Biological Samples. *Anal. Chem.* **75,** 1880–1886 (2003).

164. Zhang, R., Gong, H.-Q., Zeng, X., Lou, C. & Sze, C. A Microfluidic Liquid Phase Nucleic Acid Purification Chip to Selectively Isolate DNA or RNA from Low Copy/Single Bacterial Cells in Minute Sample Volume Followed by Direct On-Chip Quantitative PCR Assay. *Anal. Chem.* **85,** 1484–1491 (2013).

165. Yang, S. & Rothman, R. E. PCR-based diagnostics for infectious diseases: uses, limitations, and future applications in acute-care settings. *The Lancet Infectious Diseases* **4,** 337–348 (2004).

166. Drain, P. K. *et al.* Diagnostic point-of-care tests in resource-limited settings. *The Lancet Infectious Diseases* **14,** 239–249 (2014).

167. Mabey, D., Peeling, R. W., Ustianowski, A. & Perkins, M. D. Diagnostics for the developing world. *Nature Reviews Microbiology* **2,** 231–240 (2004).

168. Mirkin, C. A., Letsinger, R. L., Mucic, R. C. & Storhoff, J. J. A DNA-based method for rationally assembling nanoparticles into macroscopic materials. *Nature* **382,** 607–609 (1996).

169. Han, M. S., Lytton-Jean, A. K. R., Oh, B.-K., Heo, J. & Mirkin, C. A. Colorimetric Screening of DNA-Binding Molecules with Gold Nanoparticle Probes. *Angewandte Chemie International Edition* **45,** 1807–1810 (2006).

170. Reynolds, R. A., Mirkin, C. A. & Letsinger, R. L. Homogeneous, Nanoparticle-Based Quantitative Colorimetric Detection of Oligonucleotides. *J. Am. Chem. Soc.* **122,** 3795–3796 (2000).

171. Reynolds, R. A., III, Mirkin, C. A. & Letsinger, R. L. A gold nanoparticle/latex microsphere-based colorimetric oligonucleotide detection method*. *Pure Appl. Chem.* **72,** 229–235 (2000).

172. Storhoff, J. J., Elghanian, R., Mucic, R. C., Mirkin, C. A. & Letsinger, R. L. One-Pot Colorimetric Differentiation of Polynucleotides with Single Base Imperfections Using Gold Nanoparticle Probes. *J. Am. Chem. Soc.* **120,** 1959–1964 (1998).

173. Xu, X., Han, M. S. & Mirkin, C. A. A Gold-Nanoparticle-Based Real-Time Colorimetric Screening Method for Endonuclease Activity and Inhibition. *Angewandte Chemie International Edition* **46,** 3468–3470 (2007).

174. Hill, H. D., Vega, R. A. & Mirkin, C. A. Nonenzymatic Detection of Bacterial Genomic DNA Using the Bio Bar Code Assay. *Anal. Chem.* **79,** 9218–9223 (2007).

175. Jaroenram, W. & Owens, L. Recombinase polymerase amplification combined with a lateral flow dipstick for discriminating between infectious Penaeus stylirostris densovirus and virus-related sequences in shrimp genome. *Journal of Virological Methods* **208,** 144–151 (2014).

176. Banoo, S. *et al.* Evaluation of diagnostic tests for infectious diseases: general principles. *Nature Reviews Microbiology* **6,** S16–S29 (2010).

177. Borysiak, M. D., Thompson, M. J. & Posner, J. D. Translating diagnostic assays from the laboratory to the clinic: analytical and clinical metrics for device development and evaluation. *Lab on a Chip* **16,** 1293–1313 (2016).

178. Rouer, E. Direct neutralization of alkaline-denatured plasmid DNA in sequencing protocol by the sequencing reagent itself. **22,** 4844 (1994).

179. Wolfgang, E. *et al.* Proteinase K from Tritirachium album Limber. *European Journal of Biochemistry* **47,** 91–97 (1974).

180. ONeill, J. Antimicrobial Resistance: Tackling a crisis for the health and wealth of nations. *Review on Antimicrobial Resistance* (2014).

181. Deshpande, A. *et al.* A rapid multiplex assay for nucleic acid-based diagnostics. *Journal of Microbiological Methods* **80,** 155–163 (2010).

182. Deshpande, A. & White, P. S. Multiplexed nucleic acid-based assays for molecular diagnostics of human disease. *Expert Review of Molecular Diagnostics* **12,** 645–659 (2012).

183. Mothershed, E. A. & Whitney, A. M. Nucleic acid-based methods for the detection of bacterial pathogens: Present and future considerations for the clinical laboratory. *Clinica Chimica Acta* **363,** 206–220 (2006).

184. CLSI. Performance Standards for Antimicrobial Susceptibility Testing; Twenty-Fifth Informational Supplement. *CLSI document M100-S25* **35,** (2015).

185. Marlowe, E. M. & Bankowski, M. J. Conventional and Molecular Methods for the Detection of Methicillin-Resistant Staphylococcus aureus Staphylococcus aureus. *Journal of Clinical Microbiology* **49,** S53–S56 (2011).

186. Leekha, S., Terrell, C. L. & Edson, R. S. General Principles of Antimicrobial Therapy. *Mayo Clinic Proceedings* **86,** 156–167 (2011).

187. Xu, J. *et al.* Phenotypic and Genotypic Antimicrobial Resistance Traits of Foodborne Staphylococcus aureusIsolates from Shanghai. *Journal of Food Science* **79,** M635–M642 (2014).

188. Haveri, M., Suominen, S., Rantala, L., Honkanen-Buzalski, T. & Pyörälä, S. Comparison of phenotypic and genotypic detection of penicillin G resistance of Staphylococcus aureus isolated from bovine intramammary infection. *Veterinary Microbiology* **106,** 97–102 (2005).

189. Maynard, C. *et al.* Antimicrobial Resistance Genes in Enterotoxigenic Escherichia coli O149:K91 Isolates Obtained over a 23-Year Period from Pigs. *Antimicrobial Agents and Chemotherapy* **47,** 3214–3221 (2003).

190. Ma, M., Wang, H., Yu, Y., Zhang, D. & Liu, S. Detection of antimicrobial resistance genes of pathogenic Salmonella from swine with DNA microarray. *J Vet Diagn Invest*

19, 161–167 (2007).

191. Allen, H. K. *et al.* Call of the wild: antibiotic resistance genes in natural environments. *Nature Reviews Microbiology* **8,** 251–259 (2010).

192. Sabath, L. D. Mechanisms of Resistance to Beta-lactam Antibiotics in Strains of. *Annals of Internal Medicine* **97,** 339–344 (1982).

193. Strommenger, B., Kettlitz, C., Werner, G. & Witte, W. Multiplex PCR Assay for Simultaneous Detection of Nine Clinically Relevant Antibiotic Resistance Genes in Staphylococcus aureus. *Journal of Clinical Microbiology* **41,** 4089–4094 (2003).

194. Malhotra-Kumar, S., Lammens, C., Piessens, J. & Goossens, H. Multiplex PCR for Simultaneous Detection of Macrolide and Tetracycline Resistance Determinants in Streptococci. *Antimicrobial Agents and Chemotherapy* **49,** 4798–4800 (2005).

195. Ghidan, A., Jeney, C., Marodi, C. L., Csiszar, K. & Rozgonyi, F. PCR detection of the vanA gene in a vancomycin-resistant Enterococcus faecalis clinical isolate from Hungary. *J Antimicrob Chemother* **46,** 325–327 (2000).

196. Colom, K. *et al.* Simple and reliable multiplex PCR assay for detection of blaTEM, blaSHV and blaOXA-1 genes in Enterobacteriaceae. *FEMS Microbiology Letters* **223,** 147–151 (2003).

197. Veigas, B., Fernandes, A. R. & Baptista, P. V. AuNPs for identification of molecular signatures of resistance. *Frontiers in Microbiology* **5,** 1–11 (2014).

198. Chan, W.-S., Tang, B. S. F., Boost, M. V., Chow, C. & Leung, P. H. M. Detection of methicillin-resistant Staphylococcus aureus using a gold nanoparticle-based colourimetric polymerase chain reaction assay. *Biosensors and Bioelectronic* **53,** 105–111 (2014).

199. Storhoff, J. J., Lucas, A. D., Garimella, V., Bao, Y. P. & Müller, U. R. Homogeneous detection of unamplified genomic DNA sequences based on colorimetric scatter of gold nanoparticle probes. *Nat. Biotechnol.* **22,** 883–887 (2004).

200. Veigas, B. *et al.* Au-nanoprobes for detection of SNPs associated with antibiotic resistance in *Mycobacterium tuberculosis*. *Nanotechnology* **21,** 415101–415107 (2010).

201. Ramakrishnan, R. *et al.* Sensitive Assay for Identification of Methicillin-Resistant Staphylococcus aureus, Based on Direct Detection of Genomic DNA by Use of Gold Nanoparticle Probes. *Clinical Chemistry* **50,** 1949–1952 (2004).

202. Valiadi, M. *et al.* Simple and rapid sample preparation system for the molecular detection of antibiotic resistant pathogens in human urine. *Biomed Microdevices* **18,** 18–10 (2016).

203. Keays, M. C. *et al.* Rapid identification of antibiotic resistance using droplet

microfluidics. *Bioengineered* **7,** 79–87 (2016).

204. Conly, J. M. & Johnston, B. L. The emergence of methicillin-resistant Staphylococcus aureus as a community-acquired pathogen in Canada. *Can J Infect Dis* **14,** 249–251 (2003).

205. Fridkin, S. K. *et al.* Methicillin-Resistant Staphylococcus aureus Disease in Three Communities. *The New England Journal of Medicine* **352,** 1436–1444 (2005).

206. Fluit, A. C., Florijn, A., Verhoef, J. & Milatovic, D. Presence of Tetracycline Resistance Determinants and Susceptibility to Tigecycline and Minocycline. *Antimicrobial Agents and Chemotherapy* **49,** 1636–1638 (2005).

207. Schmitz, F.-J. *et al.* The prevalence of aminoglycoside resistance and corresponding resistance genes in clinical isolates of staphylococci from 19 European hospitals. *Journal of Antimicrobial Chemotherapy* **43,** 253–259 (1999).

208. Duran, N., Ozer, B., Duran, G. G., Onlen, Y. & Demir, C. Antibiotic resistance genes & susceptibility patterns in staphylococci. *Indian J Med Res* **135,** 389–396 (2012).

209. Argudin, M. A. *et al.* Virulence and Resistance Determinants of German Staphylococcus aureus ST398 Isolates from Nonhuman Sources. *Applied and Environmental Microbiology* **77,** 3052–3060 (2011).

210. Khan, S. A., Nawaz, M. S., Khan, A. A. & Cerniglia, C. E. Simultaneous detection of erythromycin-resistant methylase genes ermA and ermC from Staphylococcus spp. by multiplex-PCR. *Mol. Cell. Probes* **13,** 381–387 (1999).

211. Andrews, J. M. Determination of minimum inhibitory concentrations. *Journal of Antimicrobial Chemotherapy* **48,** 5–16 (2001).

212. Ibrahim, E. H., Sherman, G., Ward, S., Fraser, V. J. & Kollef, M. H. The Influence of Inadequate Antimicrobial Treatment of Bloodstream Infections on Patient Outcomes in the ICU Setting. *CHEST* **118,** 146–155 (2000).

213. Kollef, M. H., Sherman, G., Ward, S. & Fraser, V. J. Inadequate Antimicrobial Treatment of Infections. *CHEST* **115,** 462–474 (1999).

214. Kim, J., Biondi, M. J., Feld, J. J. & Chan, W. C. W. Clinical Validation of Quantum Dot Barcode Diagnostic Technology. *ACS Nano* **10,** 4742–4753 (2016).

215. Blair, J. M. A., Webber, M. A., Baylay, A. J., Ogbolu, D. O. & Piddock, L. J. V. Molecular mechanisms of antibiotic resistance. *Nature Reviews Microbiology* **13,** 42–51 (2014).

216. Fluit, A. C., Visser, M. R. & Schmitz, F. J. Molecular Detection of Antimicrobial Resistance. *Clinical Microbiology Reviews* **14,** 836–871 (2001).

217. Lambert, P. Bacterial resistance to antibiotics: Modified target sites. *Advanced Drug*

Delivery Reviews **57,** 1471–1485 (2005).

218. Guirgis, B. S. S., Abbas, R. O. & Azzazy, H. M. E. Hepatitis B virus genotyping: current methods and clinical implications. *International Journal of Infectious Diseases* **14,** e941–e953 (2010).

219. Escosura-Muñiz, A. de L. *et al.* Magnetic Bead/Gold Nanoparticle Double-Labeled Primers for Electrochemical Detection of Isothermal Amplified LeishmaniaDNA. *Small* **12,** 205–213 (2015).

220. Gorgani, N., Ahlbrand, S., Patterson, A. & Pourmand, N. Detection of point mutations associated with antibiotic resistance in Pseudomonas aeruginosa. *International Journal of Antimicrobial Agents* **34,** 414–418 (2009).

221. Sun, S., Selmer, M. & Andersson, D. I. Resistance to β-Lactam Antibiotics Conferred by Point Mutations in Penicillin-Binding Proteins PBP3, PBP4 and PBP6 in Salmonella enterica. *PLoS One* **9,** e97202–10 (2014).

222. Qin, Z., Ljubimov, V. A., Zhou, C., Tong, Y. & Liang, J. Cell-free circulating tumor DNA in cancer. *Chinese Journal of Cancer* 1–9 (2016). doi:10.1186/s40880-016-0092-4

223. Van Cutsem, E., Cervantes, A., Nordlinger, B. & Arnold, D. Metastatic colorectal cancer: ESMO Clinical Practice Guidelines for diagnosis, treatment and follow-up. *Annals of Oncology* **25,** iii1–iii9 (2014).

224. Garborg, K. *et al.* Current status of screening for colorectal cancer. *Annals of Oncology* **24,** 1963–1972 (2013).

225. Marzese, D. M., Hirose, H. & Hoon, D. S. B. Diagnostic and prognostic value of circulating tumor-related DNA in cancer patients. *Expert Review of Molecular Diagnostics* **13,** 827–844 (2013).

226. Lincoln, D., Petoumenos, K. & Dore, G. J. HIV/HBV and HIV/HCV coinfection, and outcomes following highly active antiretroviral therapy. *HIV Medicine* 241–249 (2003).

227. Dore, G. J. & Cooper, D. A. The impact of HIV therapy on co-infection with hepatitis B and hepatitis C viruses. *Current Opinion in Infectious Diseases* **14,** 749–755 (2001).

228. Sun, H.-Y. Hepatitis B virus coinfection in human immunodeficiency virus-infected patients: A review. *World J. Gastroenterol.* **20,** 14598–14614 (2014).

229. Hadziyannis, S. J. *et al.* Peginterferon- 2a and Ribavirin Combination Therapy in Chronic Hepatitis C. *Annals of Internal Medicine* **140,** 346–355 (2004).

230. Wainberg, M. A. HIV-1 subtype distribution and the problem of drug resistance. *AIDS* **18,** S63–S68 (2004).